MECHANISMS OF DRYING OF SKIN FORMING MATERIALS

by

HAYDAR MAHMOOD HASSAN

Doctor of Philosophy

THE UNIVERSITY OF ASTON IN BIRMINGHAM

October 1991

THE UNIVERSITY OF ASTON IN BIRMINGHAM

Mechanisms of Drying of Skin Forming Materials

HAYDAR MAHMOOD HASSAN

Doctor of Philosophy **October 1991**

SUMMARY

The literature relating to evaporation from single droplets of pure liquids, and to the drying of droplets containing solids and of droplet sprays has been reviewed.

The heat and mass transfer rates for a single droplet suspended from a nozzle were studied within a 42mm I.D. horizontal wind tunnel designed to supply hot dry air, to simulate conditions encountered in practical spray dryer. A novel rotating glass nozzle was developed to facilitate direct measurements of droplet weight and core temperature. This design minimised heat conduction through the nozzle.

Revised correlations were obtained for heat and mass transfer coefficients, for evaporation from pure water droplets suspended from a rotating nozzle.

$$Nu = 2.0 + 0.27 \left(\frac{1}{B}\right)^{0.18} Re^{0.5} Pr^{0.33}$$

$$Sh = 2.0 + 0.575 \left(\frac{T_a - T_s}{T_{amb}}\right)^{-0.04} Re^{0.5} Sc^{0.33}$$

Experimental drying studies were carried out on single droplets of different types of skin-forming materials, namely, custard, starch, gelatin, skim milk and fructose at air temperatures ranging from 19 °C to 198 °C. Dried crusts were recovered and examined by Scanning Electron Microscopy.

Skin-forming materials were classified into three types according to the mechanisms of skin formation. In the first type (typified by droplets of custard and starch) skin formed due to gelatinisation at high temperatures. Increasing the drying temperature resulted in increased crust resistance to mass transfer due to increased granule swelling and the crust resistance was completely transferred to a skin resistance at drying temperatures > 150 °C. In the second type e.g. gelatin droplets the skin formed immediately drying had taken place at any drying temperature. At drying temperature > 60 °C a more resistant skin was formed. In the third type (typified by droplets of skim milk and fructose) the skin appeared on the droplet surface at a certain stage of the drying process under any drying conditions. As the drying temperature was increased the resistance of the skin to mass transfer increased. The drying rate history of any material depended upon the nature of the skin formed which, in turn, depended upon the drying conditions.

A mathematical model was proposed for the drying of the first type of skin-forming material. This was based on the assumption that, once all the granules gelatinised at the gelatinisation temperature, a skin appeared instantaneously on the droplet surface. The experimentally-observed times at which the skin appeared on the droplets surfaces were in excellent agreement with those predicted from the model.

The work should assist in understanding the fundamentals of particulate drying processes, particularly when skin-formation occurs and may be a crucial factor in volatiles retention.

Key Wards : Skin Formation, Droplet Evaporation, Single Droplet Drying.

DEDICATION

To The Almighty One,

My Mother, Brothers And Sisters,

My Loving Wife, Fatin,

My Daughters, Aiya And Tebarek, And

Finally To The Memory Of My Father Al-Haj Ahmed Missed By Us All But Never Forgotten

ACKNOWLEDGEMENTS

First and foremost I would like to thank Dr. C. J. Mumford for his guidance and friendship throughout these past few years. His thorough knowledge of Chemical Engineering and his compassionate nature has been a great help for me.

I also wish to thank the following:

Mr. N. Roberts and his staff in the Department of Chemical Engineering and applied Chemistry for their co-operation.

The Department of Metallurgy, for use of their Scanning Electron Microscope, and also Mr. Roger Howell for his assistance with photographic work.

Mr. A. Sayed for his aid in preparing this thesis.

My family in Baghdad especially my mother for their continual encouragement and moral support through my studies.

My wife, for her sacrifices, patience and continual encouragement.

CONTENTS

LIST OF FIGURES

LIST OF TABLES

LIST OF PLATES

LIST OF APPENDICES

CHAPTER ONE

INTRODUCTION

INTRODUCTION

Spray drying involves the transformation of feed from a fluid state into a dried particulate form by spraying the feed into a hot drying medium. It is a one-step, continuous particle-processing operation incorporating drying (1). The feed may be either a solution, suspension or paste. The feed is atomised, to provide a large surface area, and the resulting spray is contacted with a drying medium (usually air) so that a simultaneous heat and mass transfer process occurs. The large exposed surface area facilitates rapid drying. The dried product is then recovered in a series of separation stages.

Spray drying finds applications in all major industries. For example in the food industry, milk, egg, meat, vegetable derivatives and fruit are dried for use as ingredients, such as flavour, thickeners and protein additives, or for final consumables, such as instant coffee whitener, dried eggs, dried milk and baby foods. In the chemical industry, spray drying may be used at some stage in the drying of detergents, plastics, ceramic materials, pigments, dried soups, dyestuffs, resins, surface active agents and pesticides. In the biochemical industries, e.g., for pharmaceutical products such as antibiotics and cosmetics, and for yeast products, spray drying is often employed at some stage. The use of spray drying actually dates back over 100 years, yet the process is still poorly understood. With ever increasing interest in improved product qualities, greater fundamental knowledge of the individual droplet drying behaviour is essential.

Spray drying consists of the following four process stages:

1) Atomisation of the feed into a spray.
2) Spray-air contact.
3) Drying of spray (moisture/volatiles evaporation).
4) Separation of dried product from the air.

Each stage depends upon the dryer design and operation, and together with the physical and chemical properties of the feed, determine the characteristics of the dried product.

Spray drying possesses several advantages over other drying methods. The feed

material at the dryer inlet can be any pumpable fluid, and the product at the outlet is a dry particulate of controllable size and moisture content irrespective of dryer capacity and product heat sensitivity. These characteristics are of such importance to many industrial operations that spray drying becomes the only rational choice to dry fluid feedstocks although, since it employs a convection drier, its thermal efficiency is lower than competing direct contact driers that also receive fluid feed materials. The spray drying process is easy and continuous, having a high throughput and producing a stable, easily-handled product. Furthermore with proper control, the process is applicable to both heat-sensitive and heat-resistant materials.

Spray drying is disadvantaged by high installation costs. Industrial units are also physically larger per unit of powder output than other drier types; therefore spray dryers are expensive to fabricate. Furthermore their large diameter, tall drying chambers require expensive buildings and/or supporting structures.

Particle size distribution features as a major factor in dried product specification. The ideal commercial spray-dried product is generally one which is dust -free, evenly dried (i.e. without any fraction degraded due to excessive temperature or residence time) and containing no agglomerates. The manner in which the spray contacts the air is an important factor in spray dryer design, since this affects dried product properties by influencing droplet behaviour during drying. The gas flow may be counter-current in which feed and air pass through the dryer in opposite directions. Alternatively the spray and air may pass through the dryer in the same direction i.e. co-current operation. This arrangement is often preferred for products where rapid crust formation is required and the products are heat sensitive, since the hottest gas contacts the wettest solid. Mixed flow designs are less common.

One of the prerequisites for the optimum design of a spray dryer is a knowledge of the controlling mechanisms in the heat and mass transfer processes. This can only be obtained by fundamental investigation, covering at least the first three process stages of spray drying identified earlier.

Because of the complexities and the impracticability of studying rate controlling

mechanisms for the distribution of droplet sizes travelling through a spray dryer, investigations have therefore tended to be divided into:

i) Studies of atomisation, with attempts to correlate droplet size distribution with feed characteristics, atomiser design, (rotary or nozzle) and flow rates.

ii) Gas flow patterns and residence time studies.

iii) Single droplet drying studies.

iv) Mathematical models which attempt to bring together the data from i-iii to predict dryer performance.

In general, materials which are spray dried, are classified into two major types:

(a) Crust-forming materials e.g., sodium sulphate decahydrate, sodium chloride and potassium sulphate droplets.

(b) Skin-forming materials e.g., skim milk, fructose, gelatin, starch, custard and coffee droplets.

The present study was concerned with an experimental investigation, and mathematical modelling, of the evaporation of suspended droplets of pure water and of the drying of suspensions or solutions of different skin forming materials.

Different droplet suspension techniques have been used by different investigators, for single droplet drying studies. Droplets were suspended from filaments (3,78), filament-thermocouples (8,62), or rotating nozzles (7,10). Alternatively droplets have been retained in free-flight (7,9). Suspended droplet studies have been criticised as being unrealistic for several reasons (108, 112):

i) Suspended or free flight droplets are much larger in diameter (1-5mm) than actual sprayed droplets. Big droplets are necessary because they are easier to handle and transfer, and they avoid significant drying during the initial transient period.

ii) A significant weight is required for an accurate determination if weight change is measured to establish the drying history.

iii) The droplets must be large enough to observe if visual recordings are used to follow the drying rate.

iv) Suspended and possibly free-flight droplets (except those suspended from a rotating nozzle) are not allowed to rotate freely whilst drying. This may lead to the drying rate being greatest on the side facing the air flow, and smallest in the wake region.

v) The droplet suspension device provides a heat source and a site for vapour bubble nucleation in the droplet. Later in the process it may tend to deform the droplet, if this is of a pure liquid.

Despite the above disadvantages, single suspended droplets are easy to observe and control. Of the many important investigations using single suspended droplets, the early work of Frossling (12) and Charlesworth and Marshall (3) are notable for their attempt to provide some fundamental insight into the drying process through studies of single suspended droplets.With modifications, their method of suspending droplets from devices is still in use (5).

A great many fundamental studies have been carried out on the evaporation of pure liquid droplets. Less work has been performed however on droplets containing suspended or dissolved solids, the presence of which inevitably leads to the formation of a crust or skin on the surface.This can be attributed partly to the complexities in analysing the heat and mass transfer processes after a crust or skin has formed. The majority of the work on droplets containing solids has concentrated on the crust formation process. There is little in the literature which provides any fundamental insight into the mechanisms of skin formation and its effect on the drying process or on the classification of the different types of skin-forming materials. This is possibly because the analysis of the heat and mass transfer processes after skin formation is more complex than that for crust formation. Further complications may arise after skin formation due to inflation, distortion or shrinkage of the droplet.

Following the crust or skin formation, heat is transferred by convection from the drying medium to the external crust surface and by conduction to the core. Whilst for the skin forming-materials and for those types where the interior of the droplet is semi-solid throughout the heat transfer is by conduction, in those with a liquid interior heat transfer

is by natural convection. Then mass is transferred by diffusion through the crust or skin into the surroundings. As the particle dries, the crust or skin increases in thickness resulting in an increase in the resistance to heat and mass transfer. This leads to an increase in the core temperature, resulting in a reduction in the temperature and partial pressure driving forces. Therefore the transfer process is highly complex and difficult to model mathematically, especially for skin forming materials.

The general drying characteristics of droplets containing solids are shown in Figure 1.1. The drying rate is established immediately the droplet contacts the drying medium as represented in phase AB. The droplet surface temperature increases, or decreases, until the heat transfer rate across the droplet-air interface reaches a steady value. This is reflected in the initial drying rate, which increases, or decreases. After a steady-state is established it is characterised by evaporation from a saturated (free) liquid surface, termed a constant rate drying period. This period is represented by phase BC, during which the drying rate is constant. The droplet surface is maintained saturated by sufficient migration of moisture from within the droplet to the surface. The drying rate in this period is the highest rate achieved during the entire droplet evaporation history. The constant rate drying period is controlled by the external conditions of air velocity, temperature and humidity. The gas film around the droplets represents the entire resistance to mass transfer during this period. In phase CD, point C is termed the critical point, which is attained at the end of the constant rate period. At this point the moisture within the droplet can no longer maintain surface saturation. Drying rate begins to fall, initiating the falling rate drying period, phase CD. This period can form more than one stage, if local areas of wetness remain on the droplet surface. The phase CD continues until no areas of wetness remain. In stage DE, resistance to mass transfer is wholly in the solid layer. Evaporation rate continues at a decreasing rate until the droplet acquires a moisture content at equilibrium with the surrounding drying medium. The drying process described above (Figure 1.1) is an ideal case, and in reality the drying curves may not

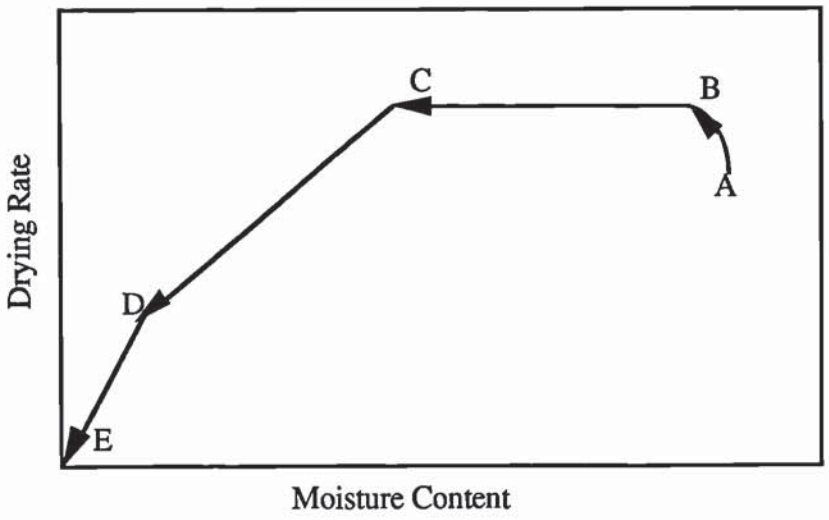

Figure 1.1 Drying of a Droplet Containing Solids

exhibit sharply defined regions. Some of the drying zones described above may not even occur. For example, if a product is heat sensitive, the air temperatures are maintained low so that stage AB can well be extended until the critical point is attained. With droplets of skin forming materials, it is found that drying rate falls immediately the droplet contacts the hot drying medium stream, and as will be shown in Chapter 9 no constant drying rate period is observed.

The present study was therefore initiated to provide fundamental insight, classification and understanding of the mechanisms involved in the drying of droplets of the different types of skin forming materials. A novel rotating nozzle developed to facilitate direct measurements of droplet weight and core temperature, was used to study the drying characteristics of single suspended droplets. This nozzle (which ensured droplet rotation during drying, thus simulating more closely conditions encountered in a spray-dryer) was placed in horizontal wind tunnel in which humidity, flow rate and temperature could be closely controlled.

CHAPTER TWO

MASS TRANSFER FUNDAMENTALS

2.1 MASS TRANSFER ACROSS A PHASE BOUNDARY

2.2 TWO-FILM THEORY

2.3 PENETRATION THEORY

2.4 FILM PENETRATION THEORY

2.5 BOUNDARY LAYER THEORY

MASS TRANSFER FUNDAMENTALS

2.1 MASS TRANSFER ACROSS A PHASE BOUNDARY

Most diffusional mass transfer operations, such as evaporation and drying of droplets involve contact between two phases which allows transfer of the diffusing vapour from one phase to the other. The driving force for mass transfer is provided by the concentration gradient which exists across the interface. The transfer process continues until either the liquid has evaporated, or the gas is saturated and the concentration gradient reduced to zero.

In 1885, Fick (14) deduced by analogy with heat transfer that the rate of diffusion of component A in a mixture of two components, A and B, is directly proportional to the concentration gradient.

$$N_a = - D_{AB} \frac{dC_A}{dZ} \qquad \text{--------2.1}$$

where D_{AB} is the diffusivity of A in B.

The rate of mass transfer between the two phases is a function of the physical properties of the phases, the interfacial area and the concentration driving force;

$$N_a = K_O A \Delta C \qquad \text{---------2.2}$$

where

K_O = Overall Mass Transfer Coefficient

A = Interfacial area

ΔC = Concentration driving force

In the majority of the important applications of mass transfer e.g. drying,

liquid-liquid extraction, distillation, etc. material is transferred across a phase boundary. Since no material accumulates at the interface, the transfer rate on each side must be equal and therefore the concentration gradients automatically adjust themselves so that they are proportional to the resistance to transfer in the particular phase.

Equation 2.2 defines the overall mass transfer coefficient, but in industrial spray drying, or in the drying of single droplets containing suspended or dissolved solids, initially evaporation takes place from a saturated surface and the entire resistance to mass transfer is only in the gas film around the droplet. The rate of vapour diffusion in the surrounding atmosphere depends on the concentration driving force between liquid and vapour around the droplet. The gas-film mass transfer coefficient, kg, is then rate controlling. However, once the critical moisture content is reached a solid crust begins to grow around the droplet and the controlling resistance to moisture movement shifts from the gas- film into the crust. The crust coefficient, k_c, then limits the overall mass transfer process. In the case of a droplet of solution/suspension which has a tendency to form a skin around the droplet, the skin mass transfer coefficient becomes rate controlling after skin formation. In some other droplets a crust forms underneath the skin as in skim milk and sucrose droplets. Hence in this case the overall mass transfer coefficient should contain a term to include for the resistance to mass transfer due to this additional barrier. Therefore, prior to crust formation, the overall mass transfer coefficient, K_O, is given by

$$\frac{1}{K_O} = \frac{1}{H_l k_g} + \frac{1}{k_s} \qquad \text{----------2.3}$$

The overall mass transfer coefficient for such a droplet once the crust forms beneath the skin reverts to,

$$\frac{1}{K_O} = \frac{1}{H_l k_g} + \frac{1}{k_c} \qquad \text{----------2.4}$$

since the external surface is , by definition, solid and not a film. The interfacial area, A, may change if the droplet expands or shrinks. Rupture may also effect a change in the value of K_O.

A number of theories have been proposed to describe the mechanism of mass transfer across a phase boundary.

2.2 TWO-FILM THEORY

In 1923, Whitman (11) attempted to describe the mechanism of mass transfer at the interface between two fluids. Equilibrium is assumed at the interface and the resistance to mass transfer in each phase is regarded as lying in a thin laminar layer on either side of the interface. The total resistance is obtained by adding the individual film resistances, in an analogous manner to that in convective heat transfer. The theory postulates that the concentration gradient is linear close to the interface and gradually becomes less at greater distances. The basis of the theory is the assumption that the zones in which the resistance to transfer occurs can be replaced by two hypothetical layers, one on each side of the interface, in which transfer is by molecular diffusion. The concentration gradient within these layer is linear and zero outside them. Using Fick's law of diffusion (14), the model predicts that the overall mass transfer coefficient K_O, is proportional to the diffusivity D_V.

2.3 PENETRATION THEORY

Higbie (137) laid the basis of the Penetration Theory for unsteady state mass transfer. It is assumed that the eddies in the bulk fluid bring discrete elements to the interface where they are exposed to the second phase for a definite interval of time, after which the surface elements are re-mixed with the bulk fluid. Thus, fluid whose initial composition corresponds with that of the bulk fluid remote from the interface is suddenly exposed to the second phase. It was assumed that equilibrium is immediately attained by the surface layer and that a process of unsteady-state molecular diffusion or penetration

of solute then occurs and that the element is re-mixed after a fixed interval of time. According to this concept the mass transfer coefficient is shown to be proportional to $(D_V)^{0.5}$.

Danckwerts (138) modified the Penetration Theory by supposing the surface to be replaced continuously by fresh fluid in a random fashion. Assuming the chance of a surface element being replaced by another is quite independent of how long it has been at the surface, and if S is the fractional rate of replacement of elements, he showed that the average mass transfer coefficient is proportional to $(D_V)^{0.5}$.

2.4 FILM PENETRATION THEORY

The Film-Penetration model, developed by Toor and Marchello (139), incorporates features of the earlier model. Mass transfer is regarded as an unsteady-state process with resistance to transfer residing within a laminar film at the interface, as in the Two-Film Theory. It is assumed that fresh surface is formed at intervals from fluid which is brought from the bulk of the fluid to the interface by the action of the eddy currents. Their analysis showed that for short exposure times, mass transfer across a boundary can be modelled by the Penetration Theory. For prolonged periods of exposure, when steady-state conditions arise, the Two-Film Theory is applicable.

2.5 BOUNDARY LAYER THEORY

The Boundary Layer Theory is applicable to the prediction of mass and heat transfer coefficients for spherical droplets. When a fluid flows over a solid surface, a velocity gradient is set up in the boundary layer. If there is a difference in temperature between the surface and the fluid, heat transfer will take place; if a concentration gradient exists mass transfer will take place simultaneously.

For flow over spherical droplets, the equations of motion, continuity and energy can be solved approximately to obtain the velocity, concentration and temperature profiles in a thin boundary layer at the interface. Frossling (12) applied this theory to

evaporating liquid droplets of nitrobenzene, aniline and water and found that the mass transfer coefficient is proportional to $(D_V)^{0.67}$.

CHAPTER THREE

DROPLET HEAT AND MASS TRANSFER

EVAPORATION FROM PURE LIQUID DROPLETS

3.1 EVAPORATION FROM SINGLE DROPLETS AND SPHERES UNDER NATURAL CONVECTION

3.2 EVAPORATION FROM SINGLE DROPLETS AND SPHERES UNDER FORCED CONVECTION

3.2.1 Mass Transfer

3.2.2 Heat Transfer

3.3 EVAPORATION FROM SINGLE DROPLETS IN A HIGH TEMPERATURE ENVIRONMENT

DROPLET HEAT AND MASS TRANSFER

EVAPORATION FROM PURE LIQUID DROPLETS

The evaporation from a single droplet and the associated phenomena of heat and mass transfer have been studied extensively since they are of fundamental significance for design in many operations, involving such processes as spray drying, humidification, cooling, absorption, desorption and combustion.

The evaporation of pure liquid droplets is a process involving simultaneous heat and mass transfer. Maxwell (6) laid down the basis of the theory related to evaporation from droplets, motionless relative to an infinite gaseous medium. It was shown that for a perfectly spherical droplet, whose vapour concentration at the surface C_S is continuously saturated, the evaporation rate was given by,

$$-\frac{dw}{dt} = 4r\pi\, D_V (C_S - C_\infty) \qquad \text{----------3.1}$$

From equation 3.1, a gas phase mass transfer coefficient can be defined under stagnant conditions as,

$$k_g = \frac{-dw/dt}{4\pi r^2 (C_S - C_\infty)} = \frac{D_V}{r} \qquad \text{---------3.2}$$

and the Sherwood number can thus be expressed as,

$$Sh = k_g . 2r / D_V = 2 \qquad \text{----------3.3}$$

For dynamic equilibrium the rate of heat transfer is equal to the product of mass transfer and latent heat of vaporisation λ. The rate of heat transfer from the saturated surface can therefore be expressed as,

$$\frac{dw}{dt} = \frac{dQ}{dt.\lambda} = h_g A_h (T_a - T_s)/\lambda \qquad \text{----------3.4}$$

Following the heat and mass transfer analogy the Nusselt number can be expressed as,

$$Nu_o = h_g \,.\, 2r / K = 2 \qquad \text{----------3.5}$$

When a finite relative velocity exists between the droplet and air, additional mass transfer takes place by convection. Frossling (12), by using a boundary-layer analysis, deduced that the right hand side of equation 3.3 should be multiplied by a wind factor, i.e.

$$Sh = 2\,(1 + \beta\, Re^{0.5}\, Sc^{0.33}) \qquad \text{----------3.6}$$

where $\beta = 0.276$

Numerous workers confirmed the validity of this equation, the main difference being in the value of β. The most widely used correlation was obtained by Ranz and Marshall (2) who evaluated β, as 0.3. However, the data relate to experiments carried out using stationary droplets or solid particles suspended at the end of a filament or a capillary or suspended in free flight. Indeed, studies of mass transfer from rotated droplets, which is the practical situation with regard to spray drying, are extremely few in number.

Therefore the literature on the evaporation of pure liquid droplets has been divided into the following categories:

a) Droplets evaporating under natural convection.

b) Droplets evaporating under forced convection.

c) Droplets evaporating under conditions of high temperature surroundings.

In the early studies experiments were carried out using droplets placed on

weighing pans. There was then a progression to using droplets placed (suspended) on the end of glass filaments or capillaries. Recently droplets were suspended from a rotating nozzle, which ensures droplet rotation thus simulating more closely conditions encountered in practical spray dryer. However other techniques have been used such as methods involving internally heated brass spheres coated with the material in question.

3.1 EVAPORATION FROM SINGLE DROPLETS AND SPHERES UNDER NATURAL CONVECTION

Evaporation from the surface of a sphere of volatile material into a still atmosphere is a diffusion-controlled process. Sreznevskii (13) was the first to determine rates of evaporation into still air. Experiments were carried out using a convex liquid meniscus at the upper end of a tube of 3mm diameter, and on droplets of liquid placed on the flat top of vertical cylindrical columns of 1.8-3.6mm diameter, such that the droplet completely covered the top. The rates of evaporation for hemispherical droplets of water, carbon disulphide, chloroform, ether and benzene were determined by following the outline of the droplet through a horizontal microscope.

In 1910 Morse (48) studied the evaporation into still air of spheres of iodine resting on the pan of a microbalance and found that the rate of evaporation was proportional to the radii of the spheres. Morse's results were examined by Langmuir (15), who derived a modified version of Maxwell's equation and hence calculated the diffusion coefficient for iodine diffusing into air at atmospheric pressure, and at 20 ^{o}C.

Experiments were later carried out by Whytlaw-Gray and Patterson (38) on droplets of water, aniline, quinoline, methyl salicylate and p-cresol with radii of 1 to 2mm, placed on the pan of a quartz microbalance. In every case the surface of the droplets decreased linearly with time, although the volume decreased by a factor of about a hundred.

No further experiments were made on droplets placed on a flat support; instead thin filaments were used to support the droplets. These give a much better approximation to the conditions of evaporation of free droplets since they remain approximately spherical and virtually all the surface area is available for convective heat and mass transfer. Therefore this technique gave more reliable and accurate results for the rates of evaporation of droplets both in still media and in an air-stream.

Measurements by this technique were first made by Topley and Whytlaw-Gray (40) on spheres of iodine of radius 1mm fused to a quartz fibre and suspended from a quartz spring-balance in a cylindrical vessel of radius 20mm. The walls and bottom of the vessel were covered with a thin layer of potassium hydroxide to absorb the iodine vapour. Their results provided the first quantitative support for Maxwell's equation.

Houghton (41) measured the rate of evaporation of droplets of water suspended from a glass fibre using a horizontal microscope. Use of different sized fibres varying from 1.25-120μm radii, facilitated the study of droplets of radii 50-100μm. The fibers were covered with a thin layer of paraffin, firstly to reduce the distortion of the droplet and secondly to prevent the droplet wetting the fibre. The temperature of the air in the chamber was 20 ^{o}C and the droplet temperature was not measured, it being assumed equal to the temperature indicated by a wet-bulb thermometer placed in the chamber.

In their study Langstroth et al (37) measured optically the evaporation rates of droplets of water and a number of organic liquids with radii of 1.4mm. A glass fibre (100μm diameter) or a constantan thermocouple was used to suspend the droplets at the centre of a spherical glass flask of 20mm inner diameter. The droplet diameter was measured by using a microscope fitted with an ocular micrometer and viewed horizontally through a small plane window. Corrections were made for the finite size of the vessel and for radiation, but the flow of heat through the glass fibre was not accounted for. The experimental results obtained agreed with calculations based on diffusion and heat transfer history.

Ranz and Marshall (2) studied the rate of evaporation of single droplets of

water, benzene and aniline, suspended from the end of a glass capillary and thermoelement, inside a special dryer. Droplet diameters ranged from 0.06 to 0.11 cm., and air temperatures ranged up to 220 °C. They correlated their experimental results by;

$$Nu_o = 2.0 + 0.6\ Pr^{0.33}\ Gr^{0.25} \quad \text{----------3.7}$$

$$Sh_o = 2.0 + 0.6\ Sc^{0.33}\ Gr^{0.25} \quad \text{----------3.8}$$

Mathers et al (121) were the first to solve the simultaneous heat and mass transfer equations numerically for natural convection. Experiments were conducted on internally-heated brass spheres coated with naphthalene. They proposed that

$$Nu_o = 2.0 + 0.282\ (Gr.Pr)^{0.37} \quad \text{----------3.9}$$

$$Sh_o = 2.0 + 0.282\ (Gr.Sc)^{0.37} \quad \text{----------3.10}$$

For Gr.Pr(or Sc) < 100

And

$$Nu_o = 2.0 + 0.5\ (Gr.Pr)^{0.25} \quad \text{----------3.11}$$

$$Sh_o = 2.0 + 0.5\ (Gr.Sc)^{0.25} \quad \text{----------3.12}$$

For $10^2 < Gr.Pr$ (or Sc) $< 10^6$

Steinberger and Treybal (42) used benzoic acid spheres of different sizes (12.7, 19.1, and 25.4mm) immersed in a Dewar flask. The flask was filled with water and allowed to stand for 8 hours on a 6.35mm thick rubber pad to damp fluid circulations. A benzoic acid sphere was gently lowered into stagnant fluid, a lucite cover being used to support the sphere and a thermometer. The next day the sphere was gently removed from the flask, and the solution was mixed and titrated for its

benzoic acid content. They divided their data according to the boundary layer becoming turbulent, which they characterised by (Gr.Sc) greater or less than 10^8. Hence,

$$Sh_o = 2.0 + 0.569\ (Gr.Sc)^{0.25} \qquad \text{----------3.13}$$

and for $(Gr.Sc) > 10^8$

$$Sh_o = 2.0 + 0.0254\ (Gr.Sc)^{0.33} \qquad \text{----------3.14}$$

However, only three data points were available for establishing equation 3.14 so that the accuracy attributed to the constants and exponents is questionable.

Frazier and Chang (106) stated that the different models developed for the vaporisation of pure liquids were based on a number of approximations and restrictions and had never been tested adequately at high temperatures. Most particularly, large changes in property values can occur through the vapour film surrounding the droplets and a question therefore arises as to how best to average the properties for acceptable agreement with experimental results. Integrated mean values of the physical and transport properties over the film length were used. A model developed by Frossling in which,

Total vaporisation rate = rate in absence of convection + rate due to convection

was used to fit the experimental results of Hoffman and Gauvin (17) for 0.4 to 1.4mm droplets of water, methanol, cumene, pentane or benzene at surrounding temperatures from 100 ^oC to 550 ^oC. Good agreement was achieved with experimental results .

Yuge (21) investigated heat transfer under natural convection conditions from internally heated carbon-chrome steel and brass spheres. The sphere was suspended from two sides by thermocouple wires. He expressed his results by,

$Nu_o = 2.0 + 0.392\ Gr^{0.25}$ ----------3.15

for $1<Gr<10^5$

The evaporation of free droplets has also been studied by supporting charged droplets in Milikan condenser. A number of investigators used this technique, notably Gudris and Kulikova (122) on droplets of water, Nestle (123) on droplets of mercury, and Woodland and Mack (124) on droplets of dibutyl tartrate and dibutyl phthalate. In this technique the droplet is introduced into the apparatus and the potential across the condenser continuously varied such that the electrostatic and gravitational fields are balanced and the droplet remains stationary. Whilst less accurate results are achieved using this technique, it does allow droplets as small as a few microns to be investigated. However surface tension may be affected by charging.

3.2 EVAPORATION FROM SINGLE DROPLETS AND SPHERES UNDER FORCED CONVECTION

The most important studies with regard to spray drying are those for the evaporation of droplets moving relative to a gaseous medium under the influence of gravity and / or interia. Most of the measurements of the rate of evaporation under forced convection have been carried out as in the previous case of stationary droplets, using fixed droplets, ventilated by a stream of gas. Very little work has been done with rotated droplets due to the experimental difficulties. Investigations in this section can be classified according to either the mass transfer or heat transfer approach.

3.2.1 Mass Transfer

The first measurements of rates of evaporation in a gas stream were carried out by Majama (16). Droplets of water and organic liquids with diameters of 0.2mm, were suspended on a horizontal glass fibre of radius 2.5μm in an air current of velocity up to 18 m/s. His analysis revealed that the rate of change of diameter squared was a constant.

The most accurate measurements of the evaporation of suspended droplets in

an air current were those of Frossling (12). Glass fibres of radius 10 to 100μm or a constantan-manganin thermocouple were used to suspend stationary droplets of water, aniline, nitrobenzene and spheres of naphthalene with initial radii in the range 0.1-0.9mm, at an air temperature of 20 °C. The droplets were suspended 20 cm above the exit of a vertical wind tunnel. The air velocity was varied from 0.2-7.0 m/s and the rate of evaporation was determined by periodically photographing the droplet and were correlated by equation 3.6.

Interesting results were obtained by Frossling on the variation in the rate of evaporation over the surface of a sphere of naphthalene; the average rate of evaporation from the (exposed) face was about ten times greater than the rate from the rear side of the sphere. These results confirm the boundary layer theory that the rate of transfer should be a maximum on the front side of the droplet (facing the oncoming air stream), decrease to a minimum value near the separation point and increase to another, but lower, maximum rate on the trailing face which experiences velocities in the reverse direction.

Vyrubov (18) investigated the rate of evaporation of freely falling droplets of 2 mm diameter in a 1 m long vertical tube. Hot air from 40-100 °C was passed down the tube at 1 m/s and droplets were collected on a weighing pan. The results were expressed in the form

$$Sh = 0.52\ Re^{0.5} \qquad \text{----------3.16}$$

at $100 < Re < 500$

Evaporation of water droplets at 0 °C to 40 °C was studied by Kinzer and Gunn (39). They carried out a theoretical and experimental investigation by using the method of instantaneous photography with side illumination. Small droplets of 10-140μm were charged and allowed to fall freely through detector rings. Droplets greater than 1mm were supported in free flight by hydrodynamic forces, and as evaporation proceeded they moved up the tube. They obtained the same relationship as

Frossling (equation 3.6) with a β value of 0.23 for $100 < Re < 1600$. They found that at very small Re (< 0.9) the wind factor was unity, i.e. $\beta = 0$. On further increasing Re the wind factor rose; β increased to a value of 0.46 at Re = 4 and then gradually fell to the above mentioned value of 0.23 at Re = 100.

The fundamental study of Ranz and Marshall (2) on pure liquids was further confirmation of Frossling's results, differing only in the value of β. They suspended single stationary droplets of aniline, benzene or water from a glass capillary sealed to the delivery tube of a microburette at air temperatures up to 220 °C. The droplets were ventilated by dry air (Re = 0 -200) from below and the droplet size was kept constant by a continuous supply of water through the burette. The rate of evaporation then equalled the rate of supply of liquid. The temperatures of the droplets were determined by inserting a constantan-manganin thermocouple into their sides. They hence derived the most widely quoted equations for heat and mass transfer i.e.,

$$Nu = 2.0 + 0.6\, Re^{0.5}\, Pr^{0.33} \qquad \text{----------3.17}$$

$$Sh = 2.0 + 0.6\, Re^{0.5}\, Sc^{0.33} \qquad \text{----------3.18}$$

In their study Hsu et al (23) used the same method as the previous investigators, i.e. keeping the droplet diameter constant, and measured the rate of evaporation of 1.8mm diameter droplets of heptane at 37 °C at Re values from 70 to 300. They paid great attention to the influence of droplet shape on the rate of evaporation. The large size of the droplets and the low surface tension of heptane, resulted in the droplet shape deviating significantly from spherical. For example on fine capillaries (0.1mm) the droplets were pear-shaped and on wide capillaries (0.8mm) truncated spheres. They expressed,their results by,

$$Sh = 2\,(1 + 0.272\, Re^{0.5}\, Sc^{0.33})\,(1 + 1.147\,(1 - E)\,(1 - 0.037\,(1 - dv/dh)) \qquad \text{---3.19}$$

where $E = 6\,V/Adh$

V	=	Volume of the droplet	m^3
A	=	surface area of the droplet	m^2
dh	=	Maximum horizontal distance	m

It was found that the evaporation rate increased rapidly with deviations from a sphere, the oblate spheroids yielding higher evaporation rates than the pendant droplets.

Maisel and Sherwood (22) used calcium silicate spheres wetted with water or benzene to measure the rate of evaporation. They found that benzene evaporated so quickly that the surface of the spheres was never really wetted. Their experiments were conducted at a Re from 2,000-50,000.

Garner and Grafton (24) measured the rate of dissolution of 1.27 cm diameter pressed benzoic acid spheres in a stream of water at room temperature. The measurements were carried out by a photographic technique and the experimental results were correlated by,

$$Sh = 44 + 0.48\ Re^{0.5}\ Sc^{0.33} \qquad \text{----------3.20}$$

for $20 < Re < 1000$.

This correlation, although of similar form, differs significantly from that of Frossling (12) and Ranz and Marshall (2); the difference is principally in the constant term and they explained that this is due to natural convection effects. However, in a later study Garner and Suckling (125), used the same apparatus and technique covering a range of 9.5mm and 12.7mm diameter spheres of adipic acid and 9.5, 12.7, 15.8 and 19.0mm diameter spheres of benzoic acid. Using an assumed limiting value of 2, they correlated their results together with earlier work above, using the expression

$$Sh = 2.0 + 0.95\ Re^{0.5}\ Sc^{0.33} \qquad \text{----------3.21}$$

for $100 < Re < 700$

Using a similar method Garner and Hoffman (49) studied the dissolution rate of organic acid spheres of 9.5mm diameter in a water tunnel at 30 °C for both upflow and downflow streams. They found that free convective effects did not disappear entirely until Re = 250 for the 9.5mm spheres compared with Re = 750 for 19.0mm spheres in the previous work (126). Garner and Keey (126) found that the overall mass transfer data tended towards the relationship,

$$Sh = 0.94\ Re^{0.5}\ Sc^{0.33} \qquad \text{----------3.22}$$

for $200 < Re < 900$

Evanochides and Thodos (32) carried out a simultaneous heat and mass transfer study, using celite spheres saturated with either water or nitrobenzene. Each sphere was suspended horizontally and rotated just above the discharge end of a 20 cm round duct. They measured the temperature of the sphere by thermocouples inserted into it. The spheres were periodically weighed in order to determine the evaporation rate.

Following the above technique, Pasternak and Gauvin (44) suspended spheres of celite saturated with water from a hypodermic needle. The spheres were placed inside a 38.1mm diameter glass column through which hot air was passed under controlled conditions of temperature, humidity and velocity. Using spheres sizes of 5.59-11.63mm diameter, they correlated their results by,

$$Sh = 0.692\ Re^{0.514}\ Sc^{0.33} \qquad \text{----------3.23}$$

In their later work (33) they confirmed this expression using radioactive celite spheres saturated with acetone in free flight. Accurate particle velocity was determined using a radioactive tracer technique.

Bowman et al (45) presented a theoretical analysis of the influence of internal circulation on the rate of mass transfer from spherical fluid particles. They assumed

that internal circulation affects the external flow pattern, thereby reducing the resistance to transfer in the external fluid. This was illustrated by the study of Ward et al (31). They measured rates of mass transfer for four liquid-liquid systems; for water droplets into cyclohexanol and from droplets of cyclohexanol, isobutanol or o-toluidine into water. Their results demonstrated a four to six fold enhancement of mass transfer over that for non-circulating droplets. These results illustrate the earlier suggestion of Fuchs (127) that internal circulation in a droplet may enhance heat and mass transfer.

Steinberger and Treybal (42) from their work with cast benzoic acid spheres, proposed that mass transfer by natural and forced convection to spheres are additive. Working with spheres of 12.7, 19.1 and 25.4mm in upward flowing streams of water and propylene glycol, they proposed,

$$Sh = Sh_o + 0.347 (Re\ Sc^{0.5})^{0.62} \qquad \text{----------3.24}$$

Where Sh_o, the natural convection contribution is given by equation 3.13 or 3.14. The above correlation gave good agreement at low Reynolds numbers but was less successful at higher values.

Pei et al (47) in a review of this area of investigation showed that Steinberger and Treybal were the only authors to come to this conclusion. All other studies have suggested that the transition from forced to natural convection, or vice-versa, was gradual and that the two convective terms were not additive.

Spheres of naphthalene, benzoic acid and camphor of 2.38 to 19.05mm diameter were freely-suspended in an air stream moving at a high velocity through rotameter tubes, and their evaporation was investigated by Jones and Smith (34). Despite the fact that the particle spun erratically, the mass transfer coefficients showed no significant difference when compared to those from fixed particles. A possible reason for this is that when one side of a spinning sphere is stationary relative to the

gas the other side meets the flow at twice its linear velocity. A relationship was proposed which takes into account the Reynolds number of the gas, Re_g. For the laminar region,

$$Sh = 2.0 + 25 (Re.Sc.Re_g^{0.5})^{0.33} \quad \text{----------3.25}$$

and for the turbulent region,

$$Sh = 2.0 + 0.055 (Re.Sc.Re_g^{0.5})^{0.5} \quad \text{----------3.26}$$

Theoretical approaches to the problem of estimating mass transfer from single spheres were reviewed by Kinard et al (107). They considered separately the forced convection in front of, and behind the separation zone of the boundary layer. They note that boundary layer theory cannot accurately predict mass transfer, since it neglects transfer from the rear surface of the sphere. They therefore added an additional term to account for this transfer in the wake of the droplet. Coefficients were evaluated from selected data of Ranz and Marshall (2), Garner and Suckling (125) and Steinberger and Treybal (42) for mass transfer due to forced convection. They proposed:

$$Sh = 2.0 + Sh_o + 0.45\ Re^{0.5}\ Sc^{0.33} + 0.00484\ Re\ Sc^{0.33} \quad \text{----------3.27}$$

A novel method of droplet suspension was used by Audu (10). He suspended hemispherical droplets from a rotating nozzle placed in a horizontal wind tunnel, exposing all sides of the evaporating droplet to the impinging air. This was a new method of droplet suspension which simulates more closely the conditions encountered in a practical spray dryer. For ambient conditions, Audu expressed his experimental data as,

$$Sh = 2.0 + 0.473\ Re^{0.5}\ Sc^{0.33} \quad \text{----------3.28}$$

A limitation may be however, that heat conducted along the suspension nozzle and that due to radiation were not taken into account.

A number of workers (128, 129, 130) have investigated the shapes, oscillations and internal circulations of droplets either falling freely or freely-suspended in a gas. In a study by Garner and Kendrick (131), they investigated mass transfer to suspended droplets of water or glycol and amine in a gas stream. The gas stream from a centrifugal fan was expanded through a horizontal duct to a settling chamber. The gas left the chamber through a suction flare and passed through a contraction section preceding the working section. They observed that droplets oscillated in three different ways,

i) Prolate-oblate oscillation

ii) Oscillations about axes 90^{o} apart in the horizontal plane

iii) Eccentric rotation about the vertical axis whilst the horizontal axes remained constant.

Miura et al (25) investigated the rate of mass and heat transfer from floating droplets in an ascending air current. The experimental apparatus was similar to that of Garner and Kendrick (131). Water droplets were floated by an inverted parabolic velocity profile, i.e. low velocity in the centre, surrounded by an annular region of high velocity. Using droplets of 2.9-3.3mm diameter, air temperatures of 53 or 75 ^{o}C and high air velocities of 7.5-9.0 m/s they found that their data gave good agreement with Ranz and Marshall's results obtained from stationary droplets suspended on a fine capillary.

Recently, Sandoval-Robles et al (26) investigated mass transfer under streamline conditions. A suspended brass sphere of 5, 7, 9 or 10mm diameter was rotated at a constant velocity around a circular channel filled with motionless electrolytic solution. This provided conditions of no turbulence and a flat velocity profile. The data showed a significant dependency on the Reynolds number and was correlated by,

$Sh = 1.032\ Re^{0.385}\ Sc^{0.33}$ $2 < Re < 20$ ----------3.29

$Sh = 0.803\ Re^{0.475}\ Sc^{0.33}$ $20 < Re < 2000$ ----------3.30

$Sh = 0.300\ Re^{0.593}\ Sc^{0.33}$ $2000 < Re < 23000$ ----------3.31

Sandoval-Robles et al (27) also studied electrochemically, mass transfer around single spheres in a highly turbulent liquid. They used a 94mm diameter, vertical column with turbulence generated by a polyethylene porous plate fixed at the bottom of the column. The mass transfer from the sphere was measured by using an electrochemical method. Their data were correlated using,

$Sh = 6.86\ Re^{0.559}\ f^{0.069}$ ----------3.32

where f = turbulence intensity.

However, at low f values the data obtained in this study are in good agreement with the previously published correlation for laminar conditions.

3.2.2 Heat Transfer

Many experimental studies have used droplets suspended from filaments, capillaries or nozzles. Heat transfer to a suspended droplet takes place by a combination of convection, radiation and conduction. Therefore the suspension device acts as a heat conductor into the droplets. This extra heat source should be taken into account when evaluating heat and mass transfer rates. However, a number of researchers ignored this term, assuming it to be insignificant. Whilst this is probably justified for data obtained at low temperatures, at elevated temperatures these heat correction terms can be quite substantial. Therefore neglecting this term can introduce errors.

Kramers (43) developed an empirical equation for the coefficient of a fluid flowing past a steel sphere heated by means of high frequency induction current and maintained at a constant, uniform temperature. Individual spheres, of 70 to 12.7mm

diameter, were suspended vertically by a pair of fine thermocouple leads in a vertical stream of air, water or oil. The correlation, proposed was,

$$Nu = 2.0 + 1.3\ Pr^{0.15} + 0.66\ Pr^{0.31}\ Re^{0.5} \qquad \text{----------3.33}$$

for Re up to 10^5 and $0.7 < Pr < 400$

The second term on the right side of equation 3.33 was necessary to bring together data for air, water and oil. However the physical properties of the liquids appear likely to have been affected by temperature gradients at the surface of the spheres.

Tsubouchi and Sato (132) investigated heat transfer between single droplets and a fluid. They suspended thermistor spheres or beads, of 0.3 to 2mm diameter in a wind tunnel. A current was passed through the thermistor and from current, voltage and resistance measurements the amount of heat dissipated and the temperature were obtained. Their results were correlated by,

$$Nu = 2.0 + 0.5\ Re^{0.5} \qquad \text{----------3.34}$$

for $0.3 < Re < 3000$

Yuge (21) in an extensive study on heat transfer using carbon-chrome steel and brass spheres in different wind tunnels, compared the effects of cross, counter and parallel flows. Metal spheres less than 6mm in diameter were preheated in an electric furnace outside the wind tunnel prior to being inserted into the flow stream. The larger spheres (6-60mm) were heated internally. The results of this study were represented by the expression

$$Nu = 2.0 + 0.493\ Re^{0.5} \qquad \text{----------3.35}$$

for $10 < Re < 1.8 \times 10^3$

$$Nu = 2.0 + 0.3\ Re^{0.5664} \qquad \text{----------3.36}$$

for $1.8 \times 10^3 < Re < 1.5 \times 10^5$

Rowe et al (30) reviewed past work on heat and mass transfer to spheres mainly in the range $10 < Re < 10^4$. New experiments were carried out in which heat transfer was measured in air and in water using internally-heated, copper spheres. Mass transfer was measured by observing the rate of dissolution of spheres of benzoic acid in water and the sublimation of spheres of naphthalene in air. The results were correlated as,

For air, $Nu \text{ (or } Sh \text{)} = 2 + 0.69\ Re^{0.5}\ Pr^{0.33} \text{ (or } Sc^{0.33} \text{)}$ ----------3.37

For water, $Nu \text{ (or } Sh \text{)} = 2 + 0.79\ Re^{0.5}\ Pr^{0.33} \text{ (or } Sc^{0.33} \text{)}$ ----------3.38

3.3 EVAPORATION FROM SINGLE DROPLETS IN A HIGH TEMPERATURE ENVIRONMENT

When a droplet evaporates, heat is transferred to the surface where it is used to transform the liquid into vapour which is in turn transferred away from the surface by diffusion. In high temperature surroundings the sensible heat required to heat the vapour from the droplet surface temperature to the gas temperature becomes significantly greater. This results in a reduction in the actual amount of heat reaching the droplet surface. It has been shown by Ranz (133) that the actual heat available for vaporisation for an evaporating droplet in high temperature surroundings may be as little as 25% of the total heat transferred, the rest being absorbed by the cold vapour in its radial flow from the droplet. This therefore has to be taken into account in the heat balance. The same consideration also applied for droplets of solutions and suspensions.

Droplet evaporation at high air temperature was studied by Marshall (28). He developed a differential heat balance over a spherical shell through which heat is passing inwards towards the droplet, whilst mass is passing outwards. Solution of this differential equation gave an expression for the temperature T, as a function of distance x, through the gas film surrounding the droplet.

$$\frac{T - T_s}{T_a - T_s} = \frac{\exp(-E/x) - \exp(-E/r_1)}{\exp(-E/r_2) - \exp(-E/r_1)} \qquad \text{---------3.39}$$

Where $E = m C_{pv} / 4 \pi k_v$

r_1 = radius of the evaporating droplet

r_2 = outer radius of the gas film

An obvious simplification was to ignore any variation in the thermal conductivity and heat capacity of the gas film caused by temperature and concentration gradients. When equation 3.39 is differentiated at the droplet surface, an expression for Nusselt number is obtained as,

$$Nu = \frac{2(E/r_1)}{\exp(E(\frac{1}{r_1} - \frac{1}{r_2})) - 1} \qquad \text{---------3.40}$$

Ranz (133) presented a similar expression but included the effects of radiation.

An experimental study of the rate of evaporation of single, stationary droplets of water, methanol, cumene, pentane and benzene within an electrically-heated stainless steel sphere containing superheated vapour was carried out by Hoffman and Gauvin (17). Droplet diameters ranged from 0.4 - 1.4mm and temperatures from 100 to 500 ^{o}C and evaporation rates were recorded photographically. They found that at high temperatures, the evaporation rate was not governed by the rate of heat transfer by natural convection, but depended on the transfer number B, where $B = C_p \Delta T / \lambda$. Their results were represented by the expression,

$$Nu = 3.2 \frac{B^{0.97}}{B'} Pr^{0.33} \qquad \text{---------3.41}$$

Where

$$B = \frac{C_{pa}\Delta T}{\lambda} \qquad \text{(Radiation not included)} \qquad \text{---------3.42}$$

$$B' = \frac{C_{pa}\Delta T}{(\lambda - \frac{q_e}{N_A})} \qquad \text{(Radiation included)} \qquad \text{---------4.43}$$

It should be noted however that this equation is only valid when the gas and the containing wall of the vessel are at the same temperature, which limits its usefulness.

In a later study, Pei and Gauvin (46), using the same apparatus as that of Hoffman and Gauvin, investigated the evaporation of water, benzene and methanol. Stationary porous, hollow spheres 6.35 to 12.7mm diameter, at 204 °C to 337 °C, were used to measure the rates of evaporation. The experimental results were satisfactorily correlated by the expression,

$$Nu = \frac{3.32}{B}(Re^{0.5}Pr^{0.33})(Gr/Re^2)^{0.007} \qquad \text{---------3.44}$$

The above experimental apparatus was subsequently modified by Pei et al (47) to provide a stream of superheated steam at 150 °C to 750 °C with Reynolds numbers ranging from 5.5 to 510. They found that the contributions of forced and natural convection were demonstrated as non-additive and that the transition from one to the other was gradual. It was concluded that when Gr / Re^2 was less than 0.2 the effect of natural convection was negligible and for values greater than 10 forced convection was negligible. However, they were unable to develop an equation to account for this dependency.

Downing (29) correlated the rates of evaporation for pure liquids evaporating in streams of high temperature air. He studied droplets of acetone, benzene, n-hexane and water suspended in a dry air stream at 27 to 340 °C with a Reynolds number

ranging from 24 to 325. The correlation of results was expressed as,

$$Nu = MN (Ln (1 + B') / B') (2 + 0.6 Re^{0.5} Pr^{0.33}) \quad \text{----------3.45}$$

$$Sh = M (2 + 0.6 Re^{0.5} Sc^{0.33}) \quad \text{----------3.46}$$

Where

$$M = 1 - 0.4 (1 - Ts) (T_g) \quad \text{----------3.47}$$

$$N = 1 - 0.4 (1 - Ln (1 + B') / B') \quad \text{----------3.48}$$

In this study the average film temperature T_f, was defined as

$$(T_f - T_s) = 0.6 (T_g - T_s) \quad \text{----------3.49}$$

and the average physical and transport properties were estimated at T_f.

Eisenklam et al (134) studied the evaporation of single droplets of water and other hydrocarbons in high temperature (upto 1000 ^oC) air streams. The Reynolds numbers varied from 0.01 to 15. The experimental data were correlated by,

$$Nu_f (1 + B_f) = 2 + 1.6 Re_f^{0.5} \quad \text{----------3.50}$$

where Nu_f and B_f are the Nusselt number and Transfer number evaluated at film conditions.

An experimental technique for the study of rapid vaporisation of pure liquid droplets in a high temperature gas stream is presented by Frazier and Hellier (35). The rates of evaporation of droplets of 440μm diameter Freon 113 were determined by injecting a stream of droplets passing through a 669 ^oC air jet and a photographic

record of the vaporisation process was made using a Graflex camera. The mass transfer coefficient was found to be higher by a factor of 4 than the value obtained by Ranz and Marshall. Using corrections for net flow through the interface based on the film theory, Crosby et al (52) recalculated the results of Frazier and Hellier and found a much smaller deviation of 33% between predicted and observed values

Evaporation of water droplets into superheated steam and air was studied by Toei et al (135). They used a correlation ratio which was similar to the equivalent correction for the temperature in the vapour film used by Downing (29) to correlate their data. The experimental results were correlated by,

$$Sh = (P_{bm} / P) (2 + 0.65 \, Re^{0.5} \, Sc^{0.33}) \qquad \text{----------3.51}$$

where P_{bm} is the average partial pressure in the boundary layer.

Lee and Ryley (53) studied the evaporation of water droplets of 230 - 1130 μm suspended on a 50μm glass fibre in a horizontal test section. The experimental apparatus provided for air or superheated steam, in the Reynolds number range 64-250, as the gaseous media and evaporation rates were determined optically using a microscope. The correlation equation found was similar to that of Ranz and Marshall (2) with a coefficient of 0.74. Radiation effects were neglected in their analysis.

The evaporation of 1.56mm diameter water droplets in superheated steam and in air at velocities of 1.6 to 2.1 m/s was investigated by Trommelen and Crosby (4). The temperature of the drying medium ranged between 150 ^{o}C and 250 ^{o}C. The experimental procedure was similar to that followed by Charlesworth and Marshall (3), suspending a stationary droplet at the junction of a chromel-constantan thermocouple which was itself fixed to the end of a fine horizontal glass fibre. This allowed the simultaneous measurement of droplet weight and temperature. They found that at equal temperatures and velocities the evaporation rate was greater for air than for superheated steam, but the difference decreased at higher temperatures. Their

results support the findings of Toei et al and confirm that the accepted correlation for heat transfer coefficients applicable for evaporation of small droplets of pure liquid in air is also valid for evaporation in a superheated vapour. In their analysis, they accounted for heat transferred by radiation and conduction through the thermocouple wires. In the estimate of the latter however, they used the cross-sectional area of the wires which underestimated the area of the bead at the junction by at least a factor of 4.

The evaporation of droplets of n-hexane in a stagnant environment at high temperature and pressure was investigated experimentally and analytically by Maltosz (136). The goal of the experimental study was to record the temperature and size of liquid droplets evaporating in a nitrogen or argon environment. Droplets of 720-910μm or 1420-1780μm were used at 286 °C with gas pressure in the range 6.8-102 atmospheres. They found that comparison of theoretical predictions for the droplet-time and radius-time histories with the experimental measurements indicated that, at the higher pressure, molecular mass transport may not be the controlling step for the evaporation process. At low (6.8 atm) pressure the effective mass diffusion coefficient was in good agreement with the predicted molecular mass diffusion coefficient. However at 102 atmospheres the effective molecular diffusion coefficient was > 6 times greater than the calculated molecular mass diffusion coefficient.

Audu (10) suspended droplets from a rotating nozzle placed in a horizontal wind tunnel to determine the rates of evaporation. At elevated temperature i.e. > 46 °C, he proposed a temperature correction factor and correlated experimental results by,

$$Sh = 2.0 + 0.44 \left(\frac{T_a - T_s}{Tamb} \right)^{-0.008} Re^{0.5} Sc^{0.33} \qquad \text{---------3.52}$$

However, an exponent of 0.008 is too small to have any significant effect.

A mathematical model of a single droplet evaporating in a high temperature and

pressure gaseous environment was derived by Kadota and Hiroyasu (54). The model included the effects of unsteady and steady-state stages of droplet evaporation considering the effects of natural convection, non-ideal behaviour, and effects of high mass transfer rate on the temperature and concentration profiles and boundary layer thickness. Results from an earlier work (56) on the evaporation of n-heptane, ethanol, benzene and water droplets in high pressure and high temperature gaseous environments were found to be in a good agreement with the model.

Using a porous sphere saturated with pure liquid in a vertical hot air tunnel, Yuen and Chen (55) measured the rates of heat transfer of ethanol and water. The experiments were restricted to a Reynolds number range of 200-2000, air temperature of 150-960 ^{o}C and a velocity of 2.1 to 11.4 m/s. Their experimental data were correlated by,

$$Nu_f (1 + B) = 2.0 + 0.6\, Re_m^{0.5}\, Pr_f^{0.33} \qquad \text{----------3.53}$$

Where

$$Re_m = \rho_g\, V_g\, d / \mu_f \qquad \text{----------3.54}$$

The experimental results therefore showed that at higher air temperatures, evaporation reduces heat transfer rates directly by a factor of (1+B). However, the study was limited to droplets with a maximum B=0.5.

Recently Renkizbulut and Yuen (57) used the same experimental technique as Yuen and Chen (55) to measure heat transfer to single water, methanol and heptane droplets. The study covered a wider Reynolds number range of 25 to 2000, and a Transfer Number range of 0.07 to 2.79. Their results were correlated by the expression,

$$Nu_f (1 + B_f)0.7 = 2.0 + 0.57\, Re_m^{0.5}\, Pr_f^{0.33} \qquad \text{----------3.55}$$

The validity of these techniques may however, be open to question because of local vapour pressure depression at micro-undulations and surface tension effects.

In summary, different techniques of droplet suspension have been used, covering an extensive range of droplet size, temperature and velocity. The droplets were investigated whilst suspended in various ways, namely,

(a) A stationary-droplet suspended on a glass filament or thermocouple. In this technique evaporation is not uniform from the surface. A higher evaporation rate occurs from the droplet side facing the direction of air flow than in the wake.

(b) A droplet suspended by means of an electric field. Such method are limited to droplets of diameter less than 10μm.

(c) A droplet suspended freely in a rising air stream. This technique has been used mainly for evaporation from a pure liquid or for gas absorption by a liquid droplet. Droplet drying studies using this technique are limited.

Therefore a rotated-suspended droplet technique which enabled direct measurement of droplet weight and temperature was developed in the present study (Chapter 6) for both evaporation and drying studies.

CHAPTER FOUR

DRYING OF DROPLETS CONTAINING DISSOLVED OR SUSPENDED SOLIDS

DRYING OF DROPLETS CONTAINING DISSOLVED OR SUSPENDED SOLIDS

The evaporation of pure liquid droplets has been studied extensively by numerous investigators. However, less work has been carried out on droplets containing soluble or suspended solids, the situation in a practical spray dryer. This is attributed to the complexities in analysing the heat and mass transfer processes after the formation of a crust or skin on the droplet surface.

With the presence of nonvolatile solution in a droplet the complexity of the process of evaporation is significantly increased. Whereas in the consideration of heat and mass transfer involving a droplet of pure liquid conditions within the droplet may be assumed uniform, they cannot be if a non-volatile material is present.

When a droplet contains dissolved, or in certain circumstances to a lesser degree suspended, solids the vapour pressure at the droplet surface is lowered; the vapour pressure driving force for mass transfer is thus reduced resulting in a reduction in the rate. The surface temperature of the evaporating droplet will consequently increase above the thermodynamic wet-bulb temperature. The drying characteristics feature the formation of solid material as a crust at the droplet surface, and thus differs from evaporation involving pure liquid droplets, since there is an additional resistance to mass transfer into the surrounding air. Furthermore with some solutions or suspensions a film or membrane may be formed which reduces the evaporation rate greatly resulting in further complication of the process.

Working with different detergent formulation droplets (a type of film or skin forming material), it has been observed (115) that these droplets undergo different types of deformation of the droplet structure. These deformations, which occurred after skin formation on the droplet surface (depending on the drying condition and nature of material), included uneven shrinkage, inflation and deflation and expansion with protrusions. Therefore the drying process can be highly complex and very difficult to model mathematically.

The drying rate of droplets containing solids is generally divided into (i) constant rate period, (ii) first falling rate period and (iii) second falling rate period. In the first period, the drying is characterised by evaporation from a free liquid surface, and proceeds by diffusion of vapour from the saturated surface through a stagnant gas-film around the droplet into the environment. The droplet surface is maintained saturated by adequate migration of moisture from within the droplet to the surface until the moisture content reaches a critical value, termed the 'Critical Moisture Content'. Any more evaporation after this stage results in formation of a solid crust gradually encasing the whole exposed surface of the droplet. If the droplet is stationary, the solid crust commences from a preferential site, usually the point of maximum mass transfer, and spreads around the droplet. The drying characteristics are then determined by the nature of the solid structure i.e. a crust with low porosity, high porosity or a very smooth film or membrane (i.e. skin). As drying proceeds, the crust thickens and its resistance to mass transfer becomes rate controlling and the evaporation rate falls. This period is termed the 'Falling Rate Period', which is usually divided into two zones; the zone of unsaturated surface drying and the zone where moisture movement controls. In the first zone, the whole evaporating surface can no longer be maintained saturated by moisture movement from inside the droplet. The drying rate reduces from the unsaturated portion and hence the rate for the total surface decreases.

As drying progresses, the point is reached where all the exterior surface is unsaturated. The plane of evaporation recedes into the solid, and the drying process enters the second falling-rate period. The drying rate is now governed by the rate of internal moisture movement and the effect of external variables diminishes. This period is usually predominant in determining the overall drying time.

4.1 MECHANISMS OF INTERNAL MOISTURE TRANSFER

Drying mechanisms control the movement of moisture within the droplet, out via paths through the solid, and hence into the surrounding gas stream. The moisture movement through a solid may occur by different mechanisms within the

material, depending on the nature of the material, the type of moisture binding, the moisture concentration, temperature and pressure in the pores, etc. This mechanism is of great interest in practical drying, since it determines the particular variables which are likely to govern the drying rate and the quality of the dried product.

There are three general theories for interpretation of moisture distribution and rate of moisture migration in porous media; diffusion theory, capillary flow theory and evaporation-condensation theory. Moisture may also be moved in a solid during the drying process by the action of gravity, by external pressure and by convection.

4.1.1 Diffusion Theory

The migration of moisture by diffusion has been proposed as the major mechanism of moisture movement by Lewis (116), and Newman (117). Sherwood's (59) theory regarded the drying process as taking place either by transfer of moisture as a liquid from the interior through the pores to the solid surface followed by evaporation of the liquid at the surface, or by vaporisation of the liquid at a point beneath the surface, followed by diffusion of water vapour through the pore to the surface and thence out into the surrounding gas. The limitation of this theory lies in the difficulty in solving the diffusion equation for cases where shrinkage occurs, or where the diffusivities are variable.

4.1.2 Capillary Flow Theory

The basic fundamentals of capillary flow theory were first introduced by Buckingham (36), who laid down the concept of capillary potential instead of a concentration potential.

The external surface of a porous solid has pore entrances of various sizes. As surface liquid is evaporated during the constant rate period, a liquid meniscus is formed across each entrance and capillary forces are set up by interfacial tension between the liquid and solid. These forces draw liquid from the interior to the external surface. At the critical moisture content, some of the menisci begin to retreat into the

pores. Wetted external surface gradually decreases and, although the drying rate per unit area of wetted external surface remains constant, drying rate based on total external surface decreases. This stage of unsaturated surface drying of porous materials is the first falling drying rate period. During this stage, gas begins to enter the pores, but the internal liquid phase is continuous; the liquid is said to be in the funicular state. If pores are small and not of uniform size, the retreat of the liquid phase is not uniform. Small pores produce stronger capillary forces than large pores; thus small pores draw liquid out of large pores. As more liquid is removed, the external surface dries completely and a point is reached where there is not enough internal liquid left to maintain a continuous phase linking all interior pores. Residual liquid retreats to isolated pockets in the smallest pores, and gas enters far enough into the material so that gas forms the continuous phase. The liquid then attaing the so-called pendular state. This point is the second critical moisture content in porous materials because there is a second break in drying rate profile. All heat for vaporisation must now pass by conduction through the material to the liquid pockets; the temperature rises, and the residual liquid vaporises and diffuses in the gas phase to the surface.

4.1.3 Evaporation-Condensation Theory

It is assumed in this theory that moisture migration takes place entirely in the gaseous phase via the pores. It was shown by some researchers (50, 51) that when the system is subjected to a temperature gradient this assumption is correct even at relatively high pore saturation. When a temperature gradient exists in a solid, there may be vapour pressure gradients set up which lead to evaporation of the liquid and its subsequent condensation on a colder surface.

4.2 LITERATURE REVIEW

Studies in the last 30 years, on the drying and evaporation of droplets containing dissolved and suspended solids, have provided fundamental knowledge into the mechanisms of phenomena controlling the heat and mass transfer processes

occurring during drying. These are of importance for the design of spray driers and the quality of spray dried products. In the last 15 years, and particularly for the drying of skin-forming materials as spray dried food products (e.g., starch, sucrose, coffee, skim milk, gelatin, etc) there has been a growing interest in particle morphology and the factors affecting it. The drying of skin forming materials includes different morphological changes, e.g., uneven shrinkage and expansion, and rupture can occur at high temperatures. The final morphology of the dried particle can determine some quality attributes. Bulk density and redispersibility are directly associated with expansion and porosity. Other factors, such as moisture content, volatile flavour and aroma retention, are affected by developing morphology.

Although investigations of the evaporation of pure liquids have been extensive, much less work has been carried out on droplets containing solids. Few of these studies concentrated on the drying of skin forming materials. The work of Ranz and Marshall (2) was the earliest, studying droplets drying whilst suspended from a filament or a thermocouple. This technique was then modified by Chralesworth and Marshall (3), and has subsequently been used by numerous researchers (4, 5, 113). However, the droplets suspended using this technique are stationary i.e., droplet rotation is not allowed. This limits the usefulness of the technique. This was overcome by suspending droplets from a rotating nozzle (10), which ensures droplet rotation during the drying process. Other droplet suspension techniques include retention of a droplet in free flight (7, 9), and more recently droplet suspension in an ultrasonic wave field (108).

4.2.1 Single Droplets Containing Dissolved or Suspended Solids Studies

In addition to their investigation of pure liquids, Ranz and Marshall (2) studied the evaporation of solutions of sodium chloride and ammonium nitrate, a non-soluble suspended green dye and reconstituted dried whole milk. Stationary droplets were suspended from a glass filament or thermocouple. For the evaporation from droplets containing dissolved solids, they assumed that during the constant rate

period (i.e. before crust formation) evaporation proceeded at all times as if the droplet surface was saturated regardless of the average concentration within the droplet. Although experiments with ammonium nitrate solutions confirm this hypothesis, this assumption was later tested using calcium chloride solutions of four different initial solids content, and challenged by Charlesworth and Marshall (3).

Duffie and Marshall (65) developed a vertical cylindrical cocurrent spray dryer, 20.32 cm in diameter and 6.1 m high, to study the drying of different crust and skin forming materials including gelatin, whole milk, coffee extract, corn syrup, inorganic salts, a water dispersible organic dyestuff and a dispersing agent. Their study concentrated firstly on the effects of feed temperature, feed concentration and air temperature on the bulk densities of the products. Secondly they classified the materials according to the nature of their spray-dried products. From their observations of dried particle characteristics, it is possible to postulate the factors contributing to the formation of hollow particles;

i) Hollow particles may arise by the rapid formation of a vapour-impervious film on the droplet surface, resulting in puffing or ballooning of the particle when the vaporising moisture within cannot readily escape.

ii) Due to the evaporation rate exceeding the rate of diffusion of solids back into the droplet, internal voids may be formed.

iii) A hollow particle may be created due to capillary suction which draws liquid and solids to the surface creating subatmospheric pressures and internal voids. The particle may eventually collapse.

iv) The presence of entrained gases in the feed may result in hollow particles.

They classified materials according to their particle structures i.e., film forming materials, crystalline materials and intermediate materials. However, they observed that the mechanism of hollow particle formation may be different within each classification.

Charlesworth and Marshall (3) made an extensive study of evaporation from single stationary droplets of sixteen different aqueous systems. The droplets to be dried

were suspended from a vertical glass filament of 340 μm diameter which was itself attached to another horizontal glass filament. The weight of the droplet was measured by measuring the deflection of the horizontal glass filament. Their experimental technique had the disadvantage of the suspended droplets being stationary. They stated that the first sign of a solid phase was indicated by the formation of crystals at the bottom of the droplet (where the evaporation rate is greatest). As drying progressed more crystals appeared to form a surface crust which grew steadily up the side of the droplet (where the evaporation rate is lowest). This mode of crust formation would not however be expected for a rotating droplet or in a practical spray dryer, in which droplets are subjected to swirling air, which causes rotation since some areas of the crust may redissolve and then reform.

They proposed a correlation for predicting the time of complete formation of a solid crust around a droplet. From their observations, they also presented a generalised description of the appearance and behaviour of a drying droplet as shown in Figure 4.1. The characteristics up to the point of crust formation were similar for all droplets regardless of the solute concentration and conditions. After crust formation however, the behaviour of the droplet was entirely controlled by the nature of the crust (i.e. porous, non porous, skin) and whether the surrounding air temperature was above or below the boiling point of the droplet.

Trommelen and Crosby (4) investigated the drying characteristics of four food products and various inorganic salts using superheated steam as the drying medium compared to air. They carried out simultaneous measurements of the droplet weight and temperature. This was achieved by using the same technique as Charlesworth and Marshall to measure the droplet weight. Thermocouple wires of 0.051mm diameter were attached to the filament to measure the droplet temperature. Although the heat conduction along the thermocouple leads was accounted for, no account was taken of heat conduction along the glass filament. They found that, with the exception of skim milk and sodium sulphate droplets, all materials dried faster in air than in steam.

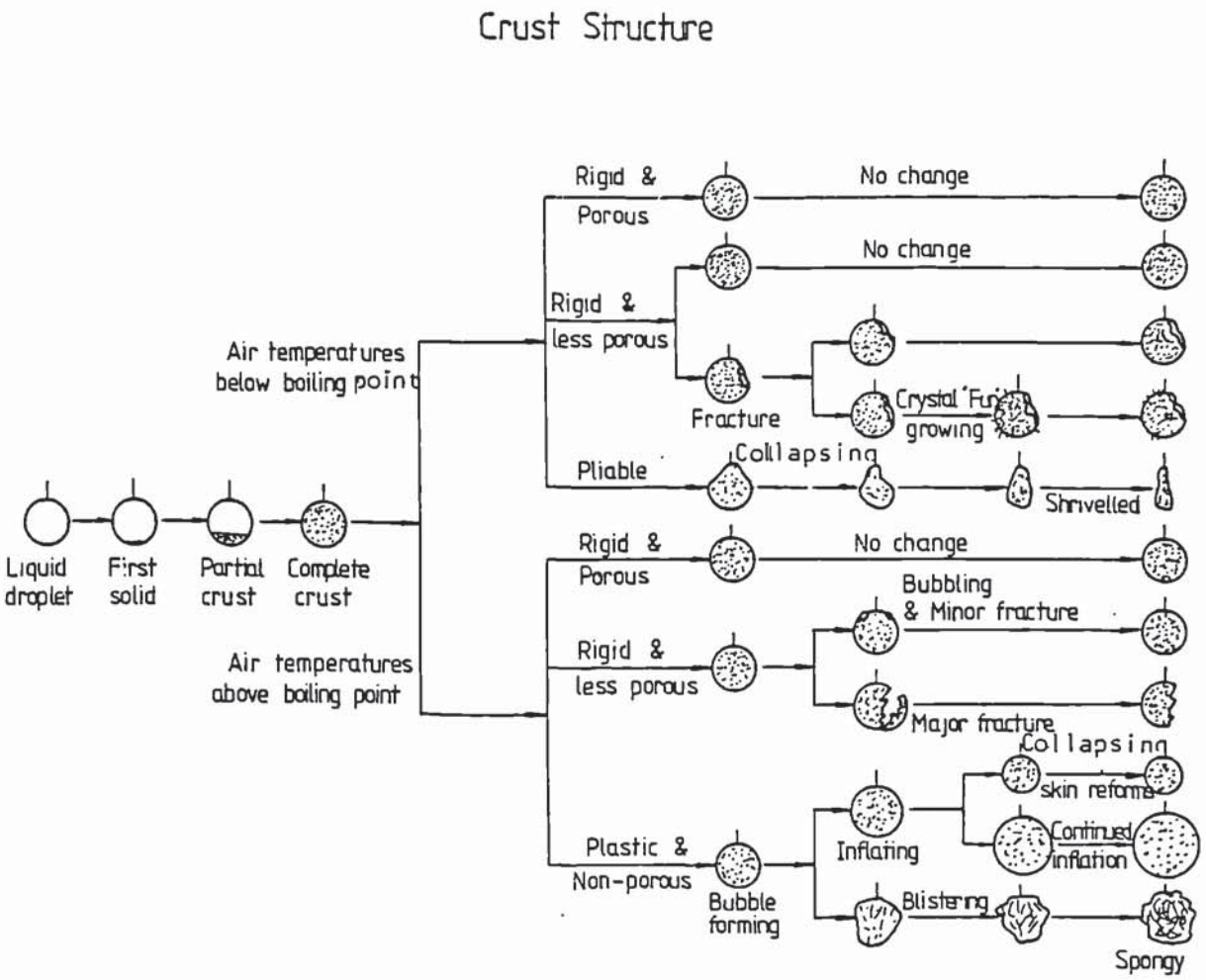

Figure 4.1 Drying Characteristics of Single Droplets (3)

Miura et al (114) used the same technique as Charlesworth and Marshall to study the drying characteristics of stationary single droplets. The materials used in the study were classified as;

(a) Crust forming, i.e. sodium sulphate, sodium chloride and ammonium chloride.

(b) Skin forming, i.e. skim milk and gelatin.

(c) Neither skin forming or crust forming, i.e. Bentonite.

They found that at an air temperature of 150 ^{o}C, a droplet of sodium sulphate dried at an initial constant rate followed by a sudden fall after completion of crust formation. After crust formation, the core temperature rose, until the crust burst open due to boiling and drying proceeded at another constant rate. When this boiling phenomena come to an end, the water in the droplet was almost totally evaporated and the drying rate accordingly decreased until the end of drying. At the lower temperature of 99 ^{o}C the drying rate was similar but, although fractures were evident, no bursting was observed. Skim milk droplets clearly showed a transition from constant rate to a falling rate when the initial moisture content was too high. However this distinction between the drying rates was not very clear at low initial moisture contents. When drying at high temperatures (> 100 ^{o}C), they observed droplet inflation after skin formation. This was not observed at low air temperatures (< 100 ^{o}C). Drying rates for Bentonite were similar to those of pure water droplets at all temperatures and initial moisture contents.

Miura et al also found that the equation for time of appearance of the crust proposed by Charlesworth and Marshall was in reasonable agreement with experimental data; the latter were generally greater than the predicted values. They proposed a mathematical model to calculate skin thicknesses based on a mass balance on the solids within a droplet.

$$Y - 1 = \frac{1 - X^3}{3AX^3 - 3A^2X + A^3} \qquad \text{---------4.1}$$

where

X	=	r_d / r_{do}	=	dimensionless diameter
Y	=	C / Co	=	dimensionless concentration
A	=	a / r_{do}	=	dimensionless thickness
a	=	thickness of skin		mm
r_d	=	radius of the droplet		mm
r_{do}	=	initial droplet radius		mm
C	=	concentration of solute		g solute/ml
C_o	=	initial concentration of solute		g solute/ml

The model was derived on the basis of an identical density for the crust and core which is a gross over-simplification. No measurements were obtained of the experimental skin thickness .

The drying of single droplets of sodium sulphate and detergent slurries, suspended from a rotating nozzle in a horizontal wind tunnel, were investigated by Audu and Jeffreys (61). They proposed a crust thickness model based on a material balance of moisture in the surrounding air. However the calculated values were as much as 20% higher than experimental results. They also proposed a crust mass transfer coefficient k_c, expressed as,

$$k_c = \frac{Dv\,\varepsilon^{1.5}}{\psi} \qquad \text{----------4.2}$$

where

Dv	=	molecular diffusivity	m^2 / s
ε	=	crust porosity	
ψ	=	crust thickness	m

With the systems studied, the crust was found to provide 64.2% of the total resistance for sodium sulphate droplets and 97.5% for detergent droplets. Their experimental technique, though allowing for droplet rotation during drying, included the following disadvantages:

(1) The nozzle material of construction was stainless steel, which is of high thermal conductivity and hence conducted additional heat into the droplet.

(2) The drying rates were determined by using a hygrometer to measure changes in air humidity before and after the droplet and were therefore dependent on homogeneity of air moisture content and instrument accuracy.

In their study some heat transfer would have occurred by conduction from the nozzle on which the droplet was suspended and, in a surrounding temperature higher than ambient, a droplet would have received a significant amount of heat by radiation. These two heat transfer sources to the droplet were not accounted for. No droplet temperatures were measured in this study.

Wijlhuizen et al (68) proposed a "solid sphere" and "hollow sphere" model for an evaporating droplet of skim milk. The model was essentially based on the work of Van der Lijn (67) who introduced a concentration and temperature dependent diffusion coefficient. The "hollow sphere" model assumed an initial gas bubble of known size in a droplet and a uniform concentration profile. The resulting diffusion equations were solved with the necessary boundary conditions to predict moisture concentrations and temperatures during drying. However, by not allowing for the formation of a crust, the model has limited applications particularly in the falling-rate period which is of primary concern in a spray drier.

A mathematical model for predicting drying rates of porous hygroscopic materials such as clay brick and burned clay, was developed by Haertling (64). The model is based on the assumption that mass transfer in the clay occurs simultaneously due to vapour diffusion and liquid movement by capillary suction. The model however, overestimates the drying rates for burned clay and clay brick with low porosities by about 21% particularly at high air temperatures e.g. at 207 ^{o}C and 247 ^{o}C. This suggests that liquid moisture migration by capillary suction is less significant in low porosity materials.

Esubiyi (66) proposed a momentum-heat transfer mathematical model. The model estimates crust mass transfer coefficient, k_c, based on an assumed velocity of vapour discharge through the pores of a solid crust described by the Kozeny equation (77). The equation for the crust coefficient was expressed as,

$$k_c = \frac{\varepsilon^3 \rho}{5(1-\varepsilon)^2 \mu S_b^2 \psi} \qquad \text{--------4.3}$$

He confirmed the validity of this model in drying five different sources of Portland cement.

Sano and Keey (5) proposed a more realistic mathematical model to describe the drying of single stationary droplets containing colloidal materials to produce solid hollow spheres. To describe the mechanisms for the formation of hollow spheres they used the assumption that, once the equilibrium vapour of the moisture inside the particle exceeds the pressure of the ambient air, the particle inflates instantaneously and ruptures. After inflation and rupture, two limiting ways of deformation of a hollow particle were assumed:

1) The maximum radius does not change, but the void radius increases due to the moisture loss; or
2) The void radius remains constant, while the outer radius shrinks.

They dried stationary droplets of skim milk at temperatures between 100 ^{o}C and 150 ^{o}C by using techniques similar to Charlesworth and Marshall (3). They found that the second assumption, i.e. a shrinking outer radius, gave a more realistic approximation to their results. Theoretical computations however, required an experimentally determined inflation ratio, which was the ratio of the maximum radius after inflation to the initial radius. Their results were computed with an inflation ratio of 0.88, but they found that a ratio of 1.1 was required to fit the data of Trommelen and Crosby (4), for droplets of skim milk at the same drying temperatures.

Using the basis of the above model, Sano and Yamemoto (100), predicted the drying rates of droplets of polyacrylonitrile in dimethyl formamide by assuming a receding interface and a constant concentration distribution. They derived empirically, a modified diffusion coefficient, which had to be used to fit the data.

Cheong (8) developed a receding interface model to describe the drying characteristics of single stationary droplets in the falling rate period. He improved the technique developed by Trommelen and Crosby (4) to measure simultaneously the droplet weight and temperature, by designing a glass filament-thermocouple as a single unit. This overcame the drawback of Trommelen and Crosby's (4) technique. The filament-thermocouple consisted of a fine nickel wire of 50μm diameter inserted through a hollow glass filament of 0.18 to 0.2mm diameter. A thin film of copper was deposited onto the outside of the filament, and a junction was made at the tip where about 0.5mm of nickel wire was exposed. The thermocouple measured the core temperature of the droplet and the deflection of the beam gave the loss in weight during drying. Three equations were derived which on simultaneous solution give the crust thickness, core temperature and weight of the droplet as a function of time. For the crust thickness predictions the model gave reasonably good results. The model however, takes no account of the constant rate period, and the effects of fractures, 'blow' holes etc. Consequently, since the model does not take into account the loss of small fragments when the crust fractures, it overestimates the droplet weight after complete crust formation. A very interesting observation was made of the droplet temperature at 33 ^{o}C. There was a sudden fall in the core temperature due to the enantiomorphic changes taking place with the decahydrate at 33 ^{o}C. When this was taken into account the model gave reasonably good agreement with the experimental results. It is interesting to note that Ali (7) also measured the core temperature history of sodium sulphate decahydrate droplets at similar air temperatures. This was achieved in his study by inserting a thermocouple into the droplet every increment of time to measure the temperature, but failed to detect the drop in the core temperature at 33 ^{o}C.

Ali et al (63) studied the drying rates of a number of materials including

sodium sulphate decahydrate and various organic dyes. They used the same experimental apparatus used by Audu (10) with slightly modified nozzles. Figures 4.2 and 4.3 show the drying rate curves for sodium sulphate decahydrate and organic pigment respectively at high air temperatures (63,7). They found that the thickness growth rate increased with an increase in air velocity, air temperature and the initial moisture content. A Scanning Electron Microscope (SEM) was used to examine the crusts . Crusts were found to be crystalline porous, rough non-crystalline, or very smooth and less or non porous. Therefore the drying after crust formation was, and in all practical drying will always be, specific to the nature of the material undergoing drying.

Recently Nescic (70) investigated the drying of droplets containing solids, by using techniques similar to Charlesworth and Marshall (3). He proposed a model, based on a number of simplifying assumptions, to describe the complete drying process including the heating-up period, equilibrium evaporation, growth of crystal formation and boiling. Good agreement was achieved between the experimental results and those predicted from the model for different materials including colloidal silica, skim milk and sodium sulphate.

More recently Bains (62) used the filament-thermocouple techniques developed by Cheong (8) to study the drying characteristics of droplets of five different inorganic salts, namely sodium sulphate decahydrate, sodium chloride, potassium sulphate, copper sulphate and sodium acetate. He developed a modified receding evaporation interface model for the drying of solutions and slurries, which was originally proposed by Cheong (8). The modified model covered both the constant rate period prior to crust formation and the subsequent falling rate period. The model was solved numerically for the variation in core temperature, droplet weight and crust thickness. Good agreement was obtained between model predictions and experimental results for materials forming rigid crusts i.e. sodium sulphate decahydrate, sodium chloride, potassium sulphate and copper sulphate. However the drying histories of droplets of 10-20% weight initial solids content sodium acetate were unpredictable since formation of a non-rigid skin deviated from the model

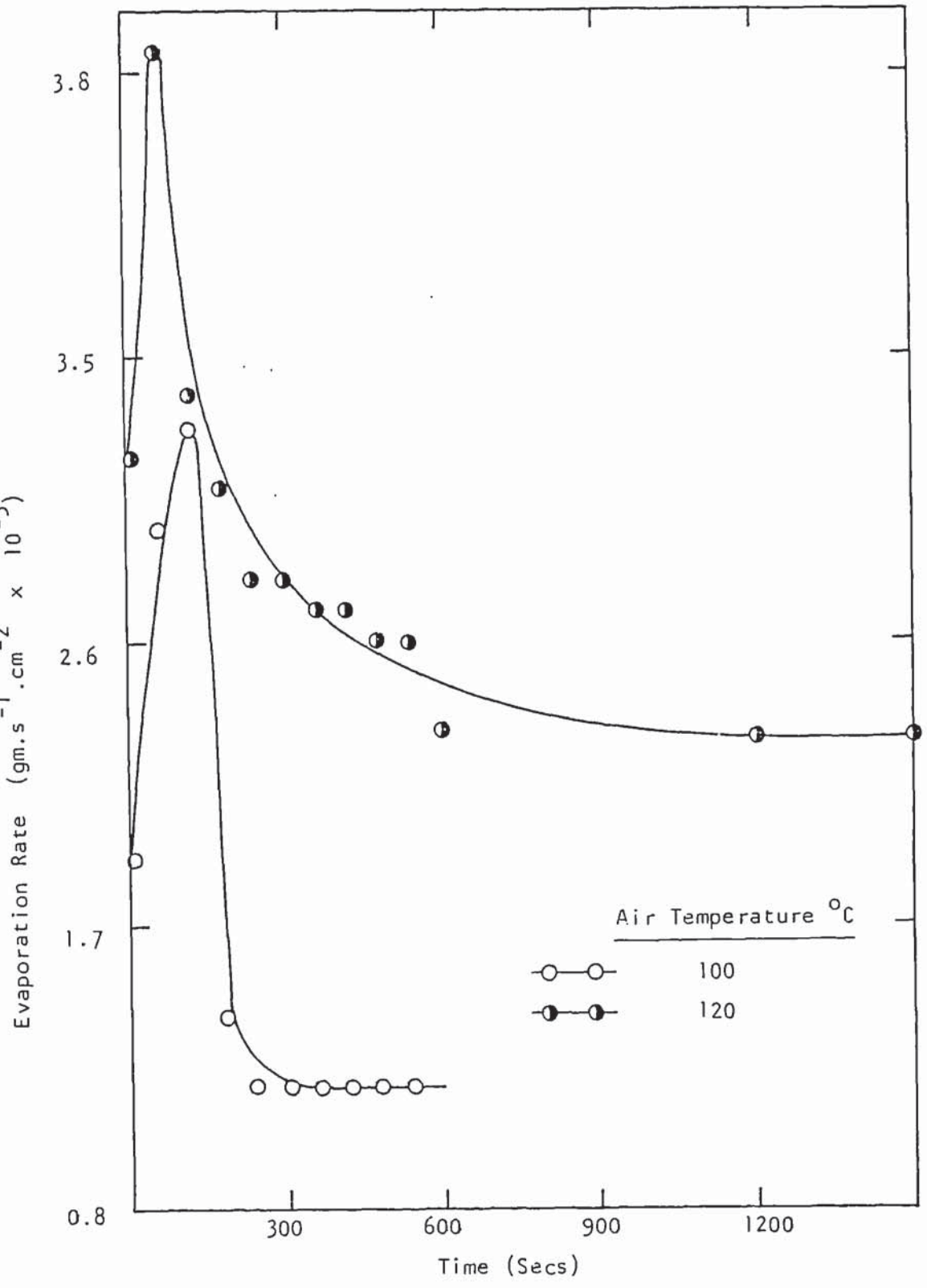

Figure 4.2 Drying Rate for Droplets of Sodium Sulphate Decahydrate (7) at Air Temperatures 100 and 120 °C

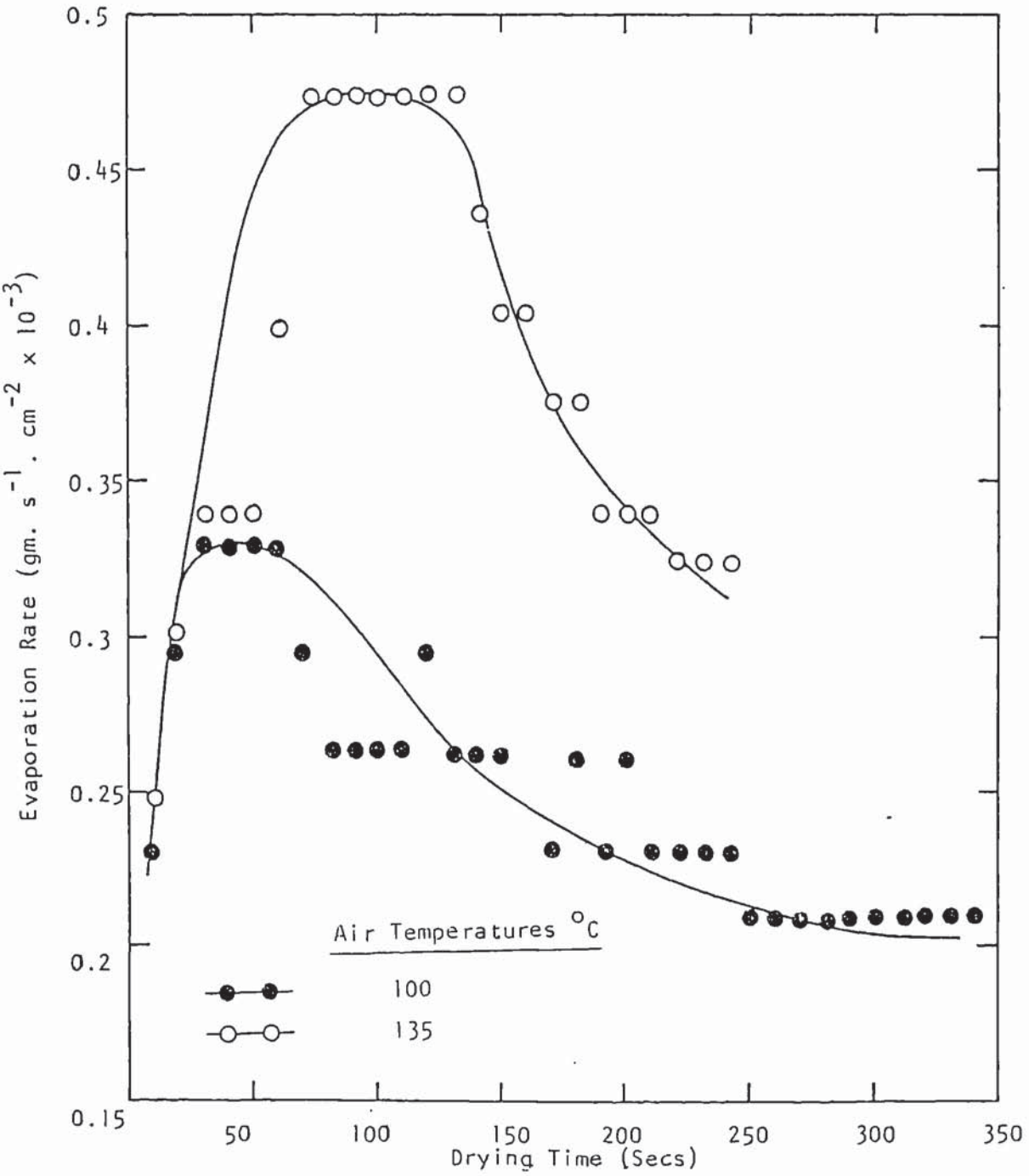

Figure 4.3 Drying Rate Histories for Droplets of Organic Pigment B at Air Temperatures 100 and 135 °C (7)

assumption of a rigid outer surface. At higher initial concentrations (40% weight), where a rigid crust was formed for sodium acetate, reasonably good agreement was obtained between experimental results and those predicted from the model.

4.3 EVAPORATION FROM SPRAYS OF DISSOLVED OR SUSPENDED SOLIDS

The evaporation characteristics of droplets within a spray differ from those of single droplets in that they represent a far more complex problem. In a practical spray dryer, under actual conditions an atomiser produces a distribution of droplet sizes, and consequently the droplets will evaporate at varying rates depending upon their initial diameters. The smallest droplets will lose their moisture first and may therefore be subject to overheating and possibly thermal degradation by prolonged exposure to high temperatures. In contrast excessively large droplets will require an inordinately longer time than the average and will, therefore, constitute the controlling time in the drying process.

Although the same fundamental concepts apply to both spray and single droplets, any full analysis of spray evaporation depends upon defining the spray in terms of a representative size distribution, and consideration of the relative velocity between any droplet and its surrounding medium, particle trajectory and droplet population density (i.e. number of droplets present at any given time per given volume of drying medium).

4.3.1 Sprays of Pure Liquids

Probert (75) presented a mathematical analysis of the variation of the size distribution in a fuel spray which was assumed to follow the Rosin-Rammler distribution function (118). Spray droplets were assumed to have no relative velocity and temperature driving force changes were considered negligible during evaporation. The prediction was that, comparing distributions with the same mean diameter, a spray with a narrow size distribution will evaporate completely in less time than one with a

wider distribution. This work was extended by Fledderman and Hanson (119) for conditions of relative velocity but assuming a Nukiyama-Tanasawa type distribution (71). However no useful results were developed.

Marshall (28) proposed a comprehensive stepwise method for the evaluation of spray distribution. This involves dividing the size distribution into small size groups, which enables the change in the average droplet diameter in each selected group to be estimated over short time intervals. Although the method was only set out for pure liquid droplets under conditions of zero relative velocity, the results were useful in illustrating the nature of changes likely to take place in a dryer. He predicted that 90% of the evaporation in the majority of spray drying operations is completed during the first 1.5 seconds, with air temperature falling to within 17 ^{o}C of the outlet air temperature during this period.

Manning and Gauvin (103) conducted a study on heat and mass transfer of water sprays in both cocurrent and countercurrent air flows. The progressive evaporation from the sprays was followed by measuring calorimetrically the increase in concentration of red dye and the droplet size distributions were determined on samples obtained by traversing the spray with an immersion cell containing Varsol. The equations presented by Frossling (12) and by Ranz and Marshall (2) for stationary droplets suspended in moving air streams were claimed to be generally applicable for correlating the Nusselt number but the scatter of the experimental data appears to be considerable. This may have arisen, in part, due to the uncertainly regarding values of relative velocities and droplet sizes in the vicinity of the atomising nozzle.

Bose and Pei (73) investigated the evaporation of water sprays in a 152.4mm I.D. cocurrent drier. They found that the relative velocity between spray and air caused a substantial increase in the heat and mass transfer rates . This is to be expected from the dependency of both Sherwood and Nusselt numbers on the Reynolds number. This is however contrary to the work by Dlouhy and Gauvin (102) using a spray dryer in which the effect of relative velocity between the droplets and the air was found to be negligible. However in contradiction to this, they showed that the Ranz and Marshall

correlations, which take account of relative velocities, represented their data well.

A computational study was presented by Dickinson and Marshall(74) to estimate the evaporation of sprays of pure liquid. They considered spray droplets under conditions of both negligible and appreciable relative velocities, and took account of non-uniform size distributions. However the basic assumptions of ideal conditions of constant droplet temperature and ideal flow, limit their usefulness.

The evaporation rates from a water droplet surrounded by glass beads were investigated by Miura et al (25). They measured the effects of droplet to droplet interaction and studied the effects of diameter and distances between the surface of the droplet and the glass bead. The experiment was set-up in three ways as shown in Figure 4.4. The water droplet and glass beads were set up in series, parallel and in a zig-zag pattern. They proposed the relationships,

Series

$b/d_g \leq 2$, Nu/Nu_o or $Sh/Sh_o = 0.71\ (b/d_g)^{0.25}\ (d_p/d_g)^{0.167} + 0.07$ ----------4.4

$b/d_g > 2$, Nu/Nu_o or $Sh/Sh_o = 0.42\ (b/d_g)^{0.125} + 0.41$ ----------4.5

Parallel

$B / d_g = 1$ i.e. no effect of the beads ----------4.6

Zig-zag

$d_p / B < 2$ Nu / Nu_o or $Sh / Sh_o = 1$ ----------4.7

$d_p / B > 4$ Nu / Nu_o or $Sh / Sh_o = 0.57$ ----------4.8

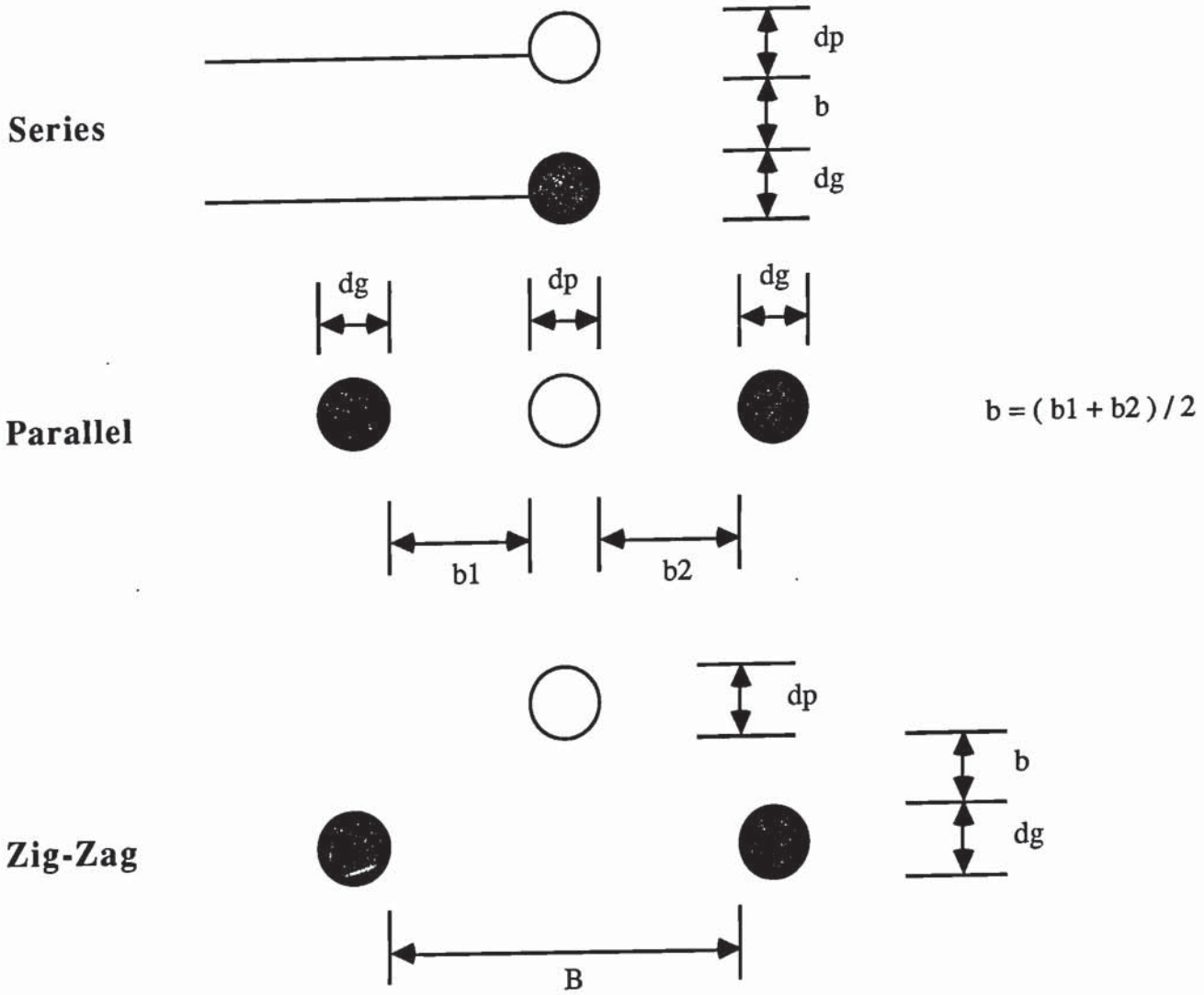

Figure 4.4 Droplet to Droplet Interaction Studies (25).

4.3.2 Sprays Containing Dissolved or Suspended Solids

If solids are present in a spray, the extent of vapour pressure lowering and resistances to mass transfer will vary throughout the size distribution. As evaporation proceeds, the concentration of solids in the smaller droplets will increase much faster than in the larger droplets, resulting in a wide variation in the concentration driving force. This phenomena also results in the solid phase not appearing simultaneously throughout the size distribution. Therefore, the analysis of spray evaporation is complex and studies in this field are limited.

Using experimental techniques similar to Manning and Gauvin (103), Dlouhy and Gauvin (102) specifically studied evaporation of sprays of calcium lignosulphonate solution in a cocurrent spray dryer of 203.2mm diameter. They found that the total spray evaporation time could be accurately predicted by employing a stepwise method of calculation proposed by Marshall (28). However, their method requires a knowledge of the droplet size distribution which must be determined experimentally.

Baltas and Gauvin (72) carried out a study to account for radial gradients of humidity, spray mass velocity and air velocity in the same dryer as Dlouhy and Gauvin (102). They developed a step-by-step prediction procedure and found that the predicted evaporation rates were 3.5 times greater than the observed rates. Results from computer calculations of local humidity and mass flow profiles showed good agreement with observed profiles. It should be noted that their model is only applicable to the free fall zone.

Equations based on assumed size distributions and ideal flow patterns in the drying chamber, were derived by Katta and Gauvin (69). The model which predicts droplet trajectories and evaporation rates was experimentally verified from a study of the drying of calcium lignosulphonate solutions in a 122 cm diameter, 183 cm high, circular cocurrent chamber with a conical bottom. They concluded that there is an optimum nozzle depth and optimum air temperature for maximum efficiency and capacity.

Spray drying of solutions of sodium chloride and skim milk were investigated experimentally by Miura et al (80) using either a two fluid pneumatic nozzle or a hollow cone nozzle for atomisation. Sprays were dried in a square cocurrent drying chamber 36 x 36 x 294 cm, and the droplet size distributions were measured at four points in the dryer. A Nukiyama-Tanasawa distribution was assumed in their analysis and the results were correlated more accurately by equations 4.4 and 4.5 for evaporation in a spray cloud, than by Ranz and Marshall's equations for single droplets(2).

4.4 TEMPERATURE OF EVAPORATING DROPLETS

To evaluate the evaporation rates and evaporation times for droplets, it is necessary to be able to specify, or estimate, the droplet surface-temperature so that the temperature driving force can be estimated for the case of a pure liquid droplet . When dynamic equilibrium is established between the rates of heat and mass transfer, and if all the heat transferred is consumed for evaporation, a simple heat balance can be expressed as,

$$Q_{in} = - N_A \lambda \qquad \text{----------4.9}$$

After substitution of the different quantities and rearrangement, the surface temperature of the droplet T_s, may be estimated from the equality,

$$\frac{T_g - T_s}{P_{wd} - P_{wa}} = \frac{k_g A_m \lambda}{h_g A_h} \qquad \text{---------4.10}$$

If A_h and A_m, which are the respective areas for heat and mass transfer , are considered to be equal then

$$\frac{T_g - T_s}{P_{wd} - P_{wa}} = \frac{k_g \lambda}{h_g} \qquad \text{----------4.11}$$

which is the familiar expression for the surface temperature or the wet-bulb temperature.

When an evaporating droplet contains solids in solution the vapour pressure of the solution is lowered and the droplet temperature will be higher than that of pure water under identical conditions. The vapour pressure lowering effect depends upon the nature of the solid in solution. When a droplet contains insoluble suspended solids, there are negligible vapour pressure lowering effects and the surface temperature of the droplet will initially approximate to that for a pure liquid droplet. However, once a crust is formed around the droplet, the additional resistance to moisture diffusion will result in the core temperature rising above the saturated wet-bulb temperature.

Williams and Schmitt (83) demonstrated that heat of crystallisation should be considered. The heat of crystallisation for ammonium nitrate solutions is, for example, 20% of the latent heat of vaporisation. Therefore equation 4.11 becomes,

$$\frac{T_g - T_s}{P_{wd} - P_{wa}} = \frac{k_g (\lambda - C_c)}{h_g} \qquad \text{----------4.12}$$

where C_C is the heat evolved by crystallisation per unit mass of water evaporated.

4.4.1 Measurements of Droplet Temperature

Different techniques were used by numerous investigators to study the droplet temperature histories (2, 3, 4, 7, 8, 62). The earliest work on single droplet investigations, notably that of Ranz and Marshall (2) and Charlesworth and Marshall (3), measured the droplet temperature by using a thermo-element of manganin-constantan wire of 0.5 mil to 2 mil embedded into the droplet. Because of the experimental difficulties they measured the heat and mass transfer histories of

evaporating droplets separately.

Simultaneous measurements of droplet temperature and weight were made for the first time by Trommelen and Crosby (4). They used a glass filament to suspend a stationary droplet and attached chromel-constantan thermocouple leads to this filament to measure the droplet temperature. However, this technique involved the disadvantage of heat conduction through the thermocouple leads which would invariably have raised the temperature at the thermojunction.

Cheong (8) improved the above method, by combining the glass filament and thermocouple wires to create a unique filament-thermocouple to measure simultaneously the heat and mass transfer for stationary suspended droplets.

The techniques of suspending a droplet in free flight (7,9) have the disadvantage that no measurement of droplet temperatures can be made, which significantly affects their usefulness.

4.4.2 Droplet Temperature Histories

Ranz and Marshall (2) and Charlesworth and Marshall (3), followed the droplet temperature histories using the same experimental technique of embedding a thermocouple into a stationary suspended droplet. Ranz and Marshall's results for the drying of a droplet of sodium chloride or ammonium nitrate showed a gradual increase in droplet temperature initially due to the effect of heat of solution followed by a rapid rise as crystallisation occurred. No correction was made for heat conduction along the thermocouple wires. Charlesworth and Marshall presented temperature histories for different materials i.e. sodium sulphate, potassium sulphate, calcium chloride, ammonium nitrate, sodium acetate and coffee extract. For droplets of sodium sulphate of 8.2% initial wt/wt, the temperature histories were similar to those observed by Ranz and Marshall. However, at a higher initial solids content of 16.4% wt/wt, crust fracture seriously affected the droplet temperature history. Again however, no allowance was made for conduction along the thermocouple leads.

Trommelen and Crosby (4) carried out measurements of droplet temperature

histories of various materials i.e. clay slurries, inorganic salts and food products. The results of their investigation showed that food products did not in general exhibit any constant temperature period, unlike clay slurry and inorganic salts. However, the rise in temperature was interrupted by one or more cycles of inflation, rupture or collapse which varied from one droplet to another.

Miura et al (114) suspended stationary droplets of skim milk, inorganic salts and Bentonite from a quartz filament of 0.3mm diameter and measured their temperature histories by inserting a 40μm maganin-constantan thermocouple into the centre of each droplet. Their results of temperature histories for skim milk droplets at high air temperatures of 100 °C -144 °C revealed no wet-bulb temperature period with the core temperature rising steadily to the air temperature. For sodium sulphate droplets they found that the droplet temperature rose initially and that there were periods of constant droplet temperature consistent with the constant rate period of mass transfer. For Bentonite, which is a suspended insoluble solid, the droplet temperature histories were similar to that of a pure liquid droplet.

In a study by Sano and Keey (5) on droplets containing colloidal material, equations were derived to predict the temperature of an evaporating droplet. Thedroplet temperature history was followed by suspending a stationary droplet on the junction of a manganin-copper thermocouple, with wire diameters of 30μm. The model was found to slightly underestimate the droplet temperature especially at high air temperature, i.e., > 150 °C. This was probably because no correction term was included to take account of heat conducted along the thermocouple wires.

Cheong (8) dried stationary droplets of sodium sulphate decahydrate by using the filament-thermocouple technique. He observed that at an air temperature of 20 °C the core temperature showed an initial transient period before equilibrium was established and the core temperature reduced to the wet-bulb temperature. There was then a steady rise in the core temperature as the resistances to heat and mass transfer increased with growing crust thickness. The trend of the core temperature curves at higher air temperatures of 40.7 and 59.3 °C was found to be rather unusual. After the

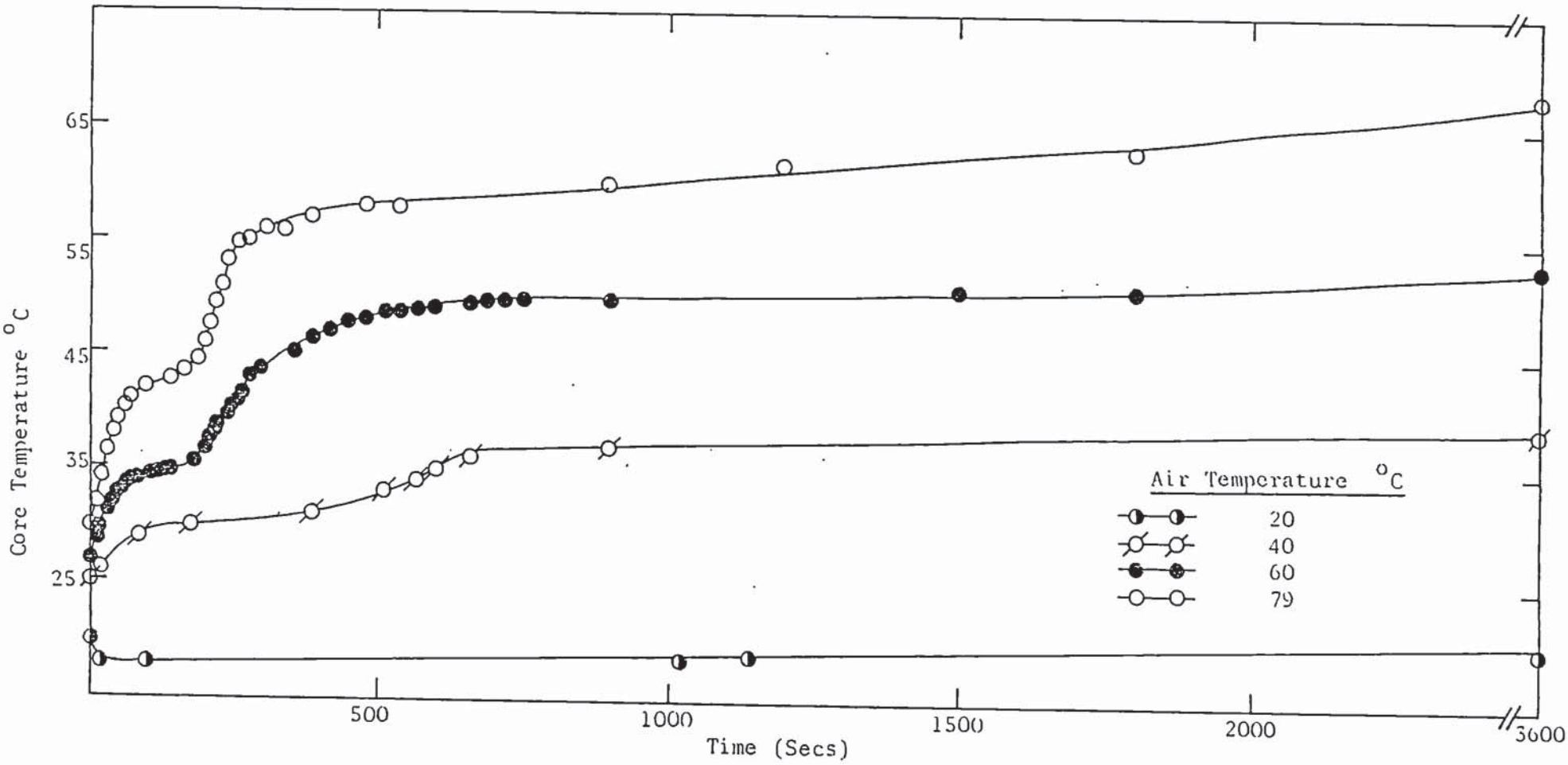

Figure 4.5 Droplet Temperature Histories for Aqueous Sodium Sulphate Decahydrate (7)

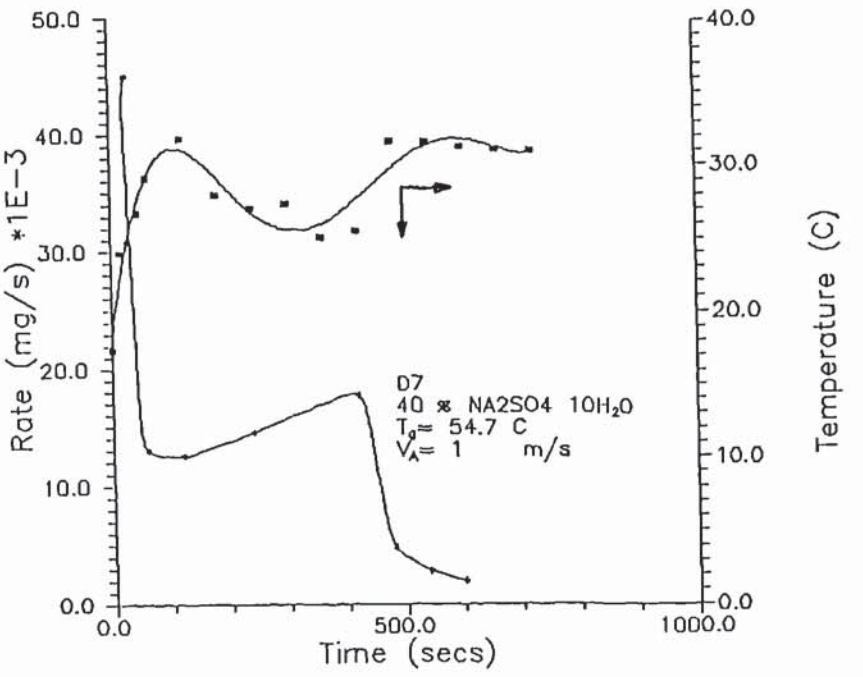

Figure 4.6 Droplet Drying Histories for Aqueous Sodium Sulphate Decahydrate at Air Temperature 54.7 ^{o}C (62)

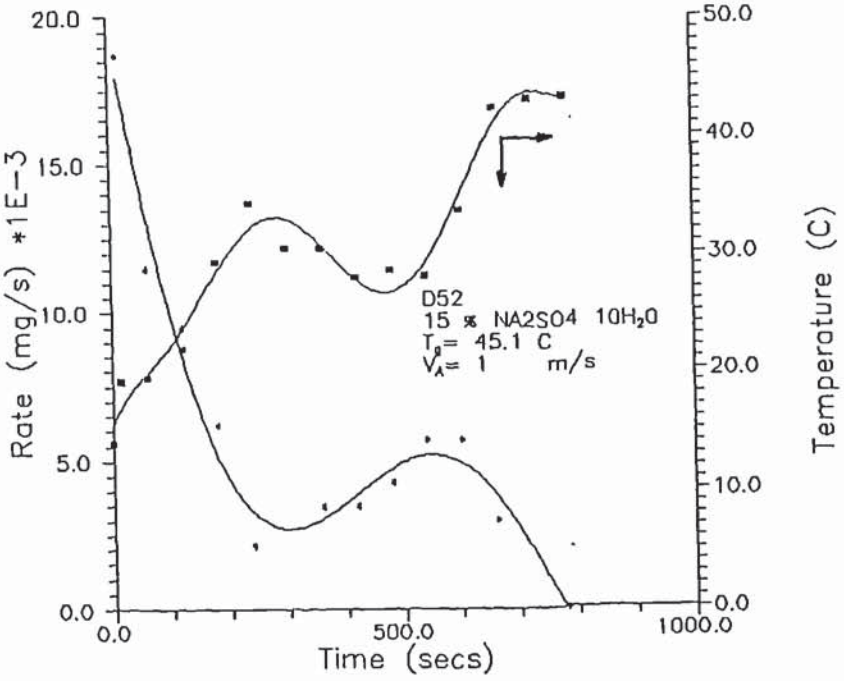

Figure 4.7 Droplet Drying Histories for Aqueous Sodium Sulphate Decahydrate at Air Temperature 45.1 ^{o}C (62)

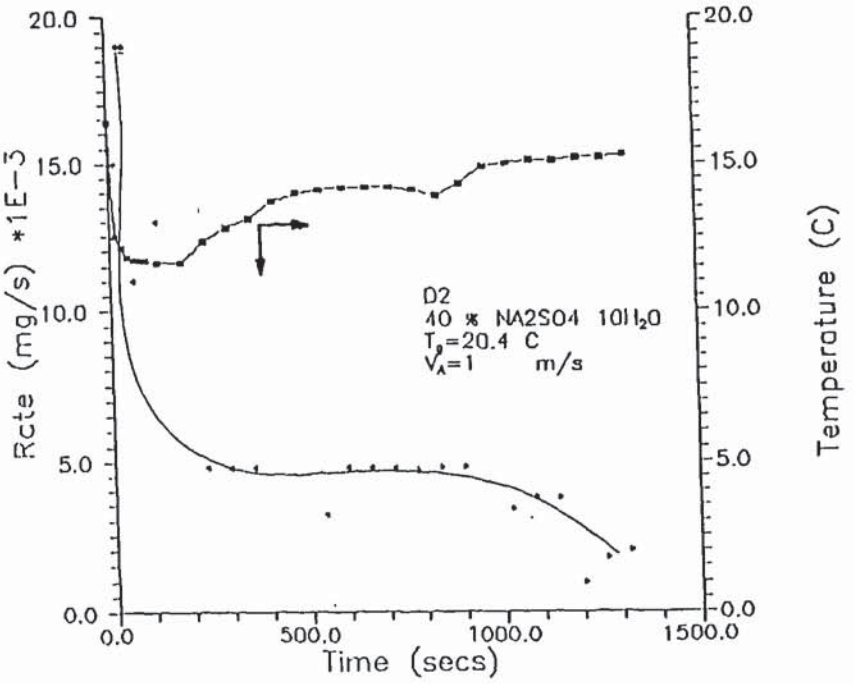

Figure 4.8 Droplet Drying Histories for Aqueous Sodium Sulphate Decahydrate at Air Temperature 20.4 ^{o}C (62)

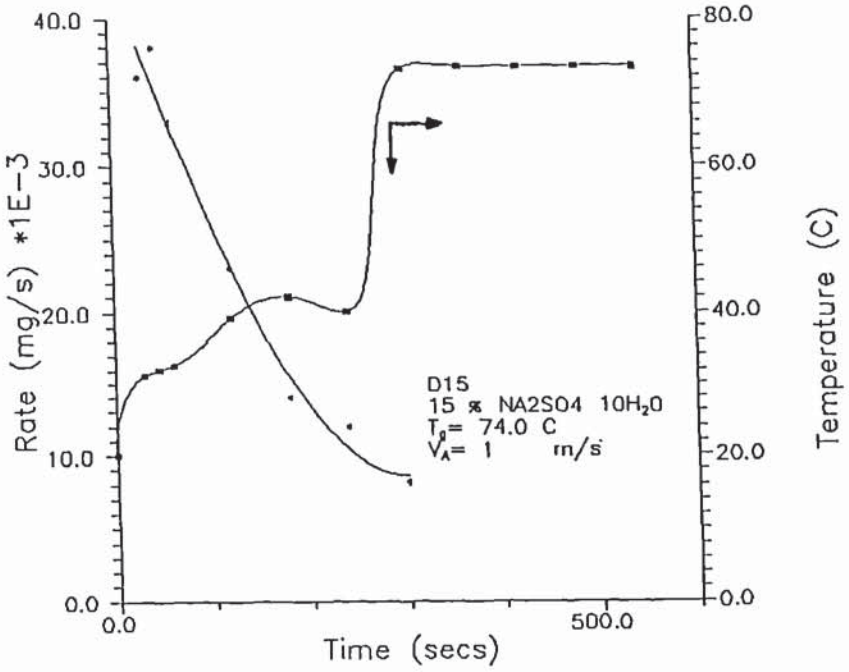

Figure 4.9 Droplet Drying Histories for Aqueous Sodium Sulphate Decahydrate at Air Temperature 74.0 ^{o}C (62)

initial transient period, the core temperature rose gradually until it reached 33 ^{o}C where there was a sudden fall, before again rising to the particular air temperature. This was explained by the knowledge that at 33 ^{o}C, sodium sulphate dechahydrate crystals melt absorbing heat in the process. Similar observations of the temperature history of sodium sulphate decahydrate droplet were made recently by Bains(62), using the above technique developed by Cheong (8) as shown in Figures 4.6-4.9. It is interesting to compare these experimental results with those obtained by Ali (7) on the same material and shown in Figure 4.5, which did not reveal this depression. By inserting an Ni-Cr/Ni-Al thermocouple into the centre of the droplet every increment of time to measure the droplet temperature, a constant temperature at ~ 33 ^{o}C for an air temperature of 60 ^{o}C was observed.

CHAPTER FIVE

MATHEMATICAL MODELS

MATHEMATICAL MODELS

5.0 INTRODUCTION

Two models which have been developed in the present work, to characterise drying of single droplets will now be discussed. In the first model for pure liquid droplets, expressions have been derived for the experimental Sherwood and Nusselt numbers. Heat transfer by conduction along the glass nozzle and by radiation have been accounted for. A second model has been developed for droplets containing solid as gelatinised material (e.g. custard/starch), to predict the time at which a skin appears at the surface of these droplets.

5.1 PURE LIQUID DROPLETS

The following discussion refers to pure water droplets but is equally applicable to other pure liquids. Figure 5.1 shows a hemispherical droplet suspended on a nozzle, in a constant flow of air which has an initial temperature T_a. Following moisture transfer the outlet air temperature is T_o.

The following assumptions were made to obtain the value of the experimental Sherwood and Nusselt numbers:

1) The droplet is hemispherical with a constant density.
2) The air flow rate and its inlet temperature are constant.
3) The physical properties of air are constant.
4) The temperature at the surface of the droplet is equal to the wet bulb temperature.
5) The partial pressure of liquid vapour at the surface is equal to the saturation partial pressure of the liquid vapour at the wet bulb temperature (saturation temperature).
6) The temperature driving force remains constant.

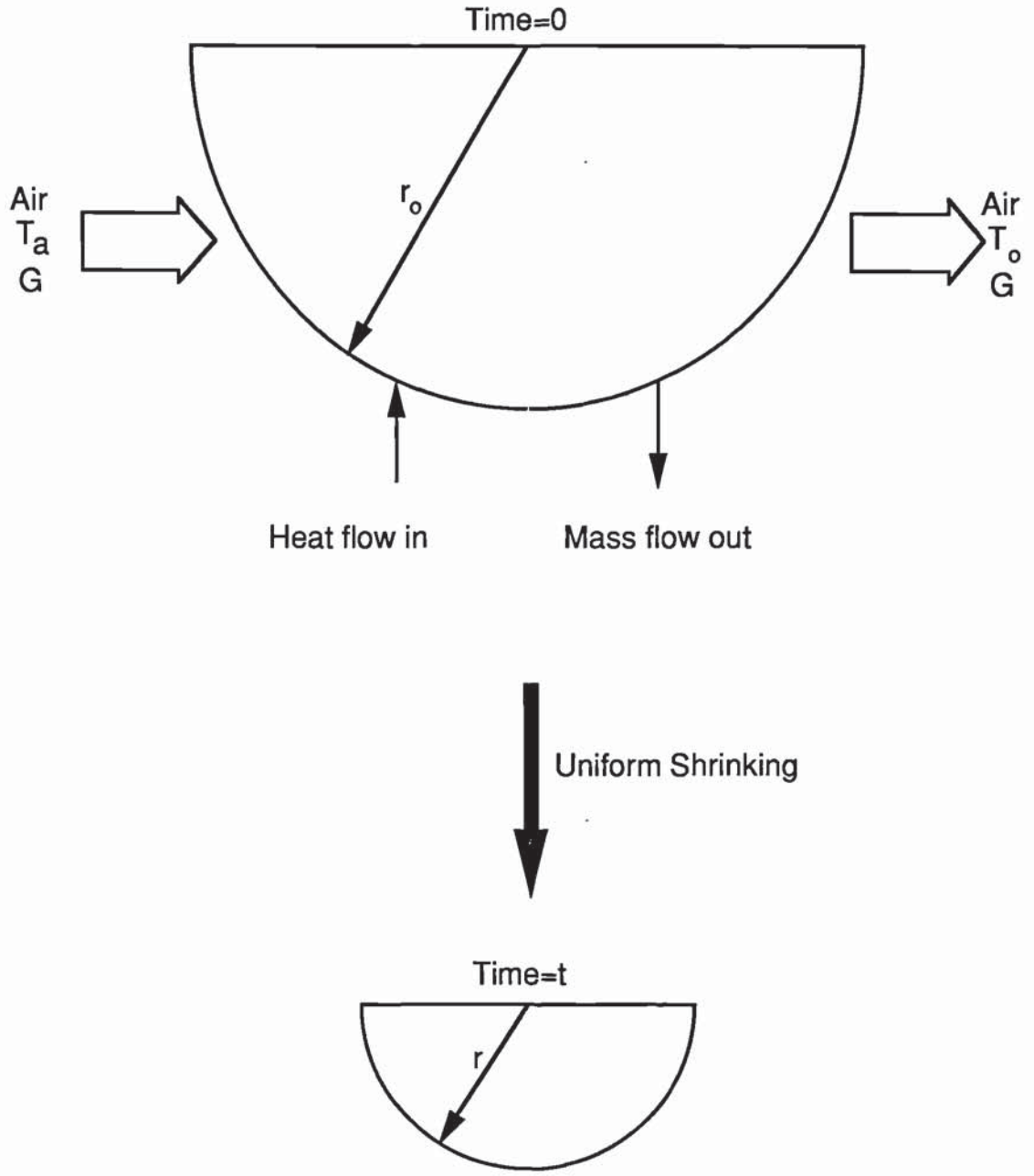

Figure 5.1 Evaporation Model of Suspended Droplet of Pure Liquid

5.1.1 Experimental Sherwood Number

From a simple mass balance on the droplet:

$$\text{Evaporation rate} = \frac{\text{Rate of Heat Transferred to the Droplet from the Drying Medium}}{\text{Latent Heat of Evaporation}}$$

$$N_A = \frac{dQ/dt}{\lambda} = k_g A \Delta P \qquad \text{----------5.1}$$

N_A can be expressed as:

$$N_A = -\frac{dw}{dt} \qquad \text{----------5.2}$$

Therefore

$$-\frac{dw}{dt} = k_g A \Delta P \qquad \text{----------5.3}$$

Where k_g is the mass transfer coefficient with units of kg / m^2 s atm. However Eqn. 5.3 can be modified to yield

$$-\frac{dw}{dt} = k_g A \Delta P \frac{M_W}{R_C (T_a + 273.15)} \qquad \text{----------5.4}$$

where

R_C = Universal Gas Constant

T_a = upstream (inlet) air temperature

A = $2 \pi r^2$, mass transfer area

ΔP = $(P_S - P)$ where P_S is the vapour pressure of water at the wet bulb temperature and P is the partial pressure of water vapour

M_W = molecular weight of water vapour

For a hemispherical droplet,

$W = \pi d_p^3 \rho_d / 12$; hence eqn. 5.4 becomes,

$$\frac{-\pi \rho_d}{12} \frac{d(d_p^3)}{dt} = k_g A \Delta P \frac{M_W}{R_C(T_a + 273.15)} \qquad \text{----------5.5}$$

By rearrangement of eqn. 5.5 the mass transfer coefficient can be expressed as,

$$k_g = \frac{-\rho_d R_C(T_a + 273.15)}{6 \Delta P M_W} \frac{1}{d_p^2} \frac{d(d_p^3)}{dt} \qquad \text{----------5.6}$$

The Sherwood Number is defined as,

$$Sh = \frac{k_g d_p}{D_V} \qquad \text{---------5.7}$$

By substitution of eqn. 5.6 into eqn.5.7

$$Sh = \frac{-\rho_d R_C(T_a + 273.15)}{6 \Delta P M_W D_V} \frac{1}{d_p} \frac{d(d_p^3)}{dt} \qquad \text{---------5.8}$$

Since,

$$\frac{d(d_p^3)}{dt} = \frac{3 d_p}{2} \frac{d(d_p^2)}{dt} \qquad \text{---------5.9}$$

Therefore

$$Sh = \frac{-\rho_d R_C (T_a + 273.15)}{4 \Delta P M_W D_V} \frac{d(d_p^2)}{dt} \qquad \text{---------5.10}$$

Under conditions of relative velocity, the derivative of d_p^2 with respect to time varies with Sh.

5.1.2 Experimental Nusselt Number

From a simple heat balance on the droplet,

Rate of Heat Transferred = Rate of Evaporation x Latent Heat of Evaporation to the Droplet from the Drying Medium

$$\frac{dQ}{dt} = - N_A \lambda \qquad \text{---------5.11}$$

The rate of heat transferred can be expressed as,

$$\frac{dQ}{dt} = h_g A \Delta T \qquad \text{---------5.12}$$

By substitution of eqn. 5.12 into eqn. 5.11,

$$- N_A \lambda = h_g A \Delta T \qquad \text{----------5.13}$$

N_A can be expressed as,

$$N_A = - \frac{dw}{dt} \qquad \text{--------5.14}$$

Therefore,

$$-\frac{dw}{dt} = \frac{h_g A \Delta T}{\lambda} \qquad \text{---------5.15}$$

For a hemispherical droplet,

$w = (\pi d_p^3 \rho_d / 12)$, eqn. 5.15 becomes,

$$h_g = \frac{-\rho_d \lambda}{6 \Delta T} \frac{1}{d_p} \frac{d(d_p^3)}{dt} \qquad \text{---------5.16}$$

The Nusselt number is defined as,

$$Nu = \frac{h_g d_p}{K} \qquad \text{---------5.17}$$

By substitution of eqn. 5.16 into eqn. 5.17

$$Nu = \frac{-\rho_d \lambda}{6 K \Delta T} \frac{1}{d_p} \frac{d(d_p^3)}{dt} \qquad \text{---------5.18}$$

Since,

$$\frac{d(d_p^3)}{dt} = \frac{3 d_p}{2} \frac{d(d_p^2}{dt} \qquad \text{---------5.19}$$

Therefore,

$$Nu = \frac{-\rho_d \lambda}{4 K \Delta T} \frac{d(d_p^2)}{dt} \qquad \text{--------5.20}$$

$d (d_p^2) / dt$ can be determined from a plot of d_p^2 versus t.

5.1.3 Heat Transferred to a Droplet by Radiation

A droplet suspended on a nozzle in a wind tunnel, or within a spray drying tower, receives some proportion of its heat by radiation in addition to the main contribution from forced convective heat transfer. Therefore radiation effects may have to be taken into consideration.

The radiative heat transfer rate q_e, can be expressed as,

$$q_e = F_a A \sigma e (T'^4_g - T'^4_s) \qquad \text{----------5.21}$$

where σ = Stefan-Boltzman constant. The geometry factor F_a, can be assumed to be unity since for all practical purposes the droplet is surrounded by the drying chamber.

5.1.4 Heat Transferred to a Droplet Through the Nozzle-Suspension Device

Any nozzle for droplet suspension inside the working section is exposed to the hot drying air. Consequently some heat is transferred from the nozzle to the droplet by conduction. Cheong (8) derived a model for conductive heat transfer to the droplet through a glass filament. In the present investigation the heat transfer took place via a similar material. Let the following assumptions, previously made by Cheong, be valid:

1) Heat is transferred to the nozzle suspension device from the surroundings by radiation and by convection;
2) The physical properties of the nozzle are constant;
3) The temperature around the nozzle is constant and equal to the dry air temperature;
4) There is no radial temperature gradient;
5) The length of the nozzle is much longer than its diameter; this will always be valid.

Considering the glass filament as a cylinder of infinite length, the final expression for the heat transferred through the glass filament was (8)

$$q_f = \frac{\pi}{2}\left(\frac{k_t d_f^3}{5}\left(2\sigma e_g\left(T_s^5 - T_g'^5\right) - 10\sigma e_g T_g'^4\left(T_s - T_g'\right) + 5h_f\left(T_S - T_g\right)^2\right)\right)^{0.5} \quad \text{---5.22}$$

In the present work q_f is equivalent to q_n, d_f is equivalent to e_n and h_f is equivalent to h_n. Therefore equation 5.22 can be written as,

$$q_n = \frac{\pi}{2}\left(\frac{k_t d_n^3}{5}\left(2\sigma e_n\left(T_s^5 - T_g^5\right) - 10\sigma e_n T_g^4\left(T_s - T_g'\right) + 5h_n\left(T_S - T_g\right)^2\right)\right)^{0.5} \quad \text{---5.23}$$

5.2 DROPLETS CONTAINING SOLIDS OF GELATINISED MATERIALS

A mathematical model has been developed in the present work to describe the drying of one type of skin forming material (first type), namely droplets containing solid in the form of gelatinised material. Such solids gelatinise when the droplet temperature reaches a specific 'gelatinisation temperature' as shown in Figure 5.2. This model is based on the following assumptions, which are borne-out in part by the experimental observations described in Section 9.1:

1) The droplet is hemispherical with a constant density, until the skin appears.
2) The droplet shrinks uniformly until the skin appears at its surface.
3) Until the skin forms the evaporation rate is equal to that of a pure-water droplet of the same size and, calculable from the mass and heat transfer correlations developed earlier.
4) All the granules gelatinise at the gelatinisation temperature.
5) The skin appears at the droplet surface instantaneously after the granules gelatinise.

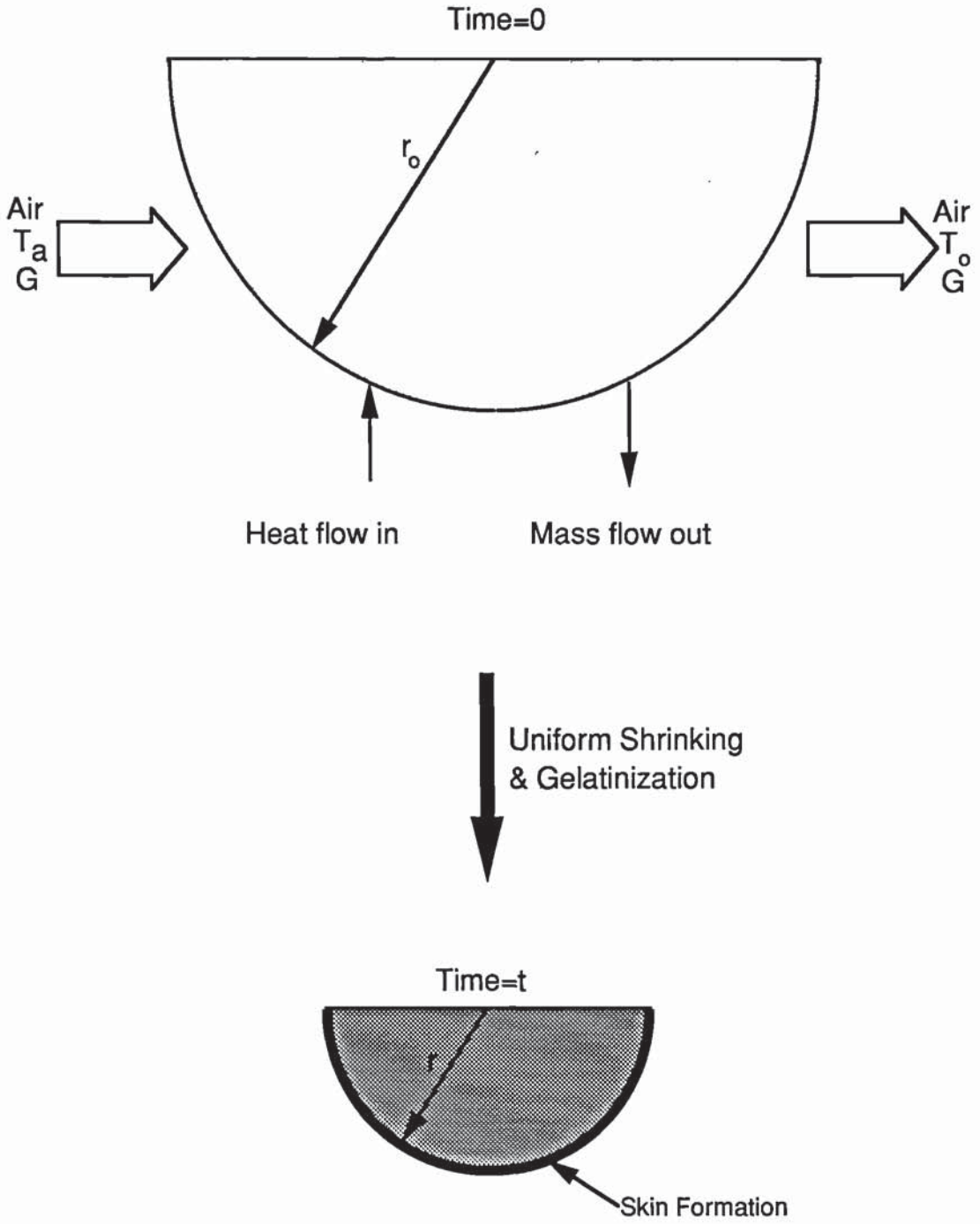

Figure 5.2 Drying Model of Suspended Droplet Containing Skin Forming Solids of the First Type e.g. Starch / Custard

A heat balance on the droplet can be expressed as,

Heat in = Heat out + Accumulation

Expressed in mathematical form for a hemispherical droplet,

$$2\pi h_g r^2 (T_a - T_s) = 2\pi r^2 k_g (P_{wd} - P_{wa}) \lambda + \frac{2}{3}\pi r^2 \rho_d C_{pa} \frac{\Delta T_s}{\Delta t} \qquad \text{---------5.24}$$

By rearrangement of equation 5.24

$$(\frac{C_{pd}}{2\pi r^2}) \frac{\Delta T_s}{\Delta t} = h_g (T_a - T_s) - k_g (P_{wd} - P_{wa}) \lambda \qquad \text{---------5.25}$$

$$\therefore \Delta t = t_s - 0 = \frac{C_{pd} / 2\pi r^2 \quad \Delta T_S}{h_g (T_a - T_s) - k_g (P_{wd} - P_{wa}) \lambda} \qquad \text{---------5.26}$$

Where t_s is the time at which the skin appears on the droplet surface and C_{pd} is the specific heat capacity of the droplet which is given by the following equation (modified after (113))

$$C_{pd} = \frac{2}{3}\pi r_o^3 [C_{ps} C_{so} + C_{pw} \{ C_{wo} - \rho_w (1 - r^3/r_o^3) \}] \qquad \text{---------5.27}$$

Equation 5.26 can be solved to give the time at which the skin appears on the surface of the droplet. A computer programme (Filename: FSTFM MODEL) has been developed to solve the equation on a Commodore BBC Microcomputer. A full listing of the programme is included in Appendix D 2.

CHAPTER SIX

EXPERIMENTAL APPARATUS

EXPERIMENTAL APPARATUS

6.0 INTRODUCTION

To study the evaporation of pure liquid droplets and the drying of droplets containing dissolved and/or suspended solids, a technique was developed where individual droplets were suspended in a controlled air stream and their weight or temperature was measured during drying.

The single suspended droplets were necessarily of larger diameter (i.e. 2-8mm) than the actual size in a practical spray-dryer (i.e. 20-250μm) since it is impracticable to support or retain single droplets < 1mm.

6.1 EXPERIMENTALAPPARATUS-OVER-ALL ARRANGEMENT

Major modifications were introduced into the experimental rig to improve the original design used by Audu (10), Esubiyi (66) and Ali (7).

The following improvements were included in the new design:

a) The drying rate measurement procedure was a completely modified, version of that used in the previous designs. A newly-designed nozzle facilitated direct measurement of the droplet weight as drying progressed. A range of nozzles were designed to facilitate suspension from a hook beneath an analytical balance with a capacity between 0.1 mg-55 gm. This arrangement enabled changes in droplet weight within 0.1 mg to be noted during drying. In the original designs (7, 10, 66), the drying rate was measured indirectly based on a humidity balance on the air stream. The latter method tended to produce inaccurate results, since there was a noticeable amount of imbalance between the air-up stream and down-stream of the suspension point when there was no droplet suspended in the working section.

b) The newly-designed nozzles were made of glass to minimise heat transfer by

conduction along the nozzle. In the original designs the nozzles were made of stainless steel, causing a higher rate of conductive heat transfer through the droplet suspension device to a droplet.

c) In the previous design (7), the droplet temperature measurements were carried out using a thermocouple wire, which could be inserted from the top inside the rotated stainless steel nozzle. The temperature inside the droplet was recorded by manually projecting the thermocouple into the centre of the droplet at fixed time increments. This technique had the following disadvantages:

1) Since the temperature of a drying droplet varies very rapidly, especially at the start and end of drying, it is desirable to measure and record the droplet temperature in as short a time as possible to produce accurate results. The droplet's temperature was measured and recorded every 10 seconds, but involved manipulation which would have made it very difficult to take accurate measurements.

2) After projecting the thermocouple into the centre of the droplet some time would be required to reach the steady state condition and so to record the droplet temperature accurately. Therefore, continuous projection of the thermocouple into the centre of the droplet would be required to achieve accurate readings.

3) Manual projection of the thermocouple into the centre of the droplet could have led to variable positioning and cause disturbances of internal flow or deformation.

4) The thermocouple wire inserted inside the rotating stainless steel nozzle, was always in contact with the inside wall of the nozzle which could disturb the correct position of the thermocouple wire.

Therefore in the present work provision was made for direct droplet temperature measurement to overcome the above disadvantages. All nozzles were made to accommodate a thermocouple sensor of 0.5mm diameter. This sensor was suspended from the top and vertically from a supported clamp stand. Plate 6.5 shows

the arrangement.

The new arrangement ensured that the thermocouple was suspended freely and vertically through the glass nozzle right to the centre of the droplet. It also ensured permanent positioning of the thermocouple in the centre of the droplet throughout the drying process.

The newly-designed glass droplet suspension device assembly was light and easily introduced into, or removed from, the working section. Therefore accurate assessment could be made of the drying time of the droplet; i.e. the actual time of exposure in the working section. Furthermore, because of the rapidity of nozzle assembly introduction into the wind tunnel, the initial droplet temperature reading was essentially ambient temperature.

The design of the flow system ensured the supply of hot dry air to the working section where the droplet was suspended, at a selected constant humidity and uniform temperature. The schematic diagram Figure 6.1, and Plate 6.1, show the single suspended droplet experimental apparatus. It consisted of an air reservoir, a metric rotameter type 18 F, heating elements, Eurotherm temperature Reader device, a T-piece of brass material, an analytical balance and a Shaw Hygrometer.

6.2 CONTROL AND MEASUREMENT OF AIR STREAM CONDITION

Air was obtained at approximately 100 psi, from the laboratory compressed air mains. The air was transferred via a reservoir, to dampen any fluctuations, into the Birlec air dryer to reduce its humidity. The air from the Birlec dryer, at a pressure of 75 psi, was reduced to 1.5 bar by passage through the valve (V4). After passing through the secondary air dryer, the air was passed to the system. The flow rate of the air was controlled by the gate valve (V6) at the inlet to the horizontal wind tunnel. By using three, 1 kw electric heating elements the air was heated to any desired temperature in the range 21 ^{o}C to 300 ^{o}C. The heating elements were controlled by means of a rotary Regavolt voltage regulator connected to the

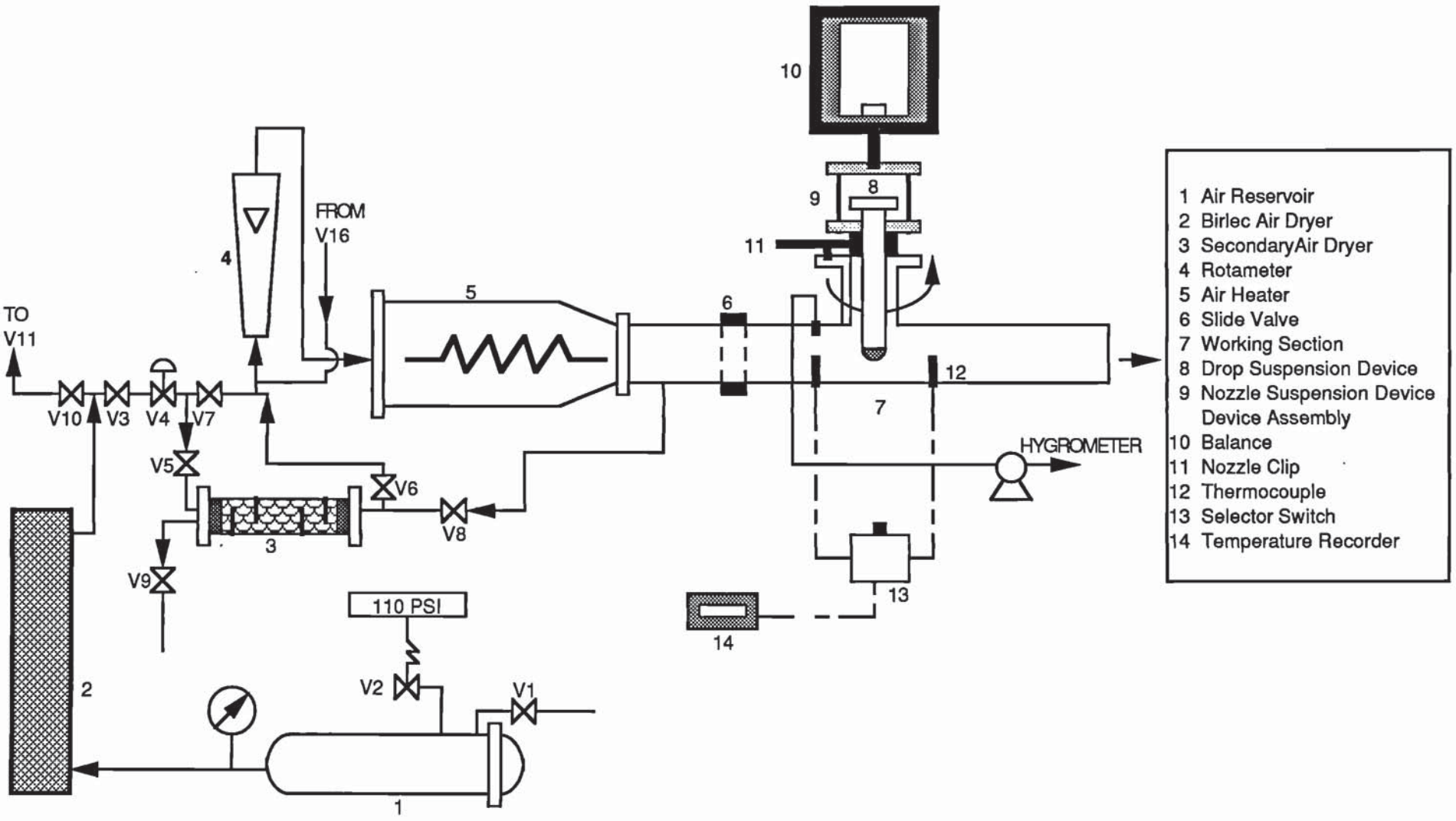

Figure 6.1 Schematic Diagram of Single Suspended-Drop Experimental Apparatus.

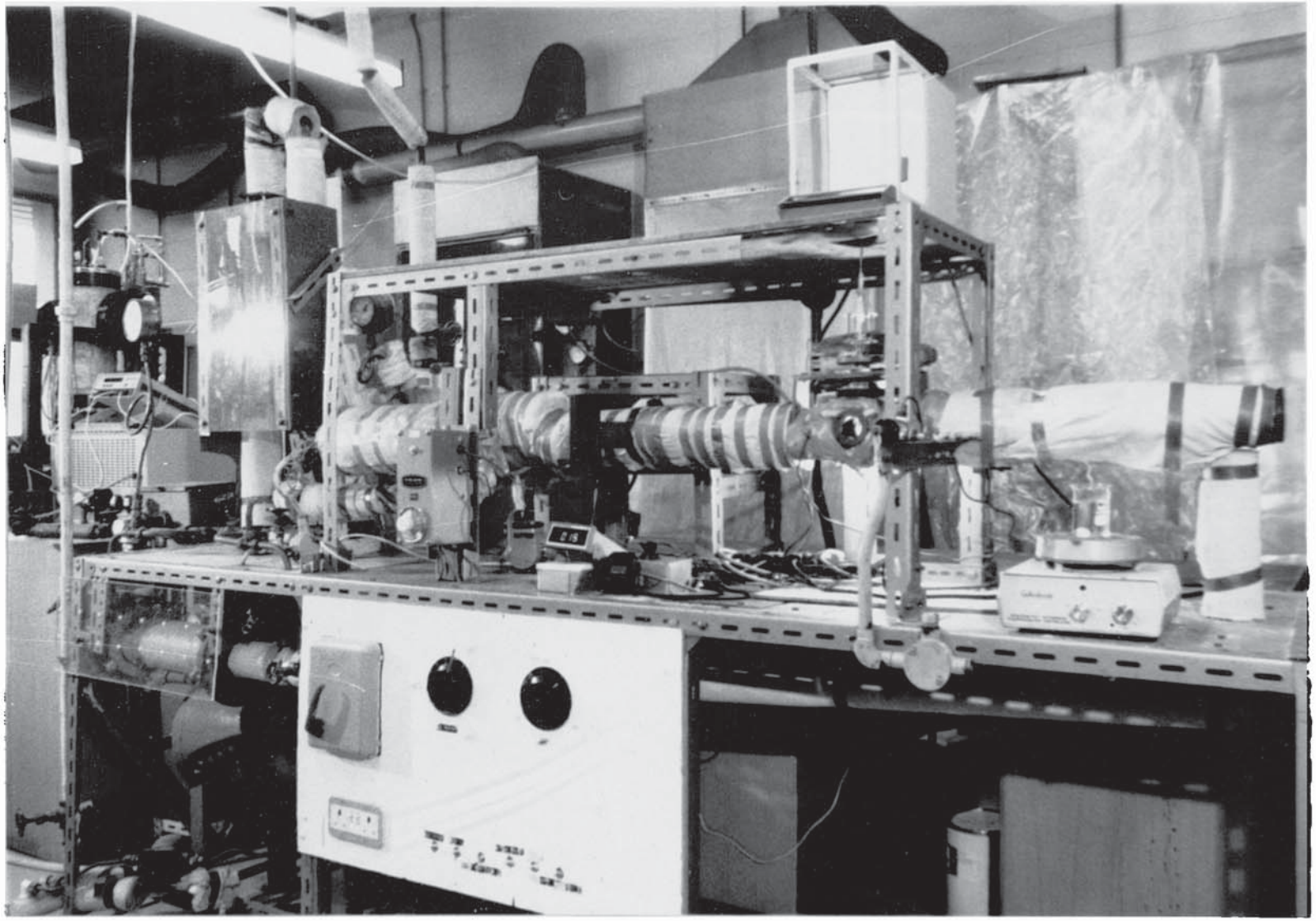

Plate 6.1 General Arrangement of the Experimental Apparatus

electrical supply.

6.2.1 Air Reservoir

The air from the laboratory supply was transferred to the air reservoir via a 12.7mm diameter Saunders diaphragm valve (V1) mounted on the inlet side. The air reservoir comprised a gas cylinder 600mm long and 300mm diameter, with a maximum working pressure of 100 psi. The valve (V2) set at 110 psi was connected to the air reservoir and served as a pressure relief valve. The outlet pipe from the cylinder was coupled to a pressure indicator and a 12.7mm diameter Spirax Sarco Strainer, and then to the Birlec Dehumidifiers.

6.2.2 Air Dryers

The air flowing to the working section was dried by passage through the Birlec Dryer Type AB30 which contained a granular Molecular Sieve. It then passed through a packed column of self-indicating silica gel and a column of self-indicating aluminate silicate Molecular Sieve (Type 4A). Figure 6.1 shows the air dryer piping system and the regeneration assembly for the secondary air dryer.

The Birlec air dryer was constructed from solid drawn steel tube with welded ends, with inlet and outlet side branches and a screw plug through which the adsorbent could be inserted or removed. An inner tube, with external longitudinal fins, contained the heating element. The maximum working pressure of the vessel was 100 psi.

The air from the Birlec dryer at a pressure of 75 psi was reduced to 1.5 bar after passage through a Spirax-Monnier type SR1 valve (V4) which acted as a pressure reducing valve. The air was then passed to the secondary dryer.

The secondary air dryer, Figure 6.2, was constructed from a 400mm long 107mm i.d. horizontal glass pipe packed with a silica-gel and molecular sieve. Five 'three-quarter' baffle plates were located evenly along the column to aid redistribution of the air.

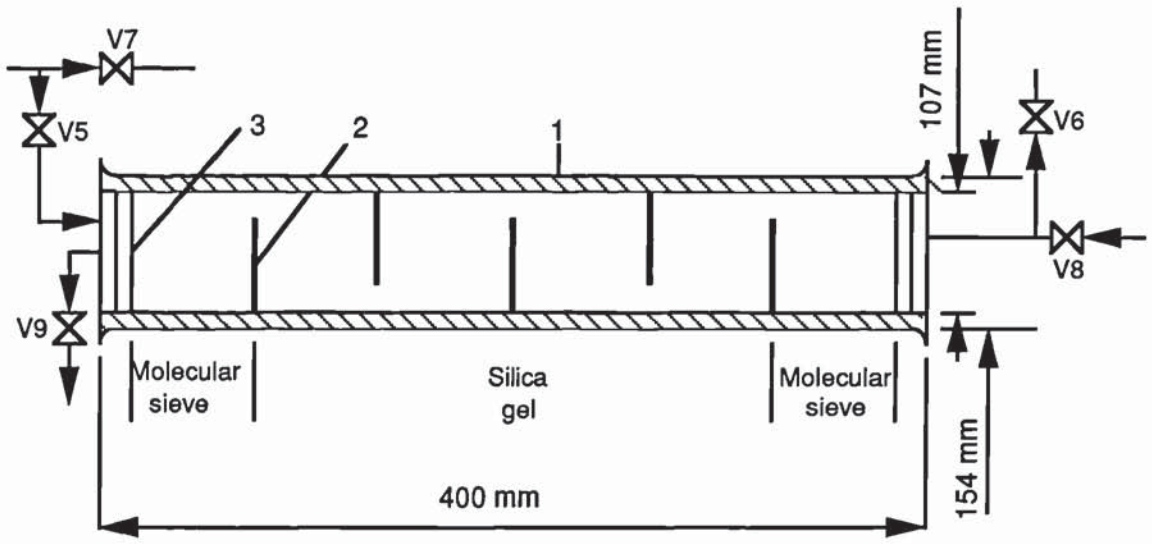

Item No	Description	Material
1	QVF Pipe Section	Glass
2	Baffle Plate	Copper
3	Wire Mesh	Stainless Steel

Figure 6.2 Secondary Air Drier Assembly.

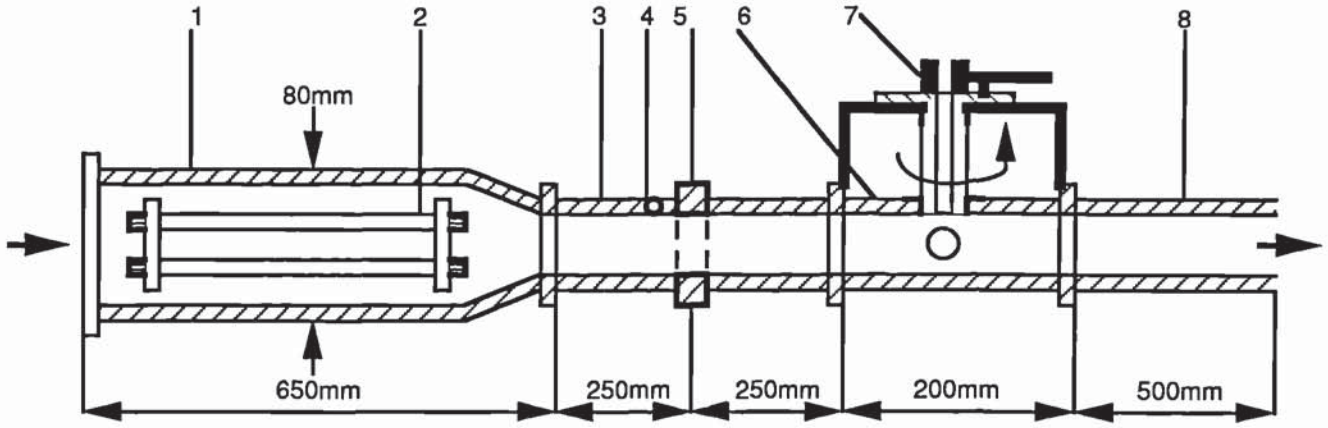

Item No	Description	Materials
1	Heater Pipe	Copper
2	Heating Elements	Tungsten
3	Upstream Pipe	Mild Steel
4	Hole	
5	Air Flow Cutter	Brass
6	Working Section	Brass
7	Clip	Brass
8	Downstream Pipe	Brass

Figure 6.3 Air Heater and Wind Tunnel Assembly

The air from the secondary air dryer passed directly into the horizontal wind tunnel. Two layers of 5mm mesh stainless steel, wire mesh were mounted at the inlet to the wind tunnel pipe, in order to prevent any particles from being carried downstream. Regeneration of the desiccants was always carried out prior to any set of experiments to sustain constant humidity inside the wind tunnel. This was carried out by closing valves V5 and V6 and opening valves V7, V8 and V9.

6.2.3 Air Heater

A 15mm gate valve (V6) was used to control the inlet air to the wind tunnel and the volumetric air flow rate was measured by means of an 18 FG.E.C. Elliott rotameter with a Duralumin float. To heat the air to the desired temperature it was passed over three 1 kw, electric-bar heaters inside a 650mm long and 80mm o.d. copper tube, The end nearest to the rotameter was flanged. The other end of this jacket tapered to a 42mm i.d. nozzle and flanged to a 500mm long standard 42mm i.d. tube which ended in a 500mm long standard 48mm o.d. mild steel tube. Figure 6.3 shows the heater and the wind tunnel assembly. A 6A, 90 ohm Cressal Torovolt voltage regulator was connected to the electrical supply of the heater to control the air temperature. The heating facility was able to raise the air temperature from ambient to over 500 ^{o}C. Three layers of fine stainless steel wire mesh (30 mesh) were spaced in series inside the mild steel tube at about 6 pipe diameters upstream from the working section. This arrangement ensured that a flat air velocity profile was presented to the suspended droplet. The velocity profiles were measured by using a pitot tube and an inclined manometer. Figure 6.4 shows a typical velocity profile across the plane of the droplet suspension in the working section.

All pipe lines upstream and downstream, the working section and the heater were insulated with 25.5mm thick glass fiber insulation.

6.2.4 Slide Valve

The air was cut-off during the weighing operation to enable an accurate

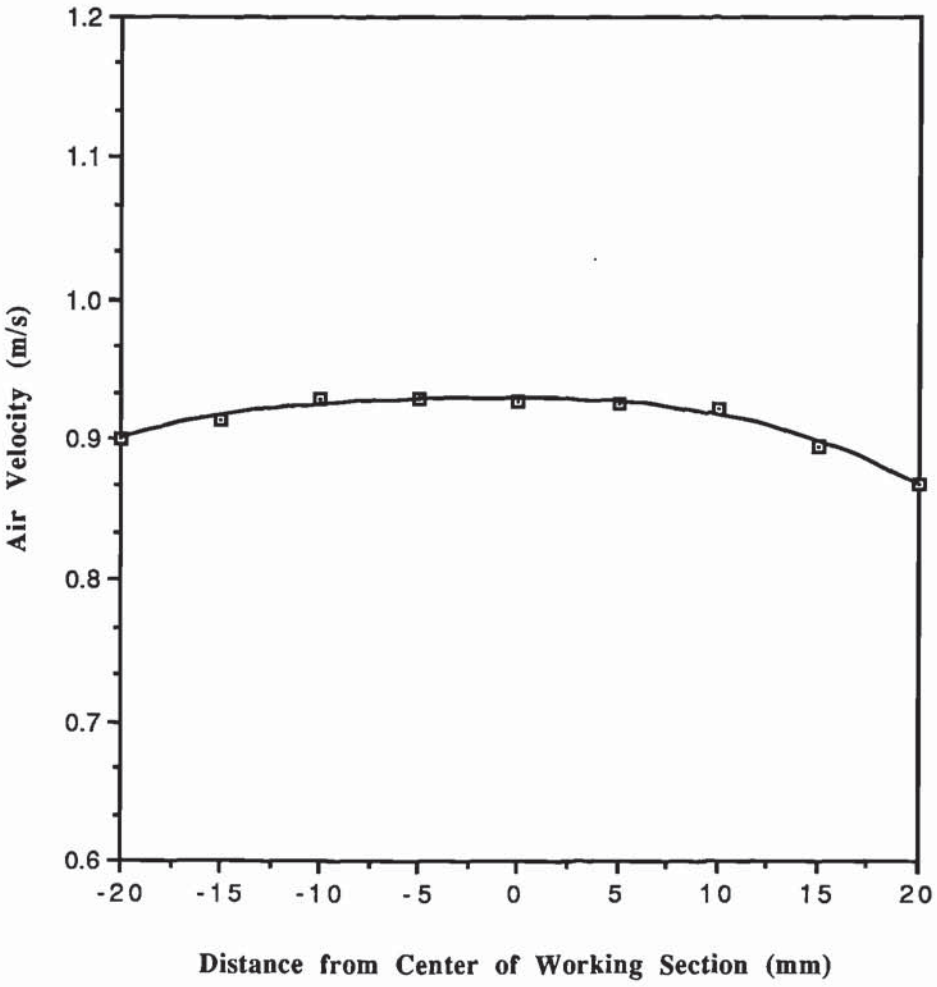

Figure 6.4 Velocity Profile across the Working Section of the Experimental Apparatus

fully-closed i.e. when the air flow to the working section was cut-off. The valve consisted of a brass plate 260mm long and 50mm wide. A hole 42mm diameter was made 65mm from one end of the brass plate; the hole diameter was identical with the pipe inside diameter. The hole allowed air flow without any obstruction when the slide valve was fully-open (i.e. when the hole was positioned in the centre of the pipe line). The other end of the brass plate terminated in a wooden hand i.e., by which the valve could be operated. Pushing the handle caused the plate to block the pipe thereby cutting-off the air flow to the working section; pulling the handle resulted in the restoration of the air flow to the working section.

The valve design eliminated any accumulation of air, and so eliminated any pressure build-up during droplet weighing (i.e. when the air flowing to the working section was cut off). To achieve this, a relief hole 10mm diameter was made in the pipe just before the sliding valve to act as an outlet for the air during the weighing process. Figure 6.3 shows the arrangement. The relief hole ensured that the air temperature and velocity remained constant since neither the heater nor the air supply were switched off. Any slight cooling during the short period of the weighing process was of little consequence because of the positioning of the slide valve very close to the working section, which allowed the temperature to return to normal in a few seconds after restoration of the air flow. Pulling the handle simultaneously restored the air flow and closed-off the relief hole. The relief hole was closed by a ring of brass tube, 12mm diameter and 27mm in length, supported by an L-shaped brass plate attached to the end of the slide valve. Plate 6.2 shows the arrangement. The front end of this tube was turned down to 10mm diameter to fit the relief hole.

6.3 WORKING SECTION

The working section is shown in plate 6.4 and illustrated diagrammatically in Figure 6.5. It was constructed from a 52mm o.d. by 42mm I.D. by 200mm long brass tube. At the mid-point of the tube there were two windows placed on opposite sides. Each window was flanged to hold a 6mm thick and 40mm diameter optical flat

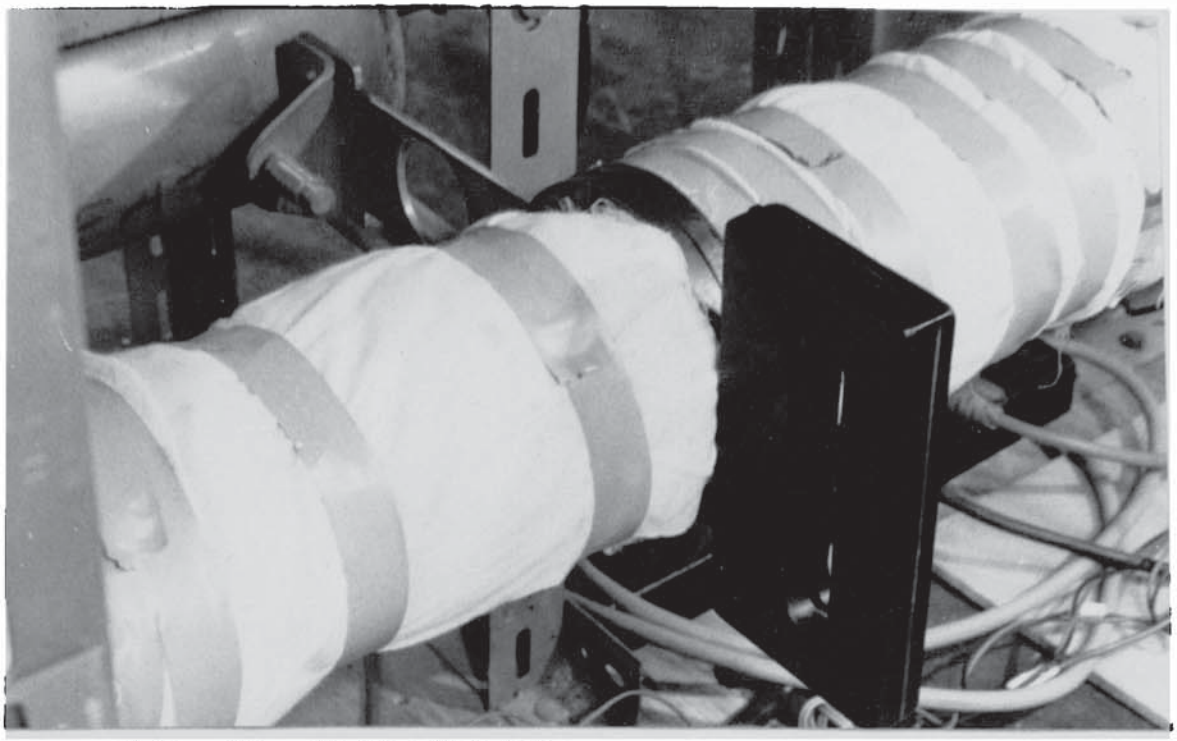

Plate 6.2 Air Flow Slide Valve

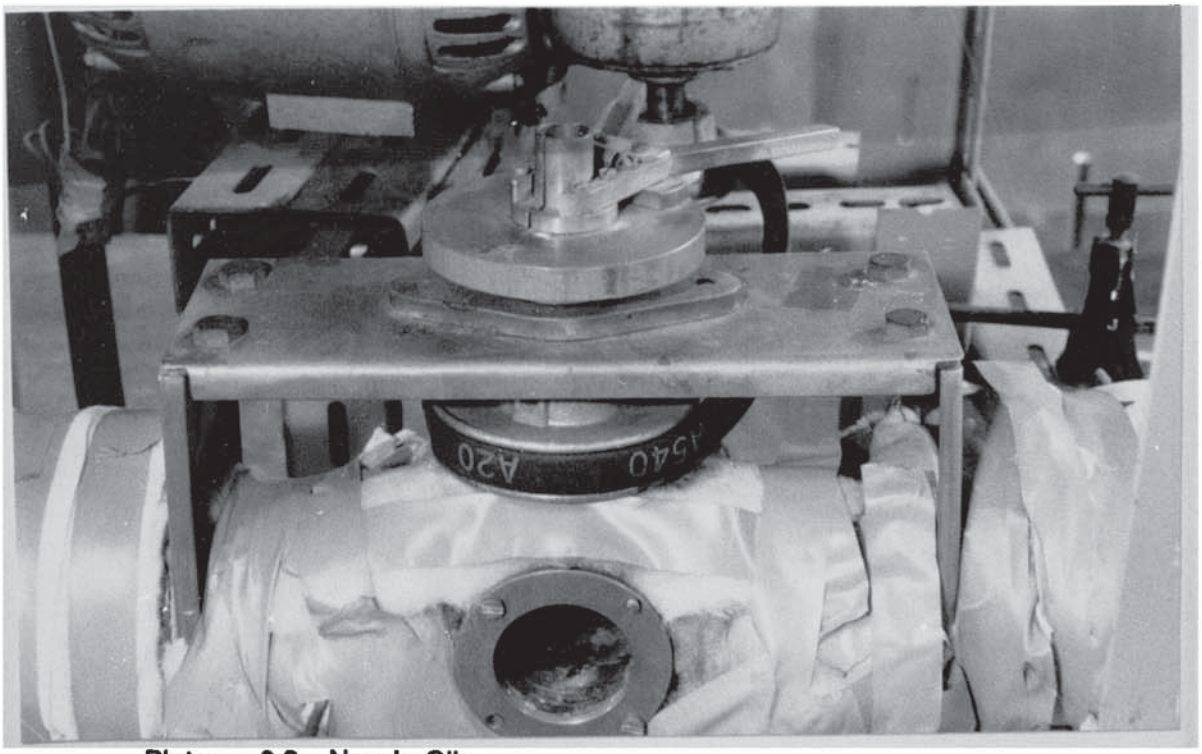

Plate 6.3 Nozzle Clip

glass, through which a suspended droplet could be observed or photographed, with the required back-lighting. The stainless steel housing of the rotated droplet suspension device was mounted midway along the top of the working section tube. It was fabricated from stainless steel tube 75mm long by 20mm o.d. by 16mm i.d. and sat upon a 210mm x 80mm wide x 70mm high brass frame. A 70mm V-shaped pulley served to drive the housing tube, and hence the glass droplet suspension device assembly, by means of a nozzle clip.

The nozzle clip is shown in Plate 6.3. It consisted of two brass arms 105mm long, connected together at the middle by a 3mm diameter spring. A half of a brass cylindrical tube with a semi circular base was mounted at the end of each arm such that when the arms were brought together, the two halves formed a complete cylinder, 9.0mm in diameter and 25mm in height, with a complete circular base 25.0mm in diameter. The glass nozzle was inserted into the working section through the stainless steel housing tube and the complete cylindrical, tube formed when the clip was closed. The tube acted as a housing for the glass droplet suspension device which fitted tightly inside, to enable the nozzle to rotate uniformly with the nozzle clip by means of a heat resistant plastic plug mounted just before the top end of the glass nozzle. While the droplet suspension device was fitted tightly inside the complete cylindrical tube of the nozzle clip there was space between the glass nozzle and the rotated stainless steel housing tube, resulting in some air leakage out of the working section. This leakage was prevented by the complete circular base formed when the nozzle clip was closed. The nozzle clip assembly fitted onto a brass ring 75mm diameter and 9mm thick, which was mounted at the top end of the rotated stainless steel housing tube. This enabled the nozzle clip, and hence the nozzle, to be rotated.

Air temperature measurement was carried out at two points, one at 50mm upstream and one at 50mm downstream of the droplet, by means of nickel-chromium/nickel-aluminium thermocouples connected via a manual selector unit to a Eurotherm digital thermocouple. Figure 6.1 shows the arrangement.

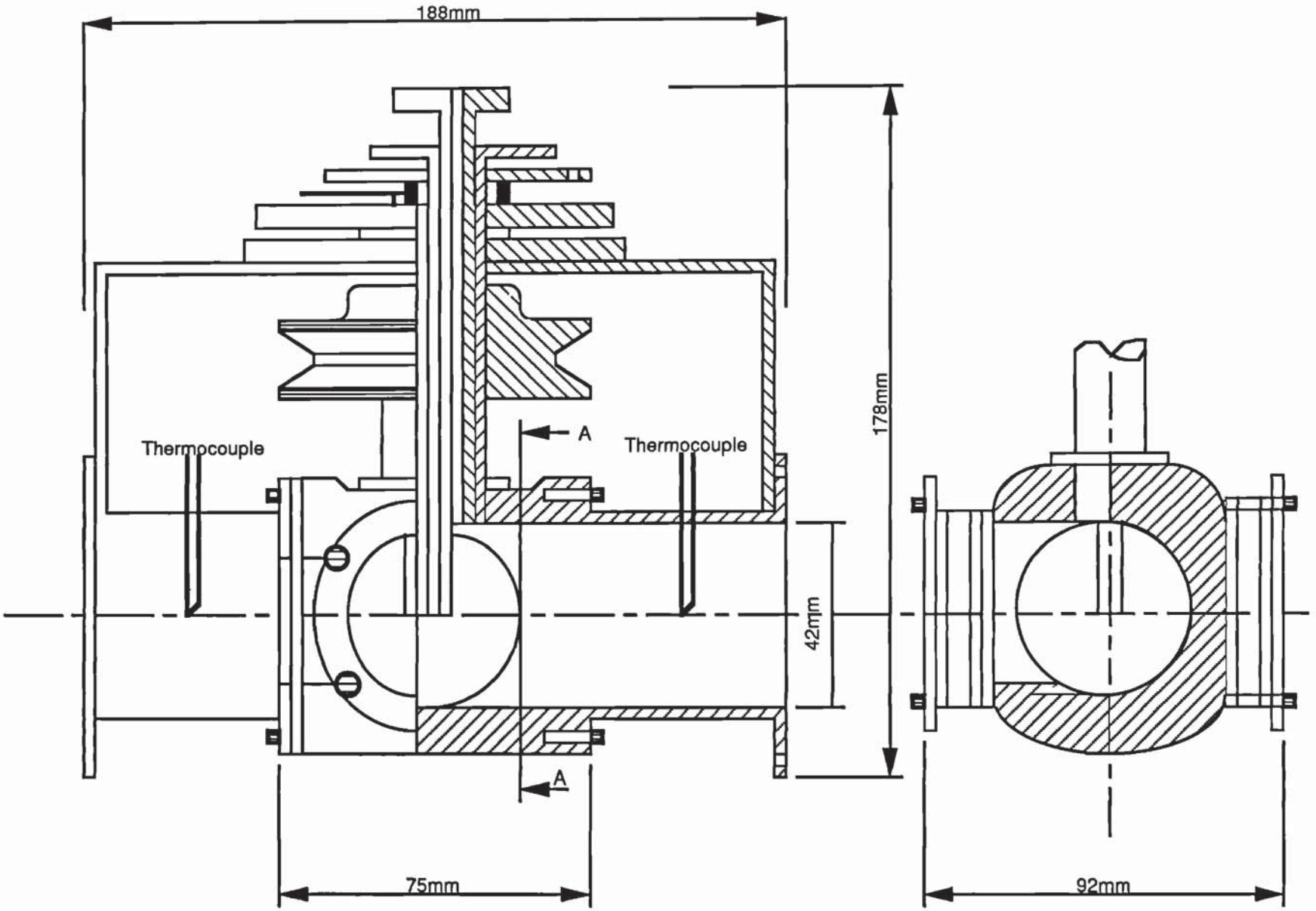

Figure 6.5 Working Section of Suspended-drop Experimental Apparatus.

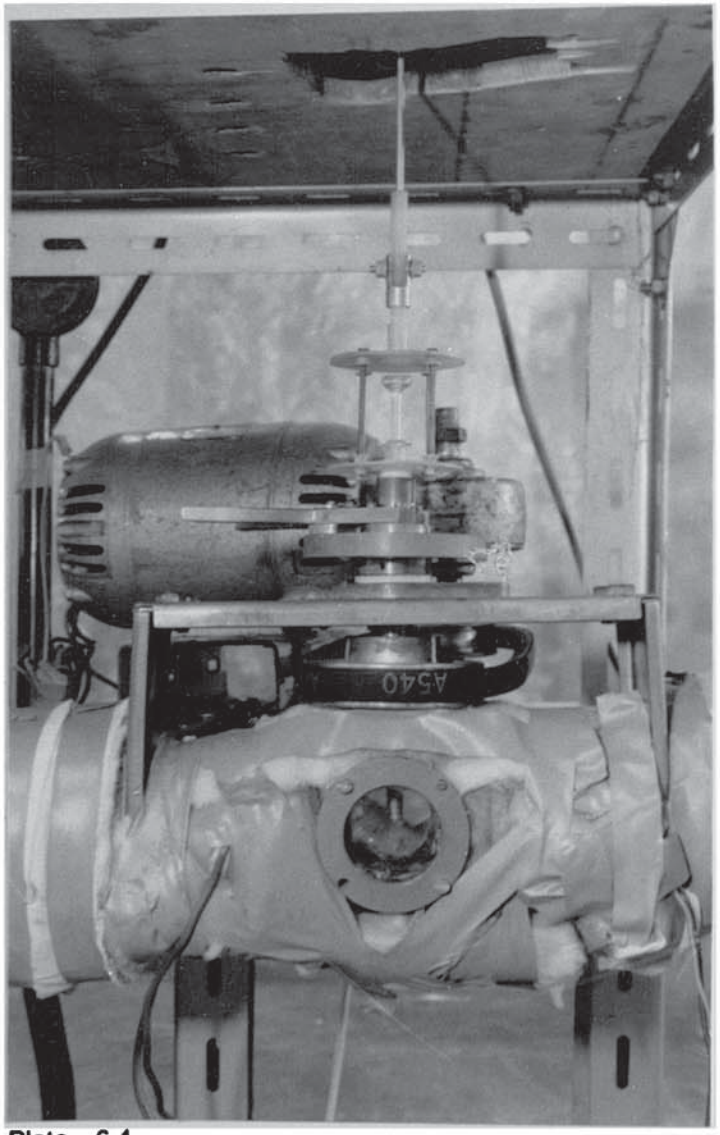

Plate 6.4
Working Section of the Experimental Apparatus

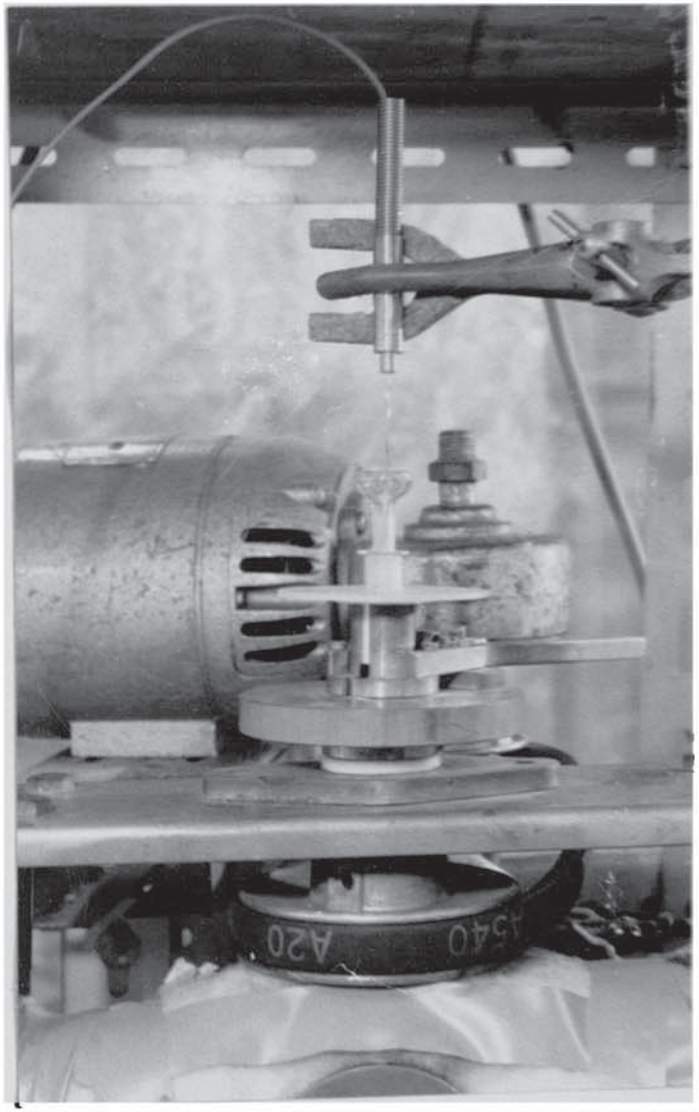

Plate 6.5 The Thermocouple Arrangement used to measure the Temperature of the Droplet

Droplet temperature measurements were carried out directly as drying proceeded by means of a Comark thermocouple sensor type K of 0.5mm diameter and 180mm long which was installed inside the glass nozzle. No manual work was involved, since the thermocouple sensor, held vertically by a support clamp stand, passed through the glass nozzle to the centre of the droplet. The droplet temperature was recorded at increments of 10-60 seconds. Plate 6.5 shows the technique used.

A Shaw hygrometer was used at 50mm upstream of the droplet to measure the humidity of the air.

6.4 DROPLET SUSPENSION DEVICE

The droplet suspension device is shown in Plate 6.6 (a, b) and Figure 6.6. It consisted of a glass plunger 170mm long. Three were constructed of 3.0, 5.0 and 8.0mm o.d. and 2.0, 4.0 and 6.0mm i.d. respectively. To enable the thermocouple to be inserted into the droplet the glass plunger had holes in the top and bottom; the bottom hole was plugged by a PTFE plug.

Three glass tubes were constructed with inside diameters of 3.0, 5.0 and 8.0mm respectively to accommodate each plunger. A glass ring of 22mm o.d. was constructed at the top end of each glass tube by which the glass nozzle (Droplet Suspension Device) was suspended from the hook beneath the balance by the nozzle suspension assembly (see Figure 6.6). The external surface of the plunger was of ground glass, to allow it to move freely inside the tube and also to prevent it sticking, by surface tension, to the inside wall of the glass tube.

The glass tubes were 145mm in length with outside diameters of 5.0, 7.0 and 11.0mm respectively. Heat resistant plastic plugs of 5.0, 7.0 and 11.0mm inside diameter and 16.0mm long, with a 25mm circular base, were mounted at the top end of each glass tube. These plugs served to secure each nozzle tightly inside the nozzle clip. This resulted in the nozzle rotating uniformly with the stainless steel housing tube

The nozzle suspension device assembly is shown in Figure 6.6 by parts (1A-1H). It consisted of two plastic circular discs of 55mm diameter. Three different

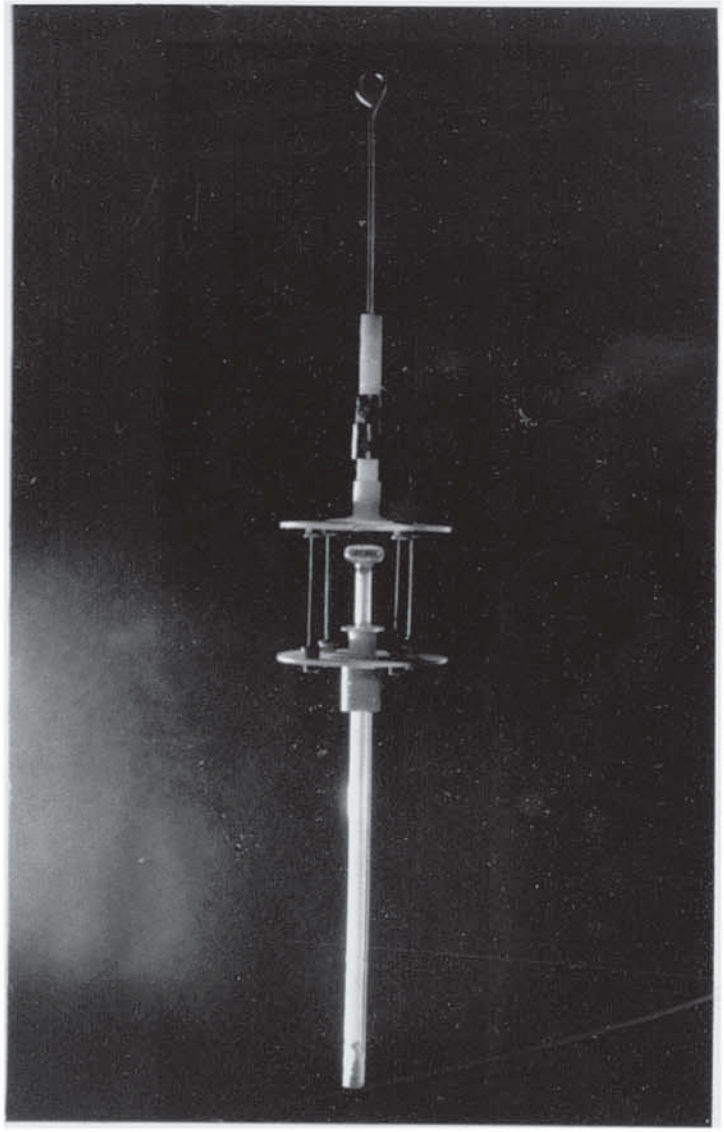

a. Normal Position

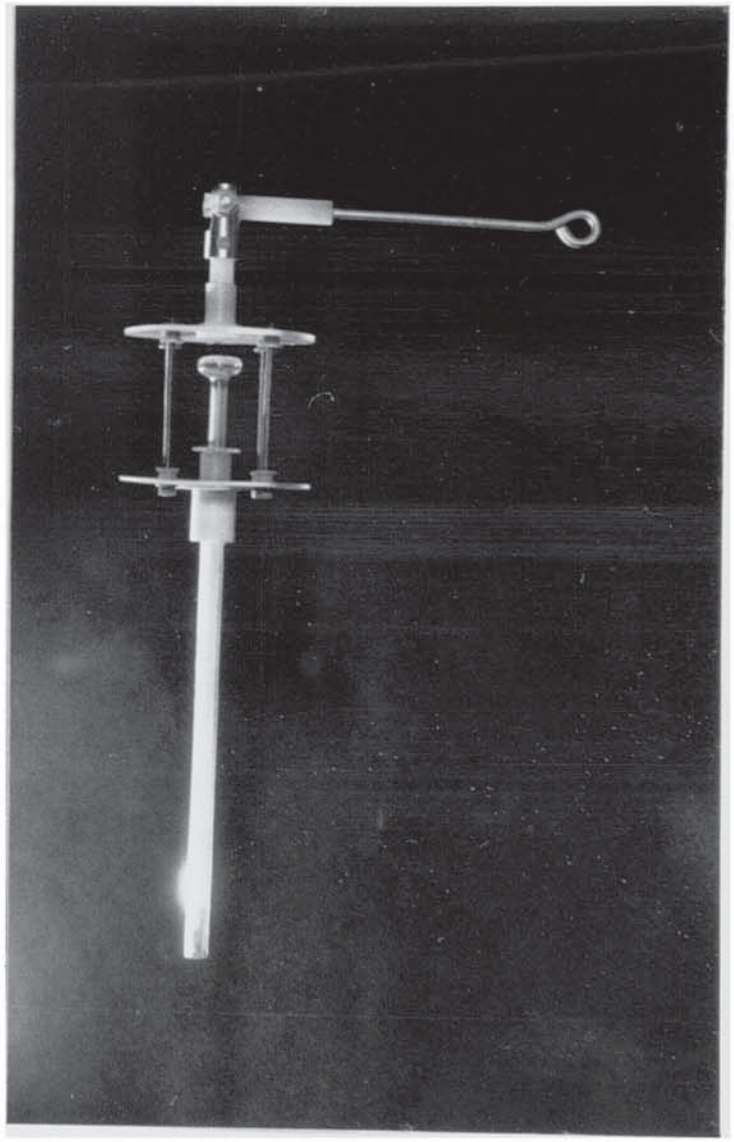

b. Bent for retraction

Plate 6.6 Drop-Suspension Device Assembly

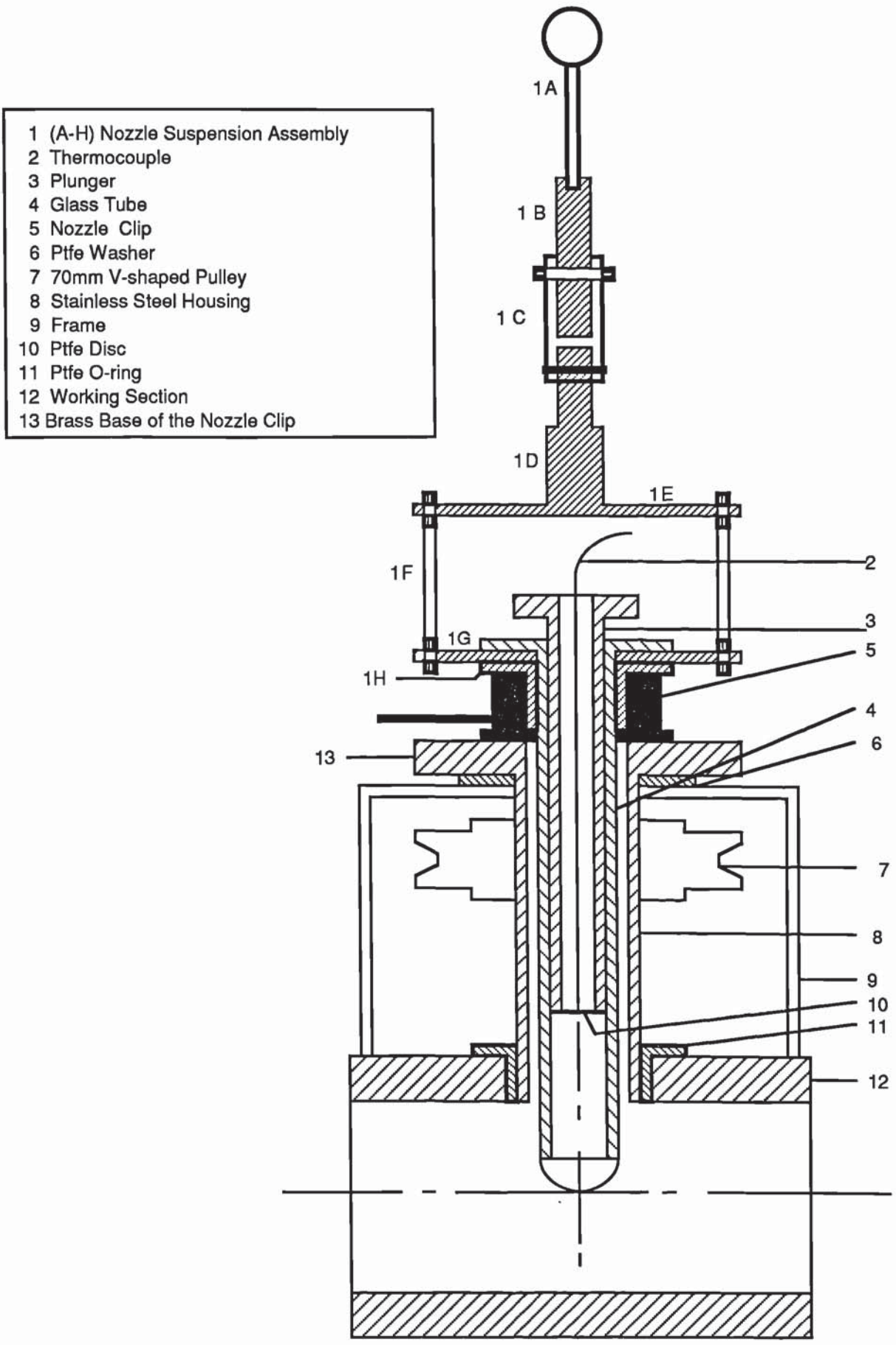

Figure 6.6 Drop-Suspension Device Assembly

lower sheets (1G) were constructed each with a central hole of 5.0, 7.0 and 11.0mm diameter respectively through which the appropriate nozzle was inserted up to the 22mm diameter glass ring of the nozzle, for suspension of the nozzle. The distance between the two discs was 45mm. This allowed easy movement of the plunger to enable a uniform hemispherical droplet to be suspended on the nozzle. The upper disc (1E) was parallel to the lower disc and contained no hole at the centre. A rigid plastic tube (1D) of 13mm length and 8mm diameter was mounted centrally on the surface of the upper disc. The upper 7mm of this tube was turned down to 6mm diameter. The two plastic discs were connected to each other by four brass screws and twelve plastic nuts and four washers.

The last part of the nozzle suspension device assembly consisted of two parts. The first part (1A) was a rigid aluminium tube 70mm long and 3mm in diameter. The top end was bent to a circular ring of 10mm diameter by which the nozzle suspension device assembly and then the nozzle were suspended from the hook beneath the balance. The aluminium tube was fitted tightly from the bottom inside the second part (1B) which was a rigid plastic tube. The top part of the nozzle suspension device assembly (1A and 1B) was connected to the lower part (1D) by an aluminium connector which allowed 1A/1B to pivot around the (bolt) of 1C enabling the nozzle assembly to be easily withdrawn from the working section.

The maximum weight of both the nozzle and nozzle suspension device assembly was less than 50.00gm, and the capacity of the balance was 55.00gm.

The maximum possible speed of rotation of the droplet was 100 r.p.m but, because it was found that speed had no effect on droplet shape and stability, each droplet was rotated at 15 r.p.m.

6.5 BALANCE

The balance comprised an analytical balance type AE50. The readability of the balance was 0.1mg, the weighing range was (0.0000-55.0000gm) and the permissible ambient conditions during operation were:

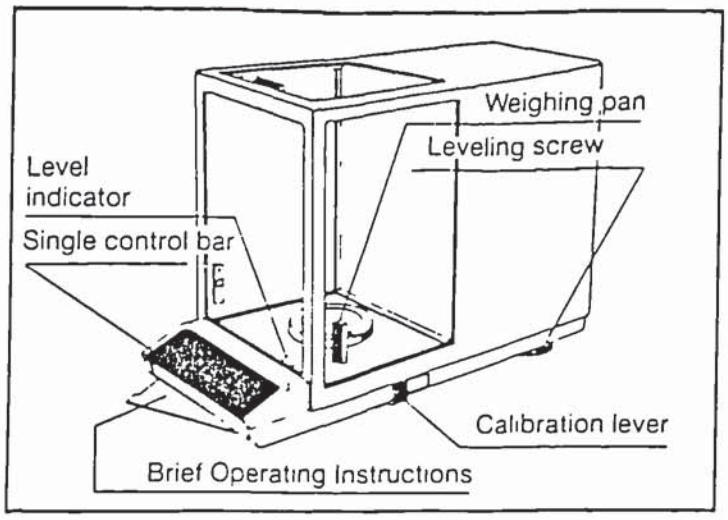

Figure 6.7 (a) The Analytical Balance

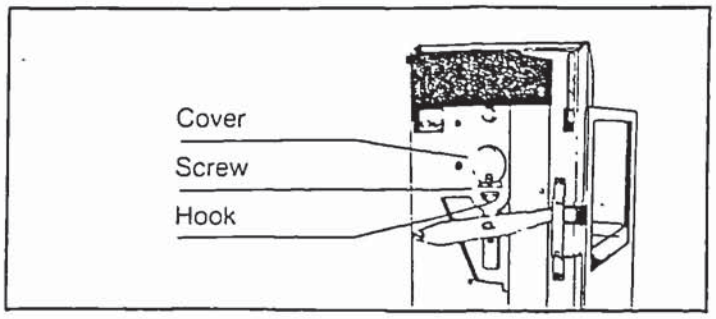

Figure 6.7 (b) Underneath the Balance

a) Temperature 10-40 ^{o}C.

b) Relative humidity 25-85% (non-condensing).

The newly-designed nozzle assembly, and the location of the balance, ensured the ambient condition to be within the admissible conditions. Figure 6.7 (a,b) shows the balance and the hook underneath from which the droplet suspension device assembly was suspended.

CHAPTER SEVEN

EXPERIMENTAL PROCEDURE

7.0 INTRODUCTION

7.1 INSTRUMENT CALIBRATION

- 7.1.1 Air Flowrate Measurement
- 7.1.2 Air Temperature and Humidity Measurements
- 7.1.3 Droplet Weight Measurement
- 7.1.4 Droplet Temperature Measurement

7.2 EXPERIMENTAL WORK

7.3 WATER DROPLETS

7.4 DROPLETS OF THE FIRST AND SECOND TYPE OF SKIN FORMING MATERIALS

7.5 DROPLETS OF AQUEOUS SOLUTIONS OF THE THIRD TYPE

EXPERIMENTAL PROCEDURE

7.0 INTRODUCTION

Air velocity, air temperature and droplet weight histories were measured in all runs. Droplet weight and droplet temperature were measured using the specially-designed rotated glass nozzle.

The method used to measure the droplet weight, or the droplet temperature, histories made it impractical to measure them simultaneously during one experiment. Parallel runs were therefore carried out under identical conditions, measuring droplet weight history in one and droplet temperature history in the other. The air humidity was also measured. The calibration of the instruments used is discussed below.

7.1 INSTRUMENT CALIBRATIONS

7.1.1 Air flowrate Measurement

The flow of air through the 42mm i.d. horizontal wind tunnel was measured by means of an 18 FG.E.C. rotameter with a Duralumin float. Calibration of the position of the rotameter float was performed against the flow rate of dry gas at ambient temperature, measured with a Parkinson gas meter placed in the outlet stream from the tunnel. A hot wire anemometer was also used to measure local air velocities. The velocities of air in the working section of the wind tunnel were then calculated at different temperatures using the appropriate air densities.

7.1.2 Air Temperature and Humidity Measurements

The air temperature in the working section upstream and downstream from a droplet were measured using Ni-Cr/Ni-Al thermocouples. The thermocouples were connected to a Eurotherm digital temperature reader via a selector unit. The air temperature was controlled by adjustment of the voltage regulator on the electrical supply of the heater.

The humidity of the air was measured by means of a Shaw hygrometer. This consisted of a hygrometer, a moisture sensing element, a constant temperature unit, coaxial cable, a sampling pump and a three-way valve. The hygrometer was scaled to read dewpoints from -20 °C to -80 °C.

The moisture sensing element operated according to the principle that the capacitance varied in direct proportion to the dewpoint of the air. The sensing element estimated the capacitance of the air and transmitted it to the hygrometer (i.e. the dewpoint meter) via the coaxial cable. The probe of the sensing element was protected from contamination by a sintered bronze filter. Once air flowed over the filter a dynamic equilibrium was set up between the water vapour pressure outside the pores of the filter and the liquid water contained within the pores.

The constant temperature unit maintained a constant temperature in the air flowing to the sensing element. It also prevented condensation on the sensing element by maintaining the air at a temperature well above its dewpoint. A constant flow of air through the unit was supplied from the working section by the sampling pump.

7.1.3 Droplet Weight Measurement

The weight of an evaporating droplet was measured by means of an analytical balance with a capacity of 55gm-0.1mg.

The balance was placed 180mm over the nozzle clip. The location of the balance ensured:

1) a stable location, virtually free from vibration;

2) no large temperature fluctuations;

3) avoidance of direct sunlight and drafts.

This resulted in accurate readings from the balance.

The following operations were performed on the balance before the start of any set of runs:

i) Levelling the Balance. The two levelling screws were adjusted so that the levelling bubble was centered in the middle of the circle.

ii) Calibration of the Balance. The balance was calibrated, so that it enabled changes in droplet weight to be noted during drying within 0.1mg. This was carried out as follows:

1- Before calibration the balance was left connected to the power supply for at least 60 minutes.

2- The single control bar was pressed and held until -CAL- appeared in the display. It was then released. The display changed to CAL-----, followed by 50.0000, then to CAL O (blinks).

3- The calibration lever was moved all the way back towards the front of the balance; the display changed to -------, followed by 0.0000.

iii) Measuring cycle/measuring accuracy. The integration cycle and stability detection step, were selected, so that the balance could be configured according to the weighing location and needs.

Integration Time

Step 1: Used for very stable, vibration-free weighing table (short measuring cycle).

Step 2: Normal setting .

Step 3: Used for unfavourable ambient conditions (long measuring cycle).

1- The control bar was pressed and held until -Int- appeared in the display. It was then released.

2- The control bar was then immediately pressed briefly; the display changed to the next step.

3- The control bar was released (i.e. stopped) when the desired step appeared in the display. Step 2 was chosen.

Stability detector

Step 1: Great sensitivity (long pause before data were released).

Step 2: Less sensitivity (short pause before data were released). Normal setting.

Step off: The stability detector was switched off.

1- The control bar was pressed and held until -ASD- appeared in the display; it was then released.

2- The control bar was then immediately pressed again briefly; the display changed to next step.

3- The control bar was then released when step 2 appeared on the display, followed by a wait for the display to return to the weighing mode (0.0000).

The procedure for droplet weighing was simple and fast. All parts, i.e. nozzle clip, droplet suspension device assembly (nozzle) and the balance were adjusted such that the nozzle was freely-suspended from the hook beneath the balance. Droplet weighing was carried-out by firstly pushing the handle of the slide valve to cut-off the air flowing to the working section. (This was done to prevent any vibration of the freely-suspended nozzle during weighing which would have affected the results). The droplet rotation was simultaneously stopped. In the second step the nozzle clip was opened manually; the droplet suspension device assembly was hence freely-suspended from the hook of the balance to enable an accurate weight measurement to be taken. The last step was to read this weight from the balance. Immediately after this the nozzle clip was closed, the slide valve opened and droplet rotation restored.

7.1.4 Droplet Temperature Measurements

As discussed in Chapter 6, the droplet temperature was measured by using the unique technique developed for this purpose. No manual work was involved.

All the equipment was carefully adjusted, so that the thermocouple was positioned precisely and rapidly in the centre of the droplet.

A droplet was suspended on the nozzle, placed in the working section and rotated at 15 r.p.m. The thermocouple sensor was then immediately inserted into the centre of the droplet and clamped from the top by the support stand. Droplet temperatures were simply recorded at fixed time increments.

7.2 EXPERIMENTAL WORK

The experimental investigation was divided into two sections. Experiments were performed with water droplets over a range of air temperatures and velocities.

This served to test the experimental apparatus and to standardise the experimental method. A major study was then made of the drying of different skin-forming materials over a range of drying conditions.

The materials selected to cover different skin formation mechanisms: were,

1) **First Type of Skin Forming Materials**

In this type, skin formed only at high drying temperatures (e.g. custard and starch suspensions). Such materials formed a skin when there was still moisture in the droplet but the droplet temperature exceeded a critical temperature (gelatinisation temperature). The dried crust obtained was not soluble or dispersible in water (e.g. granules lost their original structures and properties). The formation of skin in this type was due to the granule gelatinisation at high drying temperatures.

2) **Second Type of Skin forming Materials**

In this type, skin formed at any drying condition immediately after drying had taken place (e.g. gelatin), but at high temperature, the original granule structures and properties were irreversibly lost. This may have been due to protein denaturation.

3) **Third Type of Skin Forming Materials**

In this type, skin formed at any drying condition at a certain stage of the drying process (e.g. skim milk and fructose). The dried crust obtained had the same original structure and properties of the powder unless dried at very high temperatures.

7.3 WATER DROPLETS

Two separate sets of runs were carried out using water droplets. A set was first performed at ambient air temperature but covering different air velocities and initial droplet diameters. The velocity was varied between 0.018-0.901 m/s for a range of droplet Reynolds number between 9.5-163. A second set was carried out at higher air temperatures up to 80 ^{o}C.

Steady state conditions were first established in the wind tunnel. A droplet of distilled water was then suspended at the tip of the droplet suspension device assembly. It was then introduced into the working section, suspended from the balance and rotated at a rate of 15 r.p.m to ensure uniform evaporation from the droplet.

The air temperature, velocity and humidity were recorded at the start of each run. Droplet weight was recorded at time intervals during the evaporation process, until the droplet's hemispherical shape become distorted. This occurred when gravity could no longer sustain the droplet's hemisphericity. The droplet's hemisphericity was checked during each run, using both a cathetometer, which also allowed visual observation of the droplet, and photography using a Chinon 35mm camera with a telephoto extension lens and back lighting.

The velocity of the air flowing to the working section was controlled by adjusting the gate valve V6.

The wet bulb temperature was measured by means of a Ni-Cr/Ni-Al thermocouple with the thermojunction covered with a thin paper tissue saturated with distilled water.

7.4 DROPLETS OF THE FIRST AND SECOND TYPE OF SKIN FORMING MATERIALS

Two aqueous suspensions of custard and rice starch, and a solution of pig skin gelatin were used, with concentrations in the range 10%-40% wt/wt solids content. Gelatin and rice starch were supplied by BDH Chemicals Limited (England). Custard was Birds custard powder (a product of General Foods Ltd. (England)), the ingredients were, cornflour, salt, flavourings and colour (Annatto). Suspensions and solutions were made by mixing the desired amount of material in a fixed volume of distilled water. Suspensions of custard and starch were mixed continuously by means of a magnetic stirrer to ensure a homogeneous droplet was removed each time. This was most important for the suspensions, especially for highly concentrated samples. Too high a stirrer speed was not used to avoid problems of aeration of the feed. The

suspensions of starch and custard and the solution of gelatin were all kept at ambient temperature (~20 °C). Fresh suspensions/solutions were made up and used within 30 minutes to avoid changes in the water content.

Droplets of cooked (i.e. gelatinised) custard were also investigated; the gelatinisation temperature was in the range 60-65 °C. Samples were prepared by mixing the required amount of custard powder in a fixed volume of distilled water, which was then heated and mixed continuously with a magnetic stirrer until gelatinisation was achieved. The paste was then allowed to cool to the ambient temperature,i.e. ~20°C.

Droplet weight and temperature histories were measured in the manner described earlier. A droplet of suspension or solution of known solids content was suspended on the glass nozzle. The nozzle assembly was then immediately restored into the working section, suspended from the hook of the balance and rotated in the air flow at a steady speed of 15 r.p.m. At fixed increments of time, either the droplet weight or temperature was recorded. A range of air temperatures up to 198 °C was covered.

All the suspended droplets were hemispherical except those of the gelatinised (cooked) custard and gelatin. These tended to be cylindrical due to their high viscosities.

The drying droplets were all observed using the cathetometer. Droplets of gelatin were photographed with a 35mm Chinon camera to record their morphological changes under different drying conditions.

At the end of each experiment the crust formed on a particle was gently removed from the tip of the glass droplet suspension device and kept in a sealed dry tube to protect it from atmospheric humidity, then placed in a vacuum chamber and a thin film of gold-palladium deposited onto it by a spluttering technique. The coated sample was then introduced into the specimen chamber of the S.E.M. where it was observed on the Visual Display unit of the S.E.M. at a magnification up to 6000. Selected areas were photographed with a 35mm camera attached to the S.E.M.

7.5 DROPLETS OF AQUEOUS SOLUTIONS OF THE THIRD TYPE

Solutions of skim milk and fructose were freshly prepared by dissolving the desired amount of the skin forming material in a fixed volume of distilled water. Drying air temperatures were varied between 20-175 ^{o}C and the concentration range covered 10%-40% wt/wt.

A similar experimental procedure was then followed to that described in Section 7.4. Droplets in selected runs were photographed during drying using a 35mm Chinon camera to trace and record inflation/deflation events. Droplets were also observed using the cathetometer.

CHAPTER EIGHT

EXPERIMENTAL RESULTS

EVAPORATION OF PURE WATER DROPLETS

8.0 INTRODUCTION

8.1 WATER DROPLETS AT AMBIENT TEMPERATURE

8.2 WATER DROPLETS AT ELEVATED TEMPERATURES

EXPERIMENTAL RESULTS

EVAPORATION OF PURE WATER DROPLET

8.0 INTRODUCTION

The experimental results for water droplets are presented as Sherwood and Nusselt numbers calculated on the basis of equations 5.10 and 5.20, respectively. In these calculations corrections were made for heat transfer by conduction along the glass nozzle and by radiation. These additional heat input terms have been described in Sections 5.1.3 and 5.1.4.

8.1 WATER DROPLETS AT AMBIENT TEMPERATURE

The experimental results for the evaporation of water droplets at ambient temperature are presented in Appendix A.4.1 and summarised in Tables 8.1-8.2. These cover a Reynolds number range of 3-522. Figures 8.1 and 8.2 show the plot of Sh against $Re^{0.5}\ Sc^{0.33}$ and Nu against $Re^{0.5}\ Pr^{0.33}$ respectively.

The results were correlated according to the conventional equations.

$$Sh = 2.0 + \beta\ Re^{0.5}\ Sc^{0.33} \qquad \text{----------8.1}$$

$$Nu = 2.0 + \phi\ Re^{0.5}\ Pr^{0.33} \qquad \text{----------8.2}$$

A least squares-technique described in Appendix A.2.1 was used to correlate the results. The values of β and ϕ were found to be 0.575 and 0.552 respectively with correlation coefficients of 0.978 and 0.961 respectively, indicating a very good fit.

A computer programme (File name: PURE LIQ) written in Commodore Basic on a Commodore BBC Micro-Computer was used to analyse the experimental data. The programme is listed in Appendix A.3.1

TABLE 8.1 EVAPORATION OF WATER DROPLETS AT AMBIENT AIR TEMP.

UNITS

MEAN DIAMETER = mm
AIR VELOCITY = m/s
DROPLET & AIR TEMP. = C

SHERWOOD EQUATION = 2+0.575RE^.5*SC^.33
CORRELATION COEFF. =0.978

EXP NO	MEAN DIA.	AIR VEL.	REY NO.	AIR TEMP.	DROP TEMP.	SH EXP.	SH CORCT.	RE^.5*SC^.33
1	2.740	0.901	163.23	24.5	8	10.699	9.527	11.124
2	2.744	0.812	147.34	24.5	8	10.339	9.181	10.568
3	2.736	0.503	91.01	24.5	8	8.698	7.594	8.306
4	2.835	0.361	67.68	24.5	8	7.980	6.939	7.163
5	2.817	0.285	53.09	24.5	8	7.529	6.507	6.344
6	2.817	0.145	27.01	24.5	8	5.914	4.873	4.525
7	2.909	0.056	10.77	24.5	8	4.864	3.928	2.857
8	2.821	0.028	5.21	25.5	8.5	3.432	2.527	1.986
9	2.872	0.018	3.40	26	8.5	3.221	2.339	1.606
10	4.753	1.655	521.95	23.5	7.5	16.898	15.435	19.891
11	4.766	0.863	271.51	25	8	13.041	11.667	14.346
12	4.866	0.789	253.88	24.5	8	12.962	11.617	13.873
13	4.826	0.626	199.79	24.5	8	11.599	10.274	12.307
15	4.921	0.305	99.43	24	7.5	9.305	8.071	8.682
16	4.937	0.179	58.53	24	7.5	7.992	6.806	6.661
17	4.960	0.105	34.50	24	7.5	6.598	5.387	5.114
18	4.986	0.018	5.92	25.5	8.5	3.456	2.374	2.118
19	7.853	0.503	261.20	24.5	8	13.032	11.449	14.071
21	7.858	0.557	289.92	24	8	13.251	11.658	14.825
22	7.819	0.285	147.37	24.5	8	10.786	9.256	10.569
23	7.929	0.113	59.25	24.5	8	8.313	6.869	6.702
24	7.964	0.028	14.72	25	8	5.289	3.883	3.341
25	7.968	0.018	9.45	25.5	8.5	4.822	3.440	2.677

* Calculated values are as computed. The numbers are not intended to imply a greater degree of accuracy than is compatible with experimental procedures and discussed in Section 10.2.

TABLE 8.2 EVAPORATION OF WATER DROPLETS AT AMBIENT AIR TEMP.

UNITS

MEAN DIAMETER = mm
AIR VELOCITY = m/s
DROPLET & AIR TEMP. = C

NUSSELT EQUATION = 2+0.552RE^.5*PR^.33
CORRELATION COEFF. =0.961

EXP NO	MEAN DIA.	AIR VEL.	REY NO.	AIR TEMP.	DROP TEMP.	NU EXP.	NU CORCT.	RE^.5*PR^.33
1	2.740	0.901	163.23	24.5	8	10.603	9.432	11.371
2	2.744	0.812	147.34	24.5	8	10.247	9.089	10.803
3	2.736	0.503	91.01	24.5	8	8.655	7.551	8.490
4	2.835	0.361	67.68	24.5	8	7.909	6.868	7.322
5	2.817	0.285	53.09	24.5	8	7.474	6.451	6.485
6	2.817	0.145	27.01	24.5	8	5.862	4.820	4.626
7	2.909	0.056	10.77	24.5	8	4.835	3.899	2.921
8	2.821	0.028	5.21	25.5	8.5	3.388	2.483	2.031
9	2.872	0.018	3.40	26	8.5	3.072	2.190	1.641
10	4.753	1.655	521.95	23.5	7.5	16.893	15.430	20.333
11	4.766	0.863	271.51	25	8	12.573	11.199	14.665
12	4.866	0.789	253.88	24.5	8	12.846	11.501	14.181
13	4.826	0.626	199.79	24.5	8	11.495	10.170	12.580
15	4.921	0.305	99.43	24	7.5	9.043	7.809	8.875
16	4.937	0.179	58.53	24	7.5	7.751	6.566	6.809
17	4.960	0.105	34.50	24	7.5	6.438	5.227	5.227
18	4.986	0.018	5.92	25.5	8.5	3.417	2.334	2.165
19	7.853	0.503	261.20	24.5	8	12.972	11.389	14.384
21	7.858	0.557	289.92	24	8	13.226	11.632	15.154
22	7.819	0.285	147.37	24.5	8	10.631	9.101	10.804
23	7.929	0.113	59.25	24.5	8	8.239	6.795	6.851
24	7.964	0.028	14.72	25	8	5.092	3.686	3.415
25	7.968	0.018	9.45	25.5	8.5	4.767	3.385	2.736

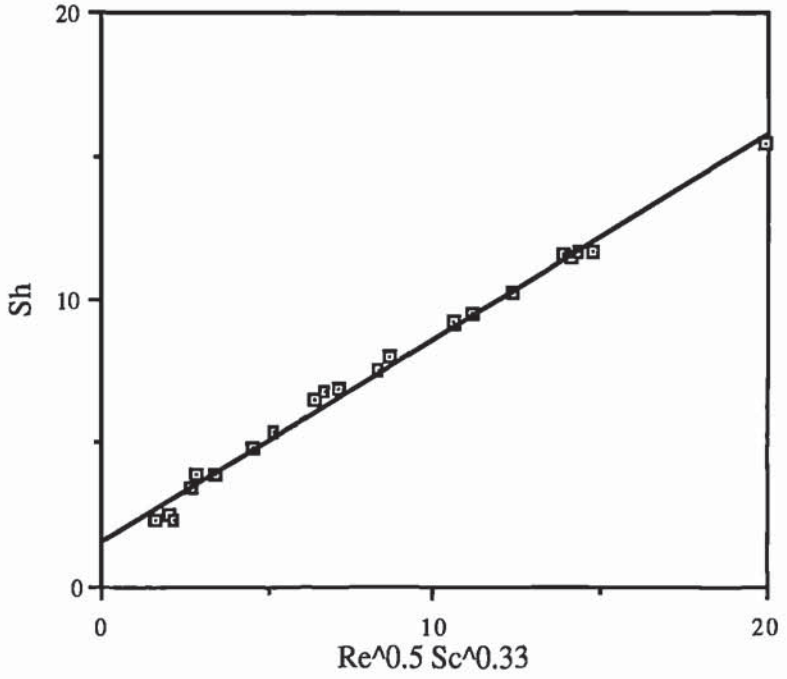

Figure 8.1 Plot of Sh Against Re^0.5 Sc^0.33 for Water Droplet at Ambient Air Temperature.

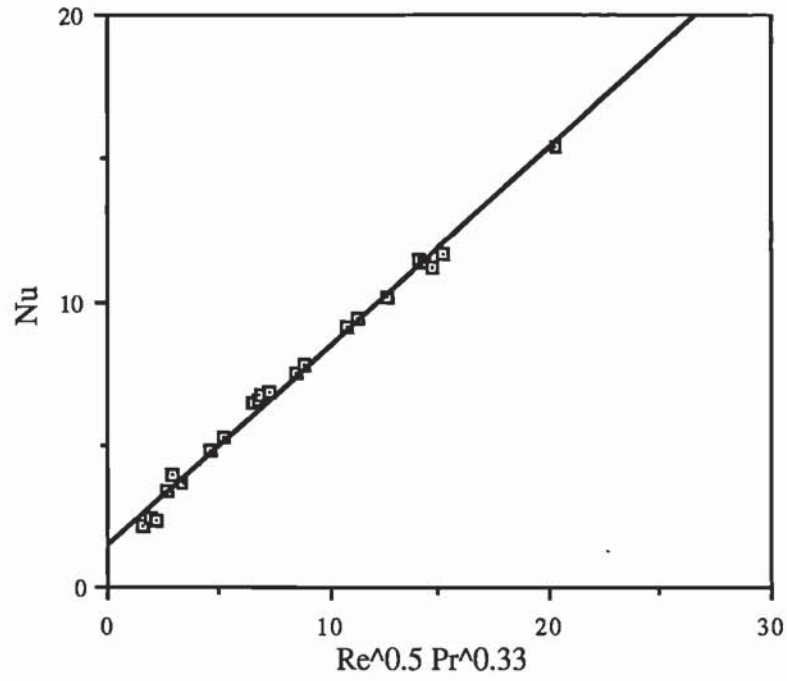

Figure 8.2 Plot of Nu Against Re^0.5 Pr^0.33 for Water Droplet at Ambient Air Temperature.

8.2 WATER DROPLETS AT ELEVATED TEMPERATURES

The experimental Sherwood and Nusselt numbers, were calculated for each droplet size during a run using equations 5.10 and 5.20 respectively. The instantaneous value of $d(d_p^2)/dt$ at each droplet size, obtained from a plot of d_p^2 against time, was used instead of a mean value for the run.

The results for the evaporation of water droplets at temperatures of 43.5, 67.0 and 80.0 ^oC are tabulated in Tables A26-A28 in Appendix A.4.2 and presented graphically in Figures 8.3-8.10.

A least squares technique was also used, as in the case for ambient temperature, to determine the values of β and ϕ in equations 8.1 and 8.2. The values of β and ϕ appear to vary with air temperature within a range $0.46 \leq \beta \leq 0.55$ and $0.44 \leq \phi \leq 0.53$. This has been observed by a number of investigators (7, 8, 10, 29).

Air Temperature (^oC)	β
43.5	0.55
67.0	0.52
80.0	0.46

Table 8.3 Values of β for Water Droplets at Elevated Air Temperatures

Air Temperature (^{o}C)	ϕ
43.5	0.53
67.0	0.51
80.0	0.44

Table 8.4 Values of ϕ for Water Droplets at Elevated Air Temperatures

Hoffman and Gauvin (17) concluded that the relatively cold vapours leaving the droplet surface can seriously reduce the heat transfer rate to it. They stated that the effect of evaporation rate on heat transfer to droplets is dependent on the magnitude of Spalding's Transfer Number $B=C_p\Delta T/\lambda$.

The results were therefore correlated by taking the sensible heat into account. Using the equation for Sherwood number proposed by Audu (10) and that proposed by Cheong (8) for Nusselt number.

$$Sh = 2.0 + \beta \left(\frac{T_a - T_s}{T_{amb}}\right)^{n} Re^{0.5} Sc^{0.33} \qquad \text{---------8.3}$$

$$Nu = 2.0 + \phi \, (1 / B)^{m} Re^{0.5} Pr^{0.33} \qquad \text{---------8.4}$$

where $B = C_p \Delta T / \lambda$

A least squares correlation technique, described in Appendix A.2.2 was used to correlate the data according to the above equations. The resulting correlations were,

$$Sh = 2.0 + 0.575 \left(\frac{T_a - T_s}{T_{amb}}\right)^{-0.04} Re^{0.5} Sc^{0.33} \qquad \text{---------8.5}$$

Table 8.5 Evaporation of Water Droplets at Elevated Temperature

Air Temperature =43.5 ^{o}C

Droplet Temperature=15.5^{o}C

Time (sec)	Reynolds Number Re	Experimental Sherwood Number Sh(exp)	Corrected Sherwood Number Sh(corctd)	Experimental Nusselt Number Nu(exp)	Corrected Nusselt Number Nu(corctd)	$Re^{0.5}$ $Sc^{0.33}$	$Re^{0.5}$ $Pr^{0.33}$
0	348.760	13.463	12.565	12.518	11.620	16.422	16.402
34	320.860	13.165	12.234	12.241	11.310	15.752	15.733
106	272.030	12.423	11.409	11.552	10.537	14.504	14.486
174	216.230	11.844	10.666	11.013	9.835	12.931	12.915
258	160.430	11.316	9.830	10.522	9.036	11.138	11.125
296	128.34	11.060	9.260	10.284	8.484	9.962	9.950
329	101.140	10.651	8.415	9.904	7.668	8.844	8.833
342	91.380	10.566	8.107	9.824	7.365	8.406	8.396

Table 8.6 Evaporation of Water Droplets at Elevated Temperature

Air Temperature =67.0 °C

Droplet Temperature=25.0°C

Time (sec)	Reynolds Number Re	Experimental Sherwood Number Sh(exp)	Corrected Sherwood Number Sh(corctd)	Experimental Nusselt Number Nu(exp)	Corrected Nusselt Number Nu(corctd)	$Re^{0.5}\ Sc^{0.33}$	$Re^{0.5}\ Pr^{0.33}$
0	325.440	12.269	11.316	12.184	11.231	16.158	15.737
28	290.940	11.973	10.974	11.889	10.890	15.278	14.880
88	236.920	11.230	10.115	11.152	10.037	13.787	13.428
159	166.620	10.389	8.961	10.317	8.888	11.562	11.261
234	104.140	9.895	7.759	9.826	7.690	9.140	8.902
265	71.600	9.890	6.857	9.821	6.788	7.579	7.382

Table 8.7 Evaporation of Water Droplets at Elevated Temperature

Air Temperature =80.0 °C

Droplet Temperature=28.5°C

Time (sec)	Reynolds Number Re	Experimental Sherwood Number Sh(exp)	Corrected Sherwood Number Sh(corctd)	Experimental Nusselt Number Nu(exp)	Corrected Nusselt Number Nu(corctd)	$Re^{0.5}$ $Sc^{0.33}$	$Re^{0.5}$ $Pr^{0.33}$
0	312.530	10.925	9.946	10.665	9.685	16.029	15.362
14	279.410	10.569	9.544	10.317	9.292	15.156	14.525
62	215.650	9.896	8.716	9.660	8.480	13.315	12.761
115	151.890	9.381	7.861	9.158	7.638	11.174	10.710
155	104.390	8.985	6.891	8.771	6.677	9.264	8.878
193	68.760	8.827	5.738	8.617	5.528	7.518	7.206

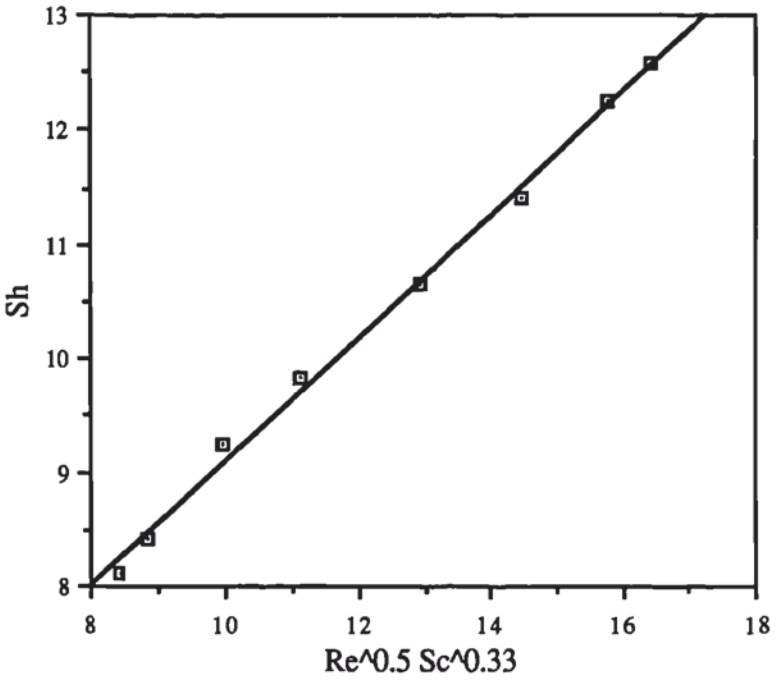

Figure 8.3 Plot of Sh Against Re^0.5 Sc^0.33 for Water Droplets at 43.5°C

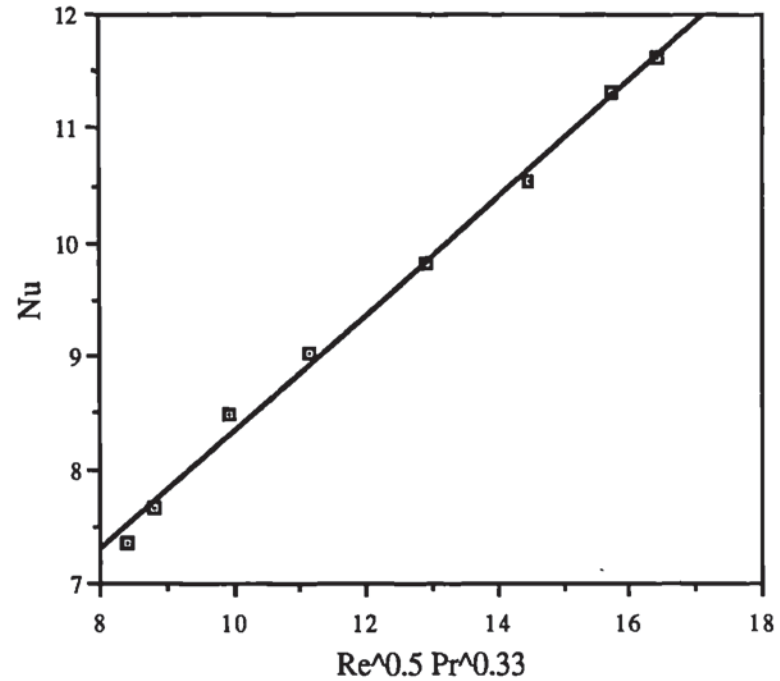

Figure 8.4 Plot of Nu Against Re^0.5 Pr^0.33 for Water Droplets at 43.5°C

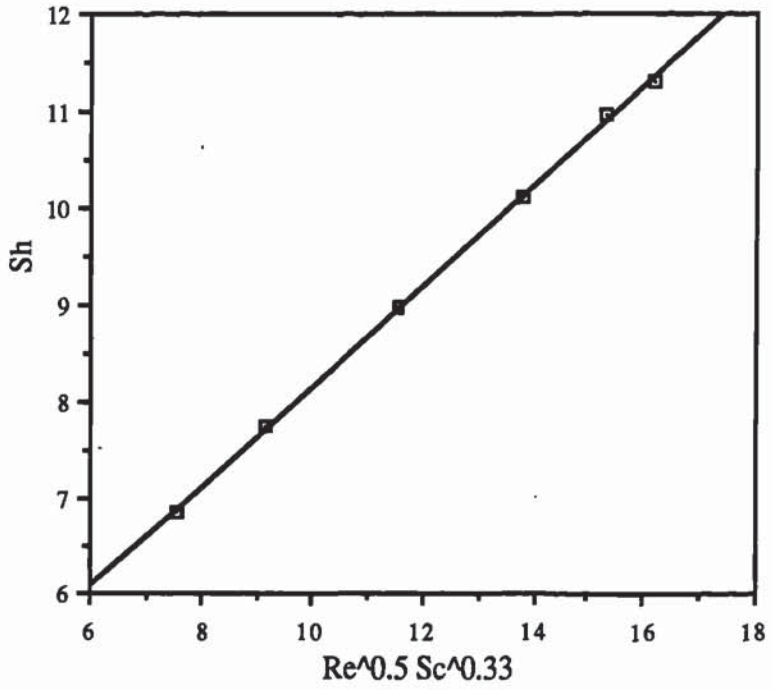

Figure 8.5 Plot of Sh Against Re^0.5 Sc^0.33 for Water Droplets at 67°C

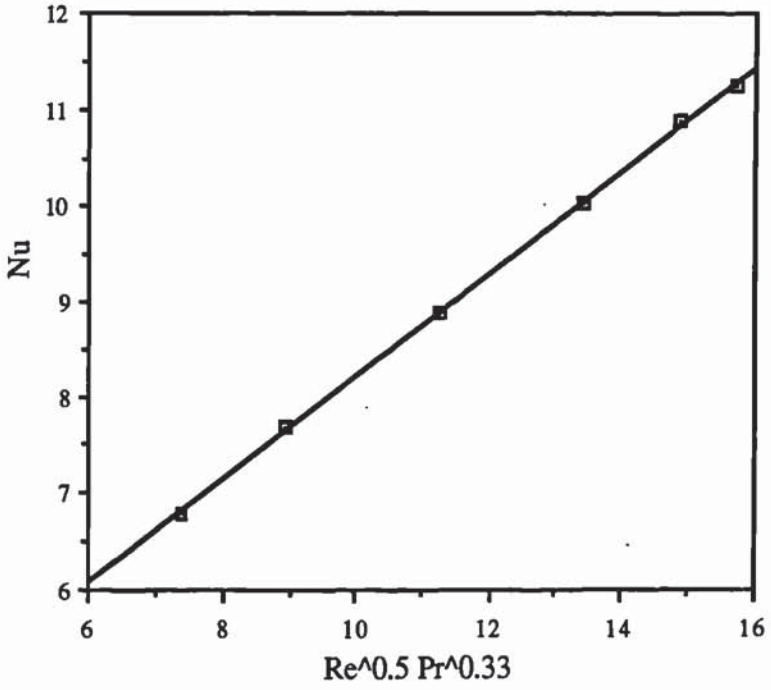

Figure 8.6 Plot of Nu Against Re^0.5 Pr^0.33 for Water Droplets at 67°C

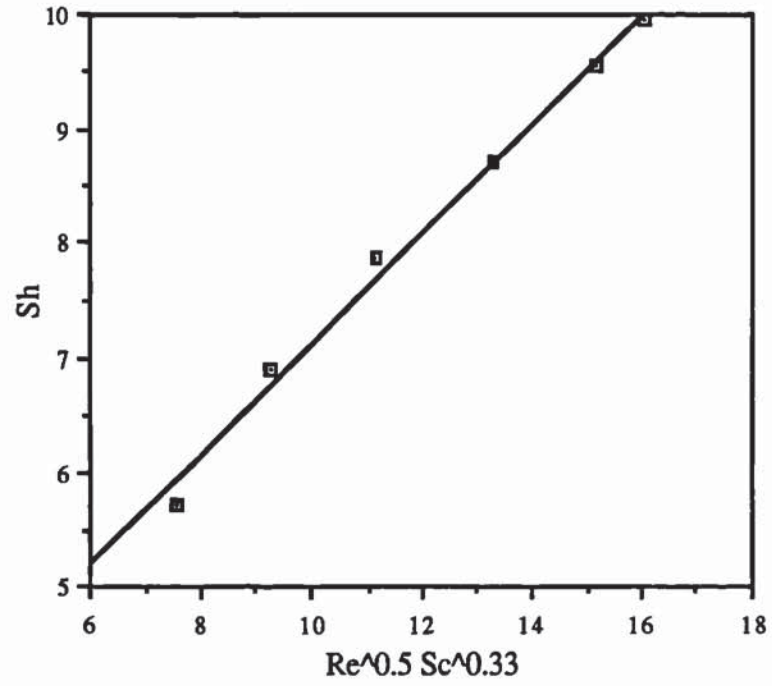

Figure 8.7 Plot of Sh Against Re^0.5 Sc^0.33 for Water Droplets at 80°C

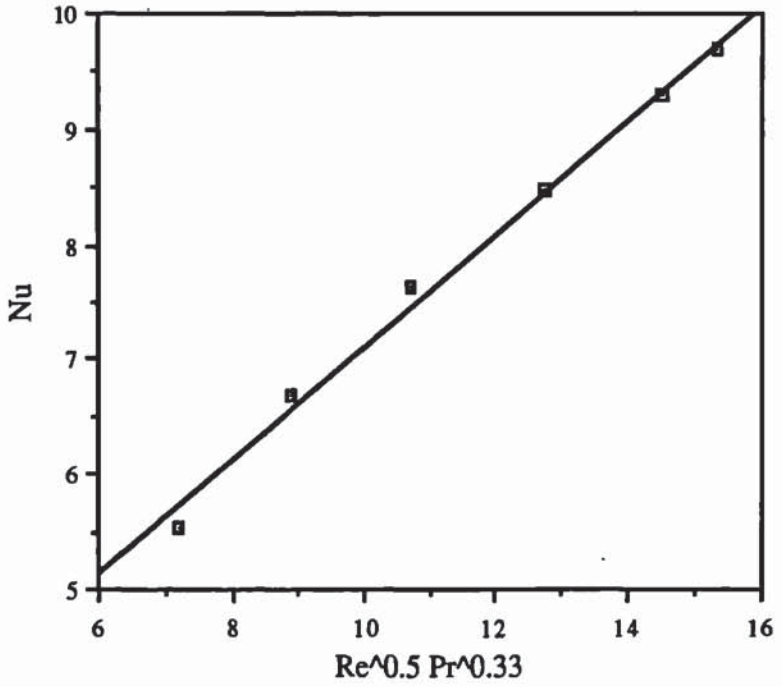

Fihure 8.8 Plot of Nu Against Re^0.5 Pr^0.33 for Water Droplets at 80°C

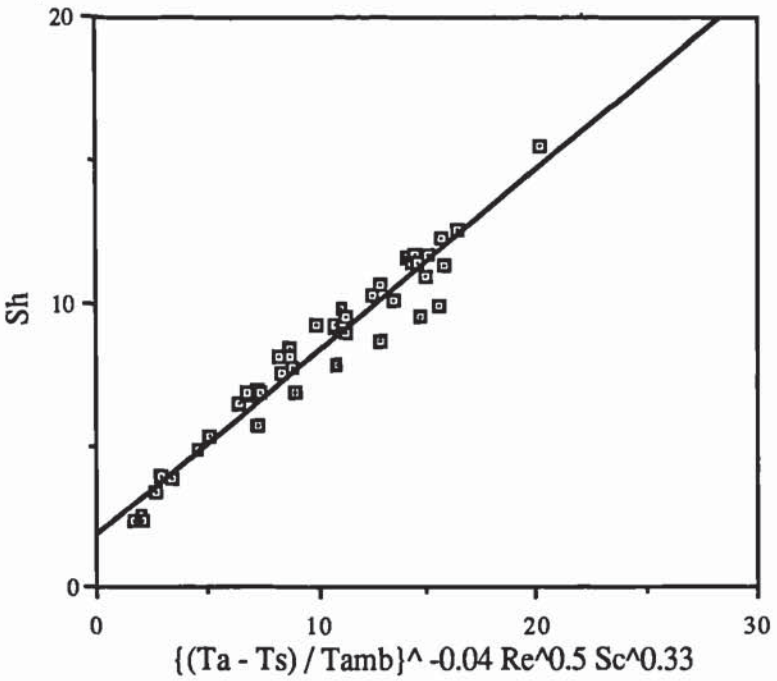

Figure 8.9 Plot of Sh Against {(Ta - Ts) / Tamb}^nRe^0.5 Sc^0.33 for Water Droplets Between 23-80°C

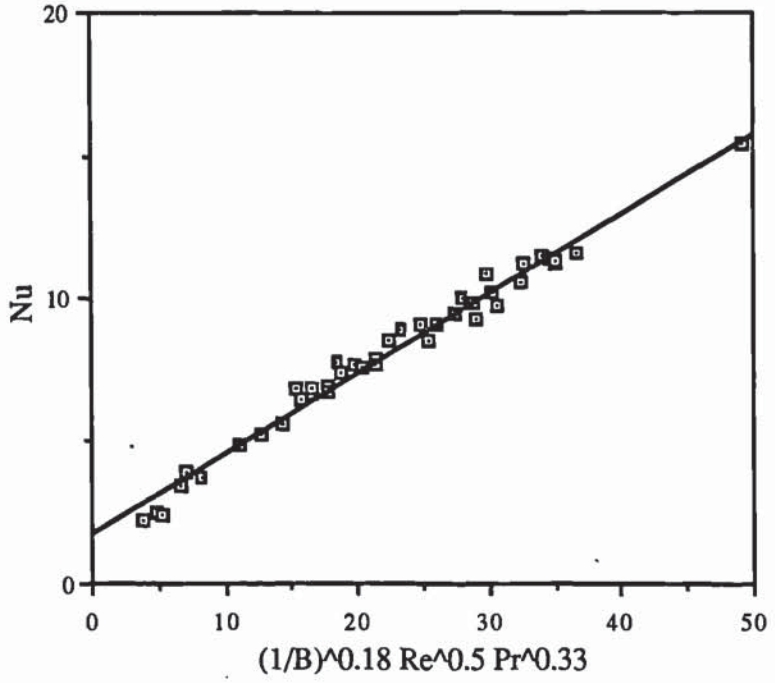

Figure 8.10 Plot of Nu Against (1/B)^0.18 Re^0.5 Pr^0.33 for Water Droplets Between 23-80°C

$$Nu = 2.0 + 0.27 \left(\frac{1}{B}\right)^{0.18} Re^{0.5} Pr^{0.33} \qquad \text{----------8.6}$$

Figures 8.9 and 8.10 show plots of Sh against $\{(T_a-T_s)/Tamb\}^{-0.04}Re^{0.5}Sc^{0.33}$ and Nu against $(1/B)^{0.18}Re^{0.5}Pr^{0.33}$. The correlation coefficients are 0.96 for equation 8.5 and 0.98 for equation 8.6, indicating a very good fit.

CHAPTER NINE

EXPERIMENTAL RESULTS-DRYING OF DROPLETS OF SKIN FORMING MATERIALS

9.0 INTRODUCTION

9.1 DROPLETS OF THE FIRST TYPE

9.1.1 DROPLETS OF CUSTARD SUSPENSION

9.1.1.1 Effect of Initial Concentration

9.1.1.2 Effect of Air Velocity

9.1.1.3 Effect of Air Temperature

9.1.1.4 Effect of Nature of Custard

9.1.2 DROPLETS OF STARCH SUSPENSION

9.1.2.1 Effect of Initial Concentration

9.1.2.2 Effect of Air Velocity and Air Temperature

9.2 DROPLETS OF THE SECOND TYPE

9.2.1 DROPLETS OF GELATIN SOLUTION

9.2.1.1 Effect of Initial Concentration

9.2.1.2 Effect of Air Velocity

9.2.1.3 Effect of Air Temperature

9.3 DROPLETS OF THE THIRD TYPE

9.3.1 DROPLETS OF SKIM MILK SOLUTION

9.3.1.1 Effect of Initial Concentration

9.3.1.2 Effect of Air Velocities

9.3.1.3 Effect of Air Temperature

9.3.2 DROPLETS OF FRUCTOSE SOLUTION

9.3.2.1 Effect of Initial Concentration

9.3.2.2 Effect of Air Velocity

9.3.2.3 Effect of Air Temperature

9.4 MATHEMATICAL MODEL PREDICTIONS

EXPERIMENTAL RESULTS-DRYING OF DROPLETS OF SKIN FORMING MATERIALS

9.0 INTRODUCTION

Single droplets of three different types of skin-forming material were investigated. These are thought to cover all types of skin forming material. The materials investigated were of three characteristic types, namely;

1) First type: Droplets of custard or starch suspension, with solids contents in the range 20%-40% wt/wt. These materials were selected since on drying they form a skin due to swelling, or gelatinisation of, the custard or starch granules at high drying temperatures i.e. > gelatinisation temperatures. At lower drying temperatures (< gelatinisation temperatures) they form a normal porous crust. After gelatinisation at high drying temperatures the dried crust loses the properties and structure of the the original powder e.g. the ability to swell or gelatinise on dispersion in water to form a suspension.
2) Second type: Droplets of gelatin solution containing up to 40% wt/wt solids. At drying temperatures < 60 ^{o}C this material forms a dry sheath which behaves like a skin in resisting mass transfer immediately after drying has taken place. At higher temperatures a more resistant dry skin forms on the droplet surface. Final crusts dried under these conditions irreversibly lose the properties and structure of the original powder e.g. the ability to absorb water on dissolution in warm water at temperatures $\geq$ 30 ^{o}C.
3) Third type: Droplets of skim milk or fructose solutions containing solids in the range 20%-40% wt/wt. These materials form a skin at some stage, under any drying conditions. The dried crust has the same properties and structure as the original powder (e.g. dissolution in water) unless the material is dried at very high drying temperatures (> 300 ^{o}C).

Investigations covered variations in the initial solids content, air velocity, air temperature and the nature of the skin forming material. The measured weights were corrected for radiation and heat conduction along the nozzle. The weight correction was expressed as,

$$Wc = ({}^{q}n + {}^{q}e) / (\lambda) \qquad \text{----------9.1}$$

where ${}^{q}n$ and ${}^{q}e$ are the total amount of heat transferred through the nozzle by conduction and by radiation respectively. For a finite change in time Δt, mean droplet diameters and temperatures are justified. Therefore,

$$q_n = \frac{\Delta t\, \pi}{2} \left[\frac{k_t\, d_f^3}{5} \{ 2\sigma\, e\, s\, (T_{sm}^5 - T_a'^5) - 10\, \sigma\, e\, s\, T_a^4 (T_{sm} - T'_a) + 5\, h_f (T_{sm} - T_a)^2 \} \right]^{0.5} \text{---9.2}$$

and

$$q_e = \sigma\, es\, \pi\, d^2_{pm}\, (T^4_a - T^4_{sm}) \qquad \text{----------9.3}$$

where T'_{sm} and d_{pm} are the mean droplet temperature and diameter respectively in Δt.

The calculated weight correction from equation 9.1 was added to the measured weight at the end of each time interval to give the corrected droplet weight. The results of the drying rates and core temperatures are tabulated in Appendices B and C respectively.

The experimental results are presented as droplet weight and core temperature histories. The weight history is presented in two ways;

a) As fractions of initial weight evaporated. This was used to smooth out any slight variations in the initial weights of the droplets. The effects of experimental variables e.g. initial solids content in the droplet, air velocity and air temperature can be easily obtained from these plots.

b) Drying rate curves. This enabled the various drying periods, e.g. the constant rate

and the falling rate periods, to be easily determined. The rate history is presented together with the core temperature history to demonstrate their inter-relationship.

9.1 DROPLETS OF THE FIRST TYPE

Custard and starch are typical examples of the first type of skin-forming material. The granules are quite insoluble in cold water, but swell in warm water (95). When an aqueous suspension of custard or starch is heated or mixed with hot water the granules swell enormously i.e. the volume of the granules increases by approximately 50-100%. The swelling is reversible until the "gelatinisation temperature" when material is leached from the granules and structural order is irreversibly lost. If the temperature of the aqueous suspension is raised above the gelatinisation range, the granules continue to swell and become more distorted.

Drying of an aqueous suspension of custard or starch at low drying air temperature (< 50 ^{o}C) results in no swelling or gelatinisation of the granules. Therefore a normal porous crust is formed and the granule's structure and properties are the same as prior to drying. Conversely drying at a high temperature leads to swelling of the granules and their structure and properties differ. Under these drying conditions a skin forms on the droplet surface which offers a very high resistance to mass transfer.

When an aqueous suspension of custard or starch is dried by hot dry air (>150 ^{o}C) at high velocity, a substantial amount of water will be evaporated before the droplet core temperature reaches the gelatinisation temperature. This will cause a great reduction in the swelling capacity and number of swollen granules. However, if the air velocity is low (0.1-0.2 m/s), enough water will remain in the droplet for perfect granule gelatinisation. This means that sufficient water should be available to obtain perfect gelatinisation and to avoid thermal degradation of the granules. Therefore the higher the air velocity the lower the degree of swelling and the swelling is reversible unless the amount of water available in the droplet at the gelatinisation temperature is enough for perfect gelatinisation.

In the drying of aqueous suspensions, swelling of the granules leads to a

major reduction in the rate of drying. This results since crust porosity is greatly reduced by swollen granules closing the pores which existed before swelling; in the case of perfect gelatinisation there is a complete transformation from a normal crust resistance to a skin resistance i.e a much higher resistance to mass transfer.

The different drying conditions i.e. air temperatures and velocities, solids concentrations and the nature of the solid, all of which affect the swelling or gelatinisation of the granules of custard or starch and hence the drying rate, are discussed in this section.

9.1.1 DROPLETS OF CUSTARD SUSPENSIONS

9.1.1.1 Effect of initial concentration

Figures 9.1 and 9.2 show the effect of the initial concentration on the rate of drying, for the same initial droplet size (all droplets were, as summarised in Appendices B and C, of 5mm diameter +/- 10%) at air temperatures of 20 ^{o}C and 54 ^{o}C respectively. These demonstrate that the initial concentration had little effect on the initial drying rate. This is because the solid custard was suspended in water and therefore had no effect in lowering the vapour pressure. However the rates diverge once a crust had formed on the surface of the droplet, since a higher initial solids content leads to a more rapid, thicker crust formation.

9.1.1.2 Effect of Air Velocity

Figure 9.3 shows the effect of air velocity upon the drying rate at 20% weight initial concentration. The curve gradients, show that doubling the air velocity from 0.49 m/s to 0.96 m/s led to a similar two-fold increase in the drying rate. However after about 500 seconds the drying rate at the lower velocity became very low and almost stopped although the droplet's moisture content at this stage was significant (> 25% of the initial moisture content). This arose because the custard granules underwent swelling under lower velocity conditions i.e. the lower evaporation rate resulted in a greater amount of water remaining in the droplet which resulted in the granules swelling.

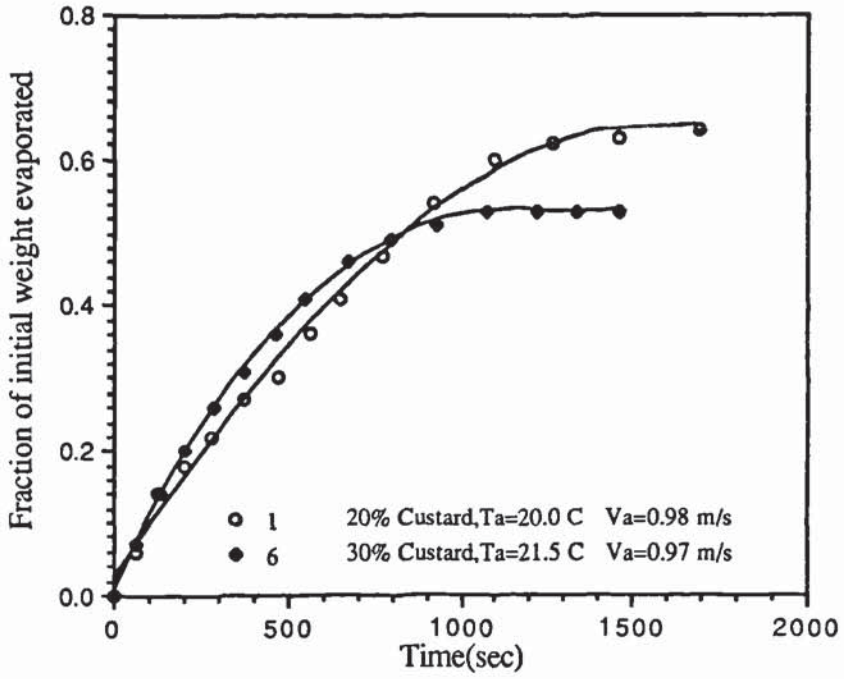

Figure 9.1 Drying of Droplets of Custard Suspension at Various Initial Concentrations.

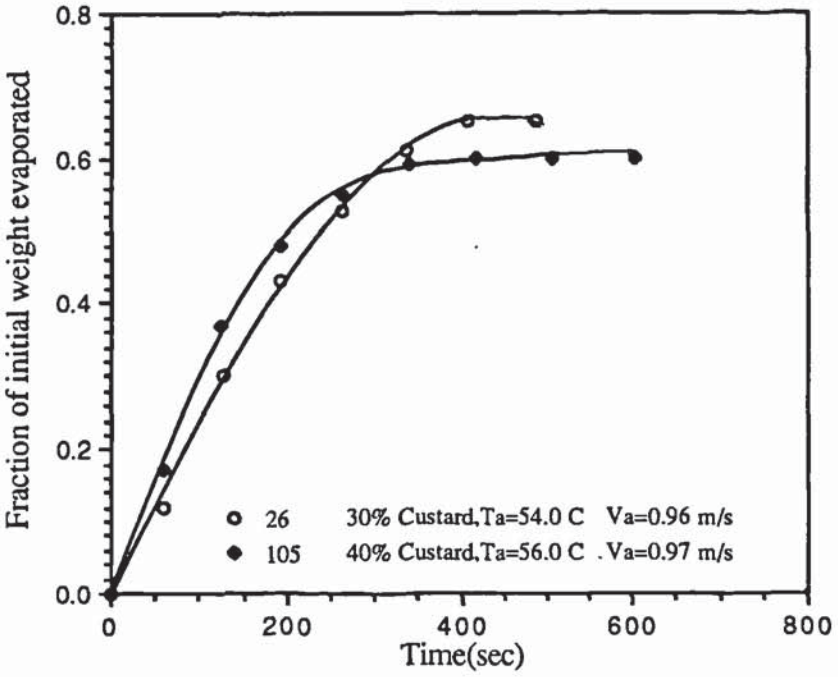

Figure 9.2 Drying of Droplets of Custard Suspension at Various Initial Concentrations.

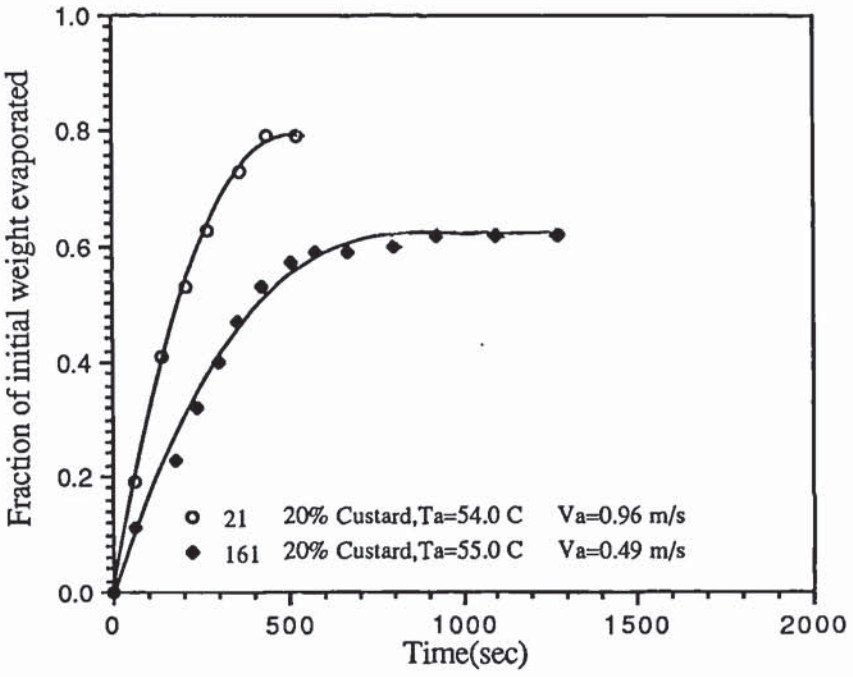

Figure 9.3 **Drying of Droplets of Custard Suspension (20% wt/wt) at Various Air Velocities.**

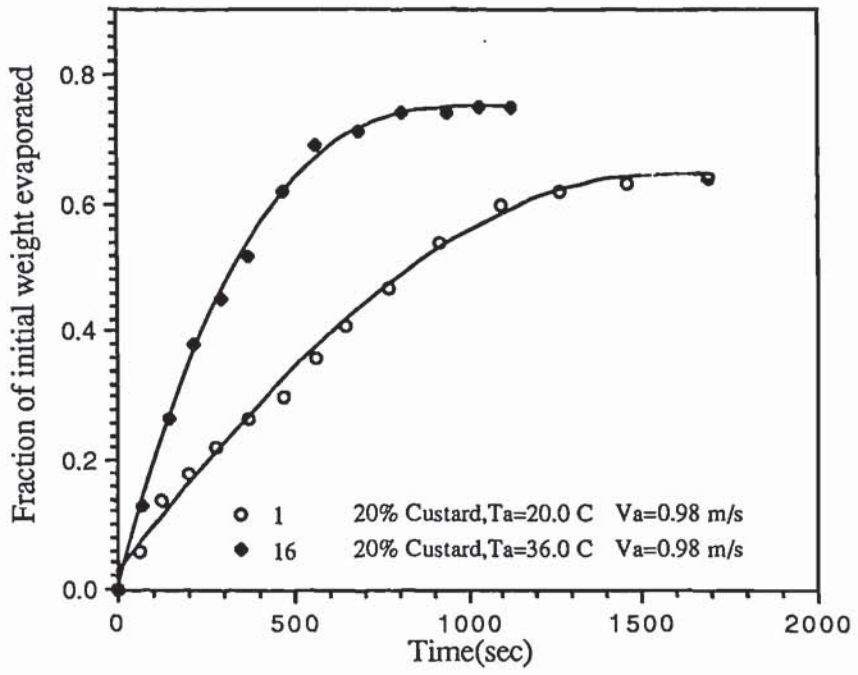

Figure 9.4 **Drying of Droplets of Custard Suspension (20% wt/wt) at Various Air Temperatures.**

As a result the crust resistance to mass transfer was significantly increased. Thus lower velocity conditions are more convenient for the granules to swell.

9.1.1.3 Effect of Air Temperature

Figures 9.4, 9.5 and 9.6 show the effects of air temperature upon the drying rate at 20% weight initial concentration. The gradients of the curves, show that the rate of drying increased by a factors of 3, 1.5 and < 1.5 when the air temperature was increased from 20 °C to 36 °C, 54 °C to 91 °C and 76 °C to 106 °C respectively. In the first case, as the air temperature was low, a porous crust was formed with no swelling of the granules. Under these conditions this porous crust provided little resistance to mass transfer. In the second and third cases as the air temperature was increased the custard granules swelled, became pliable and adhered together and thus blocked the pores. Therefore the crust became more significant as it provided an increased resistance to mass transfer. Therefore increasing the air temperature led to a thicker less porous crust (due to granules swelling), and the crust resistance became more significant. All these features are associated with the granules swelling; the higher the air temperature the higher the degree of swelling and thus the higher the resistance to mass transfer. Subsequently, as shown in Figures 9.5 and 9.6, the rate at the higher air temperature diverged after about 250 seconds at 91 °C leaving > 12% of the initial moisture in the core and, after about 180 seconds at 106 °C with > 25% of the initial moisture retained in the core. These results confirm the increasing resistance of the crust to vapour diffusion with an increase in the air temperature.

The swelling or gelatinisation of the granules led to a change in the resistance to vapour diffusion from an ordinary crust to a skin. The higher the air temperature and the lower the air velocity the greater was this degree of change. At an air temperature of 198 °C and a velocity of 0.1 m/s a complete change occurred from a crust resistance to a skin. A smooth surface on the dried crust and inflation/deflation effects were observed under these conditions which are a characteristic of a skin-forming mechanism.

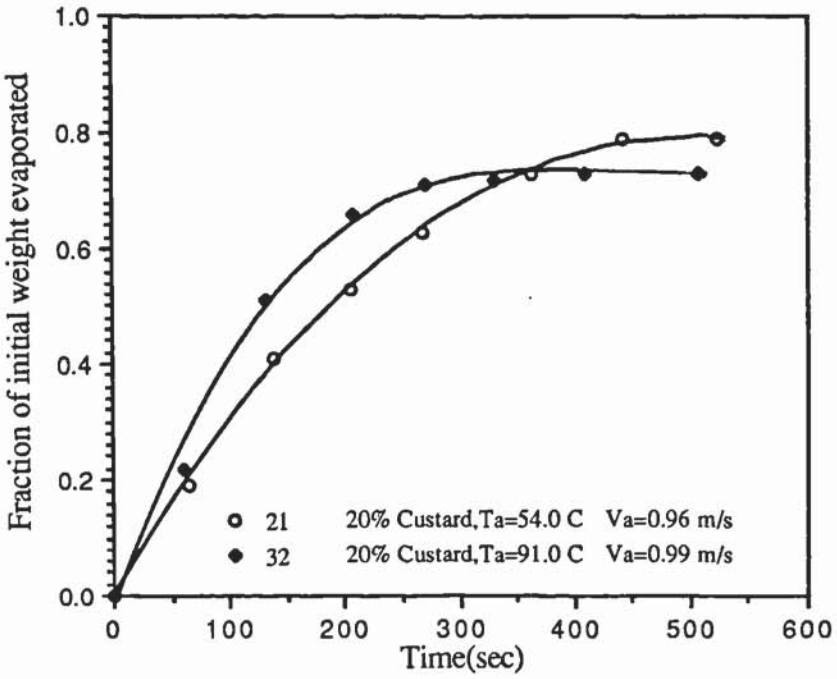

Figure 9.5 Drying of Droplets of Custard Suspension (20% wt/wt) at Various Air Temperatures.

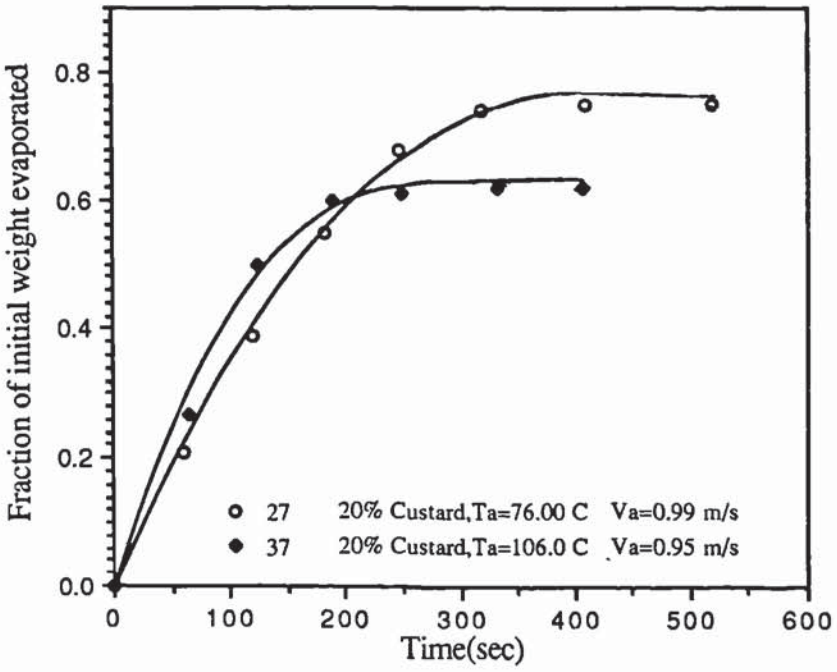

Figure 9.6 Drying of Droplets of Custard Suspension (20% wt/wt) at Various Air Temperatures.

Rate of drying and core temperatures are shown in Figures 9.10, 9.11 and 9.12, and further illustrate the effects of increasing air temperature. Figure 9.10, at 36 ^{o}C, shows that after establishment of a drying rate a very short constant rate period followed. This is reflected in the core temperature measurements. The droplet temperature initially fell to the wet-bulb temperature and remained at this temperature for a very short time before gradually rising to the air temperature as the rate of drying proceeded to fall gradually.

At higher air temperatures, i.e. 54 ^{o}C (Figure 9.11) and 76 ^{o}C (Figure 9.12) higher rates of drying were established but no constant rate period was observed. At 54 ^{o}C, upon establishment of a drying rate, the rate started to fall gradually during the first 300 seconds; it then began to fall rapidly due to crust formation as the core temperature proceeded to rise rapidly to the air temperature. At 76 ^{o}C the rate began to fall rapidly immediately after establishment of a drying rate. This is reflected in the core temperature measurements. The droplet temperature started to increase immediately the droplet contacted the hot air stream. It rose very rapidly to the air temperature. These results confirm that, as would be expected, an increase in the air temperature had a pronounced effect on the drying rate.

The electron microphotographs of the crust structure (Plate 9.1 a-d) highlight the increase in crust resistance with an increase of air temperature. (For all the electron microphotographs, at the top of each picture, the first number from the left represents the magnification, e.g. this number in plate 9.1 a is 1,09 KX which means the magnification is 1009. Underneath this number is the graticule from which, the appropriate magnification can be obtained. Finally S is the experiment reference number). Plate 9.1 represents the crust structure for a 20% weight initial concentration custard suspension dried at 20 ^{o}C and 106 ^{o}C. Plates 9.1 a and b highlight the porous nature of the crust. These Plates represent the custard crusts drying at ambient air temperature and different air velocities of 0.98 m/s and 0.49 m/s. Plates 9.1 c and d clearly show the decrease in the crust porosity due to gelatinisation. The custard granules are swollen and stuck to each other, resulting in a significant reduction in the

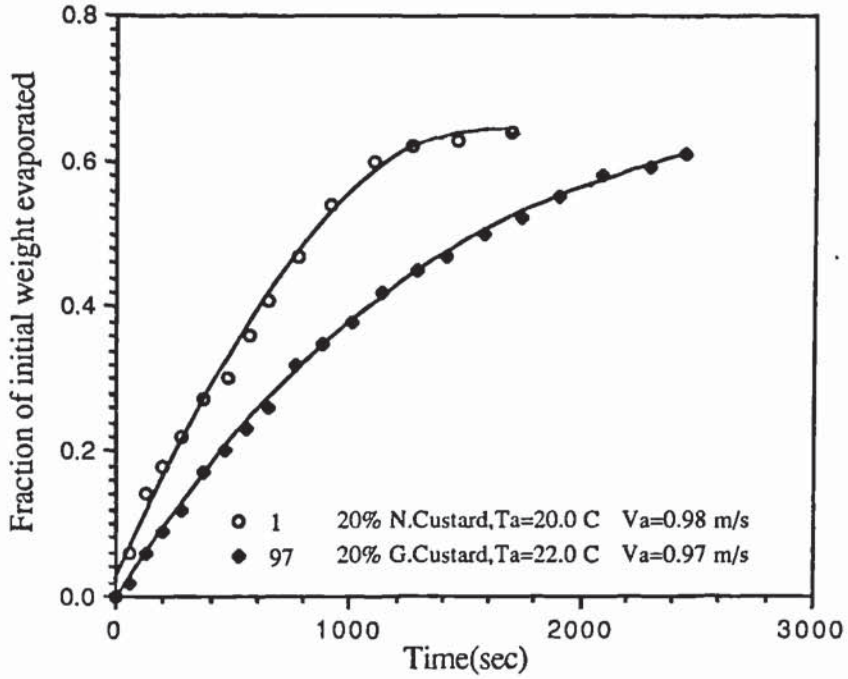

Figure 9.7 Effect of the Nature of Custard on the Drying Rate.

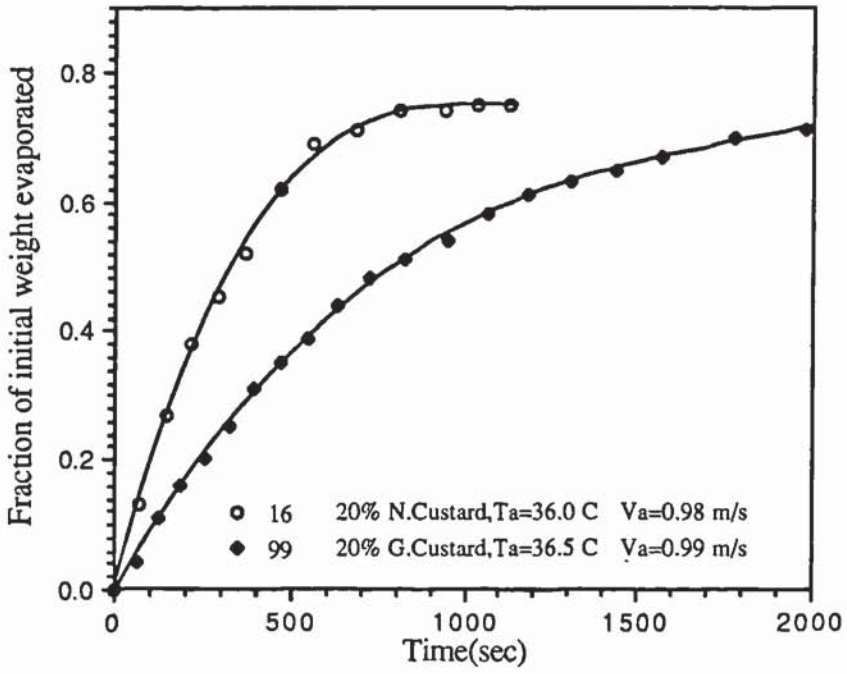

Figure 9.8 Effect of the Nature of Custard on the Drying Rate.

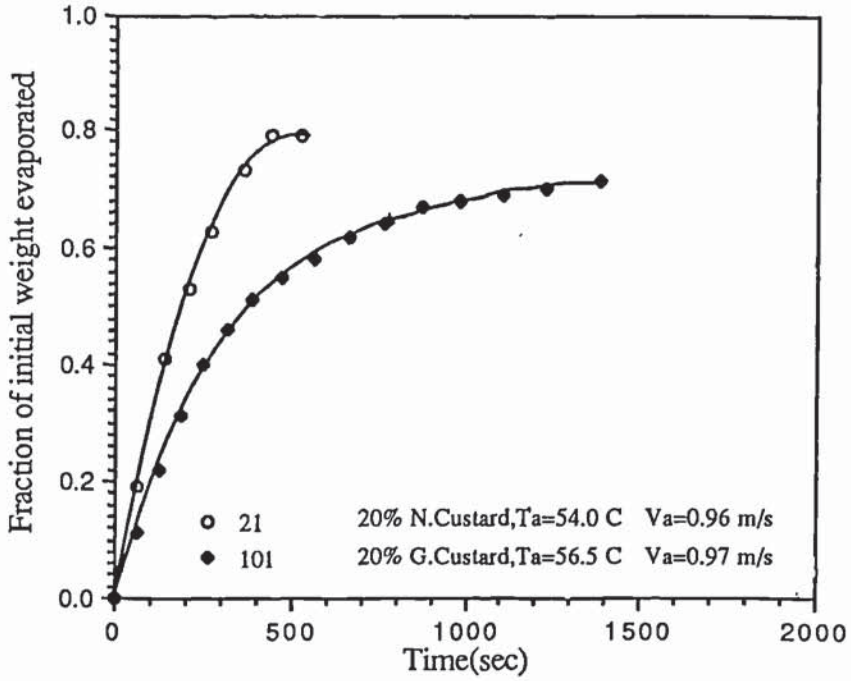

Figure 9.9 Effect of the Nature of Custard on the Drying Rate.

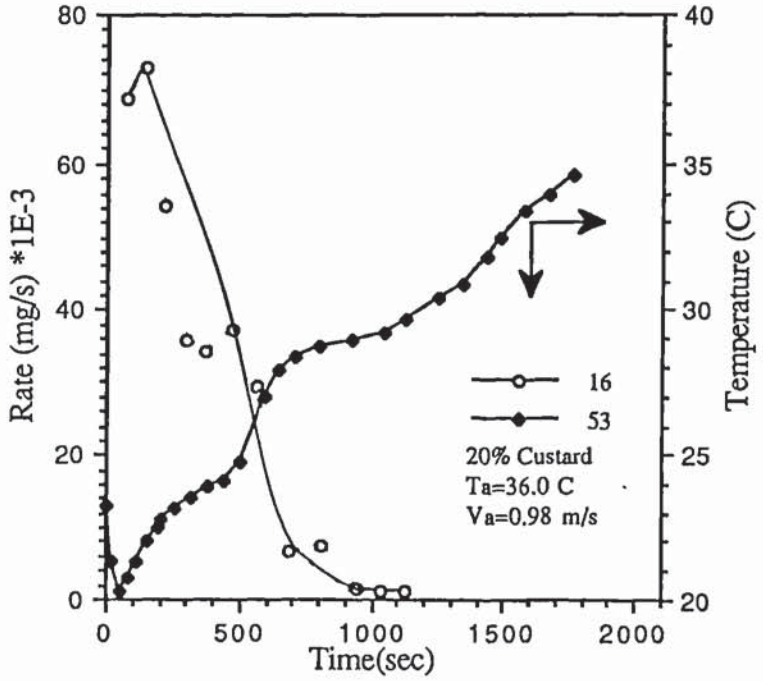

Figure 9.10 Core Temperature and Drying Rate Histories for Custard Suspension (20 wt/wt) at 36 °C

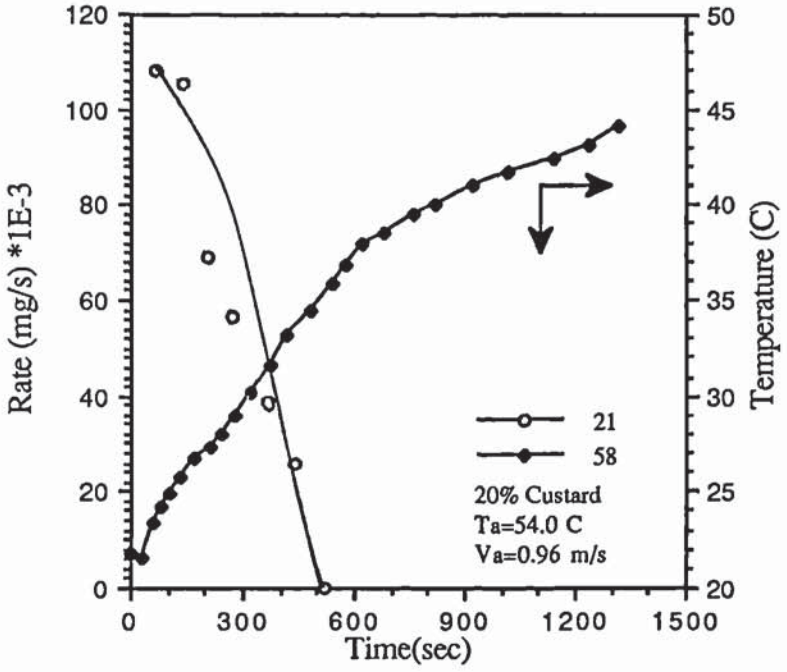

Figure 9.11 Core Temperature and Drying Rate Histories For Custard Suspension (20% wt/wt) at 54°C

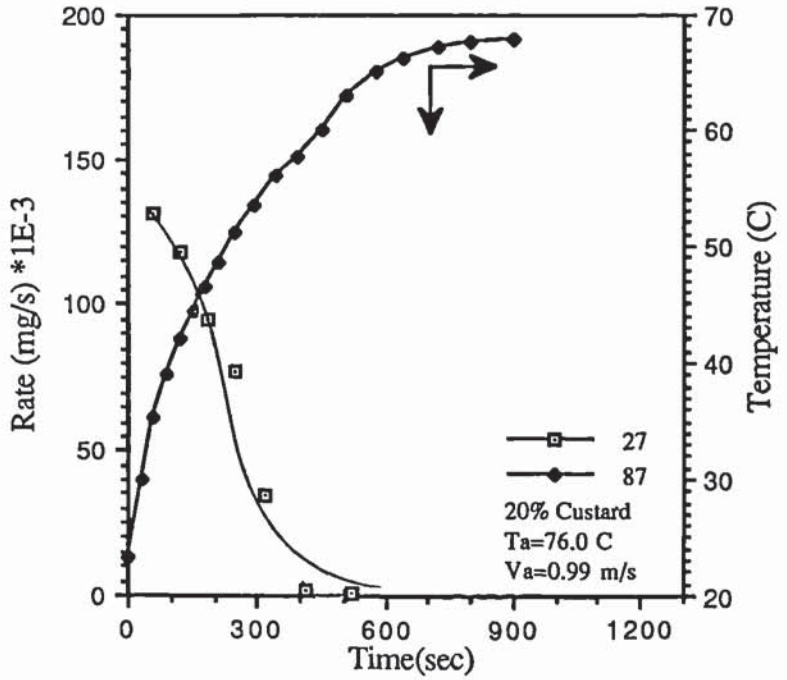

Figure 9.12 Core Temperature and Drying Rate Histories for Custard Suspension (20% wt/wt) at 76°C

crust porosity. There are several major cracks on the outer crust surface which confirms the reduction in the crust porosity. Plate 9.2 shows the outer crust structure of gelatinised custard paste (cooked custard); a skin was formed on the droplet surface, since it was smooth and contained no pores. Plates 9.3 a-d show the structure of the external and internal crust for 20% weight solids content custard suspension dried at high temperatures of 160 ^{o}C-198 ^{o}C and low air velocity of 0.1 m/s. These Plates highlight the distortion of the granules due to gelatinisation which is increased with increasing air temperature. Furthermore the resistance to mass transfer by pore diffusion increased when the air temperature was increased, since a smoother outer surface was formed, which resulted from more distorted granules due to a higher degree of swelling. The cracks on the external surface in Plate 9.3 c and d confirm this; their numbers and diameters increased with increasing air temperature. In Plate 9.3 c (179 ^{o}C) most of the recognizably discrete granules are the small granules of diameter of less than $17x10^{-6}$ m, while in Plate 9.3 d (198 ^{o}C) it is very difficult to find any discrete granules(i.e. there was total distortion at this high temperature). This suggests that larger granules may gelatinise more readily than smaller ones.

At the high drying temperature of 198 ^{o}C and low velocity of 0.1 m/s a drying droplet inflated and then deflated once or twice; it then remained at the same shape and size. This is characteristic of skin forming materials. Therefore under these conditions when the air velocity was low, the evaporation rate during the first period (i.e. prior to granules gelatinisation) was very low. This was because during this period the gas film represents the major resistance to mass transfer. This will lead to enough water being retained in the droplet to allow the granules to gelatinise completely; only the smallest granules of diameter of $< 6.5 \times 10^{-6}$ m can still be recognised as granules. This resulted in a complete transformation from a crust resistance to a skin under these severe drying conditions.

9.1.1.4 Effect of the Nature of Custard

Figures 9.7, 9.8 and 9.9 demonstrate a comparison between the drying rates

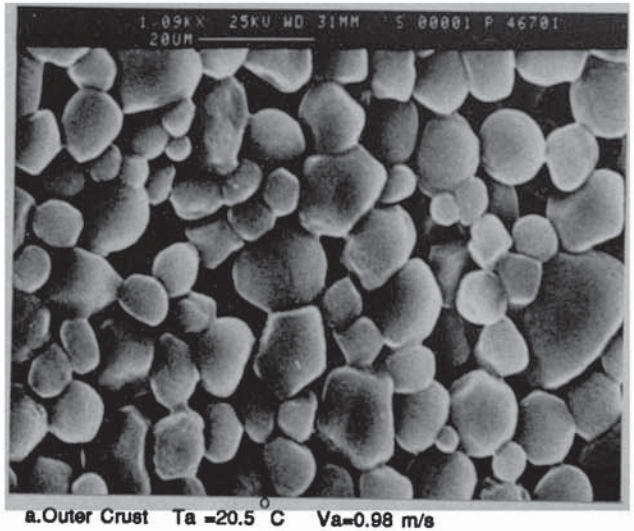

a.Outer Crust Ta =20.5 °C Va=0.98 m/s

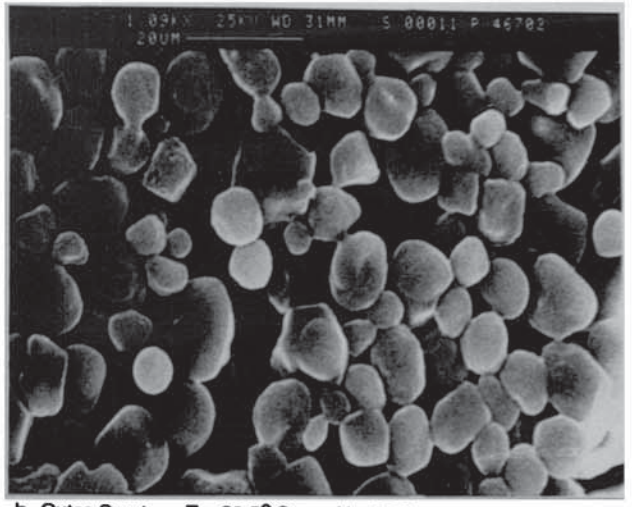

b. Outer Crust Ta=20.5°C Va=0.49 m/s

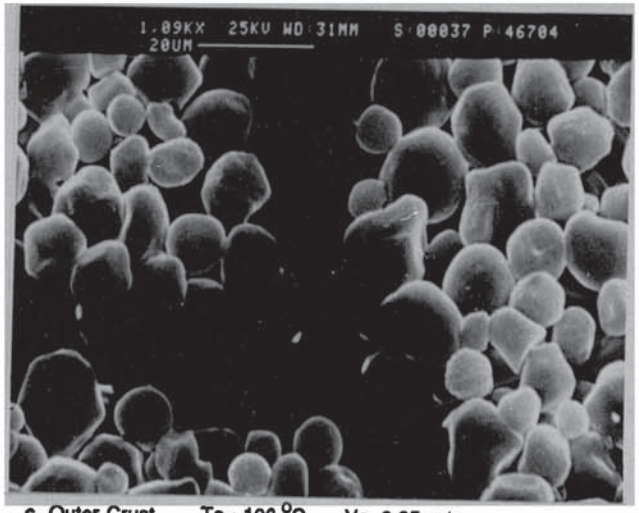

c. Outer Crust Ta= 106 °C Va=0.95 m/s

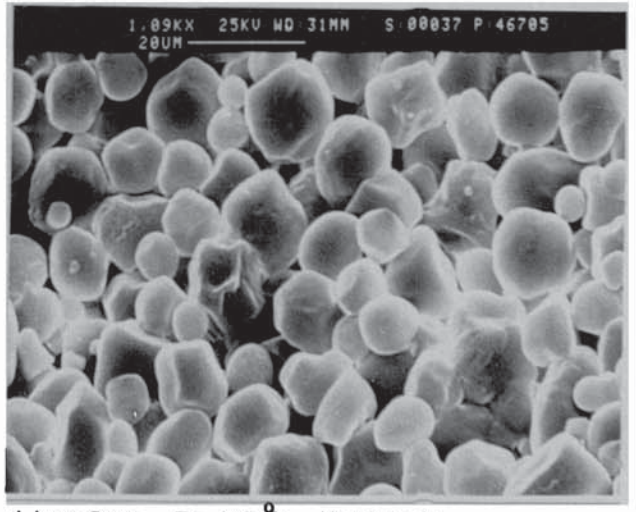

d. Inner Crust Ta= 106 °C Va=0.95 m/s

Plate 9.1 Electron microphotographs of Droplets of 20% weight Custard Suspension. Shows the effects of Air Velocity and Temperature on Crust Structure

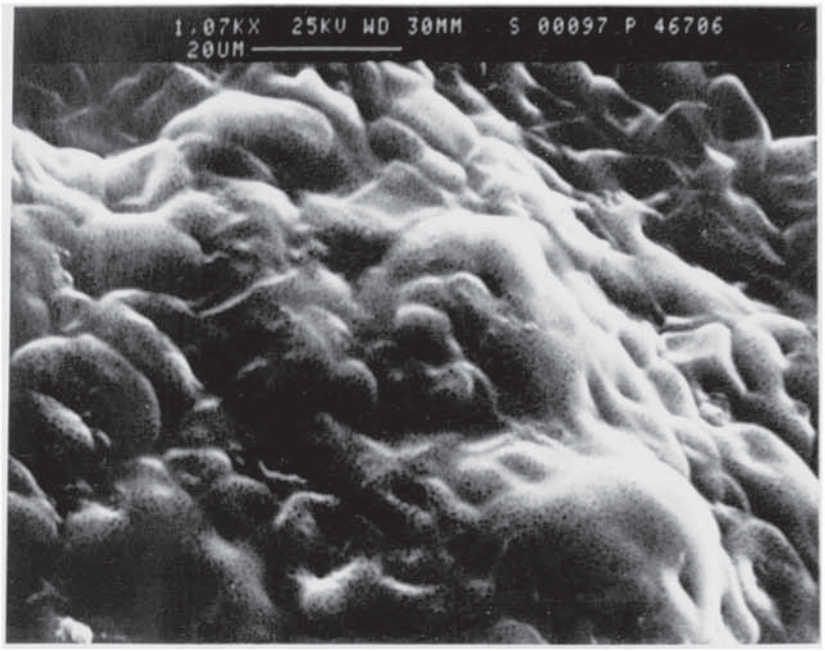

a. Outer Crust
Ta= 22°C
Va= 0.97 m/s

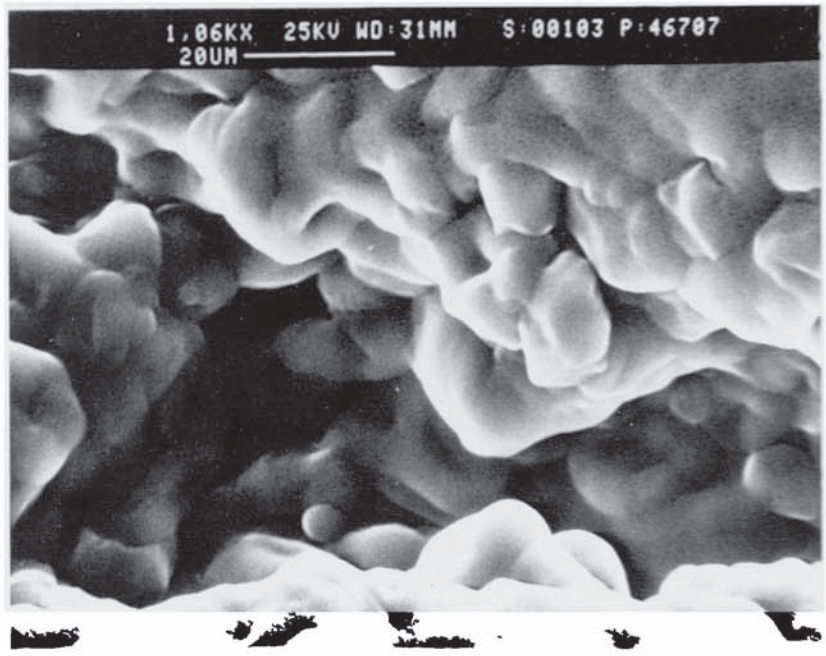

b. Outer Crust
Ta= 75.5°C
Va= 0.97 m/s

Plate 9.2 Electron microphotographs of 20% weight Gelatinized Custard Paste Dried at Different Air Temperatures

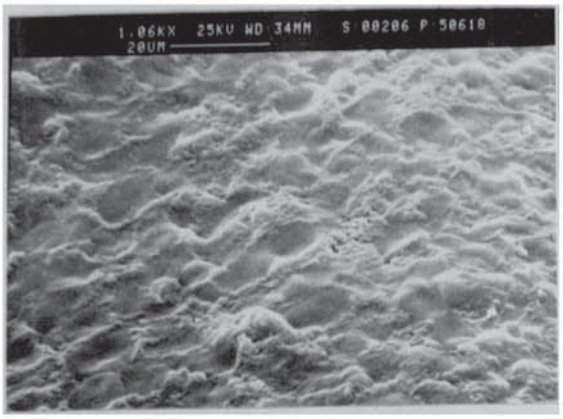

a.Inner Crust
Ta=160 °C
Va=0.1 m/s

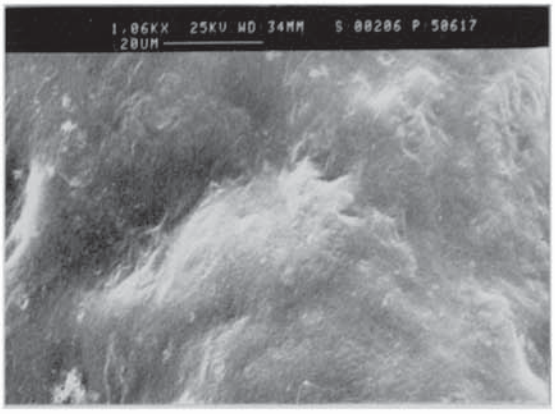

b.Outer Surface
Ta= 160 °C
Va= 0.1 m/s

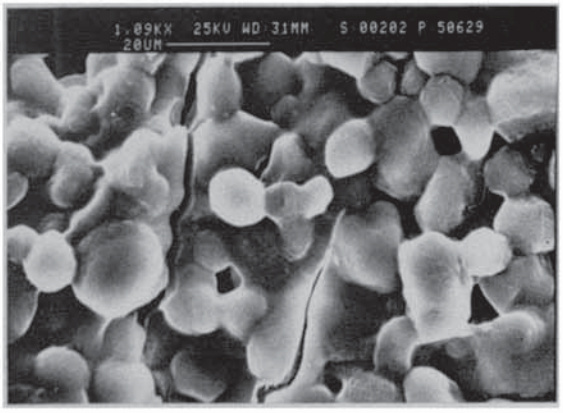

c.Outer Crust
Ta= 179 °C
Va= 0.1m/s

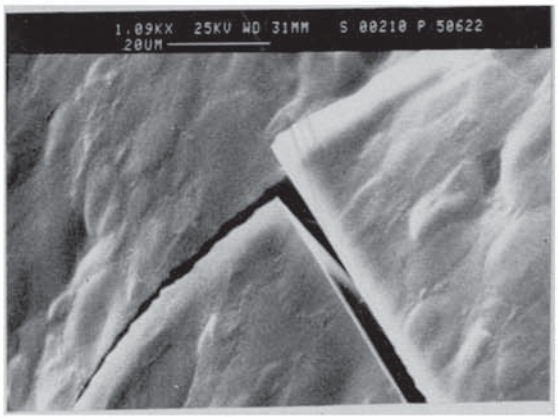

d.Outer Crust
Ta=198 °C
Va=0.1 m/s

Plate 9.3

Electron microphotographs of 20% weight Custard Droplets Dried at High Air Temperatures

of a normal custard suspension and gelatinised custard paste (i.e cooked custard) for droplets of 20% weight initial concentration. As expected the drying rate of gelatinised paste droplets was significantly less. This is due to the formation of a skin on the surface of the gelatinised paste immediately the droplet was exposed to the air stream.

At a higher air temperature of 54 °C (Figure 9.9) the difference between the rates was reduced. This is because swelling of the granules of normal custard suspension resulted in a reduction in the drying rate.

9.1.2 DROPLETS OF STARCH SUSPENSION

In this section comparisons are drawn between the drying of droplets of starch and custard suspensions under different drying conditions.

9.1.2.1 Effect of Initial Concentration

Figure 9.13 illustrates the effect of initial starch concentration on drying rate for the same initial droplet size. As with custard, the initial concentration had little effect on the initial drying rate. However after about 600 seconds, compared with 500 seconds for a custard droplet (Figure 9.1), the rates diverge due to the formation of crusts. This suggests that the formation of the crusts was faster in custard droplets. This is because the smaller starch granules absorbed less water than with custard leaving more free water in the droplet. Therefore it took longer to form the crust in the drying of starch droplets.

9.1.2.2 Effect of Air Velocity and Air Temperature

As with custard, an increase in air velocity resulted in an increased drying rate as shown in Figure 9.14.

The effect of air temperature on droplets of 20% initial weight concentration are shown in Figures 9.15 and 9.16. The trends of the drying rate curves are generally similar to those for custard i.e. an increase in air temperature increased the drying rate. The drying rate increased two fold when the air temperature was increased from 20.5 °C to 36 °C and from 36 °C to 76 °C. With custard the drying rate increased three fold

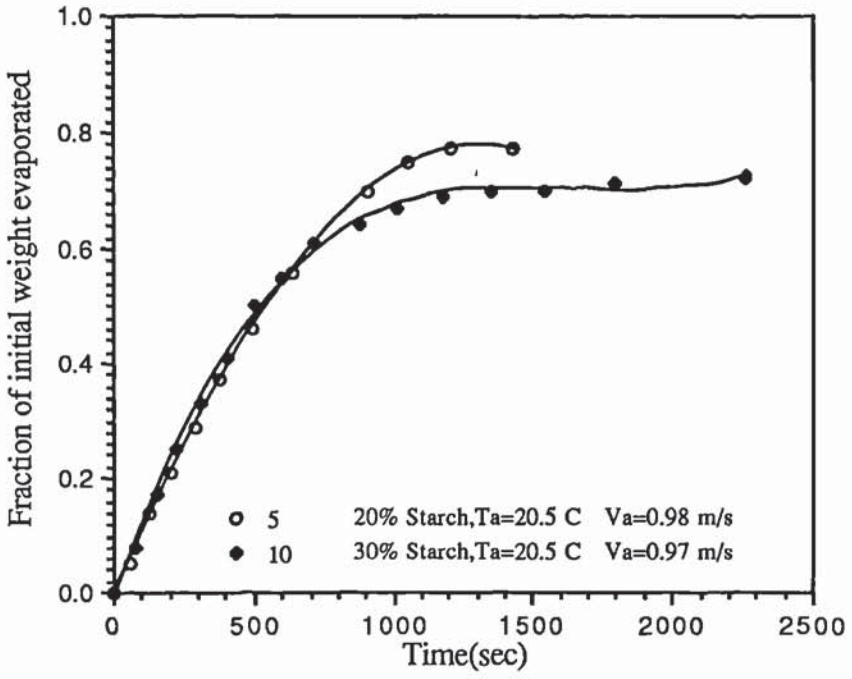

Figure 9.13 Drying of Droplets of Starch Suspension at Various Initial Concentrations.

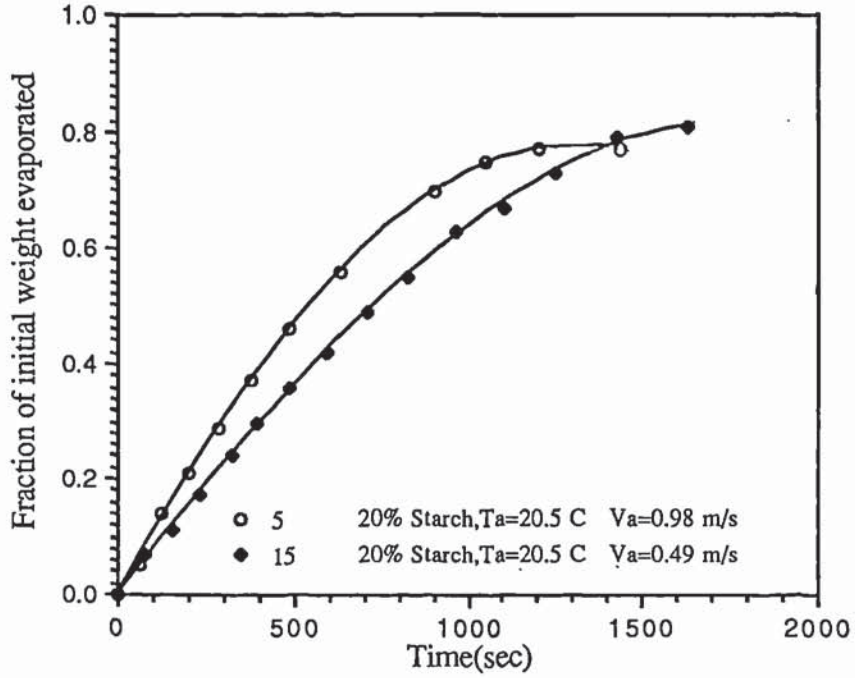

Figure 9.14 Drying of Droplets of Starch Suspension (20% wt/wt)at Various Air Velocities.

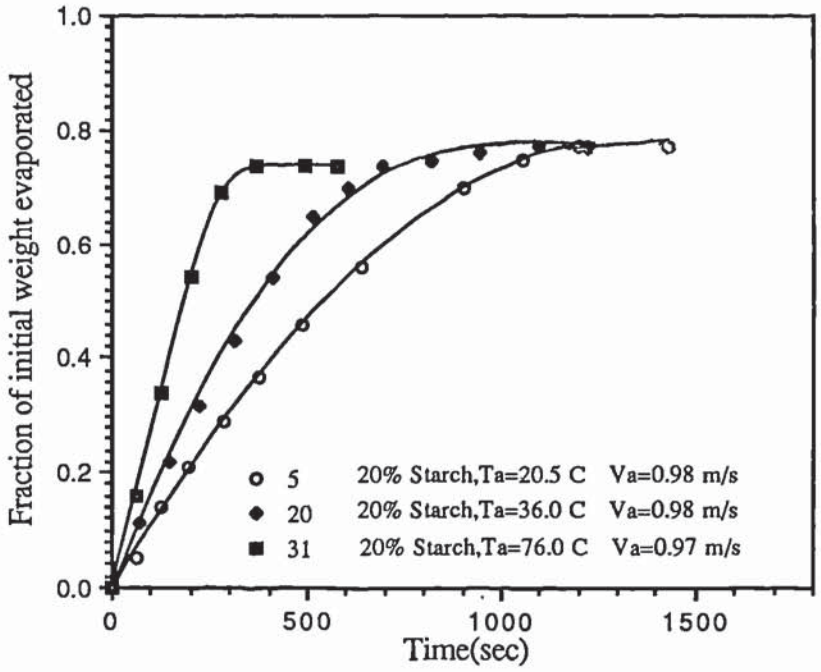

Figure 9.15 **Drying of Droplets of Starch Suspension (20% wt/wt) at Various Air Temperatures.**

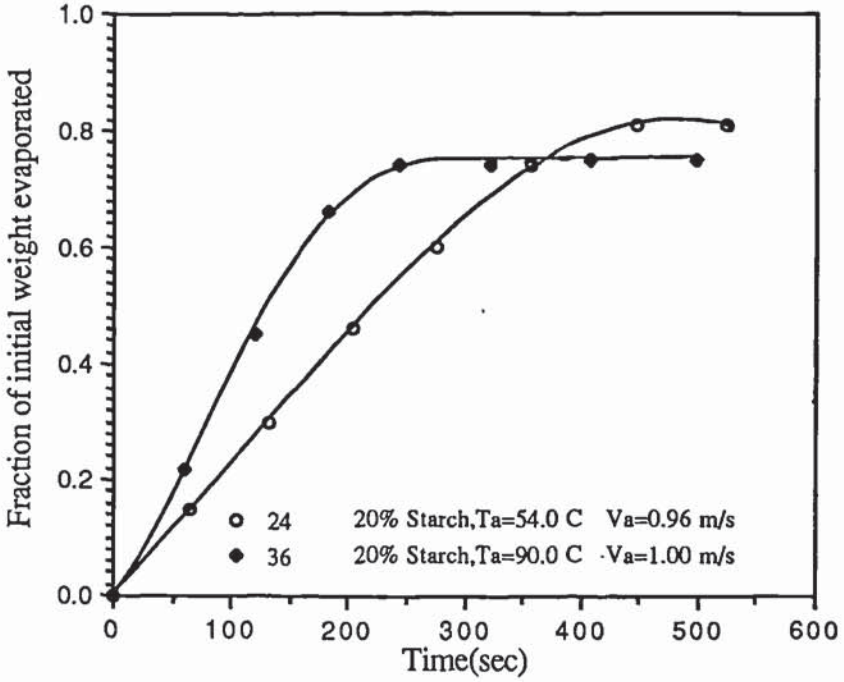

Figure 9.16 **Drying of Droplets of Starch Suspension (20% wt/wt) at Various Air Temperatures.**

when the air temperature was increased from 20 °C to 36 °C. Hence the crust of starch represents a greater resistance to mass transfer than the crust of custard. The smaller starch granules result in the pores within a starch crust being smaller in size than in the custard crust. Hence a starch crust offers a higher resistance to mass transfer.

A very interesting trend was observed at high drying temperature of 90 °C. In Figure 9.16, an increase in air temperature from 54 °C to 90 °C increased the drying rate two fold. By comparison with custard the rate was increased less than one and half fold. This is attributed to the difference in the size between the granules of custard and starch. Clearly, therefore the granules of custard (the larger granules) swelled more rapidly than the starch granules. This led to the drying rate of droplets of custard being less than the drying rate of starch. The drying process completely stopped with custard (at 91 °C in Figure 9.5) at a drying time of about 180 seconds at which the fraction of initial weight evaporated was < 0.7 compared with about 250 seconds at which the fraction of initial weight evaporated was > 0.75 in starch (Figure 9.16). Therefore a custard crust offered a higher resistance to mass transfer than a starch crust under these drying conditions.

Figures 9.17 and 9.18 show the drying rate and core temperature histories for 20% initial concentration suspensions at air temperatures of 20 °C and 54 °C respectively. The trends of the curves are similar to those for custard. At 20 °C, a short constant rate period followed establishment of a drying rate. This is reflected in the measurements of the core temperature; there was a transient period before equilibrium was established and the droplet temperature reduced to the wet-bulb temperature. The droplet temperature then rose steadily to the air temperature as the drying rate proceeded to fall steadily.

At 54 °C (Figure 9.18), as with custard droplets, a higher rate was established and no constant rate period was observed. Upon establishment of a drying rate, the rate started to fall gradually during the first 400 seconds compared with 300 seconds in custard (Figure 9.11); it then began to fall rapidly as the core temperature proceeded to rise rapidly to the air temperature. This further illustrates the effect of the granules size in starch (the smaller granules) and custard (the larger granules) on the

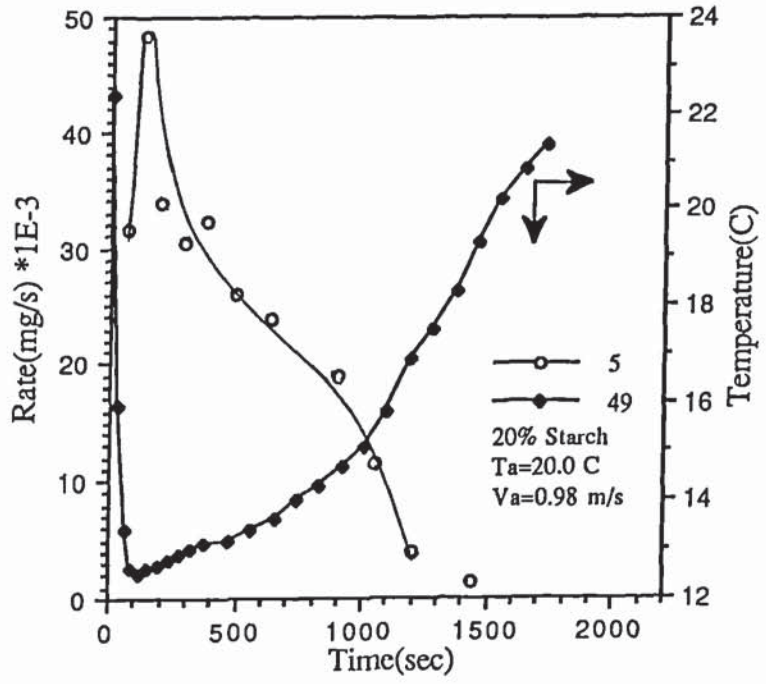

Figure 9.17 Core Temperature and Drying Rate Histories for Starch Suspension (20% wt/wt) at 20°C.

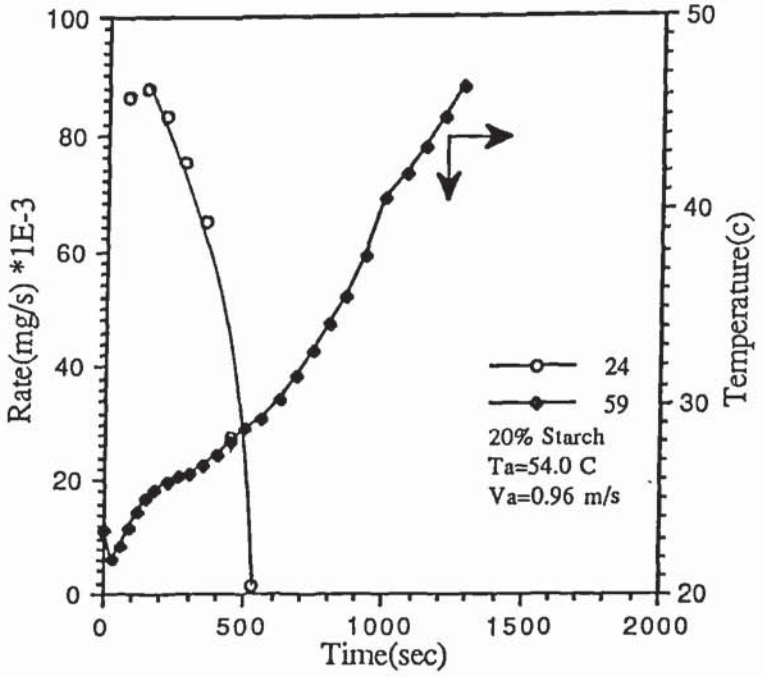

Figure 9.18 Core Temperature and Drying Rate Histories for Starch Suspension (20% wt/wt) at 54°C.

drying rate; the crust in custard forms more rapidly.

Electron microphotographs of the crust produced at different air temperatures and velocities are shown in Plates 9.4 and 9.5. These further illustrate the growth of the resistance to mass transfer, due to granules swelling with an increase in the drying temperature. The size of pores is greatly reduced as a result of granule swelling. Plates 9.5 c and d show this effect more clearly. Similar behaviour was observed with custard, except that the swelling was then more rapid and greater due to the larger granules size.

The crust produced at high air temperatures and low velocity (the ideal conditions for gelatinisation) are shown in Plates 9.6 a-e. As with custard, the degree of distortion of the granules due to gelatinisation increased with an increase in air temperature. Also, as with custard, major cracks were observed on the outer crust surface. This reflects the significant increase in the crust resistance to mass transfer due to granule gelatinisation. In comparison with custard, as shown in Plates 9.6 b and d (at temperatures of 160 ^{o}C and 179 ^{o}C respectively) the distortion of the granules was less than that in custard (Plates 9.3 b and c under the same drying conditions) due to the smaller starch granules. In Plate 9.6 e the air temperature was too high (198 ^{o}C), resulting in the granules being totally distorted and it is very difficult to find a recognisable discrete granule under these conditions; similar behaviour was observed in custard. At 198 ^{o}C and 0.1 m/s, as with custard droplets, the starch droplets inflated and deflated twice.

9.2 DROPLETS OF THE SECOND TYPE

Gelatin is a typical example of material of the second type. It is soluble in water; the solutions are very fluid when hot, but set to a clear stiff gel on cooling (85). Dry gelatin granules absorb a certain amount of water in the cold but they retain their shape and do not dissolve unless they are very impure. The rate and degree of swelling is a characteristic of the particular gelatin (149). Swelled gelatin granules dissolved rapidly in water above 35 ^{o}C.

Plate 9.4

External Crust Surface of 20% weight Starch Dried at Different Air Temperatures

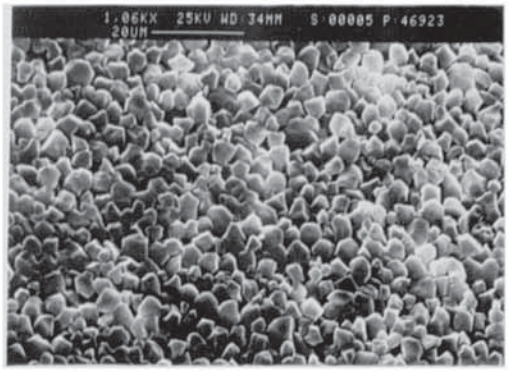

a. Ta=20.5°C
Va=0.98 m/s

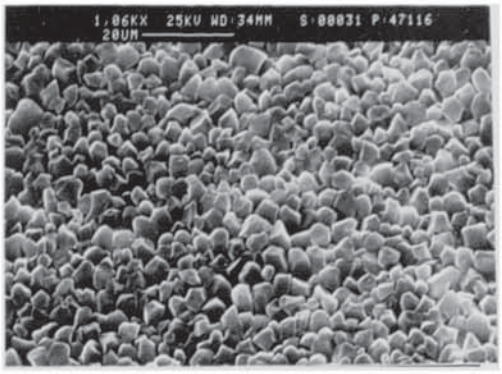

b. Ta=76°C
Va=0.97 m/s

Plate 9.5

Electron microphotographs Showing the Effect of Temperature on Crust Structure of Droplets of 20% weight Starch Suspension

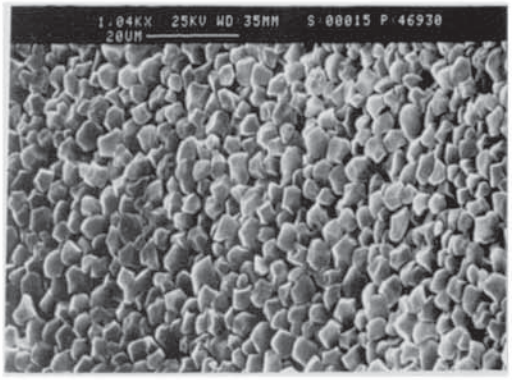

a. Internal
Ta=20.5°C
Va=0.49 m/s

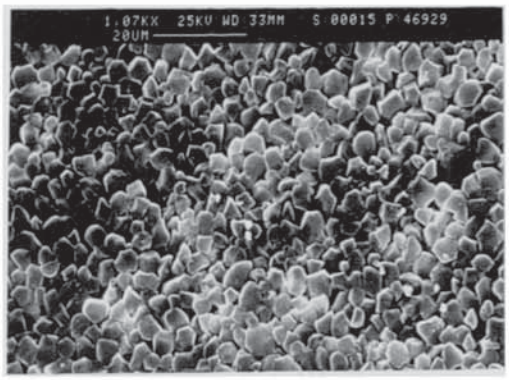

b.External
Ta=20.5 °C
Va=0.49 m/s

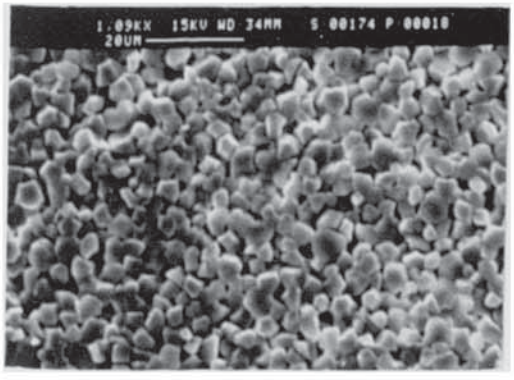

c.External
Ta=106°C
Va=0.49 m/s

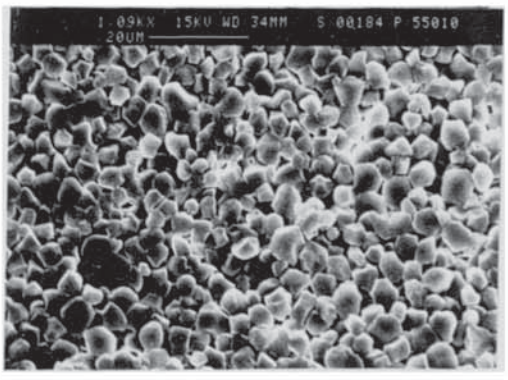

d.External
Ta=126°C
Va=0.49 m/s

Plate 9.6
Inner and Outer Crust Surfaces of 20% weight
Starch Droplets Dried at High Air Temperatures

a. Inner Crust
Ta=179 °C
Va=0.1 m/s

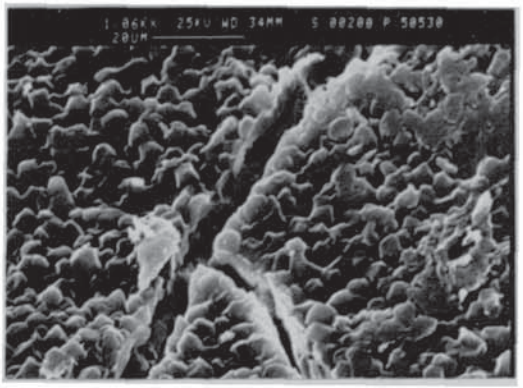

b. Outer Crust
Ta=179°C
Va=0.1 m/s

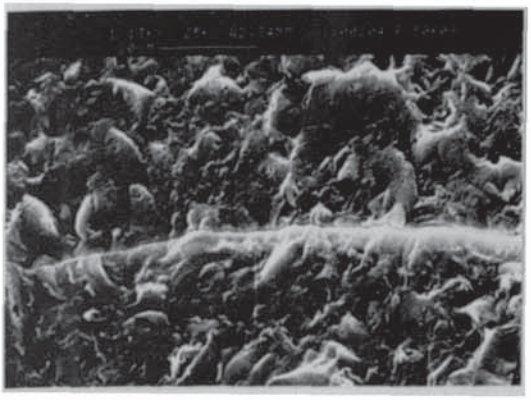

c. Inner Crust
Ta=160°C
Va=0.1 m/s

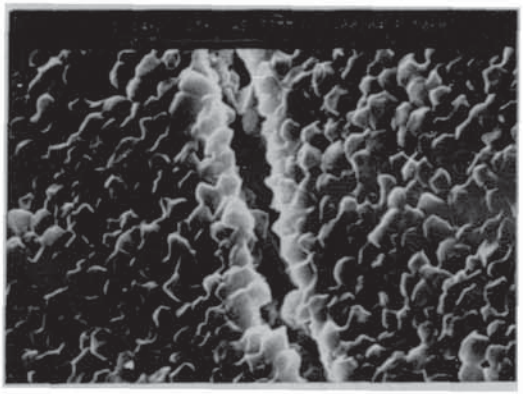

d.Outer Crust
Ta=160°C
Va=0.1 m/s

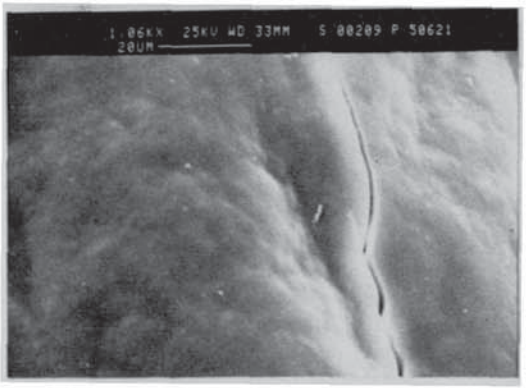

e.Outer Crust
Ta=198°C
Va=0.1 m/s

Since hydrogen bonds play a major role in maintaining the secondary and higher structures of proteins, it is not surprising that a radical change in the structure usually occurs on heating (96). This change, which occurs without severance of any covalent links, is termed denaturation. The denaturation reaction is reversible. However, if excessive heat is supplied to the protein, then covalent bonds may rupture leading to thermal degradation of the molecules (96). The possible reactions that the protein may undergo during heating are,

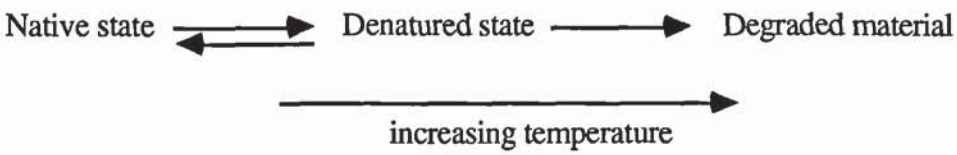

The rate of thermal degradation of a gelatin solution is appreciable above 60 °C and rapid at 100 °C (98). When a solution which has been heated in this way is cooled to a gel again, the rigidity is found to have decreased irreversibly. The more severe the conditions, the greater the loss of rigidity until, in the limit, the solution does not gel at all.

On drying, droplets of gelatin solution formed perfectly transparent films or skins immediately after exposure to the drying medium. Therefore the drying rates would be expected to be very low especially at lower drying temperatures. The dried crusts retained the structures and properties of the original powder unless dried at a high temperature (i.e. above 60 °C).

At high drying temperatures the granules melted and the droplet suspended from the nozzle became hemispherical shortly after exposure to the hot drying medium. (Initially it was cylindrical; due to the highly viscous nature of the gel it was impossible to form a hemispherical droplet). The dried crusts were different from those of the original gelatin. The type of skin formed under these conditions differed from that at lower drying temperature being smoother and offering a higher resistance to mass transfer.

In this section the different drying conditions which affect the types of skin

formation and the dried crusts will be discussed.

9.2.1 DROPLETS OF GELATIN SOLUTION

9.2.1.1 Effect of Initial Concentration

Figure 9.19 illustrates the effect of initial concentration on the drying rates of gelatin. The rate was reduced with an increase in the initial droplet concentration because (quite apart from the initially lower driving force for moisture transfer) a thicker skin was formed at the higher concentration. The increase in gel viscosity with concentration, resulting in some increase in resistance to diffusion could also have been a factor. The drying rate at the high concentration virtually stopped after about 2900 seconds although half the initial moisture content was retained in the droplet. Hence the skin which formed immediately upon exposure to the drying medium represents a major resistance to mass transfer.

9.2.1.2 Effect of Air Velocity

An interesting trend was observed when the air velocity was increased in that initially the drying rate at the higher velocity was greater as shown in Figure 9.20. However after about 100 seconds the rate diverged, because a thicker skin formed at the higher air velocity, resulting in the rate being less, due to the higher resistance.

At high air temperature (Figure 9.21) the difference between the drying rate at lower and higher velocities was reduced to half of that at the above condition (i.e. ambient temperature Figure 9.20). This arose because under these conditions the granules of gelatin dissolved in water, leading to the formation of a smoother and stronger (more resistant) skin. Therefore air velocity has less effect on the rate of drying under these conditions.

9.2.1.3 Effect of Air Temperature

As shown in Figures 9.22 and 9.23 an increase in air temperature increased the drying rate e.g. two-fold as between air temperatures of 20.5 ^{o}C and 36 ^{o}C. This

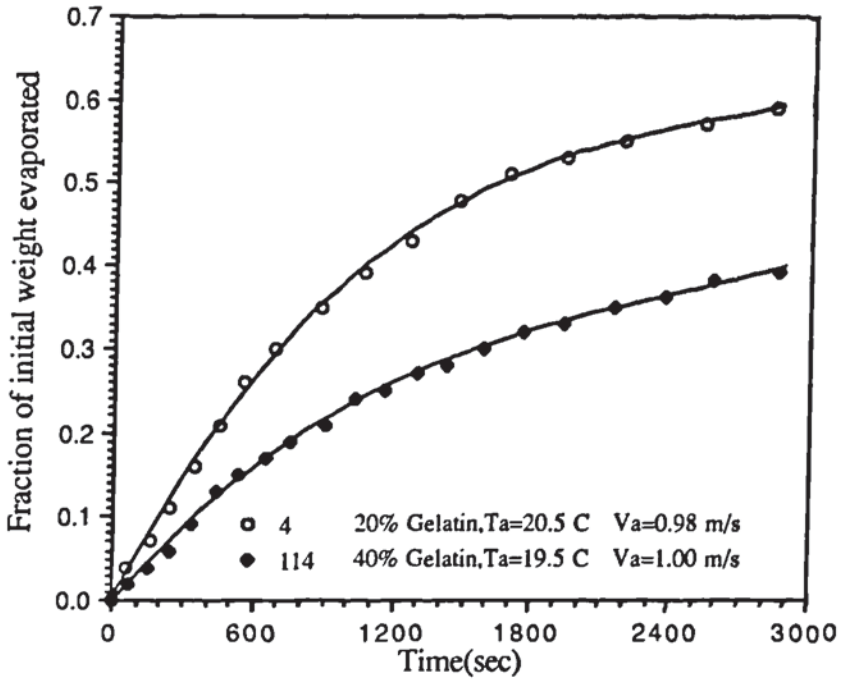

Figure 9.19 Drying of Droplets of Gelatin Solution at Various Initial Concentrations.

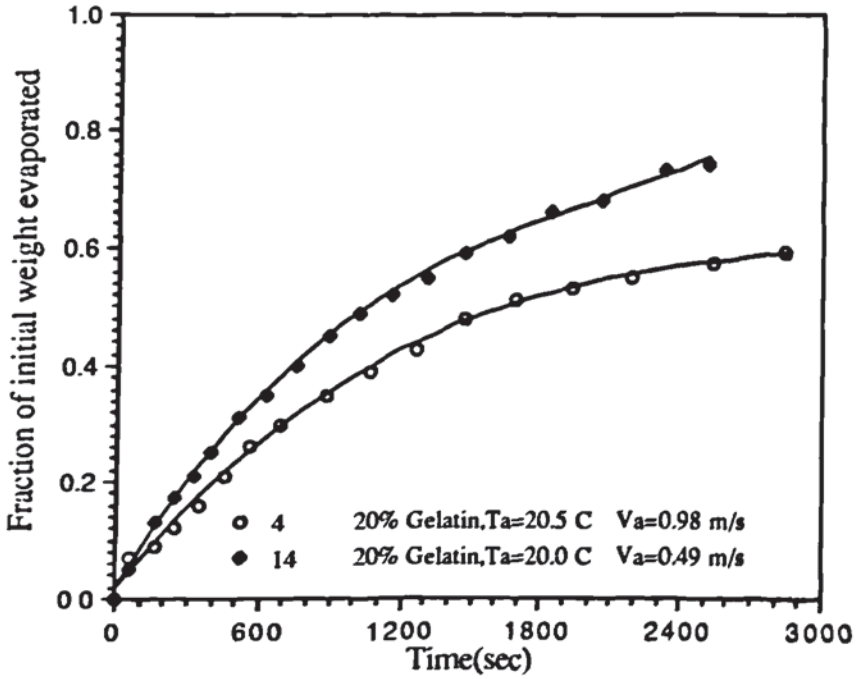

Figure 9.20 Drying of Droplets of Gelatin Solution (20% wt/wt) at Various Air Velocities.

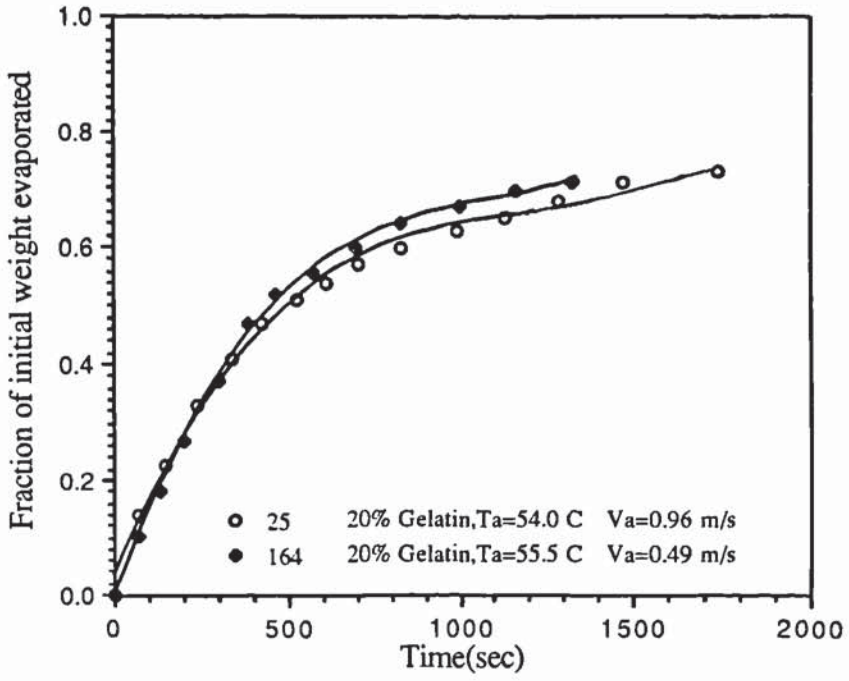

Figure 9.21 Drying of Droplets of Gelatin Solution (20% wt/wt) at Various Air Velocities.

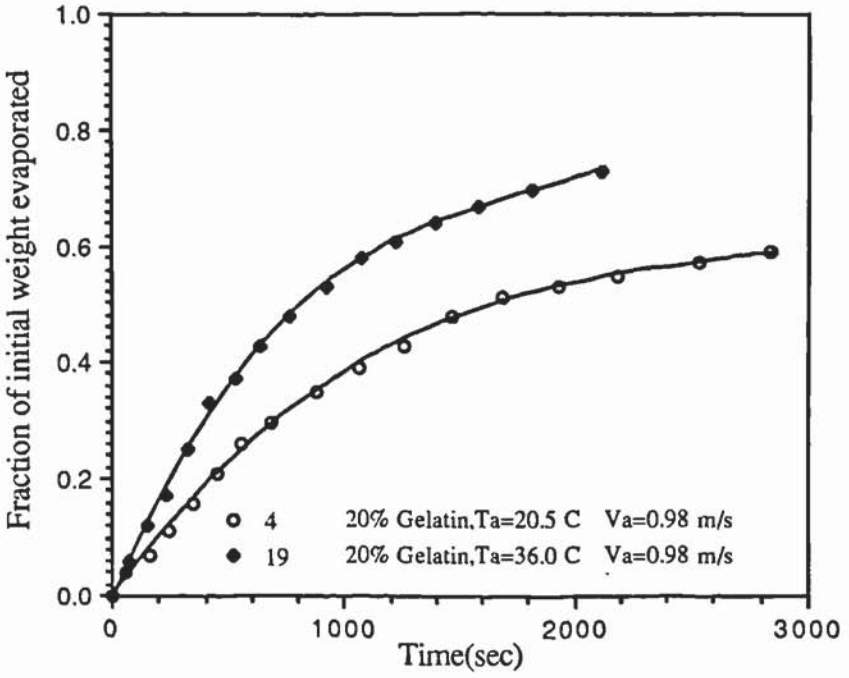

Figure 9.22 Drying of Droplets of Gelatin Solution (20% wt/wt) at Various Air Temperatures.

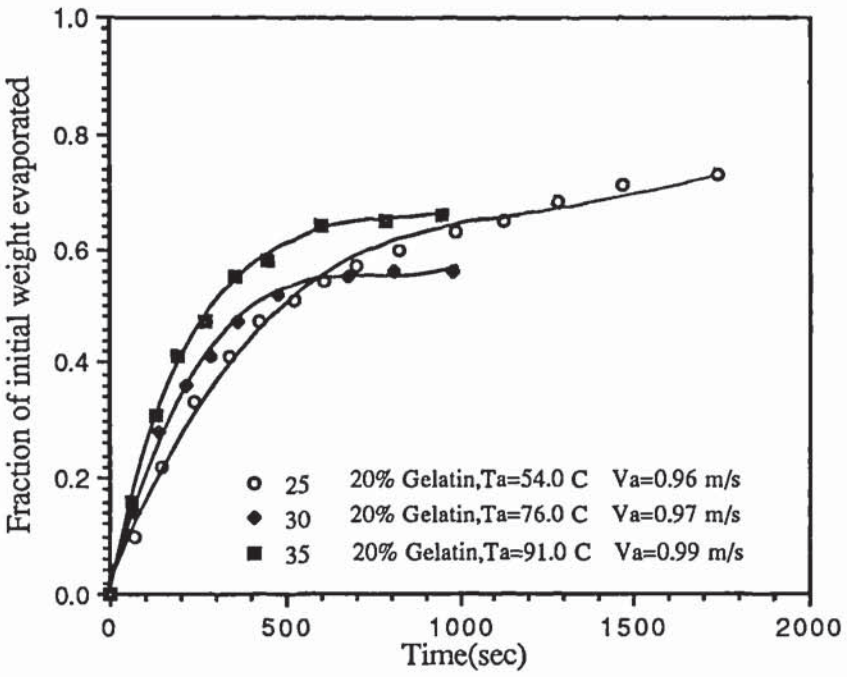

Figure 9.23 Drying of Droplets of Gelatin Solution (20% wt/wt) at Various Air Temperatures.

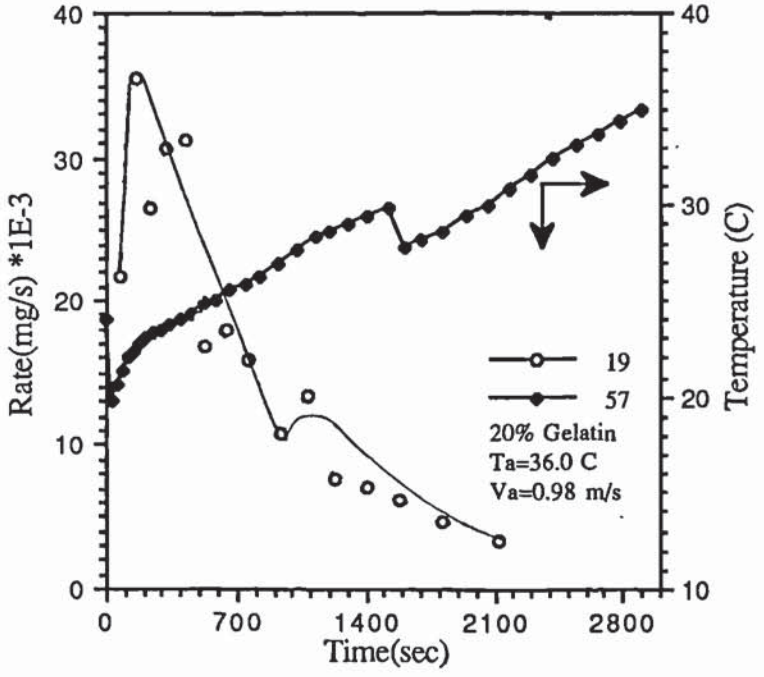

Figure 9.24 Core Temperature and Drying Rate Histories for Gelatin Solution (20% wt/wt) at 36°C.

increase in the drying rate was reduced to about the half when the air temperature was increased from 54 °C to 76 °C and from 76 °C to 91 °C as shown in Figure 9.23. At these higher drying temperatures a smoother skin formed on the droplet surface, as the gelatin granules dissolved in water, and at 76 °C and 91 °C all the granules melted. Immediately after melting a thin transparent skin formed on the surface and the droplet became less viscous. The droplet shape gradually changed from cylindrical to hemispherical during melting. All the granules had melted after about 65 seconds at 76 °C and 52 seconds at 91 °C. After all the granules melted the skin was readily visible on the surface of the droplet.

As mentioned above (Figure 9.23) an increase in the air temperature to a higher level increased the drying rate. However after about 650 seconds at 76 °C and 900 seconds at 91 °C the rates diverged and became zero while the process at 54 °C proceeded to a higher degree of drying. This confirms that a stronger skin was formed on the droplet surface at higher drying temperature particularly when the gelatin granules melted.

The effects of air temperature are clearly shown in Figures 9.24 and 9.25 which are the core temperature and drying rate histories for droplets of 20% weight initial concentration and air temperatures of 36 °C and 54 °C respectively. At an air temperature of 36 °C, a constant rate period was observed after establishment of a drying rate. This corresponds to a core temperature falling initially to the wet-bulb temperature and then steadily rising to 30 °C. At this temperature (i.e. 30 °C) a unique trend was observed in both the core temperature and drying rate histories. Once the temperature reached 30 °C, a sudden fall was observed in the core temperature to 27.5 °C. The core temperature then started to increase steadily to the air temperature. There was a simultaneous increase and decrease in the drying rate. This phenomena was associated with the dissolution of gelatin granules in water at about 30 °C, with the absorption of heat. When the core temperature fell below the dissolution point, the dissolution process was temporarily halted and the temperature subsequently rose again. (This result highlights the advantage of using the new nozzles which facilitate direct

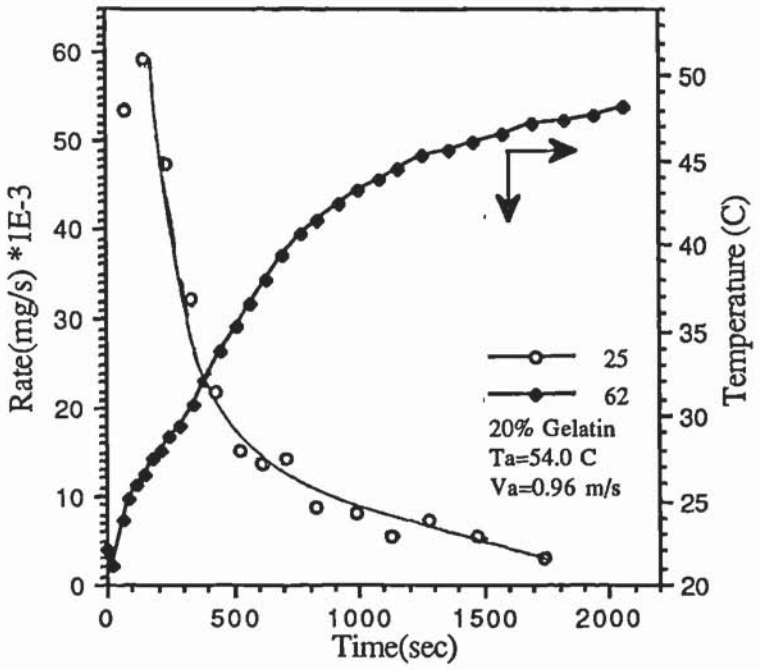

Figure 9.25 Core Temperature and Drying Rate Histories for Gelatin Solution (20% wt/wt) at 54°C.

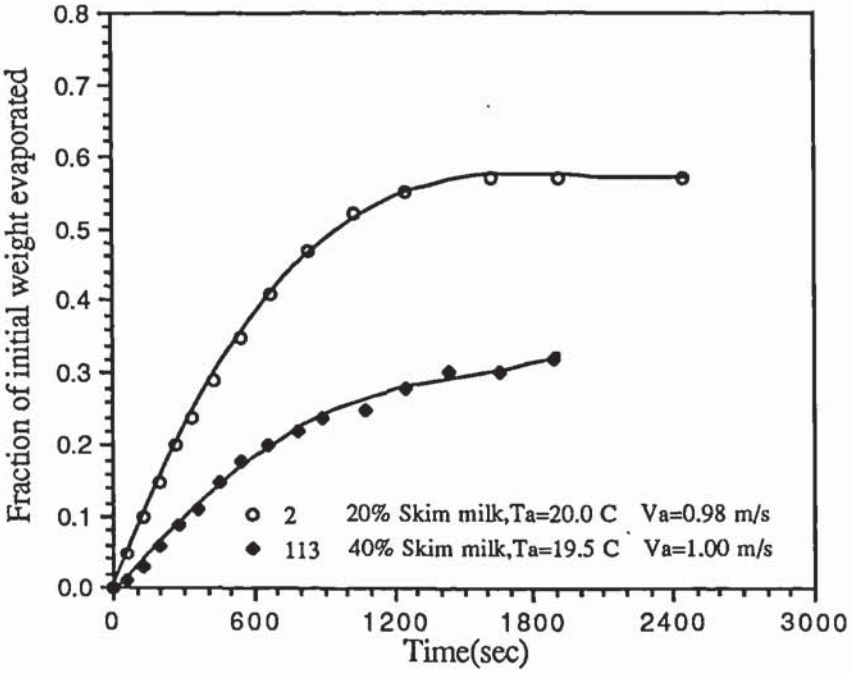

Figure 9.26 Drying of Droplets of Skim Milk Solution at Various Initial Concentrations.

measurement of the droplet weight and temperature during drying).

At higher air temperatures this sudden decrease in the core temperature at 30 ^{o}C was not noted. As shown in Figure 9.25 for a droplet of 20% weight initial concentration at 54 ^{o}C, the core temperature increased rapidly to 30 ^{o}C and then steadily to the air temperature. It is probable that the higher drying temperatures and subsequent higher heat transfer rates would tend to very rapidly re-establish the equilibrium at 30 ^{o}C. As shown in Figures 9.24 and 9.25, only at low air temperature (36 ^{o}C) was a constant drying rate period established. At higher drying temperatures after commencement of drying, a falling rate was initiated. This indicates that a more resistant skin was formed at higher temperatures.

The electron microphotographs of dried crust structure in Plate 9.7 a-f illustrate skin formation. Plate 9.7 a and 9.7 b clearly show that a thicker skin was formed at higher air velocity. The outer crust surface was smoother at lower velocity. In Plates 9.7 c and 9.7 d dissolution of the granules provided a smooth surface with major cracks. The width of the crack at the higher velocity was double that at the lower velocity consistent with the formation of a thicker skin. The cracks confirm that the skin formed at the higher air temperature shown in Plate 9.7 c and 9.7 d offers a higher resistance to mass transfer. Plates 9.7 e and 9.7 f show the skin formed at 106 ^{o}C. The skin is very smooth with a blow hole on the outer surface which confirms the very high resistance to mass transfer offered by the skin under these drying conditions. As shown in Plates 9.7 e and 9.7 f, the skin offered more resistance to mass transfer than at lower air temperature (Plates 9.7 c and 9.7 d).

Plates 9.12 shows a droplet of gelatin dried at 175 ^{o}C. A protrusion started to form after 43 seconds; this was a reproducible phenomenon under these conditions and expansion of this protrusion continued until, after 102 seconds, a smaller protrusion started to form from the original protrusion. This continued to expand with time and exploded after 169 seconds. The crust then reformed and no further expansion or explosions followed. The crust was very smooth and, being much thinner due to expansion, would offer less resistance to mass transfer.

Plate 9.7

Electron microphotographs of 20% weight Gelatin Showing the effect of Air Velocity and Temperature on the External Crust Structure

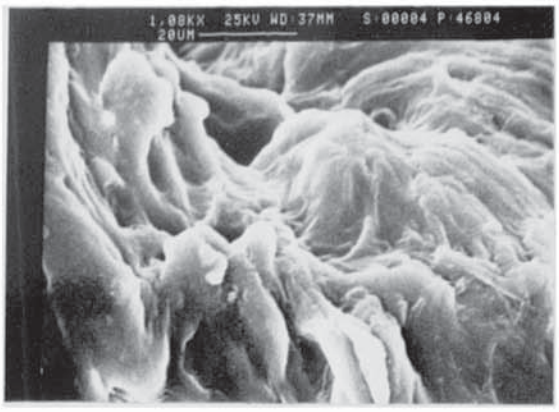

a. Ta=20.5 °C Va=0.98 m/s

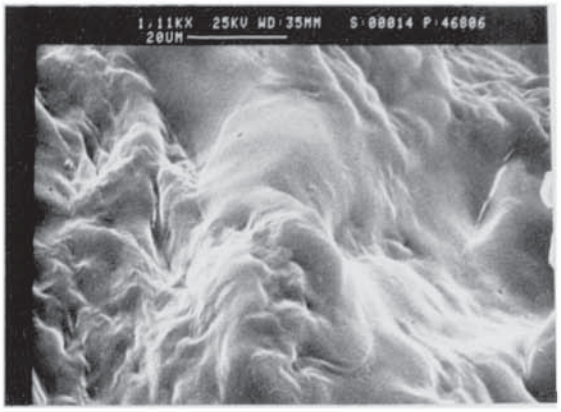

b. Ta=20.0 °C Va=0.49 m/s

c. Ta=54.0 °C Va=0.96 m/s

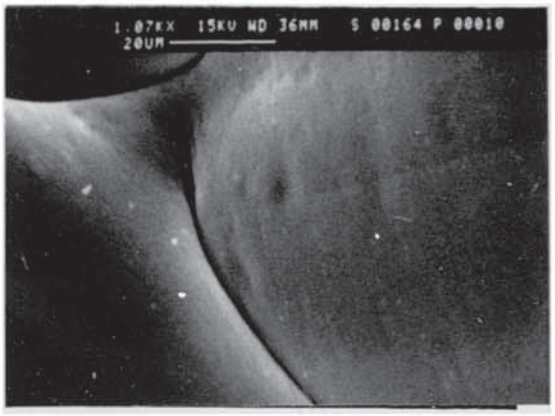

d. Ta=55.5 °C Va=0.49 m/s

e. Ta=106 °C Va=0.98 m/s

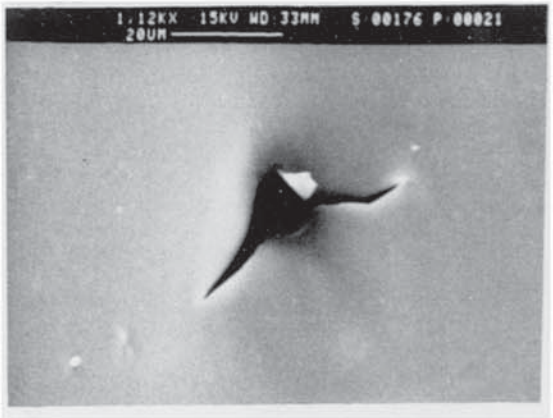

f. Ta=106 °C Va=0.49 m/s

9.3 DROPLETS OF THE THIRD TYPE

Droplets of skim milk and fructose solutions are typical examples of the third type of skin forming material. With them a skin first forms at any drying condition on the surface of the droplet at a certain stage of drying, depending upon the conditions. A crust subsequently forms underneath the skin. This phenomenon arises because there is more than one type of dissolved colloid; one is responsible for skin formation and another for crust formation. At any drying condition the final dried crust retains the structure and properties of the original powder, unless the material is dried at very high temperatures (e.g. >300 ^{o}C which result in burning of the dried crust).

The dissolved colloid responsible for skin formation is believed to deposit solid much more quickly than the material responsible for crust formation beneath it. This is attributed to the nature of each dissolved material in the solution (i.e. the nature and strength of the bonds between the dissolved molecules and water) . Therefore a skin or membrane forms first and increases in thickness until it reaches a maximum; a crust then starts to form underneath this skin leading to a major increase in the resistance to mass transfer.

The time after which the skin appears on the surface of the droplet depends upon the drying conditions; the more severe they are the more rapid the appearance of the skin. The formation of a skin represents a major resistance to mass transfer by vapour diffusion. At high drying temperature (above 100 ^{o}C), a droplet will undergo cycles of inflation/deflation. Under these conditions the majority of the mass transfer occurs due to inflation/deflation phenomena with 'explosions' releasing internal vapour pressure. In this mode of release any other volatiles in a product, e.g. flavours or odours, will also be lost. Also rupture will result in fines formation in practical drying processes.

In some materials, e.g. fructose, the vapour pressure lowering effect is significant and the skin offers a very high resistance to vapour diffusion. This results in the drying process stopping completely at some stage although a significant amount of moisture content is retained in the droplet. In such a droplet no crust formation is

observed underneath the skin, since skin formation has not finished, but due to the very high skin resistance the mass transfer is stopped completely.

9.3.1 DROPLETS OF SKIM MILK SOLUTION

9.3.1.1 Effect of Initial Concentration

The effect of initial concentration of skim milk on the drying rate is shown in Figure 9.26. A reduction in the initial solids content from 40% weight to 20% weight results in a significant increase in the drying rate. This suggests that the lowering of the vapour pressure is significant.

9.3.1.2 Effect of Air Velocities

The effects of air velocity are shown in Figures 9.27 and 9.28 for air temperatures of 20 ^{o}C and 54 ^{o}C respectively. At the lower temperature condition the rate initially was slightly higher at the higher velocity. However the rate diverged once the skin appeared on the droplet surface. This occurred because at the higher air velocity the skin formed more rapidly resulting in a reduction in the drying rate. Therefore the formation of a skin represents a major resistance to mass transfer. At the high air temperature, the air velocity again had little effect upon the initial drying rate. However the curves illustrate a growing difference in the drying rate after about 250 seconds. Droplets dried at higher air velocity exhibited higher drying rates and the difference between the curves increased with time. This suggests that at the low air velocity the skin which formed on the droplet surface after about 250 seconds offers a higher resistance to mass transfer because there is less internal turbulence. This results in a significant reduction in the drying rate, so the skin represents the major resistance to mass transfer.

9.3.1.3 Effect of Air Temperatures

Figures 9.29 and 9.30 show the effect of air temperature on droplets initially of 20% weight concentration. An increase in the air temperature from 20 ^{o}C to 36 ^{o}C

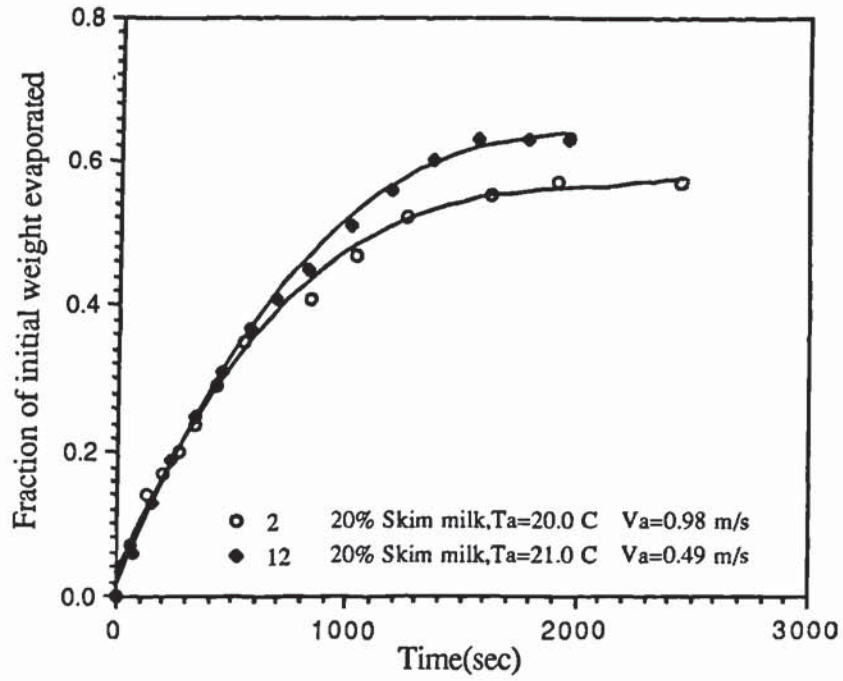

Figure 9.27 Drying of Droplets of Skim Milk Solution (20% wt/wt) at Various Air Velocities.

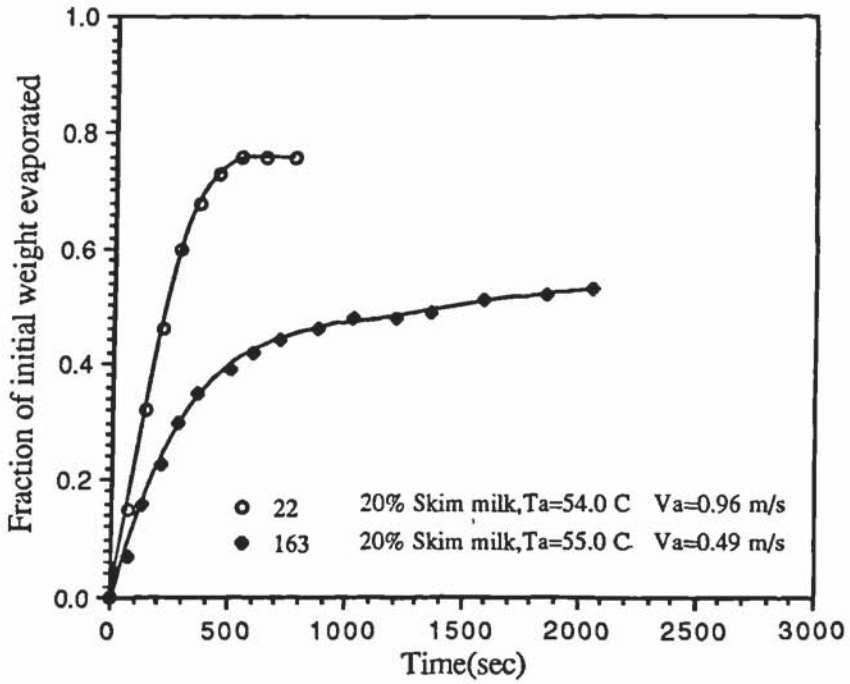

Figure 9.28 Drying of Droplets of Skim Milk Solution (20% wt/wt) at Various Air Velocities.

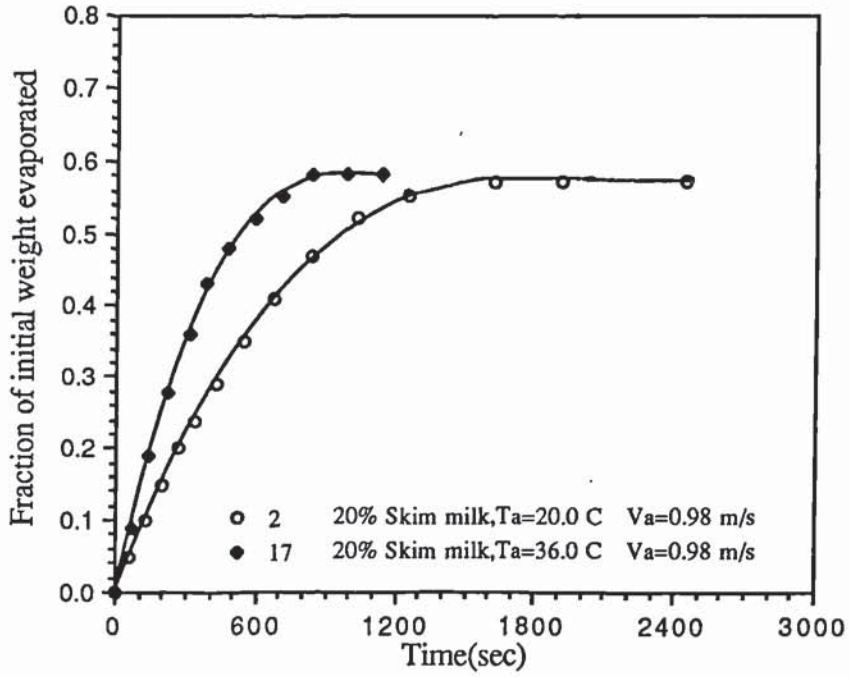

Figure 9.29 **Drying of Droplets of Skim Milk Solution (20% wt/wt) at Various Air Temperatures.**

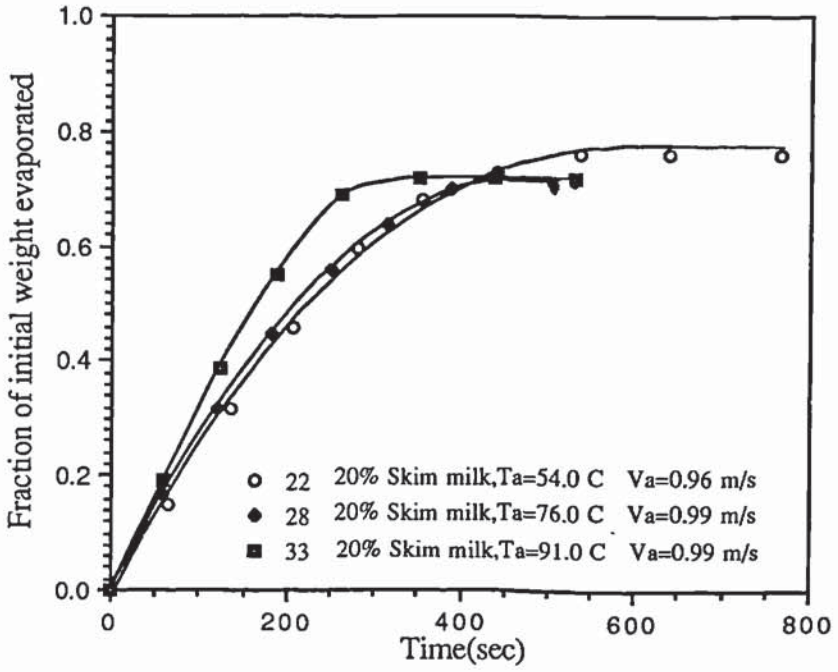

Figure 9.30 **Drying of Droplets of Skim Milk Solution (20% wt/wt) at Various Air Temperatures.**

increased the initial drying rate. However, the rate became zero (i.e. drying stopped) after about 800 seconds at 36 °C and 1300 seconds at 20 °C although over 25% of the initial moisture content was retained in the core. This suggests that the resistance had significantly increased, resulting in no more drying after this time. This was caused by the formation of a crust beneath the skin.

At higher temperatures (Figure 9.30), an increase in the air temperature had only a slight effect on the initial drying rate. This leads to the conclusion that a skin formed under these conditions represents a more significant resistance to mass transfer.

Figures 9.31 and 9.32 show the drying rate and core temperature data, and further illustrate the effect of air temperature. They confirm that at high air temperatures any increase had little effect on the drying rate. At 54 °C (Figure 9.31) no constant rate period was observed, with the rate starting to fall after establishment of a drying rate. The rate started to fall slightly more rapidly after about 350 seconds because a crust started to form underneath the skin which resulted in an increase in the resistance to vapour diffusion. This was reflected in the core temperature measurements; the droplet temperature started to increase more rapidly after about 350 seconds. A higher rate was established at 76 °C again with no constant rate period. Upon establishment of a drying rate the rate started to fall; after about 250 seconds it started to fall more rapidly due to the major increase in the resistance to vapour diffusion caused by the crust formation underneath the skin. All these were consistent with the droplet temperature which started to increase immediately the droplet contacted the hot air stream; it then increased slightly more rapidly after about 250 seconds. After about 900 seconds, it had reached the air temperature, as the drying rate proceeded to fall rapidly to the final value. At 54 °C (Figure 9.31) it took a much longer time for the droplet to reach the air temperature. Therefore the skin resistance to mass transfer is more powerful at higher drying temperatures.

Plates 9.8, 9.9 and 9.10 are electron microphotographs of skim milk crusts under different drying conditions. Plates 9.8 a-d show the crusts of 20% weight droplets dried at approximately 54 °C and different air velocities. At the lower velocity

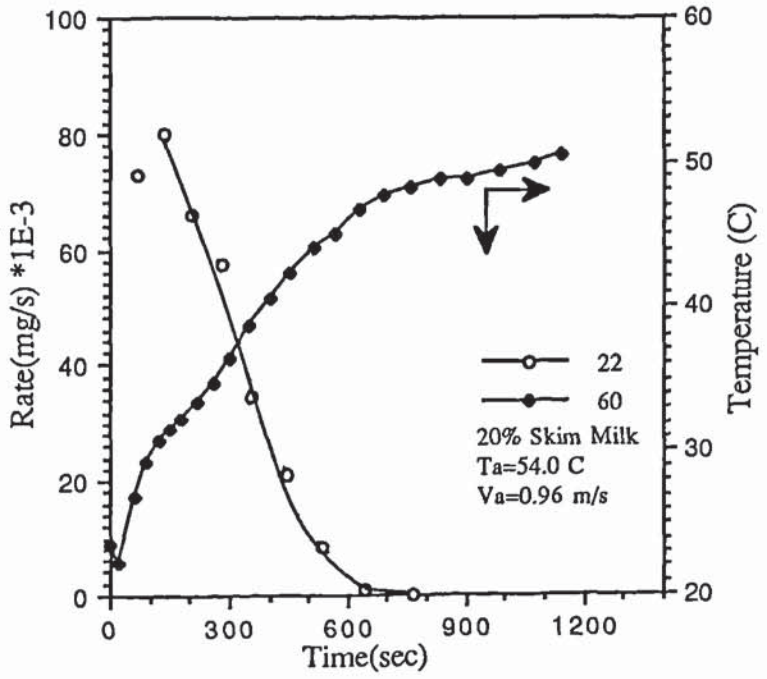

Figure 9.31 Core Temperature and Drying Rate Histories for Skim Milk Solution (20% wt/wt) at 54°C.

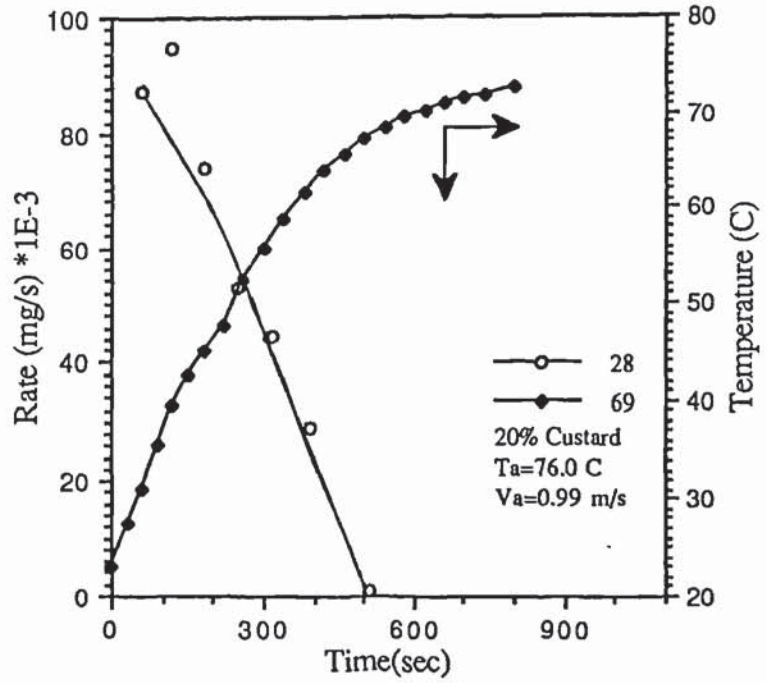

Figure 9.32 Core Temperature and Drying Rate Histories for Skim Milk Solution (20% wt/wt) at 76°C.

Plate 9.8
Electron Microphotographs of 20% weight Skim Milk Showing the Effect of Air Velocity.

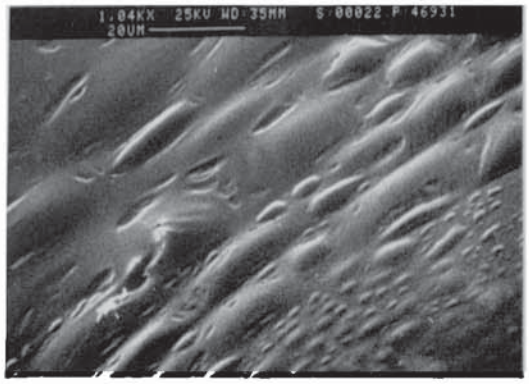

a.External
Ta=54^{o}C
Va=0.96 m/s

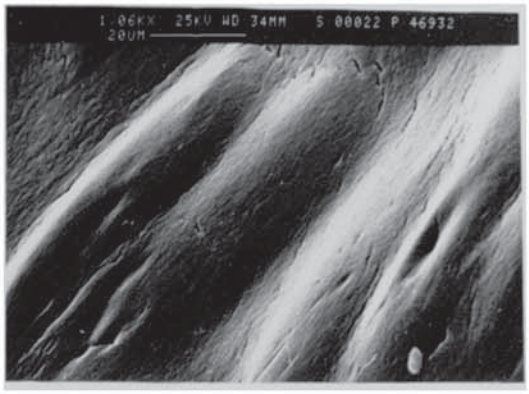

b. Internal
Ta=54^{o}C
Va=0.96 m/s

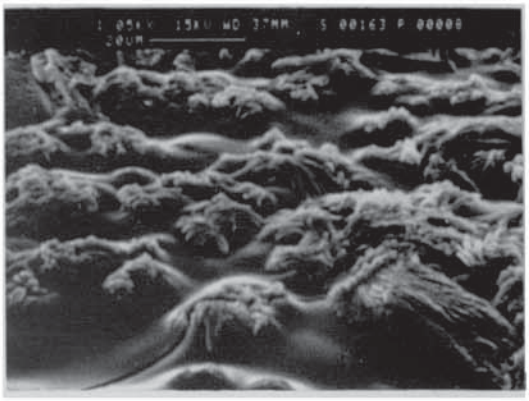

c. External
Ta=55^{o}C
Va=0.49 m/s

d. Internal
Ta=55^{o}C
Va=0.49 m/s

Plate9.9
Crust of 20% weight Skim Milk Dried at 76^{o}C And 0.99 m/s

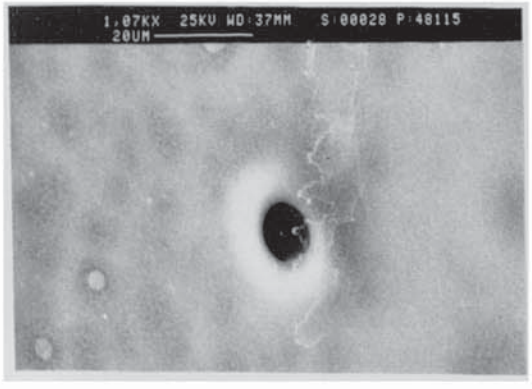

a. Outer Crust

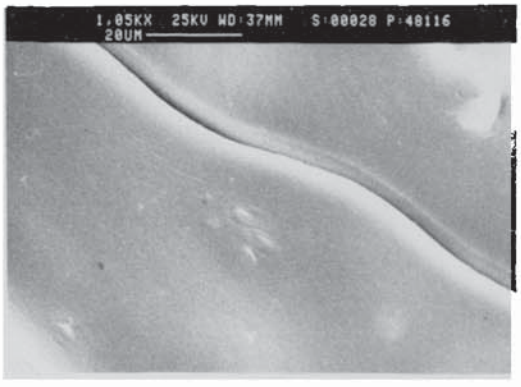

b.Inner Crust

Plate 9.10

Inner and Outer Crust Surfaces of a 40% weight Skim Milk Droplet (19.5 °C,1m/s)

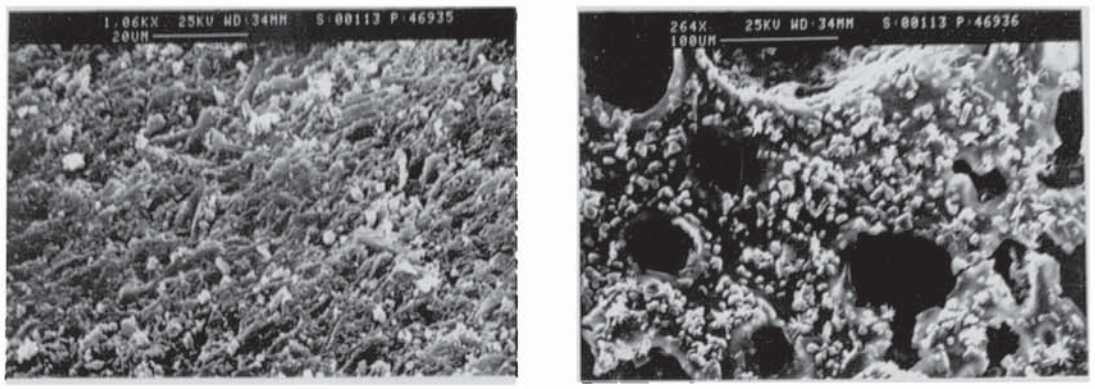

a. Outer Crust

b. Inner Crust

Plate 9.11

Electron Microphotographs of 20% weight Skim Milk Droplets Showing the Effect of Air Velocity at 20 °C

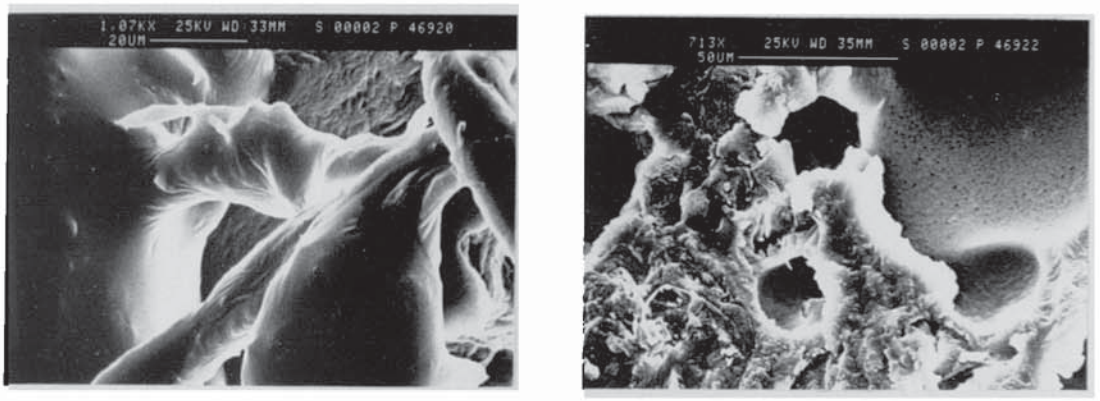

a. Outer Crust
Va=0.98 m/s

b. Inner Crust
Va= 0.98 m/s

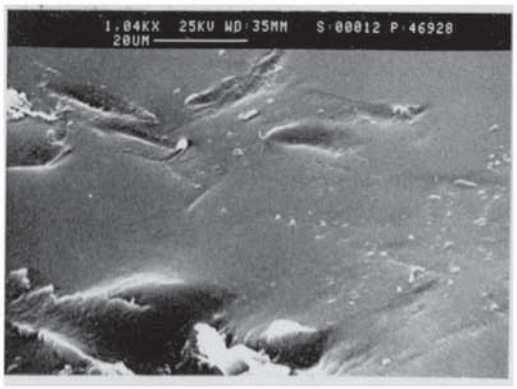

c. Outer Crust
Va= o.49 m/s

(Plate 9.8 c and d) there were cracks in the external and internal crust surfaces. This suggests that a more resistant skin was formed. Plate 9.9 shows the electron microphotographs for similar droplets dried at 76 ^{o}C and, further illustrates the skin with a higher resistance to mass transfer. The outer crust surface was very smooth with a blow holes in it; the inner surface was also very smooth with a wide crack in it. Comparisons between the crust structures in Plates 9.8 a and 9.8 c and Plate 9.9 a, indicates that as the air temperature increased a smoother skin with a higher resistance to vapour diffusion was formed on the surface.

9.3.2 DROPLETS OF FRUCTOSE SOLUTION

In this section, comparisons are drawn with the drying of droplets of skim milk.

9.3.2.1 Effect of Initial Concentration

Figure 9.33 shows the effect of initial solids content on the drying rate. As with skim milk droplets, an increase in the initial concentration significantly decreased the drying rate. However with fructose droplets the difference between the rates was much higher. This suggests that the depression of the vapour pressure was more significant with fructose solutions than that of skim milk due to the nature of the material. With fructose droplets no crust formation was observed beneath the skin. After a drying time of > 3000 seconds the droplet was very viscous especially with droplets of higher initial concentration, and the material retained a significant amount of moisture. Hence > 75% of the initial moisture content was retained in a droplet at the higher initial solids content after a drying time of > 3000 seconds.

9.3.2.2 Effect of Air Velocity

Figures 9.34 and 9.35 show the effect of air velocity at temperatures of 20 ^{o}C and 54 ^{o}C respectively. As with skim milk droplets at the lower air temperature the air velocity had little effect on the initial drying rate. However at the higher velocity after

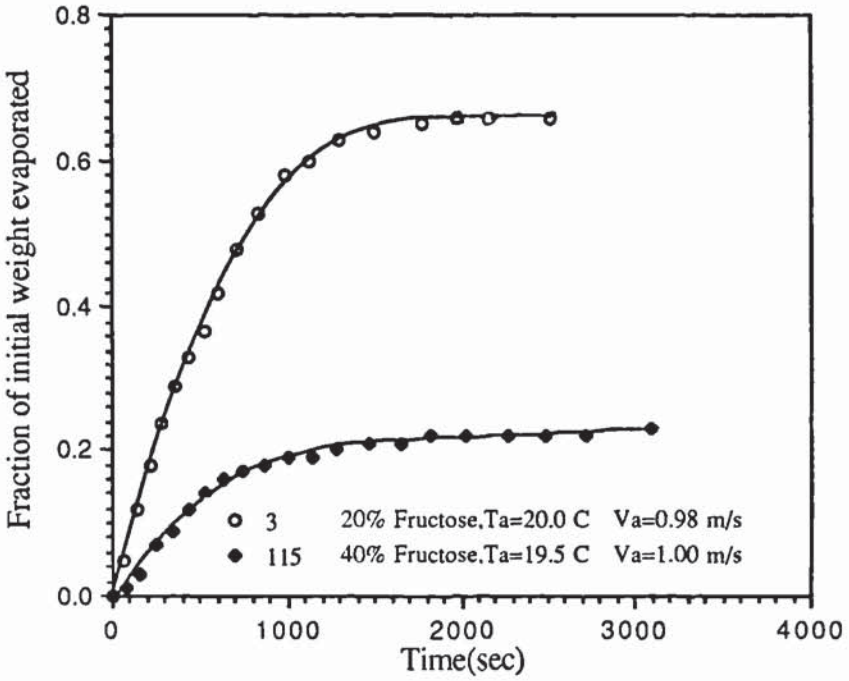

Figure 9.33 **Drying of Droplets of Fructose Solution at Various Initial Concentrations.**

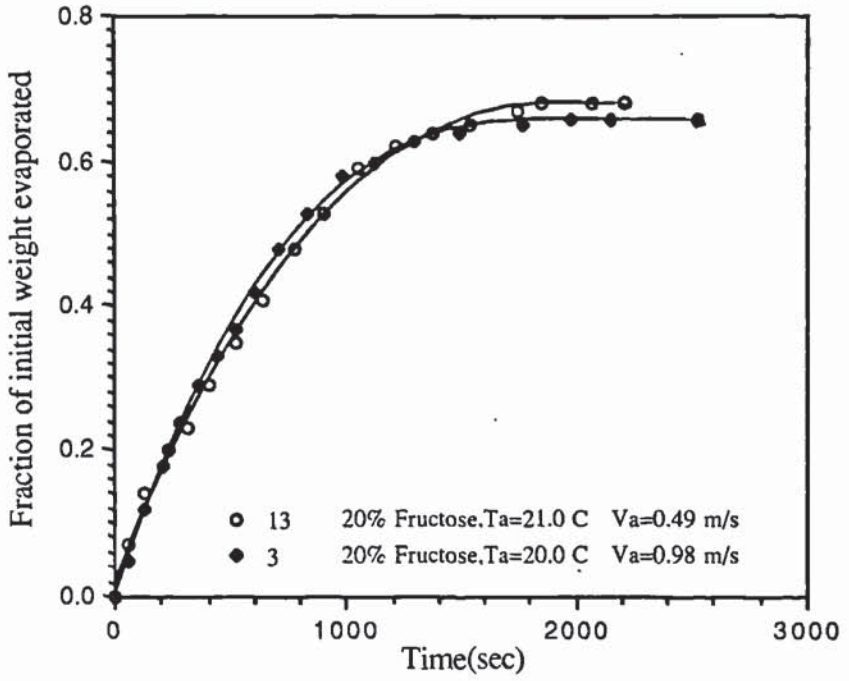

Figure 9.34 **Drying of Droplets of Fructose Solution (20% wt/wt) at Various Air Velocities.**

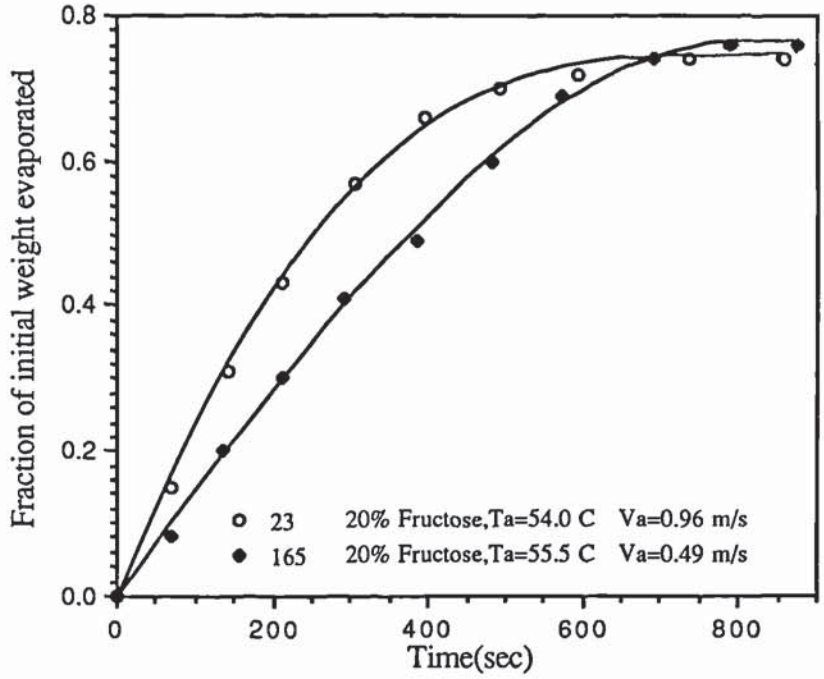

Figure 9.35 Drying of Droplets of Fructose Solution (20% wt/wt) at Various Air Velocities.

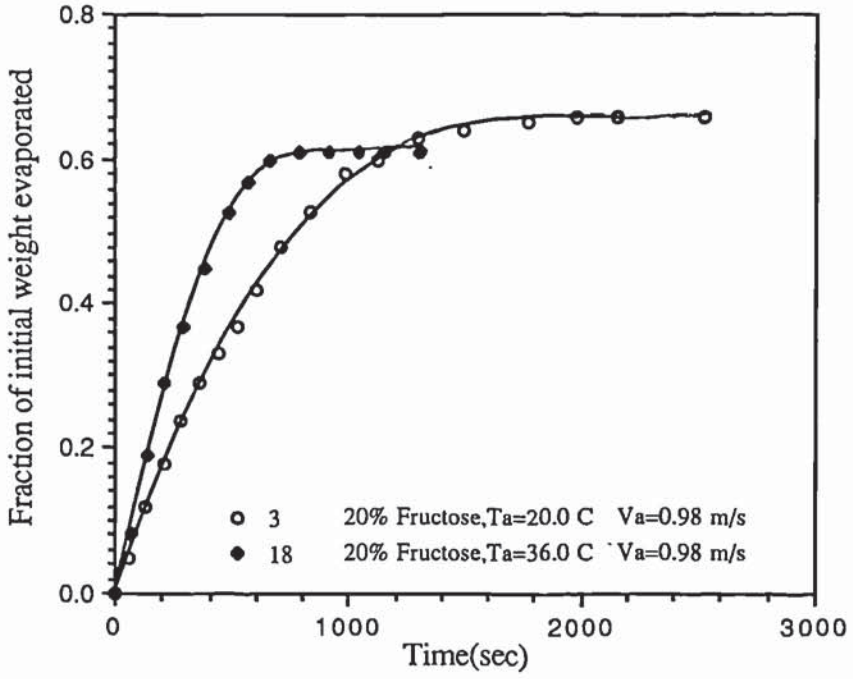

Figure 9.36 Drying of Droplets of Fructose Solution (20% wt/wt) at Various Air Temperatures.

about 1400 seconds (Figure 9.34), compared with about 500 seconds for skim milk droplets dried under similar conditions (Figure 9.27), a skin appeared on the droplet surface which resulted in the rate at the lower velocity becoming higher with both skim milk and fructose droplets. After this divergence the difference between the drying curves for fructose (Figure 9.34) was much less than with skim milk droplets (Figure 9.27). These results suggest the following,

1) The vapour pressure depression is more significant in the drying of fructose droplets.
2) The skin formed on both skim milk and fructose droplets represents a major resistance to vapour diffusion.

In comparison with the first type of skin forming material (e.g. a suspension of custard or starch), because of the need merely to lose moisture from between discrete surface particles, either a skin or crust would of course always be expected to form more readily with a suspension than with a solution.

At high air temperature (Figure 9.35) an increase in the air velocity had little effect on the drying rate. After about 600 seconds at the higher velocity conditions drying stopped; at the lower velocity drying continued to a slightly higher degree. This is because a skin appeared more rapidly on the droplet surface at the higher velocity conditions; it then thickened with time until it reached a critical thickness after which the drying process stopped. This trend is totally different to that with skim milk (Figure 9.28) and suggests that with fructose droplets the skin poses a much greater resistance to mass transfer and, once formed, represents the only major resistance until drying ceases.

9.3.2.3 Effect of Air Temperature

Figures 9.36 and 9.37 show the effect of air temperature on the drying rate for 20% weight initial solids fructose droplets. The trends of the curves at the lower and higher air temperatures are similar to those with skim milk droplets (Figures 9.29 and 9.30). They suggest that a more resistant skin formed as the air temperature was

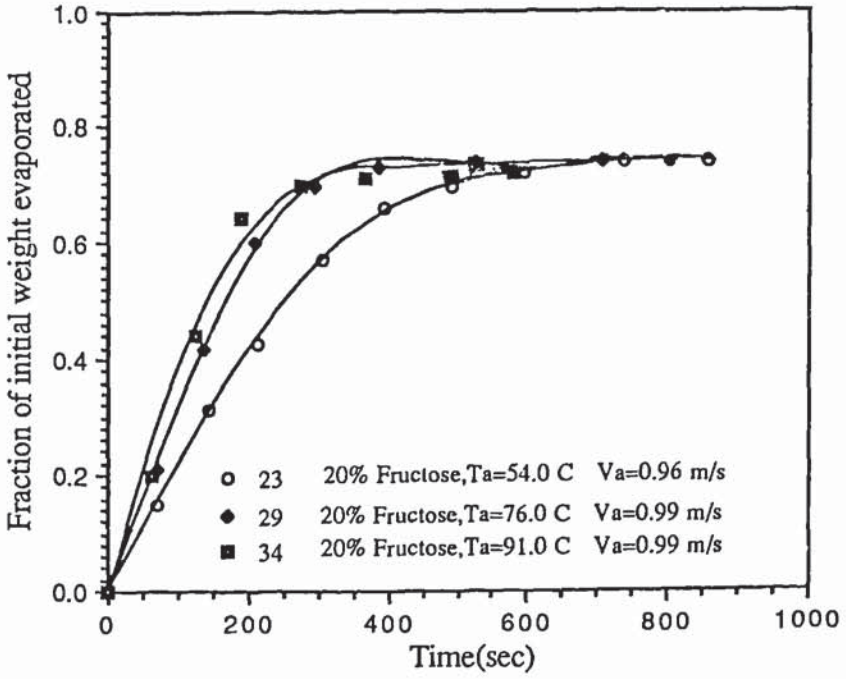

Figure 9.37 Drying of Droplets of Fructose Solution (20% wt/wt) at Various Air Temperatures.

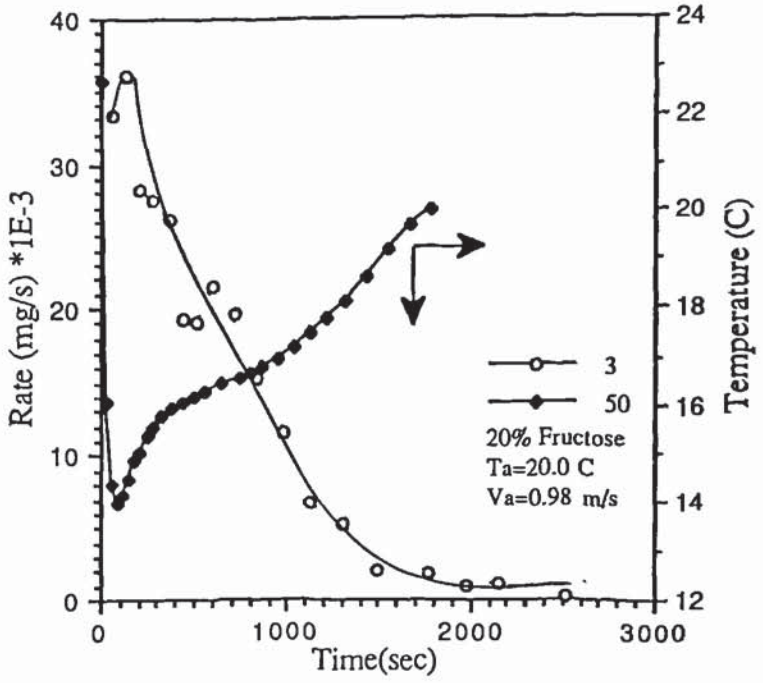

Figure 9.38 Core Temperature and Drying Rate Histories for Fructose Solution (20% wt/wt) at 20°C.

increased. The skin thickened with time and, once it reached the critical value, the drying rate became zero (i.e. drying stopped); the droplet subsequently retained the moisture content even after > 10 hours and no crust formation was observed, since the droplet remained as a viscous liquid under all the drying conditions investigated. By comparison with a skim milk droplet the drying rate became zero when the crust started to form beneath the skin. This suggests that a more resistant skin is formed on the droplet of fructose.

The core temperature and drying rate data shown in Figures 9.38 to 9.40 clearly illustrate the effect of air temperature for 20% weight solids content and air temperatures of 20 °C, 36 °C and 54 °C respectively. At the lower air temperatures of 20 °C and 36 °C, there was a short constant rate period after establishment of a drying rate. This corresponded to a core temperature history of an initial fall to the wet-bulb temperature followed by a steady rise to the air temperature. No constant rate period was observed at the higher air temperature of 54 °C (Figure 9.40); the rate started to fall after establishment of a drying rate. The rate started to fall very rapidly after about 400 seconds; this arose because at this stage the skin thickness reached the critical value which resulted in a significant increase in its resistance to vapour diffusion. These were reflected in the core temperature measurements, the droplet temperature rose immediately the droplet contacted the hot air stream; after about 400 seconds it increased very rapidly to reach the air temperature. By comparison with skim milk droplets (Figures 9.31 and 9.32), the drying rate started to decrease very rapidly after crust formation beneath the skin which led to a major increase in the resistance to vapour diffusion. With fructose it took longer for N_A but shorter for T_S to reach their final values. This confirms that lowering of the vapour pressure is more significant in fructose droplets. These results also confirm that a more powerful skin was formed offering a higher resistance to mass transfer compared to skim milk droplets. Probably the lower rate with fructose is due to a combination of factors including vapour pressure lowering. From Figures 9.29, 9.30 and 9.38 to 9.40 it is clear that a short constant rate period was established with both skim milk and fructose droplets at a low air temperatures (20 °C

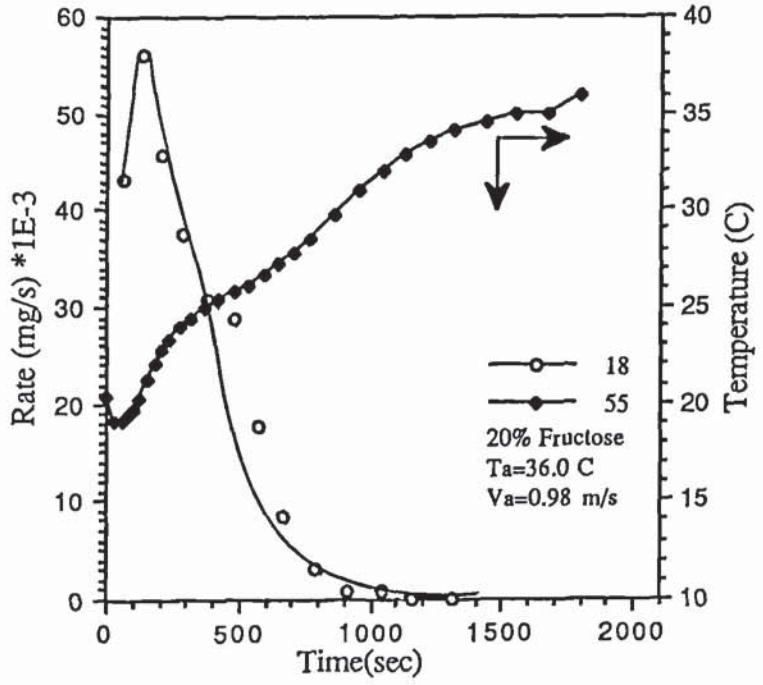

Figure 9.39 Core Temperature and Drying Rate Histories for Fructose Solution (20% wt/wt) at 36 °C.

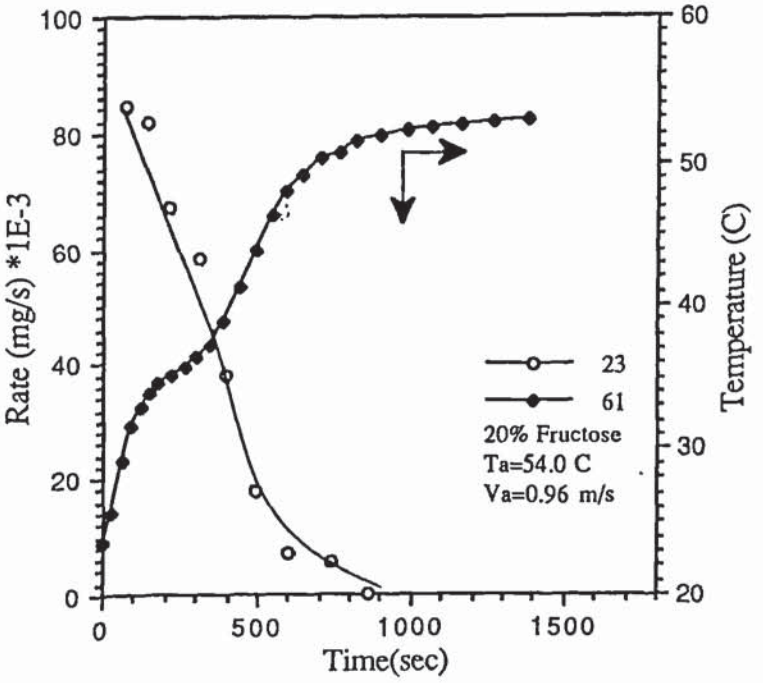

Figure 9.40 Core Temperature and Drying Rate Histories for Fructose Solution (20% wt/wt) at 54 °C.

Plate 9.12

Photographs of Droplets of 40% weight Gelatin Dried at 175 °C (Protrusion Deformation)

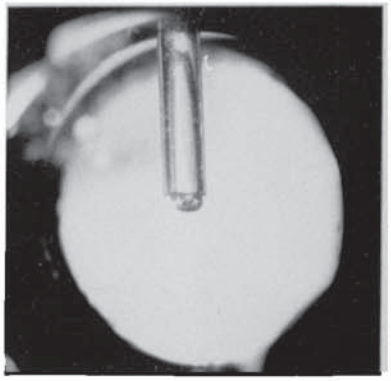

t=27 s

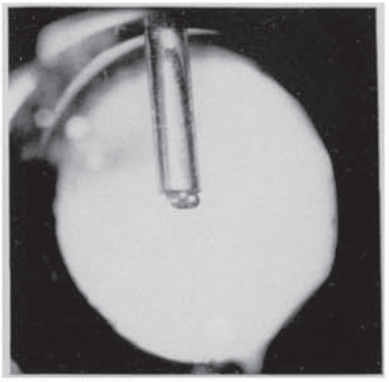

t=43 s

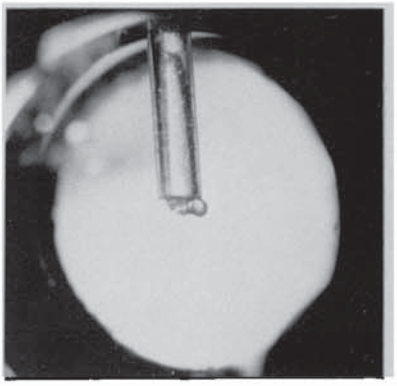

t=46 s

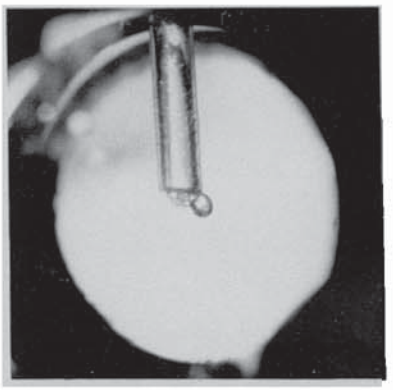

t=50 s

t=92 s

t=102 s

t=115 s

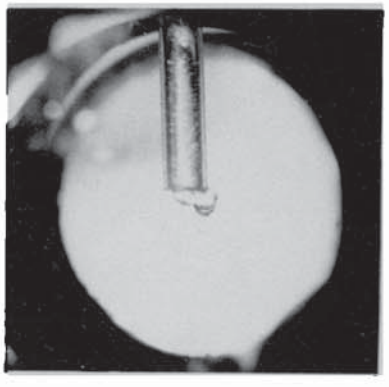

t=169 s

Plate 9.13

Photographs of a Fructose Solution (40% weight)Droplet Exhibiting an Inflation-Deflation Effect at 175 °C

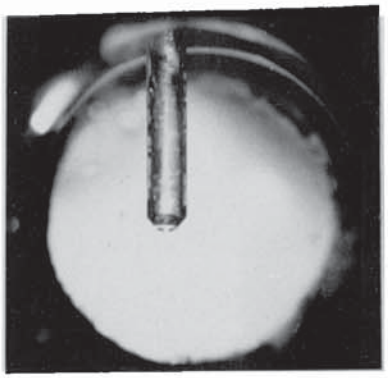

t=26 s

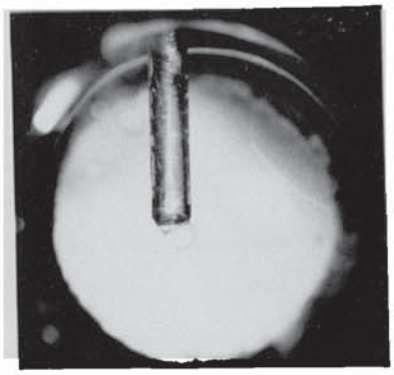

t=42 s

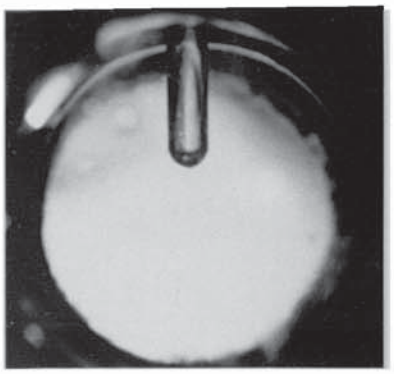

t=74 s

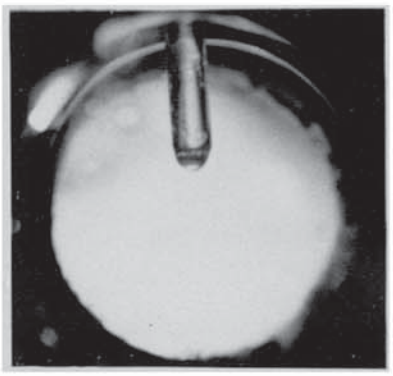

t=80 s

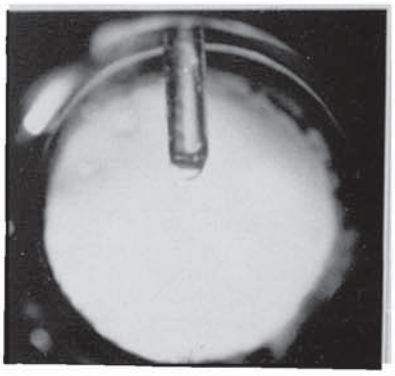

t=84 s

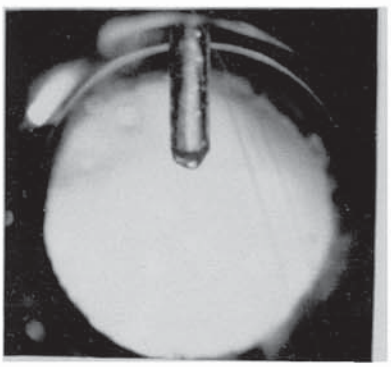

t=95 s

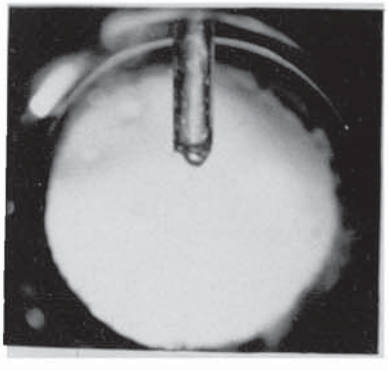

t=99 s

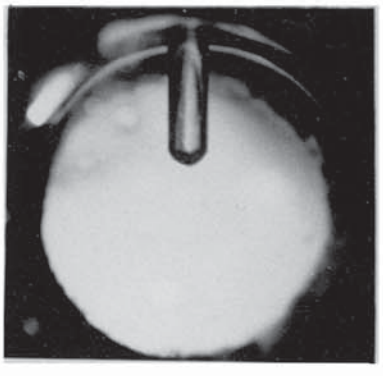

t=103 s

and 36 °C). At higher air temperatures, after commencement of drying, a falling rate was initiated; this is indicative of a very high resistance to mass transfer in the last case. At the final stage of drying a crust formed under the skin on skim milk and a final hollow shell was produced. No crust formation was observed with fructose under all the conditions investigated, and the final moisture content was retained without any change even for a drying time >10 hours. The fructose droplet also became very viscous during the final stages of drying. Therefore with fructose the skin represents the major resistance to vapour diffusion but with skim milk, once formed, the crust represented the major resistance.

Plate 9.13 represents a droplet of fructose dried at 175 °C and shows a different mechanism of expansion of the droplet after skin formation compared with gelatin droplets (Plate 9.12). The droplet started exhibiting inflation-deflation effects after 43 seconds; this was repeated a number of times until the droplet became very viscous; subsequently drying stopped completely due to the very high resistance to vapour diffusion.

9.4 MATHEMATICAL MODEL PREDICTIONS

The model discussed in Section 5.2 was used to describe the drying of single droplets of skin forming material of the first type (i.e. custard or starch suspension). The gas film heat and mass transfer coefficients were calculated according to the new correlations, equation 8.5 for mass transfer and 8.6 for heat transfer respectively.

Modelling was performed on a Commodore BBC Microcomputer and a full listing of the program is given in Appendix D.2. The change of vapour pressure with temperature and other variables required in the modelling are given in Appendix D.1.

Comparisons between the observed times at which a skin appeared on the droplet surface and those predicted, for droplets of 20% initial weight dried at different air temperatures, are shown in Table 9.1 for custard droplets and in Table 9.2 for starch droplets. Excellent agreement was achieved under all the drying conditions investigated. In general the theoretical time was higher than the experimental. This is because, it was

TABLE 9.1

MATHEMATICAL MODEL PREDICTIONS FOR DROPLETS OF CUSTARD SUSPENSION

EXP NO	AIR TEMP(C)	REY NO	SH NO	NU NO	EXPERIMENTAL TIME(sec)	THEORETICAL TIME(sec)
210	198	7.48	3.29	3.07	43.00	51.78
202	179	8.20	3.35	3.14	65.00	73.16
206	160	6.66	3.22	3.05	91.00	98.26

TABLE 9.2

MATHEMATICAL MODEL PREDICTIONS FOR DROPLETS OF STARCH SUSPENSION

EXP NO	AIR TEMP(C)	REY NO	SH NO	NU NO	EXPERIMENTAL TIME(sec)	THEORETICAL TIME(sec)
209	198	8.23	3.36	3.12	54.00	61.13
200	179	8.98	3.42	3.19	79.00	87.23
204	160	7.73	3.31	3.18	102.00	110.05

found (as discussed earlier in Section 9.1.1.3) that for both custard and starch, there is a distribution of granule sizes, and the larger granules gelatinise faster than the smaller granules. This earlier gelatinisation of the larger granules would lead to a reduction in the time required for the droplet to reach the gelatinisation temperature. The greater the gelatinisation of the larger granules the greater the reduction in time. Earlier gelatinisation of larger granules was not accounted for in the model.

The results in Tables 9.1 and 9.2 show that the time required for the appearance of the skin was lower with custard than with starch droplets. This follows because custard granules are generally larger in size than starch granules, hence they gelatinise faster, resulting in a faster appearance of the skin.

CHAPTER TEN

DISCUSSION

DISCUSSION

10.0 INTRODUCTION

The present investigation was particularly concerned with the controlling steps in the heat and mass transfer processes through the skins or crusts formed on the surface of drying droplets during the falling rate period.

Various designs of wind tunnel and different measurement techniques for evaporation rate have been used by different workers (2, 7, 39, 62). Generally the wind tunnel is designed to supply air at a constant flow rate and temperature, to simulate as closely as practicable conditions encountered in a practical spray dryer. In a spray dryer droplets are subjected to swirling air which causes droplet rotation. Therefore a single droplet suspended from a suspension device which ensures rotation during drying can be expected to simulate more closely the conditions within a spray dryer. This was achieved in the present investigation in which a single droplet was suspended from a specially designed, rotating nozzle. The design of the wind tunnel and the droplet suspension technique are discussed in the following sections. The advantages and novelty of the nozzle design are highlighted.

Different correlations have been proposed by various investigators to predict the heat and mass transfer coefficients. However, agreement between different sources is often lacking, especially at high temperatures. Correlations of Sherwood and Nusselt numbers derived in this study are discussed and compared with other published correlations. The drying mechanisms of the three types of skin-forming materials are discussed and compared. The importance of the skin structure under different drying conditions, and its effect upon the drying rate, are highlighted.

10.1 EXPERIMENTAL TECHNIQUES

Different techniques have been used by various investigators (2, 4, 7, 8, 9) for droplet suspension. With pure liquid droplets, evaporation rates were

determined by measuring the rate of supply of liquid through a suspension device such as a nozzle or capillary to maintain a constant droplet diameter (2, 10). These techniques cannot however be used to study the drying of droplets containing suspended or dissolved solids, once a skin or crust has formed on the droplet surface.

The technique of suspending a droplet from the end of a glass filament has been widely used (3, 4, 8, 62) to study the drying of single stationary droplets (i.e. droplets which did not rotate). Drying rates have been found by measuring the deflection of the filament. Such a technique, although allowing direct measurement of the droplet weight during the drying process, is limited in application since the droplet is not able to rotate in a swirling air flow, so that the rates of evaporation vary over the surface. Furthermore the drying from stationary droplets is from only one side, the rate of drying being greatest on the side facing the air flow, and lowest in the wake region.

Audu (10) and Ali (7) used stainless steel rotating nozzles as droplet suspension devices. The evaporation rates were determined using a hygrometer to measure changes in air humidity before and after the suspended droplets and were hence critically dependent on the instrument accuracy when measuring relatively small changes. Although the droplets were allowed to rotate, disadvantages arose from:

1) Since the nozzle design did not facilitate direct measurement of the changes in droplet weight and temperature as drying proceeded, reliance was placed upon a humidity balance on the air stream to measure the evaporation rate.

2) Due to the nozzle's material of construction, it conducted more heat into the droplet than with a material of lower thermal conductivity, e.g. glass.

Use of the above technique to measure the evaporation rate was probably highly inaccurate. For example a check on its reliability during the present work demonstrated a substantial difference between the upstream and downstream air humidity even when no droplet was suspended from the nozzle. This may have arisen

because of the need to identify very small changes in humidity i.e. of the order of 1-4% relative humidity. This behaviour would have led to inaccurate measurement of the evaporation rate. For example the drying rates for droplets of 50% weight initial concentration of sodium sulphate decahydrate dried at high air temperatures of 100-120 ^{o}C measured by Ali (7), exhibited significant constant rate periods as in Figure 4.2. Recently however when Bains (62) used the filament thermocouple technique and measured the drying rate of the same material, at a lower temperature of 74 ^{o}C and lower concentration of 15% weight, no constant rate period was observed, as in Figure 4.9. Also, the drying rates shown in Figure 4.3 for the material described by Ali (7) as skin forming exhibited very long constant rate periods even at a high air temperature of 135 ^{o}C. Conversely in the present investigation only very short constant rate periods were observed even at low air temperatures for all three types of skin forming materials studied. The above results suggest that the hygrometer readings in Ali's work were too high although a crust or skin had encased the droplet (i.e. falling rate period). This may have arisen because of the need to identify very small changes in humidity. This could have resulted in readings of the hygrometer for the downstream air being too high. This led to a long 'constant rate period' (7) even under drying conditions where no constant rate would be anticipated. Later in the falling rate period, when the drying rate was significantly reduced due to the increase in the skin or crust thickness (i.e. resistance to mass transfer increased), the hygrometer started to give readings of falling rate period.

The above disadvantages were overcome in the present investigation. As described in Section 6.4, a range of nozzles were designed to facilitate suspension from a hanger beneath an analytical balance. All nozzles were made to accommodate a thermocouple sensor of 0.5mm diameter for improved droplet temperature measurements. The nozzles were constructed from glass, a material of low thermal conductivity, minimising the heat conducted through the nozzle into the droplet.

The techniques of inserting a thermocouple into the centre of droplets suspended from a filament, or suspending droplets from thermojunctions, were the

most common for the studies of the core temperature histories. However, several workers ignored the heat gain through conduction via the thermocouple leads which would invariably have raised the temperature at the junction. This was overcome by Cheong (8) who improved the above technique and developed a glass filament-thermocouple as a single unit as described in Section 4.2. This technique reduced the heat conduction into the junction, but there was still some which could have affected the sensitivity. In the present design of rotating glass nozzle, conductive heat transfer to the thermojunction of the thermocouple sensor was totally avoided. This was achieved because the thermocouple sensor was contained within the glass nozzle as described in Section 6.4, i.e. no part of the thermocouple was exposed to the drying medium.

The major disadvantage of the filament-thermocouple technique (8, 62) is that a droplet drying on the tip of the filament encases the tip as it dries. Therefore complete crust recovery is impossible, so that particle morphology cannot be studied. With the present design of rotating nozzle, complete crust recovery can be achieved for further study. Furthermore with the filament-thermocouple technique it is very difficult or impossible, to transfer a droplet of high solids content or very viscous material (e.g. a droplet of gelatin solution even at very low concentration) onto the filament using a syringe. The nozzle used in the present investigation facilitated formation of a droplet of any kind of material irrespective of the concentration or viscosity.

With the previous rotating nozzle design (7) a thermocouple junction was inserted into the droplet after every increment of time to measure the core temperature, as discussed in Section 6.2. Ali measured the core temperature history of sodium sulphate decahydrate droplets using this technique but failed to detect an important phenomenon. During drying of this material when the core temperature reaches 33 ^{o}C there is a sudden decrease in temperature to 25 ^{o}C. As shown in Figure 4.5, Ali (7) did not observe this depression, but reported a constant temperature at ~33 ^{o}C for an air temperature of 60 ^{o}C. Recently Bains (62) using the filament-thermocouple,

successfully detected the decrease in temperature as shown in Figures 4.6 and 4.7. In the present investigation, a similar phenomenon (i.e. a sudden decrease in core temperature) was observed when drying gelatin droplets as shown in Figure 9.24. The present technique for measuring the drying rate also successfully detected the increase in the rate which resulted from the decrease in core temperature. These results demonstrate the sensitivity of the newly-designed rotated glass nozzle. A further advantage of the present technique of core temperature measurement, was that the thermocouple junction was positioned precisely in the centre of the core. Conversely most techniques for droplet temperature measurement were carried out with fine thermocouples by suspending droplets from thermojunctions. In these cases if any part of the junction was not completely-immersed in the droplet, an average temperature was recorded between the exposed and immersed part of the junction.

10.2 WATER DROPLET EXPERIMENTS

The horizontal wind tunnel was tested using pure water droplets. Evaporation from a saturated surface (i.e. represented by water droplets) was studied at air temperatures ranging from 23 ^{o}C to 80 ^{o}C and air velocities between 0.018 and 1.65 m/s. At ambient temperature, the values of β and ϕ in equations 8.1 and 8.2 were 0.575 and 0.552 respectively; this is in very good agreement with the values of β and ϕ of 0.6 reported by Ranz and Marshall (2), and the value of β of 0.552 reported by Frossling (12). This agreement confirmed the reliability of the present design of wind tunnel and droplet suspension technique.

No expression is available in the literature to estimate the experimental Sherwood number applicable to the evaporation of a pure liquid droplet which decreased in diameter during the process. A mathematical model was therefore proposed for estimating the experimental Sherwood number for pure liquid droplets; this is presented in section 5.1.1. The novelty of the model is that the values of β and ϕ were almost identical at ambient and elevated temperatures. The small difference may be due to some inaccuracy in the physical properties (e.g. diffusivity) upon

which the calculation was based. This confirmed the mass and heat transfer analogy (110). In a previous investigation, Ali (7) obtained widely different values for β and ϕ, for example 0.516 and 0.668 respectively at ambient temperature. This may have arisen from the use of Audu's (10) model to calculate the mass transfer coefficients, a model applicable for droplets of constant diameter (this criterion was achieved in Audu's experimental technique, since liquid was supplied continuously via the feeding device).

At ambient and elevated temperatures, the experimental Sherwood and Nusselt numbers were corrected for heat conduction through the glass suspension device and heat transferred by radiation, as described in Sections 5.1.3 and 5.1.4.

Ali (7) and Ranz and Marshall (2) ignored these corrections assuming them to be insignificant. This may be justified at low temperatures, but at high temperatures these corrections could be significant. At elevated temperatures, the values of β varied from 0.55 to 0.46 and values of ϕ varied from 0.53 to 0.44 for air temperatures between 43.5 ^{o}C to 80 ^{o}C.

Spalding (111) proposed that heat transferred to the outward diffusing vapour at high temperatures can be accounted for by the transfer number B. Audu (10) has proposed a temperature correction term (T_a-T_s)/(ambient temperature) with an index of -0.008 to fit his results. Consequently the transfer number and the temperature correction term were included in equations 8.1 and 8.2 to correlate the results at high temperature, resulting in the modified Sherwood and Nusselt equations,

$$Sh = 2.0 + 0.57 \left(\frac{T_a - T_s}{T_{amb}}\right)^{-0.04} Re^{0.5} Sc^{0.33} \qquad \text{--------10.1}$$

$$Nu = 2.0 + 0.27 \left(\frac{1}{B}\right)^{0.18} Re^{0.5} Pr^{0.33} \qquad \text{--------10.2}$$

10.3 DROPLETS OF SKIN FORMING MATERIALS

10.3.1 DROPLETS OF THE FIRST TYPE

10.3.1.1 Effects of Initial Concentration

As discussed earlier, and shown in Figures 9.1, 9.2 and 9.13, with both custard and starch, an increase in the initial solids content had little effect on the drying rate.

The larger custard granules absorbed more water than the starch granules. Therefore the drying rate became zero when the fraction evaporated for the higher custard concentration reached 0.53 (Figure 9.1), compared to a possible 0.8. For starch the fraction evaporated was 0.72 (Figure 9.13). These confirm that the custard granules absorbed more water, leaving less free water in the suspension. As a consequence drying stopped completely after evaporation of the free water, since it was extremely difficult to remove the remaining moisture from within the swollen granules of custard under the drying conditions used.

10.3.1.2 Effect of Air Temperatures

As shown in Figures 9.10 and 9.17 at low air temperatures for both custard and starch at a concentration of 20% wt/wt, there was a short initial constant rate period prior to the falling rate period. The droplet core temperature also remained at the wet-bulb temperature for a short time before rising to the air temperature. A much greater drying rate was established at 36 ^{o}C. This indicates that the crust provided a reduced resistance to mass transfer because, under these conditions of air temperature, no gelatinisation took place. This resulted in the formation of a normal porous crust providing little resistance to the mass transfer process. This behaviour was confirmed by the electron microphotographs of the final dried crust. As is evident from Plates 9.1 a and 9.4 a, the final dried crust consisted of an open crystalline structure. After crust formation on the droplet surface, the gradients of the curves diverge to fall more rapidly due to the increase in the resistance to vapour diffusion.

At the high drying temperatures, no constant rate periods were observed for either custard or starch, as shown in Figures 9.11, 9.12 and 9.18. Upon establishment of a drying rate, it proceeded to fall rapidly. The fall was more rapid at the higher air temperature (Figure 9.12), which resulted in a higher degree of swelling of granules. With custard droplets after about 300 seconds at 54 ^{o}C (Figure 9.11) compared with about 220 seconds at 76 ^{o}C (Figure 9.12) and, about 400 seconds at 54 ^{o}C with starch droplets (Figure 9.18), the gradients of the curves diverge to fall more rapidly. These were consistent with core temperature measurements and coincided with the appearance of the crust on the droplet surface. Hence, as would be expected, the crust forms more rapidly at higher air temperature. The faster appearance of the crust on the droplet surface of custard arose because the larger custard granules absorbed more water than the starch granules; as a result less free water was left in a custard droplet and hence it took less time for the appearance of the crust.

It can be concluded that a crust offering an increased resistance to mass transfer was formed at higher air temperatures. This is associated with increased swelling of granules at increased air temperature and hence an increased crust resistance. The granules become pliable and easily adhere to each other due to swelling or gelatinisation and thus block the pores, resulting in a significant increase in the resistance to mass transfer. The microphotographs of the final dried crusts highlight this behaviour. Plates 9.1 c and d and Plates 9.5 c and d, clearly illustrate that granules are swollen to a larger extent at high temperature compared with those at low temperature (Plates 9.1 a and 9.5 a).

10.3.2 DROPLETS OF THE SECOND TYPE

10.3.2.1 Effect of Air Velocity

Figures 9.20 and 9.21 show the effect of air velocity at ambient temperature and 54 ^{o}C respectively. At ambient temperature the air velocity had little effect on the initial drying rate. However after about 200 seconds, a reduction in air

velocity, resulted in a significant increase in the drying rate. The curves shown in Figure 9.20 show that the difference (distance) between them increases with time.This occurs because initially free moisture is removed by the drying medium; subsequently there is believed to be a tendency to form a sheath of partly-dried gelatin around the granules. The formation of this sheath causes the drying rate at this stage to be significantly reduced. Since the sheath forms more rapidly at higher velocity, the drying rate at the lower velocity becomes higher and drying continues to a greater extent. Hence under these drying conditions a lower air velocity is actually preferable to dry the gelatin droplets.

At an air temperature of 54 ^{o}C (Figure 9.21), the air velocity had little effect on the initial drying rate. Under these conditions the granules dissolved in water, which led to transformation of the gel into a sol. The formation of the partly-dried gelatin sheath was thus delayed and, when it formed, its effect on the mass transfer process was reduced because it enclosed a solution; this resulted in water migration to the surface being faster. Hence the difference (distance) between the drying rate curves at low and high velocity is significantly reduced, i.e. about half that at ambient temperature. Also due to the delay in the formation of the sheath around the granules, the initial drying rates for both the higher and lower velocity are slightly different up to about 400 seconds compared with 200 seconds at ambient temperature. Moreover at 54 ^{o}C and 0.49 m/s (Figure 9.21) the fraction of initial weight evaporated reached 0.71 in a drying time of 1317 seconds, while for a similar velocity at ambient temperature a value of 0.74 was reached after a drying time of > 2500 seconds. Therefore since the dried crust at 54 ^{o}C keeps the structure and properties of the original powder the best drying conditions for gelatin under the conditions studied were an air temperature of 54 ^{o}C and a velocity of 0.49 m/s.

10.3.2.2 Effect of Air Temperatures

In normal drying practice, the removal of moisture proceeds more rapidly the higher the air temperature, because of the higher coefficients of heat and mass

transfer and the increased temperature driving force. Drying of droplets of gelatin gel represents a difficult case because the initial stages of drying cannot be performed at too high a temperature, as the gel will liquefy. From Figure 9.22, increasing the air temperature from 20.5 °C to 36 °C increased the drying rate. After a drying time of 2838 s at 20.5 °C, only 74% of the initial moisture content was removed; at 36 °C after 2121 seconds, over 91% of the initial moisture content was removed. Clearly under these conditions an increase in the air temperature greatly improved the drying rate. Figure 9.23 shows that increasing the air temperature to 54 °C improved the drying rate further.

The gel does not liquefy at 36 °C or 54 °C. Hence the dried crust has the same structure and properties as the original powder. Therefore 54 °C was the optimum temperature for drying the gel under the conditions studied. Increasing the air temperature above this value has a deleterious effect on the drying rate and the quality of the dried crust. From Figure 9.23, at 76 °C and 91 °C since the wet-bulb temperature of the air is higher than the melting point of the granules the gel liquefies. As a result the initial drying rates are improved slightly. However after about 500 seconds at 76 °C and 420 seconds at 91 °C drying stopped although a significant amount of moisture remained in the core. This behaviour is attributed to formation of a dry thin skin immediately after the granules melt; the mass transfer is then by diffusion through this skin. The skin gradually increases in thickness and the mass transfer is progressively reduced; when the skin thickness reaches a critical value the mass transfer process stops. After the gel melts, the original structure and properties are irreversibly lost, which is not desirable in a dried product. Therefore the optimum drying temperature is the maximum air temperature possible at which the wet-bulb temperature remains below the gel melting point.

Electron microphotographs in Plate 9.7 show the external crust structure of gelatin droplets dried under different conditions of air velocity and temperature. At ambient temperature the outer surface at the higher velocity (Plate 9.7 a) is very rough with no pores; at lower velocity (Plate 9.7 b) the surface is smoother. As the air

temperature was increased to 54 °C (Plate 9.7 c and 9.7 d) the granules dissolved in water, resulting in a smooth outer surface. Increasing the air temperature further led to melting of the gel and a very smooth dried skin formed on the surface. This behaviour is shown in Plates 9.7 e and 9.7 f, demonstrating a smoother surface with a blow hole.

10.3.3 DROPLETS OF THE THIRD TYPE

At low air temperatures (20 °C and 36 °C) the drying rates of single suspended droplets of skim milk and fructose increased initially to maximum values before the falling rate period commenced. Figures 9.38 and 9.39 demonstrate that the core temperatures also decreased to minimum values (the wet-bulb temperature) before rising to the air temperature. At high air temperatures (54 °C and 76 °C) no constant rate period was observed. For droplets of 20% initial solids content, upon establishment of a drying rate it immediately proceeded to fall. This was reflected in the core temperature history, i.e. the droplet temperature began to increase immediately the droplet contacted the hot air stream (Figures 9.13, 9.32 and 9.40). Under all the drying conditions investigated, the rate began to decrease more rapidly (due to an increase in the resistance to vapour diffusion) after the crust started to form beneath the skin in droplets of skim milk or after the skin thickness reached the critical value in fructose droplets. All these observations were consistent with the core temperature measurements i.e. the core temperature began to increase more rapidly.

The formation of a more resistant skin with an increase in the drying temperature was confirmed by the electron microphotographs of the final dried crust. As is evident from Plates 9.8 and 9.9, a smoother skin was formed on the surface at the higher temperatures; this would offer a higher resistance to mass transfer. A blow hole was observed on the outer crust dried at 76 °C (Plate 9.9 a) and major fissures on the inner crust surface (Plate 9.9 b). These confirm the higher resistance to diffusion offered by the skin formed at higher drying temperatures.

10.3.4 COMPARISONS BETWEEN THE THREE TYPES

The skin on materials of the first type forms due to granules swelling or gelatinisation at high drying temperatures. At low temperatures no skin formation was observed and a normal porous crust was formed. Increase in the air temperature resulted in an increase in the swelling of the granules. This led to a less porous crust and the crust resistance became more significant. When the air temperature was increased to 198 ^{o}C at a low air velocity of 0.1 m/s, all the granules gelatinised perfectly. This resulted in complete transformation from a crust resistance to a skin resistance. Under these conditions the droplet exhibited the inflation-deflation effects characteristic of skin forming materials. In summary, an increase in air temperature led to a gradual transfer from a crust to a skin (i.e. increased resistance) and the original granular structure and properties were irreversibly lost.

With the second type , partly dried sheaths were formed around the swollen granules at low temperatures (less than 30 ^{o}C). This sheath behaved like a skin in resisting the mass transfer. As the air temperature was increased above 30 ^{o}C, up to the maximum air temperature at which the wet-bulb temperature was less than the melting point of the granules, a smoother dried surface crust was formed which offered a higher resistance to mass transfer. This is due to the transformation of the gel into a sol resulting from dissolution of the granules in water. Under these conditions the original granular structure and properties were retained, which may be a very important feature of a dried product. When the wet-bulb temperature exceeded the melting point of the granules, all the granules melted (liquefied) and a dry skin formed immediately on the surface. This skin thickened with time and mass transfer decreased until it stopped completely leaving a significant amount of moisture in the core. Under these drying conditions the original structure and properties of the granules were irreversibly lost. When drying at very high temperature (>100 ^{o}C) the droplet exhibited multiple inflation-deflation effects.

With the third type of material a skin always appeared on the surface of the droplet at a certain stage depending on the drying conditions. An increase in air

temperature resulted in the formation of a smoother skin offering a higher resistance to mass transfer. At temperatures over 100 ^{o}C droplets of this type exhibited puffing or ballooning phenomena; the droplet inflated and deflated many times before forming the final dried crust.

CHAPTER ELEVEN

CONCLUSIONS AND RECOMMENDATIONS

CONCLUSIONS AND RECOMMENDATIONS

11.1 CONCLUSIONS

1) The present investigation comprised a first attempt to directly measure droplet weight and core temperature for suspended rotating droplets, using a novel rotating glass nozzle developed specially for this purpose. A range of nozzles was designed to facilitate suspension from an analytical balance with a capacity up to 55gm-0.1mgm. Each nozzle was of glass to minimise heat gain by conduction and it accommodated a thermocouple sensor of 0.5mm diameter for improved droplet temperature measurement.

2) None of the previously published correlations adequately predicted the Sherwood and Nusselt numbers obtained experimentally for pure liquid droplets. The experimental data were however well correlated by the modified Sherwood and Nusselt equations 8.5 and 8.5 respectively.

3) Most previous researchers who measured evaporation rates from suspended droplets ignored heat gain along the droplet suspension device (e.g. nozzle or filament) resulting in significant experimental errors. Heat conduction through the nozzle and gains by radiation heat were accounted for in the present work.

4) Skin-forming materials were classified for the first time into three different types. In the first type, formation of a skin was due to granule gelatinisation at high drying temperatures. The skin in the second type formed under any drying conditions immediately drying took place, but at higher drying temperature, a more resistant skin was formed. With the third type of material the skin appears on the droplet surface at a certain stage of the drying process under any drying conditions and its resistance to mass transfer increased with an increase in the drying temperature.

5) A mathematical model has been developed for the drying of droplets of skin forming material of the first type. The model is based on the assumption of the formation of a skin instantaneously after granule gelatinisation as soon as the droplet

temperature reaches the gelatinisation temperature. Excellent agreement was obtained between model predictions for time to skin formation and those observed experimentally.

6) Drying rate and core temperature studies were carried out on suspensions (custard and starch) / solutions (skim milk, gelatin and fructose) of the three types of skin forming material. Air velocities of 0.49 m/s to 1.0 m/s, air temperatures of 20 ^{o}C to 106 ^{o}C and initial solids contents between 20% wt/wt to 40% wt/wt were used. A number of experiments were also carried out at very high temperature (> 150 ^{o}C) with air velocities of 0.1 m/s-0.5 m/s. A Scanning Electron Microscope was used to determine the nature of the final dried crust.

For single suspended droplets of gelatin (the second type), the newly-designed rotating glass nozzle apparatus successfully detected the decrease in core temperature and increase in drying rate resulting from granule dissolution at 30 ^{o}C. This is in contrast to previous studies of Audu (10) and Ali (7) which failed to detect such phenomena.

In general all three types of skin forming materials dried at an initial constant rate in low temperature air (e.g. 20 ^{o}C and 36 ^{o}C). The rate then fell as the skin or crust (in the first type), grew in thickness, and its resistance to mass transfer increased. At high temperatures (e.g. 54-106 ^{o}C) no constant rate period was observed because a more resistant skin or crust was formed.

11.2 RECOMMENDATIONS FOR FUTURE WORK

1) The mathematical model for skin formation should be extended to cover the third type of skin forming material. In this type a skin forms first on the droplet surface; this will increase in thickness until it reaches the maximum then a crust starts to form. Therefore the model should be based on the assumption that when the concentration of the colloidal materials which are responsible for the formation of the skin reaches a critical value, any further evaporation results in the appearance of the skin instantaneously on the droplet surface.

2) For the materials of the third type the model could be extended further to cover the "puffing or ballooning" phenomena occurring at drying temperatures of > 100 °C. The model should based on the assumption that when the droplet temperature reaches the elevated boiling point, inflation starts instantaneously. The model could predict the time at which inflation of the droplets start, for comparison with experimental data on materials of this type e.g. skim milk, sucrose, coffee.

3) The effects of experimental variables i.e. initial concentration, air temperature and velocity on the morphology of all the three types, and especially the third type, of skin forming materials should be studied. The rotating glass nozzle which has been developed would be ideal for such a study, since it facilitates direct measurement of the droplet weight and temperature during drying and allows a recovery of an intact, final dried crust. The suspended droplet is also allowed to rotate freely whilst drying.

4) Studies could be undertaken of the effect of additives to improve drying characteristics of skin forming materials especially materials of the third type since this includes a wide range of materials of natural products such as sucrose, skim milk, coffee etc.

5) Consideration could be given to how industrial drying processes could benefit from application of some of the fundamentals established in this work e.g. spray drying of coffee. The objective would be to promote skin formation, to 'seal in' flavour, but to ensure that this skin was sufficiently porous that under the temperatures of operation it did not undergo inflation-rupture-deflation effects. The limitations on additives to specific natural products does not apply to formulations so that 4 can be one approach. Moreover it is far from proven that for every product rapid drying at high temperature (i.e. countercurrent spray drier operation) is necessarily worse for product degradation than slower drying at lower temperature (cocurrent operation) (143). The final desired morphology for product use is another complicating factor (142).

NOMENCLATURE

A	-----	Surface area	m^2
A_h	-----	Surface area for heat transfer	m^2
A_m	-----	Surface area for mass transfer	m^2
a	-----	Thickness of skin	m
b	-----	Distance between glass bead surface and water droplet	m
C	-----	Concentration of solute	g solute/ml
C_o	-----	Initial concentration of solute	g solute/ml
C_A	-----	Molar concentration of A	
ΔC	-----	Concentration driving force	kg/m^3
C_∞	-----	Concentration at an infinite distance	kg/m^3
C_c	-----	Heat of crystallisation per kg of water evaporated	J/kg
C_p	-----	Heat capacity of air	J/kg/K
C_{pa}	-----	Specific heat capacity of air	J/kg/K
C_{pd}	-----	Specific heat capacity of droplet	J/kg/K
C_{ps}	-----	Specific heat capacity of solid	J/kg/K
C_{pv}	-----	Heat capacity of diffusing vapour	J/kg/K
C_{pw}	-----	Specific heat capacity of water	J/kg/K
C_r	-----	Constant	
C_s	-----	Concentration at the droplet's surface	kg/m^3
C_{so}	-----	Initial concentration of solid	kg/m^3 suspension
C_{wo}	-----	Initial concentration of water	kg/m^3 suspension
d	-----	Diameter	m

d_f	-----	Diameter of filament	m
d_g	-----	Glass bead diameter	m
dh	-----	Maximum horizontal distance	m
d_n	-----	Diameter of nozzle	m
d_p	-----	Diameter of the particle	m
D_{AB}	-----	Diffusion coefficient of A in a mixture of A and B	m^2/s
D_v	-----	Molecular diffusivity	m^2/s
e	-----	Emissivity of the droplet	
e_g	-----	Emissivity of the glass nozzle	
e_n	-----	Emissivity of the nozzle	
f	-----	Turbulence factor	
Fa	-----	Geometry factor	
g	-----	Acceleration due to gravity	m^2/s
G	-----	Dry air mass flow rate	kg/s
h_f	-----	Heat transfer coefficient for glass filament	$W/m^2/K$
h_g	-----	Gas film heat transfer coefficient	$W/m^2/K$
h_n	-----	Heat transfer coefficient for glass nozzle	$W/m^2/K$
H_l	-----	Henry's law constant	
H_N	-----	Heat transfer coefficient of nozzle	W/m^2K
k_c	-----	Crust mass transfer coefficient	m/s
K	-----	Thermal conductivity of air	W/m/K
k_g	-----	Gas film mass transfer coefficient	m/s
K_o	-----	Overall mass transfer coefficient	m/s
k_s	-----	Skin mass transfer coefficient	m/s
k_t	-----	Thermal conductivity of glass	W/m/K

k_v	-----	Thermal conductivity at film conditions	W/m/K
m	-----	Mass flow rate	kg/s
M_w	-----	Molecular weight of water	
N_a	-----	Rate of mass transfer per unit area	$kg/m^2/s$
N_A	-----	Rate of evaporation	kg/s
N_{Ao}	-----	Rate of evaporation in a stagnant medium	kg/s
P	-----	Gas pressure	atmos
ΔP	-----	pressure drop across the gas film	atmos
P_{bm}	-----	Average partial pressure in the boundary layer	atmos
P_{wd}	-----	Vapour pressure at the droplet's surface	atmos
P_{wa}	-----	Partial pressure of water vapour in the air	atmos
Q	-----	Rate of heat transfer	W
q_e	-----	Rate of heat transfer by radiation	W
q_f	-----	Rate of heat transfer to a droplet through glass filament	W
Q_{in}	-----	Total rate of heat transferred to the droplet	W
q_n	-----	Rate of heat transfer to a droplet through the nozzle	W
r	-----	Radius of the droplet	m
rd	-----	Radius of the droplet	m
rdo	-----	Initial droplet radius	m
r_1	-----	Outer radius of an evaporating droplet	m
r_2	-----	Radius of the gas film	m
r_o	-----	Initial radius of the droplet	m
R_c	-----	Universal gas constant	atmos m^3/kgmole/K

S	-----	Rate of production of fresh surface	s^{-1}
S_b	-----	Specific surface area of the pores	m^{-1}
t	-----	Time	s
T	-----	Temperature	K
Δt	-----	Time interval	s
ΔT	-----	Temperature driving force	K
ΔT_s	-----	Change in droplet temperature from initial value to gelatinisation temperature	K
T_a, T'_a	-----	Air temperature in ^oC and K respectively	
T_{amb}	-----	Ambient temperature	K
ΔT_d	-----	Temperature driving force	K
T_g, T'_g	-----	Gas temperature in ^oC and K respectively	
T_o	-----	Outlet air temperature	K
t_s	-----	Time at which skin forms on the droplet surface	s
T_s, T'_s	-----	Droplet temperature in ^oC and K respectively	
V_a	-----	Velocity of air	m/s
V_A	-----	Velocity of air (in Figures 4.6-4.9)	m/s
V_g	-----	Velocity of gas	m/s
w	-----	Weight of the droplet	kg
x	-----	Radius of the core	m
X	-----	Dimensionless diameter	
Y	-----	Dimensionless concentration	
Z	-----	Distance in the direction of diffusion	m

DIMENSIONLESS GROUPS

B	-----	Transfer number	$C_{pa}\,\Delta T / \lambda$
B'	-----	Transfer number	$C_{pa}\Delta T / (\lambda - q_e/N_A)$
B_f	-----	Transfer number at film conditions	
Gr	-----	Grashof number	$d_p^3\,\rho\,g\,\beta_1\,\Delta T/\mu^2$
Nu	-----	Nusselt number	$h_g\,d_p / k$
Nu_f	-----	Nusselt number at film conditions	"
Nu_o	-----	Nusselt number under stagnant conditions	"
Pr	-----	Prandtl number	$C_{pa}\,\mu / k$
Pr_f	-----	Prandtl number at film conditions	"
Re	-----	Reynolds number	$d_p\,V_a\,\rho_a / \mu$
Re_g	-----	Reynolds number for the gas stream	"
Re_m	-----	Reynolds number defined as	$\rho_g\,V_g\,d / \mu_f$
Re_n	-----	Reynolds number for glass nozzle	$\rho_a\,V_a\,d_n / \mu_a$
Sc	-----	Schmidt number	$\mu\,D_v / \rho_a$
Sh	-----	Sherwood number	$k_g\,d_p / D_v$
Sh_o	-----	Sherwood number under stagnant conditions	"

GREEK SYMBOLS

β	-----	Wind factor in Frossling's equation

ψ	-----	Crust thickness	m
ε	-----	Crust porosity	
λ	-----	Latent heat of vaporisation	J/kg
σ	-----	Stefan-Boltzman constant	
ϕ	-----	Constant	
ρ	-----	Density	kg/m^3
ρ_a	-----	Density of air	kg/m^3
ρ_d	-----	Droplet density	kg/m^3
ρ_g	-----	Density of gas	kg/m^3
ρ_w	-----	Density of water	kg/m^3
μ	-----	Viscosity	kg/m/s
μ_a	-----	Viscosity of air	kg/m/s
μ_f	-----	Viscosity at film conditions	kg/m/s
μ_g	-----	Viscosity of gas	kg/m/s
π	-----	Constant = 3.1416	

REFERENCES

1. Masters, K.,
"Spray Drying Handbook",
4th ed., George Godwin Limited., London (1985).

2. Ranz, W. E., Marshall, W.R.,
"Evaporation from Drops",
Chem. Eng. Prog., 48, 3, 141 (1952).

3. Charlesworth, D., Marshall, W.R.,
"Evaporation from Drops Containing Dissolved Solids",
A.I.Ch.E. Journal., 6, 9 (1960).

4. Trommelen, A.M., Crosby, E.J.,
"Evaporation and Drying of Drops in Superheated Vapours",
A.I.Ch.E. Journal., 16, 5, 857 (1970).

5. Sano, Y., Keey, R.B.,
"The Drying of a Spherical Particle Containing Colloidal Material into a Hollow Sphere",
Chem. Eng. Sci., 37, 6, 881 (1982).

6. Maxwell, J.C.,
"Diffusion",
Collected Scientific Papers Cambridge., 11, 625 (1890).

7. Ali, H.H,
"The Mechanisms of Drying of Single Droplets",
Ph.D Thesis., University of Aston in Birmingham, England (1985).

8. Cheong, H.W.,
"The Drying of Small Drops of Particulate Slurries",
Ph.D Thesis, University of Aston in Birmingham, England (1983).

9. Akbar, S.,
"The Drying of Drops in Free-Flight",
Ph.D Thesis, University of Aston in Birmingham, England (1988).

10. Audu, T.O.K.,
"Studies of the Drying of Particulate Slurries",
Ph.D Thesis, University of Aston in Birmingham, England (1973).

11. Whitman, W.G.,
Chem. Eng., 29, 147 (1923).

12. Frossling, N.,
"On the Evaporation of Falling Drops",
Gerlands. Beitrage. Zur. Geophysics. AERE Harwell Translation.,
August 1963, 52, 170 (1978).

13. Sreznevskii, V.,
Zh. R. Ph. Kh. O., 14, 420, 483 (1882).

14. Fick, A.,
Ann. Phys., 94, 59 (1855).

15. Langmuir, I.,
"The Evaporation of Small Spheres",
Physics Review., 12, 368 (1918).

16. Majama, T.,
Bll. Inst. Phys. Chem. Res. (Tokyo)., 9, 339 (1930).

17. Hoffman, T.W., Gauvin, W.H.,
"Evaporation of Stationary Droplets in High Temperature Surroundings",
Can. J. Chem. Eng., 129 (1960).

18. Vyrubov, D.N.,
"Droplet Thermal Emission and Evaporation",
Trans. J. Techn. Physics (USSR)., 9, 21, 1923 (1939).

19. Garner, F.H., Lane, J.J.,
"Mass Transfer to Drops of Liquid Suspended in a Gas Stream",
Trans. Inst. Chem. Engrs., 37, 162 (1959).

20. Frazier, G.C.,
"Water Droplet Vaporisation in Humid Atmospheres",
Can. J. Chem. Engr., 55, 678 (1977).

21. Yuge, T.,
"Experiments on Heat Transfer from Spheres Including Combined Natural and Forced Convection",
Trans. A. S. M. E. 82, Series C, 214 (1960).

22. Maisel, D.S., Sherwood, T.K.,
"Evaporation of Liquid into Turbulent Gas Streams",
Chem. Eng. Prog., 46, 3, 131 (1950).

23. Hsu, N.T., Sato, K., Sage, B.H.,
"Material Transfer in Turbulent Gas Streams",
Ind. Eng. Chem., 46, 870, (1954).

24. Garner, F.H., Grafton, R.W.,
"Mass Transfer in Fluid Flow from a Solid Sphere",
Proc. R. Soc., A224, 64 (1954).

25. Miura, K., Miura, T., Ohtani, S.,
"Heat and Mass Transfer to and from Droplets",
A. I. Ch. E. Symp. Ser., 73,95 (1977).

26. Sandoval-Robles, J.G., Riba, J.P., Conderc, J.P.,
"Mass Transfer around a Sphere",
Trans. Inst. Chem. Engrs., 58, 132 (1980).

27. Sandoval-Robles, J.G., Pelmas, H., Conderc, J.P.,
"Influence on Mass Transfer between a Liquid and a Solid Sphere",
A. I. Ch. E. Journal., 27, 819 (1981).

28. Marshall, W.R. Jr.,
"Heat and Mass Transfer in Spray Drying",
Trans. A. S. M. E., 77, 1377 (1955).

29. Downing, G.C.,
"The Evaporation of Drops of Pure Liquid at Elevated Temperatures: Rates of Evaporation and Wet-Bulb Temperatures",
A. I. Ch. E. Journal., 12, 4, 760 (1966).

30. Rowe, P.N., Claxton, K.T., Lewis, J.B.,
"Heat and Mass Transfer from a Single Sphere in an Extensive Flowing Fluid",
Trans. Inst. Chem. Engrs., 43, T14-T31 (1965).

31. Ward, D.M., Trass, O., Johnson, A. I.,
"Mass Transfer from Fluid and Solid Spheres at low Reynolds Numbers-Part II",
Can. J. Chem. Eng., 40, 164 (1962).

32. Evanochides, S., Thodos, G.,
"Simultaneous Mass and Heat Transfer in the Flow of Gases Past Single Spheres",
A. I. Ch. E. Journal., 7, 78 (1961).

33. Pasternak, I. S., Gauvin, W.H.,
"Turbulent Convective Heat and Mass Transfer from Accelerating Particles",
A. I. Ch. E. Journal., 7, 254 (1961).

34. Jones, S.J.R., Smith, W.,
"Mass Transfer from Solids Freely Suspended in an Air Stream",
Proc. Symp. Interaction between Fluids and Particles, Inst. Chem. Engrs. London., 190 (1962).

35. Frazier, G.C. Jr., Hellier, W.W. Jr.,
"Vaporisation of Liquid Droplets in High Temperature Air Streams",
Ind. Eng. Chem. Fundam., 8, 807 (1969).

36. Buckingham, E.,
U. S. Dept. Agr. Bur. Solids. Bull., 38 (1907).

37. Langstroth, G.O., Diehl, C.H., Winhold, E.J.,
"The Evaporation of Droplets in Still Air",
Can. J. Res., 24A, 580 (1950).

38. Whytlaw-Gray, R., Patterson, H.,
Smoke (Dym)., 149 (1934).

39. Kinzer, G.D., Gunn, R.,
"The Evaporation, Temperature and Thermal Relaxation-Time of Freely Falling Water Drops",
J. Meteor., 81, 71 (1951).

40. Topley, B., Whytlaw-Gray, R.,
"On the Rate of Evaporation of Small Spheres",
Phil. Mag., 4, 873 (1927).

41. Houghton, H.G.,
"A Study of the Evaporation of Small Water Drops",
Physics., 4, 419 (1933).

42. Steinberger, R.L., Treybal, R.E.,
"Mass Transfer from a Solid Soluble Sphere to a Flowing Liquid Stream",
A. I. Ch. E. Journal, 6, 227 (1960).

43. Kramers, H.,
Physica's. Frav., 12, 61 (1946).

44. Pasternak, I.S., Gauvin, W.H.,
"Turbulent Heat and Mass Transfer from Stationary Particles",
Can. J. Chem. Eng., 38, 35 (1960).

45. Bowman, C.W., Ward, D.M., Johnson, A.I., Trass, O.,
"Mass Transfer from Fluid and Solid Spheres at Low Reynolds Numbers",
Can. J. Chem. Eng., 39, 9 (1961).

46. Pei, D.C.T., Gauvin, W.H.,
"Natural Convection Evaporation from Spherical Particles in High-Temperature Surroundings",
A. I. Ch. E. Journal., 9, 3, 375 (1963).

47. Pei, D.C.T., Narasimhan, C., Gauvin, W.H.,
"Evaporation from Drops and Particles in High Temperature Surroundings",
Proc. Chem. Engrs. (London)., 243 (1962).

48. Morse, H.W.,
"Evaporation from the Surface of a Solid Sphere",
Proc. Am. Acad. Sci., 45, 363 (1910).

49. Garner, F.H., Hoffman, J.M.,
"The Evaporation from Free to Forced Convection in Mass Transfer from Solid Spheres",
A. I. Ch. E. Journal., 6, 4, 581 (1960).

50. Gurr, C.G., Marshall, T.J., Hutton, J.T.,
"Movement of Water in Soil due to a Temperature Gradient",
Soil Sci., 74, 5, 335 (1952).

51. Kuzmak, J.M., Sereda, P.J.,
"The Mechanism by which Water Moves Through a Porous Material Subjected to a Temperature Gradient",
Soil Sci., 84, 419 (1957).

52. Crosby, E.J., Stewart, W.E.,
"Vaporisation of Droplets in High-Temperature Gas Streams",
Ind. Eng. Chem. Fundam., 9, 3, 515 (1970).

53. Lee, K., Ryley, D.J.,
"The Evaporation of Water Droplets in Superheated Steam",
J. Heat. Transfer., 445 (1968).

54. Kadota, T., Hiroyasu, H.,
"Evaporation of a Single Droplet at Elevated Pressures and Temperatures",
Bull. J. S. M. E., 19, 138, 1515 (1976).

55. Yuen, M.C., Chen, L.W.,
"Heat Transfer Measurements of Evaporating Liquid Droplets",
Int. J. Heat and Mass Transfer., 21, 537-542 (1978).

56. Hiroyasu, H.,
"Trans. J. S. M. E., 40, 3147 (1974).

57. Renkizbulut, M., Yuen, M.C.,
"Experimental Study of Droplet Evaporation in a High-Temperature Air Stream",
J. Heat. Transfer., 105, 384 (1983).

58. Sherwood, T.K.,
"The Air Drying of Solids",
Trans. Am. Inst. Chem. Engrs., 32, 150 (1936).

59. Sherwood, T.K.,
"The Drying of Solids-II",
Ind. Eng. Chem., 13, 427 (1921).

60. Hormathy, T.Z.,
"Simultaneous Moisture and Heat Transfer in Porous Systems with Particular Reference to Drying",
Ind. Eng. Chem. Fund., 8, 92 (1969).

61. Audu, T.O.K., Jeffreys, G.V.,
"The Drying of Drops of Particulate Slurries",
Trans. Inst. Chem. Eng., 53, 165 (1975).

62. Bains, G.S.,
"Mechanisms of Drying of Particulate Slurries",
Ph.D Thesis, University of Aston in Birmingham, England (1990).

63. Ali, H.H., Mumford, C.J., Jeffreys, G.V., Bains, G.S.,
"A Study of Evaporation from, and Drying of, Single Droplets",
6th International Drying Symposium, IDS'88, Versailles, France (1988).

64. Haertling, M.,
"Prediction of Drying Rate",
Drying 80., Vol 1, Hemisphere Publ. Corp., N.Y. (1980).

65. Duffie, J.A., Marshall, W.R. Jr.,
"Factors Influencing the Properties of Spray-Dried Materials",
Chem. Eng. Prog., 49, 417 (1953).

66. Esubiyi, A.O.,
"Drying of Portland Cement Raw Material Slurries",
Ph.D Thesis, University of Aston in Birmingham, England (1980).

67. Van der Lijn, J.,
"Simulation of Heat and Mass Transfer in Spray Drying",
Ph.D Thesis, Agricultural University, Wagoninsen, Netherlands (1976).

68. Wijlhuizen, A.E., Kerkhof, R.J.A.M., Bruin, S.,
"Theoretical Study of the Inactivation of Phosphatase during Spray Drying of Skim-Milk".
Chem. Eng. Sci., 34, 651 (1979).

69. Katta, S., Gauvin, W.H.,
"Some Fundamental Aspects of Spray Drying",
A. I. Ch. E. Journal., 21, 1, 143 (1975).

70. Nescic, s.,
"The Evaporation of Single Droplets-Experiments and Modelling",
6th International Drying Symposium., IDS'88, Versailles, France (1988).

71. Nukiyama, S., Tanasawa, Y.,
Trans. Soc. Mech. Eng. (Japan)., 4, 86 (1937).

72. Baltas, L., Gauvin, W.H.,
"Performance Predictions for a Co-current Spray Dryer",
A. I. Ch. E. Journal., 15, 5, 764 (1969).

73. Bose, A.K., Pei, D.C.T.,
"Evaporation Rates in Spray Drying",
Can. J. Chem. Eng., 42, 259 (1964).

74. Dickinson, D.R.., Marshall, W.R. Jr.,
"The Rates Of Evaporation of Sprays",
A. I. Ch. E. Journal., 14, 4, 541 (1968).

75. Probert, R.P.,
"The Influence of Spray Particle Size and Distribution in the Combustion of Oil Droplets",
Phil. Mag., 37, 94 (1946).

76. Cheong, H.W., Jeffreys, G.V., Mumford, C.J.,
"A Receding Evaporation Interface Model for the Drying of Slurry Droplets",
A. I. Ch. E. Journal., 32, 81, 1334 (1986).

77. Coulson, J.M., Richardson, J.F.,
"Chemical Engineering",
Volume 2., Pergamon Press., Oxford (1970).

78. Abdul-Rahman, Y.A.K., Crosby, E.J., Bradley, R.L. Jr.,
J. Dairy. Sci., 54, 111 (1971).

79. Crosby,E.J., Weyl, R.W.,
"Foam Spray Drying: General Principles",
A. I. Ch. E. Symp. Ser., 73, 163, 82 (1977).

80. Miura, T., Ohtani, S., Maeda, S.,
"Drying 80",
Vol. 1., Hemisphere Publ. Corp., N.Y. (1980).

81. Keey, R.B.,
"Drying Principles and Practice",
1st ed., Pergamon Press, Oxford (1972).

82. Perry, R.H., Chilton, C.H.,
"Perry's Chemical Engineers Handbook",
6th ed., McGraw-Hill Ltd., N.Y. (1985).

83. Williams, G.C., Schmitt, R.O.,
"Humidity Measurements in Presence of Water Soluble Salts",
Ind. Eng. Chem., 38, 967 (1940).

84. Furuta, T., Okazaki, M., Toei, R., Crosby, E.J.,
"Formation of Crystals on the Surface of Non-Supported Droplets in Drying",
Drying 82., 157-164, Hemisphere Publ., N. Y. (1983).

85. Stocks, H.B.,
"Colloid Chemistry of Starch, Gums, Hemicelluloses, Albumin, Casein, Gluten, and Gelatin",
Reports on Colloid Chemistry and its Applications, 46-78, Department of Scientific and Industrial Research, London (1917).

86. Samuel, H.Maron, Carl, F.Prutton,
"Principles of Physical Chemistry",
4th ed., The Mocuillan Company, N. Y. (1965).

87. Thomas, J.Schoch, Eilean, C.Maywald,
"Industrial Microscopy of Starchs",
Starch: Chemistry and Technology, Volume 2, 637-647,
Academic Press, New York (1967).

88. Araham, C., Bernard, S.,
"Biochemistry",
4th ed., W. B. Saunders Company, Philadelphia (1967).

89. Galt, H.,
"The Microscopy of the Starchs",
Bailliere, Tindall and Cox, London (1900).

90. Hawthorn, J.,
"Foundations of Food Science",
W. H. Freeman and Company Ltd., Oxford (1981).

91. Leitch, J.M., Rhodes, D.N.,
"Recent Advances in Food Science-3",
Butter worths, London (1963).

92. Leach, H.W.,
"Gelatinisation of Starch",
Starch: Chemistry and Technology, Volume 1, 289-306, Academic Press, N.Y. (1965).

93. Eynon, L., Lane, J.H.,
"Starch: Its Chemistry, Technology and Uses",
W. Heffer and Sons Ltd., Cambridge (1928).

94. Radely, J.A.,
"Starch and its Derivatives",
4th ed., Chapman and Hall Ltd., London (1968).

95. Banks, W., Greenwood, C.T.,
"Starch and its Components",
University Press, Edinburgh (1975).

96. Ledward, D.A.,
"Proteins",
Effects of Heating on Foodstuffs, 1-33, Applied Science Publishers Ltd., London (1979).

97. Greenwood,C.T., Munro, D.N.,
"Carbohydrates",
Effects of Heating on Foodstuffs, 35-71, Applied Science Publishers Ltd., London (1979).

98. Stainsby, G.,
"The Gelatin Gel and the Sol-Gel Transformation",
The Science and Technology of Gelatin, Academic Press, London (1977).

99. Finch, C.A., Jobling, A.,
"The Physical Properties of Gelatin",
The Science and Technology of Gelatin, Academic Press, London (1977).

100. Sano, Y., Yamamoto, S.,
Proc. Third. Int. Drying. Symp., 1, 535 (1982).

101. Fledderman, R.G., Hanson, A.R.,
Univ. Michigan Res. Dept., Cm 677 (1951).

102. Dloughy, J., Gauvin, W.H.,
"Heat and Mass Transfer in Spray Drying",
A. I. Ch. E. Journal., 6, 1, 29 (1960).

103. Manning, W.P., Gauvin, W.H.,
"Heat and Mass Transfer to Decelerating Finely Atomised Sprays",
A. I. Ch. E. Journal., 6, 184 (1960).

104. Greenwald, C.G., Judson King, C.,
"The Mechanism of Particle Expansion in Spray Drying of Foods",
A. I. Ch. E. Symp. Ser., 78, 218, 101 (1982).

105. Judson King, C.,
"Control of Food-Quality Factors in Spray Drying",
4th Int. Drying. Symp., Kyoto, Japan, July 9-12 (1984).

106. Frazier, G.C., Chang, H.W.,
"Droplet Vaporisation in Moderately High Temperature Stationary Media",
Can. I. Chem. Eng., 55, 736 (1977).

107. Kinard, G.E., Manning, F.S., Manning, W.P.,
"A New Correlation for Mass Transfer from Single Spheres",
Brit. Chem. Eng., 8, 326 (1963).

108. Toei, R., Furuta, T.,
"Drying of a Droplet in a Non-Supported State",
A. I. Ch. E. Symp. Series., 78, 218, 111 (1982).

109. Davis, E.J., Ray, A.K., Chang, R.A.,
A. I. Ch. E. Symp. Ser., 74, 190 (1978).

110. Coulson, J.M., Richardson, J.F.,
"Chemical Engineering",
Volume 1, Pergamon Press., Oxford (1985).

111. Spalding, D.B.,
4th Int. Symp. On Combustion., 847, Williams and Williams, Baltimore, Maryland (1953).

112. Greenwald, G.C.,
"Particle Morphology in the Spray Drying of Foods",
Ph.D Thesis., University of California, Berkeley (1980).

113. Furuta, T., Okazaki, M., Toei, R.,
"Flavour Retention on Drying of a Single Droplet under Various Drying Conditions",
Drying'85, Int. Drying. Symp., Kyoto, Japan (1985).

114. Miura, K., Atarashiya, K., Ouchi, I., Ohtani, S.,
"Experimental Study of Drying Characteristics of Single Drops Containing Solids",
Kagaku Kogaku, 35, 643 (1971)-Translation- Heat. Transfer. Jap. Res., 1, 11 (1972).

115. Hassan, H.M.,
Unpublished Work., Chemical Engineering Department,
University of Aston in Birmingham (1988).

116. Lewis, W.K.,
Ind. Eng. Chem., 13, 427 (1921).

117. Newman, A.B.,
Trans. Am. Inst. Ch. Eng., 27, 203, 310 (1931).

118. Rosin, P., Rammler, E.,
J. Inst. Fuel., 7, 29 (1933).

119. Fledderman, R.G., Hanson, A.R.,
Univ. Michigan Res. Dept., Cm 677 (1951).

120. Miura, T., Ohtani, S.,
Kogaku Kogaku Ronbunshu, 5, 130 (1979).

121. Mathers, W.G., Madden, A.J., Piret, E.L.,
"Simultaneous Heat and Mass Transfer in Free Convection",
Ind. Eng. Chem., 49, 16, 961 (1957).

122. Gudris, N., Kulikova, L.,
Z. Physik., 25, 121 (1924).

123. Nestle, R.,
Physics., 77, 174 (1932).

124. Woodland, O.J., Mack, E.,
"The Effect of Curvature of Surface on Surface Energy. Rate of Evaporation of Liquid Droplets. Thickness of Saturated Vapour Films",
J. Amer. Chem. Soc., 55, 3149 (1933).

125. Garner, F.H., Suckling, R.D.,
"Mass Transfer from a Soluble Solid Sphere",
A. I. Ch. E. Journal., 4, 1, 114 (1958).

126. Garner, F.H., Keey, R.B.,
Chem. Eng. Sci., 9, 119 (1958).

127. Fuchs, N.A.,
"Evaporation and Droplet Growth in Gaseous Media",
Pergammon Press., London (1959).

128. Garner, F.H., Skelland, A.H.P.,
Ind. Eng. Chem., 46, 1255 (1954).

129. Finlay, B.A.,
Ph.D Thesis, University of Birmingham, England (1957).

130. Jarvis, J.,
Ph.D Thesis, University of Birmingham, England (1960).

131. Garner, F.H., Kendrick, P.,
Trans. Inst. Chem. Eng., 37, 155 (1959).

132. Tsubouchi, T., Sato, S.,
"Heat Transfer between Single Particles and Fluids in Relative Forced Convection",
Chem. Eng. Prog. Symp. Ser., 56, 269, 285 (1960).

133. Ranz, W.E.,
"On the Evaporation of a Drop of Volatile Liquid in High-Temperature Surroundings",
Trans. A. S. M. E., 78, 909 (1956).

134. Eisenklam, P., Armachalam, S.A., Weston, J.A.,
"Evaporation rates and Drag Resistance of Burning Drops",
In the Eleventh Symposium (International) on Combustion, PP 715-725 (1967).

135. Toei, R., Okazaki, M., Kubota, K., Ohaski, K., Mizata, K.,
Chem-Eng (Japan)., 30, 43 (1966).

136. Matosz, R.L., Leipziger, S., Torda, T.P.,
"Investigation of Liquid Drop Evaporation in a High Temperature and High Pressure Environment",
Int. J. Heat and Mass Transfer, 15, 831 (1972).

137. Higbie, R.,
"The Rate of Absorption of a Pure Gas into a Still Liquid during Short Periods of Exposure",
Trans. Amr. Inst. Chem. Eng., 31, 365 (1935).

138. Danckwerts, P.V.,
"Significance of Liquid Film Coefficients in Gas Absorption",
Ind. Eng. Chem., 43, 1460 (1951).

139. Toor, H.L., Marchello, J.M.,
"Film Penetration Model for Mass and Heat Transfer",
A. I. Ch. E. Journal., 4, 97 (1958).

140. Sharma, S.
"Spray Drier Simulation and Air Flow Patterns",
Ph.D. Thesis, University of Aston in Birmingham, England (1990).

141. Sudlow, C.A.,
Unpublished Work., University of Aston in Birmingham, England (1991).

142. Walton, D.,
Unpublished Work., University of Aston in Birmingham, England (1991).

143. Sayed, A.,
Unpublished Work., University of Aston in Birmingham, England (1991).

144. International Critical Tables.,
Vol., 3 1 st ed., McGraw-Hill Ltd., N.Y. (1933)

145. International Critical Tables.,
Vol. 5, 1 st ed., McGraw-Hill Ltd., N.Y. (1933).

146. Himmelblau, D.M.,
"Basic Principles and Calculations in Chemical Engineering",
4 th ed., Prentice-Hall, New Jersey (1982).

147. Kaye, G.W.C., Laby, T.H.,
"Tables of Physical and Chemical Constants,
13 th ed., Longmans, London (1966).

148. Kirk-Othmer Encyclopaedia of Chemical Technology.,
Vol. 21, 492, 3 rd ed., John Wiley and Sons., N.Y. (1983).

149. Kirk-Othmer Encyclopaedia of Chemical Technology.,
Vol. 11, 712, 3 rd ed., John Wiley and Sons., N.Y. (1983).

150. Kirk-Othmer Encyclopaedia of Chemical Technology.,
Vol 11, 911, 3 rd ed., John Wiley and Sons., N.Y. (1983).

APPENDIX A

PURE WATER DROPLETS

A.1 PHYSICAL PROPERTIES USED IN ANALYSIS OF WATER DROPLETS

A.1.1 Water

A.1.2 Air

A.1.3 Glass Nozzle

A.2 LEAST-SQUARES METHOD FOR DATA CORRELATION

A.2.1 Constant Air Temperature

A.2.2 Elevated Air Temperature

A.3 COMPUTER PROGRAMME LISTINGS

A.3.1 Programme Filename: PURE LIQ

A.3.2 Programme Filename: ELEVATED

A.3.3 Programme Filename: CRRELATN

A.4 TABULATION OF RESULTS

A.4.1 Water droplets at Ambient Temperature

Tables A1- A25

A.4.2 Water Droplets at Elevated Temperatures

Tables A26 - A28

A.1 PHYSICAL PROPERTIES USED IN ANALYSIS OF WATER DROPLETS

This section presents the physical and transport properties of water, air and properties of the glass nozzle on which calculations were made.

A.1.1 Water

1) Density of Water

Droplet Temperature ^{o}C	Density kg/m^{3}
8.0	999.85
15.5	999.00
25.0	997.04
28.5	996.10

2) Vapour Pressure of Water Droplet

Droplet Temperature ^{o}C	Vapour Pressure kN/m^{2}
8.0	1.0726
15.5	1.8001
25.0	3.3624
28.5	3.9614

3) Latent Heat of Vaporisation

$\lambda = 2805198 - 331.829\ T'_s - 3.0848\ T'^2_s$ J/kg

4) Diffusivity

$D_v = -4.6 \times 10^{-6} + 5.39 \times 10^{-8}\ T'_s + 1.62 \times 10^{-10}\ T'^2_s$ m^2/s

5) Emissivity of Droplet and Stefan-Boltzman Constant

Emissivity of Droplet, e = 0.955

Stefan-Boltzman Constant, $\sigma = 5.669 \times 10^{-8}$ W/m^2K^4

A.1.2 Air

1) Heat Capacity of Air

$C_{pa} = 1018.17 - 0.13376\ T'_g + 3.393 \times 10^{-4}\ T'^2_g$ J/kg K

2) Thermal Conductivity

$K = -3.3496 \times 10^{-4} + 1.0153475 \times 10^{-4} - 4.524765 \times 10^{-8}\ T'^2_g + 1.2226 \times 10^{-11}$

T'^{-3}_g W/m K

3) Viscosity

$\mu_g = 4.568 \times 10^{-8} (T_g - T_s) / 2 + 1.72 \times 10^{-5}$ kg/ms

4) Density

$\rho_g = 1.2929 (273.15 / 273.15 + T_g)$ kg/m^3

A.1.3 Glass Nozzle

Diameter of Nozzles, $D_N = 3, 5$ and 8mm

Thermal Conductivity, $k_t = 0.6404$ W/mK

Emissivity of Nozzle, $e_g = 0.94$

Heat Transfer Coefficient of Nozzles,

$H_N = C_r Re^m Pr^{0.33} K / d_n$ W/m^2K

where $C_r = 0.989$ and $m = 0.33$ for $Re_n < 4$

$C_r = 0.911$ and $m = 0.385$ for $4 \leq Re_n < 40$

$C_r = 0.683$ and $m = 0.466$ for $Re_n \geq 40$

A.2 LEAST SQUARE TECHNIQUE FOR DATA CORRELATION

A.2.1 Constant Air Temperature

From equation 8.1

$$Sh = 2.0 + \beta\, Re^{0.5}\, Sc^{0.33}$$

By rearrangement and taking logarithms to the base e,

$$\log_e (Sh - 2) = \log_e \beta + \log_e (Re^{0.5}\, Sc^{0.33}) \qquad \text{----------A.1}$$

Let, $X_1 = \log_e (Sh - 2)$

$X_2 = \log_e (Re^{0.5}\, Sc^{0.33})$

$X_3 = \log_e \beta$

The error between the given data and the approximating function at X_{2i} can be expressed by,

$$e (X_{1i}) = X_{1i} - X_{2i} - X_3 \qquad \text{----------A.2}$$

The objective function is to minimise the sum of the errors squared, expressed as,

$$e (X_{1i})^2 = S = \sum_{i=1}^{n} (X_{1i} - X_{2i} - X_3)^2 \qquad \text{----------A.3}$$

Differentiating S with respect to X_3, and setting the differential equation to zero,

$$\frac{ds}{dX_3} = -2 \sum_{i=1}^{n} (X_{1i} - X_{2i} - X_3) = 0 \qquad \text{----------A.4}$$

Thus,

$$\sum X_{1i} - \sum X_{2i} - \sum n\, X_3 = 0 \qquad \text{---------A.5}$$

Therefore,

$$X_3 = \frac{1}{n}\left(\sum X_{1i} - \sum X_{2i} \right) \qquad \text{---------A.6}$$

The value of β can be the evaluated from equation A.6 by taking the exponential of X_3, that is:

$$\beta = \exp (X_3) \qquad \text{---------A.7}$$

The correlation coefficient C is represented by,

$$C = \left[1 - \frac{\sum (X_{1i} - X_{2i} - X_3)}{\sum (X_{1i} - X'_1)^2} \right]^{1/2} \qquad \text{---------A.8}$$

where,

$$X'_1 = \frac{1}{n} \sum X_{1i}$$

The same analytical procedure was followed to find the values of ϕ in equation 8.2 for water droplets at ambient temperature data, and hence equation A.7 becomes,

$$\phi = \exp (X_3) \qquad \text{---------A.9}$$

and let $X1 = \log_e (Nu - 2)$

$$X_2 = \log_e (Re^{0.5}\, Pr^{0.33})$$

$$X_3 = \log_e \phi$$

A computer Programme filename "PURE LIQ", listed in Appendix A.3.1 for data

analysis at constant temperature.

A.2.2 Elevated Air Temperature

From the applied proposed correlation 8.3,

$$Sh = 2.0 + \beta \left[\frac{T_a - T_s}{T_{amb}} \right]^{\eta} Re^{0.5} Sc^{0.33}$$

Rearranging and taking logarithms to the base e,

$$\log_e (Sh - 2) = \log_e \beta + \eta \log_e \left[\frac{T_a - T_s}{T_{amb}} \right] + \log_e Re^{0.5} Sc^{0.33} \qquad \text{---------A.10}$$

Let,

$$X_1 = \log_e (Sh - 2)$$

$$X_2 = \log_e (Re^{0.5} Sc^{0.33})$$

$$X_3 = \log \beta$$

$$X_4 = \log_e \left[\frac{T_a - T_s}{T_{amb}} \right]$$

The errors squared e $(X1i)^2$, is thus expressed as,

$$e (X_{1i})^2 = S = \sum_{i=1}^{n} (X_{1i} - X_{2i} - X_3 - \eta X_{4i})^2 \qquad \text{----------A.11}$$

Differentiating S with respect to X_3 and η respectively, and equating both equations to zero,

$$\frac{ds}{dX_3} = -2\sum_{i=1}^{n}(X_{1i} - X_{2i} - X_3 - \eta X_{4i} = 0 \qquad \text{----------A.12}$$

and

$$\frac{ds}{d\eta} = -2\sum_{i=1}^{n} X_{4i}(X_{1i} - X_{2i} - X_3 - \eta X_{4i} = 0 \qquad \text{---------A.13}$$

Equation A.12 can be written as,

$$\sum X_{1i} - \sum X_{2i} - \eta \sum X_{4i} = 0 \qquad \text{----------A.14}$$

Thus,

$$X_3 = \frac{1}{n}(\sum X_{1i} - \sum X_{2i} - \eta \sum X_{4i}) \qquad \text{---------A.15}$$

expanding equation A.13,

$$\sum(X_{4i} \,.\, X_{1i}) - \sum(X_{4i} \,.\, X_{2i}) - X_3 \sum X_{4i} - \eta \sum(X_{4i})^2 = 0 \qquad \text{----------A.16}$$

Substituting equation A.15 into A.16 and rearranging,

$$\eta = \frac{n\sum(X_{4i} \,.\, X_{1i}) - n\sum(X_{4i} \,.\, X_{2i}) - (\sum X_{4i})(\sum X_{1i} + (\sum X_{4i})(\sum X_{2i})}{n\sum(X_{4i})^2 - (\sum X_{4i})^2} \qquad \text{-----A.17}$$

The value of η can then be used in equation A.15 to evaluate X_3, and

$$\beta = \exp(X_3) \qquad \text{----------A.18}$$

The same procedure was used for equation 8.4, where

$$X_1 = \log_e(Nu - 2)$$

$$X_2 = \log_e (Re^{0.5} Pr^{0.33})$$

$$X_3 = \log_e \phi$$

$$X_4 = \log_e (1 / B)$$

The correlation coefficient is expressed as,

$$C = [\, 1 - \frac{\sum(X_{1i} - X_{2i} - X_3 - \eta X_{4i})^2}{\sum(X_{1i} - X'_1)^2}]^{1/2} \qquad \text{---------A.19}$$

A computer Programme "ELEVATED" listed in Appendix A.3.2 was used to correlate the results at Elevated air temperatures according to equations A.15, A17 and A.18.

A.3 COMPUTER PROGRAMME LISTINGS

A.3.1 Programme Filename : PURELIQ

```
 10 REM EVALUATION OF SHERWOOD AND NUSSELT NOS.
 14 REM FOR WATER DROPLETS AT AMBIENT AIR TEMP.
 16 REM  SYMBOLS
 17 REM C      = CONST.OF REGRESS LINE
 19 REM DA(J) =AIR DENSITY
 21 REM DD(I) =DROPLET DIAMETER
 23 REM DF(J) =DIAMETER OF NOZZLE
 24 REM DN     =DROPLET DENSITY
 25 REM DW(I) =DROPLET WEIGHT
 26 REM DV(J) =DIFFVSITY OF VAPOUR IN AIR
 27 REM ED     =EMISIVITY OF DROPLET
 29 REM EG     =EMISIVITY OF NOZZLE
 31 REM HT     =H.T.C OF NOZZLE
 33 REM K(J)  =THERM. COND. OF AIR
 35 REM KT     =THERM. COND. OF NOZZLE
 37 REM LA(J) =LATENT HEAT OF EVAP.
 39 REM M      =SLOPE OF REGRESS LINE
 40 REM MD(J) =MEAN DIAMETER
 41 REM MW     =MOLECULAR WEIGHT OF WATER VAP.
 42 REM NC     =NUSSELT CORRECTIONS
 44 REM NE(J) =EXP. NUSSEL NO.
 45 REM NU(J) =CORRECTED NUSSEL NO.
 46 REM P(J)  =PARTIAL PRESSURE OF WATER VAP. IN UP STREAM AIR
 47 REM PI     =PIE (3.14159)
 48 REM PS(J) =VAPOUR PRESSURE OF WATER AT WET BULB TEMP.
 49 REM PR     =PRANDTL NO. OF AIR
 50 REM QF     =HEAT THRW. NOZZLE
 51 REM QR     =HEAT RADIATION
 52 REM R      =CORR. COEFF. OF REGRESS LINE
 53 REM RE(J) =REYNOLDS NO. OF DROP
 55 REM RG     =REYNOLDS NO. OF NOZZLE
 56 REM RC     =UNIVERSAL GAS CONSTANT
 57 REM S      =STEFAN_BOLTZMAN CONST.
 58 REM SC     =SCHMIDT NO. OF AIR
 59 REM SH(J) =CORRECTED SHERWOOD NO.:REM SHE(J) EXPERIMENTAL
    SHERWOOD NO.
 60 REM TA(J) =AIR  TEMP.
 62 REM TD(J) =DROPLET TEMP.
 64 REM VA     =VISCOSITY OF AIR
 66 REM V(J)  =AIR VELOCITY
 68 REM W5     =COFF. OF RE^.5*PR^.33 IN NU. EQN.
 70 REM W9     =CORR. COEFF IN NU. EQN.
 71 REM
100 DIMX(500),Y(500),WW(50),N2(50),V(50),TA(50),TD(50),DF(50),
    DA(50),LA(50),K(50)
113 DIM DW(150),DD(150),MD(150),RE(40),DN(40),NU(40),F1(40)
115 DIM NE(40),W1(40),W2(40),SHE(40),SH(40),F2(40),P(40),
    PS(40),DV(40)
119 REM
120 REM INPUT EXPERIMNTAL CONDITIONS
125 REM INPUT NUMBER OF SETS OF DATA
126 READ N1
130 REM INPUT THE EXPT.NOS.
135 FOR J=1 TO N1
137 READ WW(J)
139 NEXT J
140 REM INPUT NO.OF READINGS IN EACH SET
>
```

```
 142 FOR J=1 TO N1
 143 READ N2(J)
 145 NEXT J
 146 REM INPUT VELOCITY IN EACH SET
 147 FOR J=1 TO N1
 148 READ V(J)
 150 NEXT J
 151 REM INPUT VISCOSITY OF AIR
 152 READ VA
 153 REM INPUT PRANDTL NO. OF AIR
 155 READ PR
 160 REM INPUT EMISIVTY OF DROP
 164 READ ED
 168 REM INPUT EMISIVITY OF NOZZLE
 170 READ EG
 171 REM INPUT UNIVERSAL GAS CONSTANT AND MOLECULAR WEIGHT
 172 READ RC
 173 READ MW
 174 REM INPUT PARTIAL PRESSURE OF AIR AND VAPOUR PRESSURE
     OF WATER
 175 FOR J=1 TO N1
 176 READ P(J)
 178 NEXT J
 179 FOR J=1 TO N1
 180 READ PS(J)
 181 NEXT J
 182 REM INPUT AIR TEMP. FOR EACH SET
 184 FOR J=1 TO N1
 187 READ TA(J)
 193 NEXT J
 200 REM INPUT DROP TEMP. FOR EACH SET
 205 FOR J=1 TO N1
 206 READ TD(J)
 209 NEXT J
 212 REM INPUT DENSITY OF DROP
 215 READ DN
 220 REM
 225 REM INPUT DIAMETER OF NOZZLES
 230 FOR J=1 TO N1
 231 READ DF(J)
 232 DF(J)=DF(J)/1000
 234 NEXT J
 235 REM
 236 REM INPUT SCHMIDT NO. OF AIR
 237 READ SC
 238 REM INPUT THERMAL CONDUC. OF NOZZLE
 240 READ KT
 241 REM
 242 REM SET VALUE OF CONSTANTS
 243 LEPI=22/7
 245 S=5.6697E-8
 250 REM
 260 REM EVALUATE PHYSICAL PROPS.
 265 FOR J=1 TO N1
 270 LET DA(J)=1.2929*273.15/(273.15+TA(J))
 272 NEXT J
 273 REM CONVERT TEMP. TO K
>
```

```
 274 FOR J=1 TO N1
 275 LET TA(J)=TA(J)+273.15
 276 LET TD(J)=TD(J)+273.15
 277 NEXT J
 280 FOR J=1 TO N1
 281 LET LA(J)=2805198-331.892*TD(J)-3.0848*TD(J)^2
 284 NEXT J
 290 FOR J=1 TO N1
 291 LET K(J)=(-3.3496E-4)+(1.0153475E-4)*TA(J)-(4.584765E-8)*
     TA(J)^2+(1.222604E-11)*TA(J)^3
 295 NEXT J
 308 REM
 310 FOR J=1 TO N1
 312 LET DV(J)=-4.6E-6+(5.39E-8)*TD(J)+(1.62E-10)*TD(J)^2
 315 NEXT J
 350 REM
 352 REM DATA ANALYSIS
 380 REM DROP WEIGHT/TIME DATA INPUT.
 410 FORJ=1TON1
 420 FORI=1TON2(J)
 422 READ X(I)
 425 NEXTI
 430 NEXT J
 435 FOR J=1 TO N1
 440 FORI=1TON2(J)
 441 READDW(I)
 443 NEXT I
 460 REM
 465 REM CALCULATE DROP DIA. AND RATE OF CHANGE OF D^2
 470 FOR I=1 TO N2(J)
 471 LET DD(I)=((DW(I)/1E6)/(DN)/(PI/12))^(1/3)
 475 Y(I)=DD(I)^2
 482 NEXT I
 487 LET NN=N2(J)
 490 GOSUB 5000
 500 LET SA=M
 510 LET C2=C
 512 LET R2=R
 515 REM TEST FOR LINEARITY
 517 IF (1-R)>.015 THEN 519
 518 GOTO 520
 519 PRINT
 520 REM
 530 REM REYNOLDS NUMBER CALCULATION
 531 C3=0
 535 FOR I=1 TO N2(J)
 545 LET C3=DD(I)+C3
 547 NEXT I
 552 LET MD=C3/N2(J)
 555 MD(J)=MD
 556 LET MD=MD/1000
 559 REM
 561 LET RE(J)=V(J)*MD(J)*DA(J)/VA
 570 LET F1(J)=RE(J)^.5*PR^(1/3)
>
```

```
573 LET F2(J)=RE(J)^.5*SC^(1/3)
580 REM
589 REM RADIATION CALC.
600 QR=(S*PI*MD(J)^2*ED*(TA(J)^4-TD(J)^4))*.5
610 REM
620 REM HEAT THROW. NOZZLE
630 LET RG=V(J)*DF(J)*DA(J)/VA
640 IF RG>=40 THEN CR=.683
642 LET G=.466
650 IF RG<40THEN CR=.911
652 LET G=.385
660 IF RG<4 THEN CR=.989
662 LET G=.33
672 LET HT=CR*RG^G*PR^(1/3)*K(J)/(2*DF(J))
685 LET QF=2*S*EG*(TD(J)^5-TA(J)^5)
687 QF=QF-(10*S*EG*TA(J)^4*(TD(J)-TA(J)))
690 LET QF=QF+(5*HT*(TD(J)-TA(J))^2)
700 LET QF=(QF*KT*DF(J)^3/5)^.5
710 LET QF=QF*PI/4
720 REM
730 REM HEAT CORRCTION FACTOR
740 LET NC=(QR+QF)/(2*(MD(J)*PI*(TA(J)-TD(J))*K(J)))
760 REM
780 REM NUSSELT CALCULATION
795 LET NE(J)=-(LA(J)*DN/4/(TA(J)-TD(J))/K(J)*SA)
797 LET NU(J)=NE(J)-NC
800 SHE(J)=-(DN*RC*TA(J)/4/(PS(J)-P(J))/MW/DV(J)*SA)
805 LET SH(J)=SHE(J)-NC
820 REM
825 REM RETURN TO EVALUATE NEXT SET OF RESULTS
850 NEXT J
906 REM CALCULATE COFF. FOR RE^.5*PR^.33
907 GOSUB 10000
908 REM
909 REM NUMBERS ARE ROUNDED OFF
910 FOR J=1 TO N1
912 LET V(J)=INT(V(J)*1E3+.5)/1E3
913 LET RE(J)=INT(RE(J)*1E2+.5)/1E2
914 LET TA(J)=TA(J)-273.15:TD(J)=TD(J)-273.15
916 LET NU(J)=INT(NU(J)*1E3+.5)/1E3
917 LET SH(J)=INT(SH(J)*1E3+.5)/1E3
918 LET F1(J)=INT(F1(J)*1E3+.5)/1E3
919 LET F2(J)=INT(F2(J)*1E3+.5)/1E3
920 LET NE(J)=INT(NE(J)*1E3+.5)/1E3
921 LET SHE(J)=INT(SHE(J)*1E3+.5)/1E3
922 NEXT J
924 LET W5=INT(W5*1E3+.5)/1E3
926 LET W9=INT(W9*1E3+.5)/1E3
930 REM
931 @%=131850
932 REM PRINTING RESULTS
945 A$="EVAPORATION OF WATER DROPS AT AMBIENT AIR TEMP."
987 PRINT TAB(7);"TABLE 8.1",A$
995 PRINT TAB(7);"_____";
>
```

```
 998 PRINT "_____"
1001 PRINT
1009 PRINT TAB(10);" UNITS"
1018 PRINT TAB(10);"       "
1028 PRINT TAB(7);"MEAN DIAMETER        = mm"
1039 PRINT TAB(7);"AIR VELOCITY         = m/s"
1047 PRINT TAB(7);"DROPLET & AIR TEMP. = C"
1050 PRINT
1055 PRINT TAB(7);"SHERWOOD EQUATION    = 2+";W5;"RE^.5*SC^.33"
1057 PRINT TAB(7);"CORRELATION COEFF.   =";W9
1061 PRINT
1065 PRINT
1067 PRINT
1071 PRINT TAB(7);"EXP";
1072 PRINT TAB(12);"MEAN";
1073 PRINT TAB(20);"AIR";
1074 PRINT TAB(29);"REY";
1075 PRINT TAB(39);"AIR";
1076 PRINT TAB(45);"DROP";
1077 PRINT TAB(53);"SH";
1078 PRINT TAB(60);"SH"
1079 PRINT TAB(7);"NO";
1080 PRINT TAB(12);"DIA.";
1081 PRINT TAB(20);"VEL.";
1082 PRINT TAB(29);"NO.";
1083 PRINT TAB(39);"TEMP.";
1084 PRINT TAB(45);"TEMP.";
1085 PRINT TAB(53);"EXP.";
1086 PRINT TAB(60);"CORCT.";
1087 PRINT TAB(67);"RE^.5*SC^.33"
1093 PRINT TAB(6);"___";
1094 PRINT TAB(12);"____";
1095 PRINT TAB(20);"_____";
1096 PRINT TAB(29);"_______";
1097 PRINT TAB(39);"____";
1098 PRINT TAB(45);"____";
1099 PRINT TAB(52);"_____";
1100 PRINT TAB(60);"_____";
1101 PRINT TAB(67);"____________"
1105 PRINT
1145 FORJ=1TON1
1148 @%=10
1150 PRINT TAB(7);WW(J);
1152 @%=131850
1153 PRINT TAB(12);MD(J)*1000;
1154 PRINT TAB(20);V(J);:@%=131594
1156 PRINT TAB(29);RE(J);:@%=10
1158 PRINT TAB(39);TA(J);
1159 PRINT TAB(46);TD(J);:@%=131850
1161 PRINT TAB(52);SHE(J);
1162 PRINT TAB(60);SH(J);
1163 PRINT TAB(68);F2(J)
1166 NEXT J
>
```

```
 3500 END
 5000 REM
 5004 REM SUBROUTINE FOR LINEAR REGRESS
 5007 S1=0:S2=0:S3=0:B2=0:B3=0:S4=0:S5=0:S6=0:S7=0:M=0:C  :
 5012 FORA=1TONN
 5020 S1=S1+X(A)*Y(A)
 5030 S2=S2+X(A)
 5040 S3=S3+Y(A)
 5050 NEXTA
 5060 B2=S2/NN:B3=S3/NN
 5070 FORA=1TONN:S4=S4+((X(A)-B2)^2):S5=S5+((Y(A)-B3)^2 ·N
 5080 S6=S4/NN:S7=S5/NN
 5090 M=((S1/NN)-(B2*B3))/S6:C=B3-M*B2:R=(M^2*S6/S7)^.5
 5100 RETURN
10000 REM
10010 REM SUBROUTINE FOR LEAST SQUARESS FITTING
10020 FORJ=1TON1
10030 W1(J)=LN(SH(J)-2)
10040 W2(J)=LN(F2(J))
10050 NEXT
10060 W3=0:W4=0:W5=0:W6=0:W7=0:W8=0:W9=0
10070 FORJ=1TON1
10080 W3=W3+W1(J)
10090 W4=W4+W2(J)
10100 NEXT
10110 W5=(W3-W4)/N1:W6=W3/N1
10120 FORJ=1TON1
10130 W7=W7+(W1(J)-W5-W2(J))^2
10140 W8 =W8+(W1(J)-W6)^2
10150 NEXT
10160 W9=(1-(W7/W8))^.5
10170 W5=EXP(W5)
10180 RETURN
>
```

A.3.2 Programme Filename : ELEVATED

```
 10 REM EVALUATION OF SHERWOOD AND NUSSELT NOS.
 14 REM FOR WATER DROPLETS AT ELEVATED AIR TEMP.
 16 REM  SYMBOLS
 19 REM DA(J)    =AIR DENSITY
 21 REM DD(J,I) =DROPLET DIAMETER
 23 REM DF       =DIAMETER OF NOZZLE
 24 REM DN(J)    =DROPLET DENSITY
 26 REM DV(J)    =DIFFVSITY OF VAPOUR IN AIR
 27 REM ED       =EMISIVITY OF DROPLET
 29 REM EG       =EMISIVITY OF NOZZLE
 31 REM HT       =H.T.C OF NOZZLE
 33 REM K(J)     =THERM. COND. OF AIR
 35 REM KT       =THERM. COND. OF NOZZLE
 37 REM LA(J)    =LATENT HEAT OF EVAP.
 41 REM MW       =MOLECULAR WEIGHT OF WATER VAP.
 42 REM NC(J,I) =NUSSELT CORRECTIONS
 44 REM NE(J,I) =EXP. NUSSEL NO.
 45 REM NU(J,I) =CORRECTED NUSSEL NO.
 46 REM P(J)     =PARTIAL PRESSURE OF WATER VAP. IN UP STREAM
    AIR
 47 REM PI       =PIE (3.14159)
 48 REM PS(J)    =VAPOUR PRESSURE OF WATER AT WET BULB TEMP.
 49 REM PR(J)    =PRANDTL NO. OF AIR
 50 REM QF       =HEAT THRW. NOZZLE
 51 REM QR(J,I) =HEAT RADIATION
 52 REM R        =CORR.COFF.OF REGRESS LINE
 53 REM RE(J,I) =REYNOLDS NO. OF DROPLET
 55 REM RG       =REYNOLDS NO. OF NOZZLE
 57 REM S        =STEFAN BOLTZMAN CONSTANT
 58 REM SC(J)    =SCHMIDT NO. OF AIR
 59 REM SH(J,I) =CORRECTED SHERWOOD NO. :REM SHE(J) EXP.
    SHERWOOD NO.
 60 REM TA(J)    =AIR TEMP.
 62 REM TD(J)    =DROPLET TEMP.
 64 REM VA(J)    =VISCOSITY OF AIR
 66 REM V(J)     =AIR VELOCITY
120 DIM X(5,35),Y(5,35),N2(6),V(6),TA(6),TD(6),DA(6),WW(6),
    PR(6),SC(6),DN(6)
130 DIM LA(6),K(6),DD(5,35),RE(5,35),NU(5,35),SA(5,35)
140 DIM F1(5,35),NE(5,35),VA(6),QR(5,35),NC(5,35),W1(2,10),
    W2(2,10)
150 DIM SHE(5,35),SH(5,35),F2(5,35),P(6),PS(6),DV(6),CP(6)
155 REM
160 REM INPUT EXPERIMENTAL CONDITIONS
170 REM INPUT NUMBER OF SETS OF DATA
175 READ N1
180 REM INPUT THE EXPT. NOS.
190 FOR J=1 TO N1
200 READ WW(J)
210 NEXT J
220 REM INPUT NO. OF READING IN EACH SET
230 FOR J=1 TO N1
240 READ N2(J)
245 NEXT J
250 REM INPUT VELOCITY IN EACH SET
255 FOR J=1 TO N1
>
```

```
260 READ V(J)
265 NEXTJ
290 REM INPUT AIR TEMP. FOR EACH SET
295 FOR J=1 TO N1
300 READ TA(J)
305 NEXT J
315 REM INPUT DROPLET TEMP. FOR EACH SET
320 FOR J=1 TO N1
325 READ TD(J)
330 NEXT J
335 REM EVALUATE PHYSICAL PRORERTIES
340 FOR J=1 TO N1
350 LET VA(J)=(4.568E-8)*(TA(J)+TD(J))/2+1.720E-5
360 NEXT J
370 FOR J=1 TO N1
375 LET DA(J)=1.2929*273.15/(273.15+TA(J))
380 NEXT J
390 REM CONVERT TEMP. TO K
395 FOR J=1 TO N1
400 LET TA(J)=TA(J)+273.15
405 LET TD(J)=TD(J)+273.15
410 NEXT J
412 FOR J=1 TO N1
414 LET CP(J)=1017.441-.1356588*TA(J)+(3.39147E-4)*TA(J)^2
416 NEXT J
420 FOR J=1 TO N1
425 LET LA(J)=2805198-331.892*TD(J)-3.0848*TD(J)^2
430 NEXT J
440 FOR J=1 TO N1
445 LET K(J)=(-3.3496E-4)+(1.0153475E-4)*TA(J)-(4.584765E-8)*
    TA(J)^2+(1.2226E-11)*TA(J)^3
450 NEXT J
455 REM
460 FOR J=1 TO N1
465 LET DV(J)=-4.6E-6+(5.39E-8)*TD(J)+(1.62E-10)*TD(J)^2
470 NEXT J
475 REM
480 FOR J=1 TO N1
485 LET PR(J)=CP(J)*VA(J)/K(J)
490 NEXT J
495 FOR J=1 TO N1
500 LET SC(J)=VA(J)/(DV(J)*DA(J))
505 NEXT J
510 REM INPUT EMISIVITY OF DROPLET
515 READ ED
520 REM INPUY EMISIVITY OF NOZZLE
525 READ EG
530 REM INPUT UNIVERSAL GAS CONSTANT
535 READ RC
540 REM INPUT MOLECULAR WEIGHT OF WATER VAP.
545 READ MW
550 REM INPUT PARTIAL PRESSURE OF AIR
555 FOR J=1 TO N1
560 READ P(J)
565 NEXT J
570 REM INPUT VAPOUR PRESSURE OF WATER DROP AT WET BULB TEMP.
>
```

```
575 FOR J=1 TO N1
580 READ PS(J)
585 NEXT J
590 REM INPUT DENSITY OF DROP
595 FOR J=1 TO N1
600 READ DN(J)
605 NEXT J
615 REM INPUT DIAMETER OF NOZZLE
620 READ DF
625 REM INPUT THERMAL CONDUCTIVITY OF NOZZLE
630 READ KT
640 REM SET VALUE OF CONSTANTS
645 LEPI=22/7
650 S=5.6697E-8
655 REM DATA ANALYSIS
660 FOR J=1 TO N1
665 FOR I=1 TO N2(J)
670 READ X(J,I)
675 NEXTI
680 NEXTJ
685 FOR J=1 TO N1
690 FOR I=1 TO N2(J)
695 READ DD(J,I)
700 LET Y(J,I)=DD(J,I)
705 NEXT I
706 NEXT J
708 FOR J=1 TO N1
710 FOR I=1 TO N2(J)
715 READ SA(J,I)
720 NEXT I
730 REM REYNOLDS NUMBER CALCULATION
750 FOR I=1 TO N2(J)
755 LET RE(J,I)=V(J)*(DD(J,I)/1000)*DA(J)/VA(J)
780 LET F1(J,I)=RE(J,I)^.5*PR(J)^(1/3)
785 LET F2(J,I)=RE(J,I)^.5*SC(J)^(1/3)
795NEXT I
800 REM
805 REM RADIATION CALCULATION
815 FOR I=1 TO N2(J)
820 QR(J,I)=(S*PI*(DD(J,I)/1000)^2*ED*(TA(J)^4-TD(J)^4))*.5
825 NEXT I
830 REM
835 REM HEAT THROW NOZZLE
850 LET RG=V(J)*(DF/1000)*DA(J)/VA(J)
860 IF RG>=40 THEN CR=.683
870 LET G=.466
875 IF RG<40 THEN CR=.911
880 G=.385
890 IF RG<4 THEN CR=.989
895 LET G=.33
900 LET HT=CR*RG^G*PR(J)^(1/3)*K(J)/(2*(DF/1000))
915 LET QF=2*S*EG*(TD(J)^5-TA(J)^5)
930 QF=QF-(10*S*EG*TA(J)^4*(TD(J)-TA(J)))
940 LET QF=QF+(5*HT*(TD(J)-TA(J))-2)
950 LET QF=(QF*KT*(DF/1000)^3/5)^.5
960 LET QF=QF*PI/4
>
```

```
  970 REM
  980 REM HEAT CORRECTION FACTOR
  990 FOR I=1 TO N2(J)
  995 LET NC(J,I)=(QR(J,I)+QF)/(2*((DD(J,I)/1000)*PI*(TA(J)-
      TD(J))*K(J)))
 1000 REM
 1020 REM NUSSELT AND SHERWOOD CALCULATION
 1030 LET NE(J,I)=(LA(J)*DN(J)/4/(TA(J)-TD(J))/K(J)*SA(J,I))
 1040 LET NU(J,I)=NE(J,I)-NC(J,I)
 1050 SHE(J,I)=(DN(J)*RC*TA(J)/4/(PS(J)-P(J))/MW/DV(J)*SA(J,I))
 1060 LET SH(J,I)=SHE(J,I)-NC(J,I)
 1070 REM
 1080 REM RETURN TO EVALUATE NEXT SET OF RESULTS
 1085 NEXT I
 1090 NEXT J
 1120 REM CALCULATE COFF. FOR RE^.5*PR^.33
 1140 REM
 1150 REM NUMBERS ARE ROUNDED OFF
 1170 FOR J=1 TO N1
 1180 FOR I=1 TO N2(J)
 1190 LET V(J)=INT(V(J)*1E3+.5)/1E3
 1195 LET RE(J,I)=INT(RE(J,I)*1E2+.5)/1E2
 1205 LET TA(J)=TA(J)-273.15:TD(J)=TD(J)-273.15
 1215 LET NU(J,I)=INT(NU(J,I)*1E3+.5)/1E3
 1230 LET SH(J,I)=INT(SH(J,I)*1E3+.5)/1E3
 1240 LET F1(J,I)=INT(F1(J,I)*1E3+.5)/1E3
 1250 LET F2(J,I)=INT(F2(J,I)*1E3+.5)/1E3
 1260 LET NE(J,I)=INT(NE(J,I)*1E3+.5)/1E3
 1270 LET SHE(J,I)=INT(SHE(J,I)*1E3+.5)/1E3
 1280 NEXT I
 1290 NEXT J
 1330 REM
 1335 REM PRINTING RESULTS
 1338 FOR J=1 TO N1
 1340 @%=10
 1345 B$="EVAPORATION OF WATER DROPS AT ELEVATED TEMP."
 1350 PRINT TAB(9);"TABLE 7.    ";B$
 1355 PRINT TAB(9);"___________";
 1360 PRINT"_____________________________________________________________"
 1375 PRINT
 1390 PRINT TAB(19);"UNITS"
 1400 PRINT TAB(19);"_____"
 1410 PRINT
 1420 PRINT TAB(9);"AIR TEMP. (C)          =";TA(J)-273.15
 1430 PRINT TAB(9);"DROP TEMP.(C)          =";TD(J)-273.15
 1450 PRINT
 1480 PRINT
 1485 PRINT
 1490 PRINT TAB(9);"TIME";
 1500 PRINT TAB(19);"REY";
 1510 PRINT TAB(30);"SH";
 1520 PRINT TAB(39);"SH"
 1530 PRINT TAB(9);"(sec)";
 1540 PRINT TAB(19);"NO.";
 1550 PRINT TAB(29);"(EXP)";
 1560 PRINT TAB(39);"CORCT.";
>
```

```
 1570 PRINT TAB(49);"RE^.5*SC^. 3"
 1580 PRINT TAB(9);"    ";
 1590 PRINT TAB(19);"     ";
 1600 PRINT TAB(29);"     ";
 1610 PRIN  TAB(39);"      ";
 1620 PRINT TAB( 9);"              "
 1630 PRI
 1640 FOR I=1 TO N2(J)
 1642 @%=10
 1650 PRINT TA (10);X(J,I);
 1655 @%=131594
 1660 PRINT TAB(19);RE(J,I);
 1665 @%=131850
 1670 PRINT TAB(29);SHE(J,I);
 1680 PRINT TAB(39);SH(J,I);
 1690 PRINT TAB(50);F2(J,I)
 1700 PRINT
 1750 NEXT I
 1800 PRINT
 1810 PRINT
 1820 PRINT
 1830 PRINT
 1835 PRINT
 1840 PRINT
 1842 PRINT
 1845 PRINT
 1850 NEXT J
 1950 END
1  00 REM
10010 REM  UBR UTINE FOR LEAST SQUARE S FITTI
1 020 F R J=1 TO N1
1  30 F R I=1 TO  2(J)
1  40 W1(J,I)=LOG(NU(J,I)-2)
10050 W2(J,I)=LOG(F1(J,I)
10 60 NEXT I
1  65 NEXT J
1  7  W3=0:W4=0:W5=0:W6=0:W7= :W =0:W -
1  80 FOR  J=1 TO N1
10090 W3=W3+W1(J,I)
10100 W4=W4+W2(J,I)
1011  W5(J)=(W3-W4)/N2(J):W6=W /N2 J
10120 NEXT I
10125 NEXT J
10130 FOR J=1 TO N1
101 0 FOR I=1 TO N2(J)
1 150 W7(J)=W7+(W1(J,I)-W5(J)-W2(J, )
1 155 W8(J)=W8+(W1(J,I)-W
10160 NEXTI
10170 NEXT J
10180 FOR J=1 TO N1
10190 W9(J)=(1-(W7(J)/W8(J) .
10200 W5(J)=EXP(W5(J))
10210 RETURN
```

A.3.3 Programme Filename : CORELATION

```
  10 REM CORRELATION OF THE RESULTS OF PURE WATER DROPLETS
  20 REM AT ELEVATED AIR TEMP.
  30 REM SYMBOLS
  40 REM B(I)          =TRANSFER NUMBER (CP(I)/(TA(I)-TD(I))/LA(I)
  50 REM CP(I)         =HEAT CAPACITY (J/KG/K)
  60 REM F1(I,J)       =THE VALUE OF RE^.5*PR^.33
  70 REM LA(I)         =LATENT HEAT OF EVAP.(J/KG)
  80 REM N             =NO. OF SETS OF DATA
  90 REM N2(I)         =NO. OF READING IN EACH SET
  95 REM NU(I,J)       =CORRECTED NU. NO.
 100 REM PR(I)        =PR.NO. OF AIR
 110 REM RE(I,J)      =DROPLET REY. NO.
 150 DIM TA(17),TD(17),LA(17),N2(17),CP(17),B(17)
 160 DIM F1(16,45),W1(16,45),W2(16,45),Y3(16,45),NU(16,45)
 170 REM INPUT NO. OF SETS OF EXP.
 180 READ N
 190 REM INPUT NO. OF READING IN EACH SET
 200 FOR I=1 TO N
 210 READN2(I)
 220 NEXT I
 230 REM INPUT AIR TEMP.
 240 FOR I=1 TO N
 250 READTA(I)
 260 NEXT I
 270 REM INPUT DROP TEMP.
 280 FOR I=1 TO N
 290 READ TD(I)
 300 NEXT I
 301 REM CONVERT TEMP. TO K
 302 FOR I=1 TO N
 303 LET TD(I)=TD(I)+273.15
 304 LET TA(I)=TA(I)+273.15
 306 NEXT I
 308 REM EVALUATE PHYSICAL PROP.
 310 FOR I=1 TO N
 312 LET CP(I)=(1018.17-.13376*TA(I)+(3.3939E-4)*TD(I)^2)
 350 NEXT I
 490 FOR I=1 TO N
 500 LET LA(I)=(2805198-331.892*TD(I)-3.0848*TD(I)^2)
 520 LET B(I)=(CP(I)*(TA(I)-TD(I))/LA(I))
 530 NEXT I
 540 REM
 550 REM INPUT NU. NUMBER AND RE^.5*PR^.33
 560 FOR I=1 TO N
 570 FOR J=1 TO N2(I)
 580 READ NU(I,J)
 590 NEXT J
 600 FOR J=1 TO N2(I)
 610 READ F1(I,J)
 620 NEXT J
 630 NEXT I
 650 REM
 660 REM EVALUATE COFF. OF NU EQN. AND CORRELATION COEFF.
 670 FOR I=1 TO N
 680 FOR J=1 TO N2(I)
 690 LET W1(I,J)=LOG(NU(I,J)-2)
>
```

```
  700 LET W2(I,J)=LOG(F1(I,J))
  710 LET Y3(I,J)=LOG(1/B(I))
  720 NEXT J
  730 NEXT I
  740 W3=0:W4=0:W5=0:W6=0:W7=0:W8=0:W9=0:N3=0:Y1=0:Y2=0:Y4=0:Y5=0
  750 FOR I=1 TO N
  760 FOR J=1 TO N2(I)
  770 LET W3=W3+W1(I,J)
  780 LET W4= W4+W2(I,J)
  790 LET Y1=Y1+(Y3(I,J)*W1(I,J))
  800 LET Y2=Y2+(Y3(I,J)*W2(I,J))
  810 LET Y4=Y4+(Y3(I,J)^2)
  820 LET Y5=Y5+Y3(I,J)
  830 LET N3=N3+1
  840 NEXT J
  850 NEXT I
  860 LET B1=(N3*Y1-N3*Y2+W4*Y5-Y5*W3)/(N3*Y4-Y5^2)
  870 LET B2=(W3-B1*Y5-W4)/N3
  880 LET W6=W3/N3
  890 FOR I=1 TO N
  900 FOR J=1 TO N2(I)
  910 LET W8=W8+(W1(I,J)-W6)^2
  920 LET Y6=Y6+(W1(I,J)-B2-B1*Y3(I,J)-W2(I,J))^2
  930 NEXT J
  940 NEXT I
  950 LET Y7=(1-Y6/W8)^.5
  960 REM
  970 REM NUMBERS ARE ROUNDED OFF
  980 B1=INT(B1*1E3+.5)/1E3
  990 B2=EXP(B2):B2=INT(B2*1E3+.5)/1E3
 1000 LET Y7=INT(Y7*1E3+.5)/1E3
 1010 REM
 1020 REM PRINTING RESULTS
 1030 PRINT "COEFF. OF NU. EQN.     =";B2
 1040 PRINT "INDEX FOR (1/B)        =";B1
 1060 PRINT "CORRELATION COEFF.     =";Y7
 1090 END
>
```

A.4 TABULATION OF RESULTS

A.4.1 Water Droplets at Ambient Temperature

Tables A1-A25

TABLE A1

EXP. NO.	=1
AIR TEMP.(C)	=24.5
DROP TEMP.(C)	=8
VAP.PRES.DRIV.FORC.(ATM)	=0.010
MEAN DROP DIAM.(mm)	=2.740
AIR VELOCITY (m/s)	=0.901
REYNOLDS NO.	=163.23
SHERWOOD NO. (EXP.)	=10.699
SHERWOOD NO. (CORRECTED)	=9.527
RE^.5*SC^.33	=11.124
NUSSELT NO. (EXP.)	=10.603
NUSSELT NO. (CORRECTED)	=9.432
RE^.5*PR^.33	=11.371

TIME(Sec)	DROP WEIGHT(mg)
0	7.20
69	6.40
153	5.50
229	4.60
315	3.70

TABLE A2

EXP. NO.	=2
AIR TEMP.(C)	=24.5
DROP TEMP.(C)	=8
VAP.PRES.DRIV.FORC.(ATM)	=0.010
MEAN DROP DIAM.(mm)	=2.744
AIR VELOCITY (m/s)	=0.812
REYNOLDS NO.	=147.34
SHERWOOD NO. (EXP.)	=10.339
SHERWOOD NO. (CORRECTED)	=9.181
RE^.5*SC^.33	=10.568
NUSSELT NO. (EXP.)	=10.247
NUSSELT NO. (CORRECTED)	=9.089
RE^.5*PR^.33	=10.803

TIME(Sec)	DROP WEIGHT(mg)
0	7.20
102	6.30
179	5.50
271	4.80
392	3.70

TABLE A3

EXP. NO.	=3
AIR TEMP.(C)	=24.5
DROP TEMP.(C)	=8
VAP.PRES.DRIV.FORC.(ATM)	=0.010
MEAN DROP DIAM.(mm)	=2.736
AIR VELOCITY (m/s)	=0.503
REYNOLDS NO.	=91.01
SHERWOOD NO. (EXP.)	=8.698
SHERWOOD NO. (CORRECTED)	=7.594
RE^.5*SC^.33	=8.306
NUSSELT NO. (EXP.)	=8.655
NUSSELT NO. (CORRECTED)	=7.551
RE^.5*PR^.33	=8.490

TIME(Sec)	DROP WEIGHT(mg)
0	7.20
80	6.90
159	5.70
223	5.10
301	4.30
381	3.60

TABLE A4

EXP. NO.	=4
AIR TEMP.(C)	=24.5
DROP TEMP.(C)	=8
VAP.PRES.DRIV.FORC.(ATM)	=0.010
MEAN DROP DIAM.(mm)	=2.835
AIR VELOCITY (m/s)	=0.361
REYNOLDS NO.	=67.68
SHERWOOD NO. (EXP.)	=7.980
SHERWOOD NO. (CORRECTED)	=6.939
RE^.5*SC^.33	=7.163
NUSSELT NO. (EXP.)	=7.909
NUSSELT NO. (CORRECTED)	=6.868
RE^.5*PR^.33	=7.322

TIME(Sec)	DROP WEIGHT(mg)
0	7.20
97	6.80
179	6.00
268	5.70
397	4.40

TABLE A5

EXP. NO.	=5
AIR TEMP.(C)	=24.5
DROP TEMP.(C)	=8
VAP.PRES.DRIV.FORC.(ATM)	=0.010
MEAN DROP DIAM.(mm)	=2.817
AIR VELOCITY (m/s)	=0.285
REYNOLDS NO.	=53.09
SHERWOOD NO. (EXP.)	=7.529
SHERWOOD NO. (CORRECTED)	=6.507
RE^.5*SC^.33	=6.344
NUSSELT NO. (EXP.)	=7.474
NUSSELT NO. (CORRECTED)	=6.451
RE^.5*PR^.33	=6.485

TIME(Sec)	DROP WEIGHT(mg)
0	7.20
79	6.50
163	5.90
258	5.30
352	4.60

TABLE A6

EXP. NO.	=6
AIR TEMP.(C)	=24.5
DROP TEMP.(C)	=8
VAP.PRES.DRIV.FORC.(ATM)	=0.010
MEAN DROP DIAM.(mm)	=2.817
AIR VELOCITY (m/s)	=0.145
REYNOLDS NO.	=27.01
SHERWOOD NO. (EXP.)	=5.914
SHERWOOD NO. (CORRECTED)	=4.873
RE^.5*SC^.33	=4.525
NUSSELT NO. (EXP.)	=5.862
NUSSELT NO. (CORRECTED)	=4.820
RE^.5*PR^.33	=4.626

TIME(Sec)	DROP WEIGHT(mg)
0	7.20
75	6.70
169	6.20
257	5.60
336	5.10
411	4.60

TABLE A7

EXP. NO.	=7
AIR TEMP.(C)	=24.5
DROP TEMP.(C)	=8
VAP.PRES.DRIV.FORC.(ATM)	=0.010
MEAN DROP DIAM.(mm)	=2.909
AIR VELOCITY (m/s)	=0.056
REYNOLDS NO.	=10.77
SHERWOOD NO. (EXP.)	=4.864
SHERWOOD NO. (CORRECTED)	=3.928
RE^.5*SC^.33	=2.857
NUSSELT NO. (EXP.)	=4.835
NUSSELT NO. (CORRECTED)	=3.899
RE^.5*PR^.33	=2.921

TIME(Sec)	DROP WEIGHT(mg)
0	7.20
68	6.90
155	6.60
226	6.10
313	5.50

TABLE A8

EXP. NO.	=8
AIR TEMP.(C)	=25.5
DROP TEMP.(C)	=8.5
VAP.PRES.DRIV.FORC.(ATM)	=0.010
MEAN DROP DIAM.(mm)	=2.821
AIR VELOCITY (m/s)	=0.028
REYNOLDS NO.	=5.21
SHERWOOD NO. (EXP.)	=3.432
SHERWOOD NO. (CORRECTED)	=2.527
RE^.5*SC^.33	=1.986
NUSSELT NO. (EXP.)	=3.388
NUSSELT NO. (CORRECTED)	=2.483
RE^.5*PR^.33	=2.031

TIME(Sec)	DROP WEIGHT(mg)
0	7.20
99	6.40
195	6.10
273	5.80
354	5.50
436	5.30
534	5.00

TABLE A9

EXP. NO.	=9
AIR TEMP.(C)	=26
DROP TEMP.(C)	=8.5
VAP.PRES.DRIV.FORC.(ATM)	=0.010
MEAN DROP DIAM.(mm)	=2.872
AIR VELOCITY (m/s)	=0.018
REYNOLDS NO.	=3.40
SHERWOOD NO. (EXP.)	=3.221
SHERWOOD NO. (CORRECTED)	=2.339
RE^.5*SC^.33	=1.606
NUSSELT NO. (EXP.)	=3.072
NUSSELT NO. (CORRECTED)	=2.190
RE^.5*PR^.33	=1.641

TIME(Sec)	DROP WEIGHT(mg)
0	7.20
69	6.50
144	6.20
208	6.10
383	5.80
460	5.50

TABLE A10

EXP. NO.	=10
AIR TEMP.(C)	=23.5
DROP TEMP.(C)	=7.5
VAP.PRES.DRIV.FORC.(ATM)	=0.010
MEAN DROP DIAM.(mm)	=4.753
AIR VELOCITY (m/s)	=1.655
REYNOLDS NO.	=521.95
SHERWOOD NO. (EXP.)	=16.898
SHERWOOD NO. (CORRECTED)	=15.435
RE^.5*SC^.33	=19.891
NUSSELT NO. (EXP.)	=16.893
NUSSELT NO. (CORRECTED)	=15.430
RE^.5*PR^.33	=20.333

TIME(Sec)	DROP WEIGHT(mg)
0	33.70
93	32.00
185	29.80
278	27.80
367	25.90
582	20.80

TABLE A11

EXP. NO.	=11
AIR TEMP.(C)	=25
DROP TEMP.(C)	=8
VAP.PRES.DRIV.FORC.(ATM)	=0.010
MEAN DROP DIAM.(mm)	=4.766
AIR VELOCITY (m/s)	=0.863
REYNOLDS NO.	=271.51
SHERWOOD NO. (EXP.)	=13.041
SHERWOOD NO. (CORRECTED)	=11.667
RE^.5*SC^.33	=14.346
NUSSELT NO. (EXP.)	=12.573
NUSSELT NO. (CORRECTED)	=11.199
RE^.5*PR^.33	=14.665

TIME(Sec)	DROP WEIGHT(mg)
0	33.70
113	31.20
212	29.10
316	27.60
400	25.80
519	23.40

TABLE A12

EXP. NO.	=12
AIR TEMP.(C)	=24.5
DROP TEMP.(C)	=8
VAP.PRES.DRIV.FORC.(ATM)	=0.010
MEAN DROP DIAM.(mm)	=4.866
AIR VELOCITY (m/s)	=0.789
REYNOLDS NO.	=253.88
SHERWOOD NO. (EXP.)	=12.962
SHERWOOD NO. (CORRECTED)	=11.617
RE^.5*SC^.33	=13.873
NUSSELT NO. (EXP.)	=12.846
NUSSELT NO. (CORRECTED)	=11.501
RE^.5*PR^.33	=14.181

TIME(Sec)	DROP WEIGHT(mg)
0	33.70
89	32.20
183	30.60
279	28.60
393	26.10

TABLE A13

EXP. NO.	=13
AIR TEMP.(C)	=24.5
DROP TEMP.(C)	=8
VAP.PRES.DRIV.FORC.(ATM)	=0.010
MEAN DROP DIAM.(mm)	=4.826
AIR VELOCITY (m/s)	=0.626
REYNOLDS NO.	=199.79
SHERWOOD NO. (EXP.)	=11.599
SHERWOOD NO. (CORRECTED)	=10.274
RE^.5*SC^.33	=12.307
NUSSELT NO. (EXP.)	=11.495
NUSSELT NO. (CORRECTED)	=10.170
RE^.5*PR^.33	=12.580

TIME(Sec)	DROP WEIGHT(mg)
0	33.70
93	32.30
185	30.80
278	28.30
367	27.10
582	25.00

TABLE A15

EXP. NO.	=15
AIR TEMP.(C)	=24
DROP TEMP.(C)	=7.5
VAP.PRES.DRIV.FORC.(ATM)	=0.010
MEAN DROP DIAM.(mm)	=4.921
AIR VELOCITY (m/s)	=0.305
REYNOLDS NO.	=99.43
SHERWOOD NO. (EXP.)	=9.305
SHERWOOD NO. (CORRECTED)	=8.071
RE^.5*SC^.33	=8.682
NUSSELT NO. (EXP.)	=9.043
NUSSELT NO. (CORRECTED)	=7.809
RE^.5*PR^.33	=8.875

TIME(Sec)	DROP WEIGHT(mg)
0	33.70
93	32.70
187	31.50
305	29.90
428	28.40

TABLE A16

EXP. NO.	=16
AIR TEMP.(C)	=24
DROP TEMP.(C)	=7.5
VAP.PRES.DRIV.FORC.(ATM)	=0.010
MEAN DROP DIAM.(mm)	=4.937
AIR VELOCITY (m/s)	=0.179
REYNOLDS NO.	=58.53
SHERWOOD NO. (EXP.)	=7.992
SHERWOOD NO. (CORRECTED)	=6.806
RE^.5*SC^.33	=6.661
NUSSELT NO. (EXP.)	=7.751
NUSSELT NO. (CORRECTED)	=6.566
RE^.5*PR^.33	=6.809

TIME(Sec)	DROP WEIGHT(mg)
0	33.70
95	32.60
194	31.80
311	30.50
434	29.00

TABLE A17

EXP. NO.	=17
AIR TEMP.(C)	=24
DROP TEMP.(C)	=7.5
VAP.PRES.DRIV.FORC.(ATM)	=0.010
MEAN DROP DIAM.(mm)	=4.960
AIR VELOCITY (m/s)	=0.105
REYNOLDS NO.	=34.50
SHERWOOD NO. (EXP.)	=6.598
SHERWOOD NO. (CORRECTED)	=5.387
RE^.5*SC^.33	=5.114
NUSSELT NO. (EXP.)	=6.438
NUSSELT NO. (CORRECTED)	=5.227
RE^.5*PR^.33	=5.227

TIME(Sec)	DROP WEIGHT(mg)
0	33.70
99	33.00
200	32.20
292	31.00
417	29.90

TABLE A18

EXP. NO.	=18
AIR TEMP.(C)	=25.5
DROP TEMP.(C)	=8.5
VAP.PRES.DRIV.FORC.(ATM)	=0.010
MEAN DROP DIAM.(mm)	=4.986
AIR VELOCITY (m/s)	=0.018
REYNOLDS NO.	=5.92
SHERWOOD NO. (EXP.)	=3.456
SHERWOOD NO. (CORRECTED)	=2.374
RE^.5*SC^.33	=2.118
NUSSELT NO. (EXP.)	=3.417
NUSSELT NO. (CORRECTED)	=2.334
RE^.5*PR^.33	=2.165

TIME(Sec)	DROP WEIGHT(mg)
0	33.70
102	32.80
195	32.40
298	32.00
525	31.40

TABLE A19

EXP. NO.	=19
AIR TEMP.(C)	=24.5
DROP TEMP.(C)	=8
VAP.PRES.DRIV.FORC.(ATM)	=0.010
MEAN DROP DIAM.(mm)	=7.853
AIR VELOCITY (m/s)	=0.503
REYNOLDS NO.	=261.20
SHERWOOD NO. (EXP.)	=13.032
SHERWOOD NO. (CORRECTED)	=11.449
RE^.5*SC^.33	=14.071
NUSSELT NO. (EXP.)	=12.972
NUSSELT NO. (CORRECTED)	=11.389
RE^.5*PR^.33	=14.384

TIME(Sec)	DROP WEIGHT(mg)
0	134.50
98	131.80
203	128.80
309	125.60
425	121.80
537	118.50

TABLE A21

EXP. NO.	=21
AIR TEMP.(C)	=24
DROP TEMP.(C)	=8
VAP.PRES.DRIV.FORC.(ATM)	=0.010
MEAN DROP DIAM.(mm)	=7.858
AIR VELOCITY (m/s)	=0.557
REYNOLDS NO.	=289.92
SHERWOOD NO. (EXP.)	=13.251
SHERWOOD NO. (CORRECTED)	=11.658
RE^.5*SC^.33	=14.825
NUSSELT NO. (EXP.)	=13.226
NUSSELT NO. (CORRECTED)	=11.632
RE^.5*PR^.33	=15.154

TIME(Sec)	DROP WEIGHT(mg)
0	134.50
99	132.10
201	129.10
310	125.90
425	122.10
536	118.80

TABLE A22

EXP. NO.	=22
AIR TEMP.(C)	=24.5
DROP TEMP.(C)	=8
VAP.PRES.DRIV.FORC.(ATM)	=0.010
MEAN DROP DIAM.(mm)	=7.819
AIR VELOCITY (m/s)	=0.285
REYNOLDS NO.	=147.37
SHERWOOD NO. (EXP.)	=10.786
SHERWOOD NO. (CORRECTED)	=9.256
RE^.5*SC^.33	=10.569
NUSSELT NO. (EXP.)	=10.631
NUSSELT NO. (CORRECTED)	=9.101
RE^.5*PR^.33	=10.804

TIME(Sec)	DROP WEIGHT(mg)
0	134.50
86	131.80
195	129.70
325	127.40
438	124.70
575	121.20
720	118.00
843	114.80

TABLE A23

EXP. NO.	=23
AIR TEMP.(C)	=24.5
DROP TEMP.(C)	=8
VAP.PRES.DRIV.FORC.(ATM)	=0.010
MEAN DROP DIAM.(mm)	=7.929
AIR VELOCITY (m/s)	=0.113
REYNOLDS NO.	=59.25
SHERWOOD NO. (EXP.)	=8.313
SHERWOOD NO. (CORRECTED)	=6.869
RE^.5*SC^.33	=6.702
NUSSELT NO. (EXP.)	=8.239
NUSSELT NO. (CORRECTED)	=6.795
RE^.5*PR^.33	=6.851

TIME(Sec)	DROP WEIGHT(mg)
0	134.50
92	132.50
185	130.50
275	128.60
370	126.50

TABLE A24

EXP. NO.	=24
AIR TEMP.(C)	=25
DROP TEMP.(C)	=8
VAP.PRES.DRIV.FORC.(ATM)	=0.010
MEAN DROP DIAM.(mm)	=7.964
AIR VELOCITY (m/s)	=0.028
REYNOLDS NO.	=14.72
SHERWOOD NO. (EXP.)	=5.289
SHERWOOD NO. (CORRECTED)	=3.883
RE^.5*SC^.33	=3.341
NUSSELT NO. (EXP.)	=5.092
NUSSELT NO. (CORRECTED)	=3.686
RE^.5*PR^.33	=3.415

TIME(Sec)	DROP WEIGHT(mg)
0	134.50
100	133.60
180	132.60
315	131.00
440	129.50

TABLE A25

EXP. NO.	=25
AIR TEMP.(C)	=25.5
DROP TEMP.(C)	=8.5
VAP.PRES.DRIV.FORC.(ATM)	=0.010
MEAN DROP DIAM.(mm)	=7.968
AIR VELOCITY (m/s)	=0.018
REYNOLDS NO.	=9.45
SHERWOOD NO. (EXP.)	=4.822
SHERWOOD NO. (CORRECTED)	=3.440
RE^.5*SC^.33	=2.677
NUSSELT NO. (EXP.)	=4.767
NUSSELT NO. (CORRECTED)	=3.385
RE^.5*PR^.33	=2.736

TIME(Sec)	DROP WEIGHT(mg)
0	134.50
99	133.70
181	132.80
315	131.30
442	129.80

A.4.2 Water Droplets at Elevated Temperatures

Tables A26-A28

Table A26

Air Temperature =43.5^{o} C

Droplet Temperature=15.5^{o}C

Droplet Velocity =1.16 m/s

Time (sec)	Droplet Diameter Dp	Reynolds Number Re	Experimental Sherwood Number Sh(exp)	Corrected Sherwood Number Sh(corctd)	Experimental Nusselt Number Nu(exp)	Corrected Nusselt Number Nu(corctd)	$Re^{0.5} Sc^{0.33}$	$Re^{0.5} Pr^{0.33}$
0	5.000	348.760	13.463	12.565	12.518	11.620	16.422	16.402
34	4.600	320.860	13.165	12.234	12.214	11.310	15.752	15.733
106	3.900	272.030	12.423	11.409	11.552	10.537	14.504	14.486
174	3.100	216.230	11.844	10.666	11.013	9.835	12.931	12.915
258	2.300	160.430	11.316	9.830	10.522	9.036	11.138	11.125
296	1.840	128.340	11.060	9.260	10.284	8.484	9.962	9.950
329	1.450	101.140	10.651	8.415	9.904	7.668	8.844	8.833
342	1.310	91.380	10.566	8.107	9.824	7.365	8.406	8.396

Table A27

Air Temperature =67.0^{o} C

Droplet Temperature=25.0^{o}C

Droplet Velocity =1.21 m/s

Time (sec)	Droplet Diameter Dp	Reynolds Number Re	Experimental Sherwood Number Sh(exp)	Corrected Sherwood Number Sh(corctd)	Experimental Nusselt Number Nu(exp)	Corrected Nusselt Number Nu(corctd)	$Re^{0.5}$ $Sc^{0.33}$	$Re^{0.5}$ $Pr^{0.33}$
0	5.000	325.440	12.269	11.316	12.184	11.231	16.158	15.737
28	4.470	290.940	11.973	10.974	11.889	10.890	15.278	14.880
88	3.640	236.920	11.230	10.115	11.152	10.037	13.787	13.428
159	2.560	166.620	10.389	8.961	10.317	8.888	11.562	11.261
234	1.600	104.140	9.895	7.759	9.826	7.690	9.140	8.902
265	1.100	71.600	9.890	6.857	9.821	6.788	7.579	7.382

Table A28

Air Temperature =80.0° C

Droplet Temperature=28.5° C

Droplet Velocity =1.23 m/s

Time (sec)	Droplet Diameter Dp	Reynolds Number Re	Experimental Sherwood Number Sh(exp)	Corrected Sherwood Number Sh(corctd)	Experimental Nusselt Number Nu(exp)	Corrected Nusselt Number Nu(corctd)	$Re^{0.5}\,Sc^{0.33}$	$Re^{0.5}\,Pr^{0.33}$
0	5.000	312.530	10.925	9.946	10.665	9.685	16.029	15.362
14	4.470	279.410	10.569	9.544	10.317	9.292	15.156	14.525
62	3.450	215.650	9.896	8.716	9.660	8.480	13.315	12.761
115	2.430	151.890	9.381	7.861	9.158	7.638	11.174	10.710
155	1.670	104.390	8.985	6.891	8.771	6.677	9.264	8.878
193	1.100	68.760	8.827	5.738	8.617	5.528	7.518	7.206

APPENDIX B

EXPERIMENTAL RESULTS FOR THE DRYING OF DROPLETS OF SKIN FORMING MATERIALS

B.1 CUSTARD

B.2 RICE STARCH

B.3 GELATIN

B.4 SKIM MILK

B.5 FRUCTOSE

B.1 CUSTARD

TABLE B1

EXPERIMENT NUMBER =1
CUSTARD(WT%) =20
AIR TEMPERATURE (C) =20
AIR VELOCITY(m/s) =0.98

TIME (sec)	ACTUAL WT.(mg)	CORRECTED WT.(mg)	FRACTION EVAPORATED
0	38.1	38.10	0.00
60	35.8	36.00	0.06
127	32.5	32.70	0.14
199	31.1	31.30	0.18
275	29.4	29.60	0.22
371	27.7	27.90	0.27
471	26.4	26.60	0.30
563	24.1	24.30	0.36
650	22.2	22.40	0.41
772	19.9	20.10	0.47
917	17.2	17.40	0.54
1097	15.1	15.30	0.60
1268	14.4	14.60	0.62
1460	13.9	14.10	0.63
1691	13.7	13.90	0.64

TABLE B2

EXPERIMENT NUMBER =6
CUSTARD(WT%) =30
AIR TEMPERATURE (C) =21.5
AIR VELOCITY(m/s) =0.97

TIME (sec)	ACTUAL WT.(mg)	CORRECTED WT.(mg)	FRACTION EVAPORATED
0	38	38.00	0.00
60	35.3	35.53	0.07
130	32.4	32.63	0.14
204	30	30.23	0.20
288	27.9	28.13	0.26
374	26.1	26.33	0.31
460	24.1	24.33	0.36
551	22.2	22.43	0.41
670	20.3	20.53	0.46
797	19.1	19.33	0.49
927	18.5	18.73	0.51
1075	17.8	18.03	0.53
1217	17.7	17.93	0.53
1338	17.6	17.83	0.53
1456	17.6	17.83	0.53

TABLE B3

EXPERIMENT NUMBER =16
CUSTARD(WT%) =20
AIR TEMPERATURE (C) =36
AIR VELOCITY(m/s) =0.98

TIME (sec)	ACTUAL WT.(mg)	CORRECTED WT.(mg)	FRACTION EVAPORATED
0	37.6	37.60	0.00
70	32.4	32.79	0.13
144	27	27.39	0.27
216	23.1	23.49	0.38
294	20.3	20.69	0.45
373	17.6	17.99	0.52
470	14	14.39	0.62
565	11.2	11.59	0.69
687	10.4	10.79	0.71
809	9.5	9.89	0.74
941	9.3	9.69	0.74
1034	9.2	9.59	0.75
1130	9.1	9.49	0.75

TABLE B4

EXPERIMENT NUMBER =21
CUSTARD(WT%) =20
AIR TEMPERATURE (C) =54
AIR VELOCITY(m/s) =0.96

TIME (sec)	ACTUAL WT.(mg)	CORRECTED WT.(mg)	FRACTION EVAPORATED
0	36.4	36.40	0.00
65	28.9	29.48	0.19
138	21.1	21.68	0.41
206	16.4	16.98	0.53
268	12.9	13.48	0.63
364	9.2	9.78	0.73
442	7.2	7.78	0.79
523	7.2	7.78	0.79

TABLE B5

EXPERIMENT NUMBER =26
CUSTARD(WT%) =30
AIR TEMPERATURE (C) =54
AIR VELOCITY(m/s) =0.96

TIME (sec)	ACTUAL WT.(mg)	CORRECTED WT.(mg)	FRACTION EVAPORATED
0	38.1	38.10	0.00
60	33.1	33.68	0.12
127	26	26.58	0.30
192	21.1	21.68	0.43
264	17.3	17.88	0.53
336	14.4	14.98	0.61
408	12.8	13.38	0.65
489	12.7	13.28	0.65

TABLE B6

EXPERIMENT NUMBER =27
CUSTARD(WT%) =20
AIR TEMPERATURE (C) =76
AIR VELOCITY(m/s) =0.99

TIME (sec)	ACTUAL WT.(mg)	CORRECTED WT.(mg)	FRACTION EVAPORATED
0	38.2	38.20	0.00
60	29.5	30.36	0.21
120	22.4	23.26	0.39
182	16.5	17.36	0.55
249	11.3	12.16	0.68
319	8.9	9.76	0.74
411	8.7	9.56	0.75
520	8.6	9.46	0.75

TABLE B7

EXPERIMENT NUMBER =32
CUSTARD(WT%) =20
AIR TEMPERATURE (C) =91
AIR VELOCITY(m/s) =0.99

TIME (sec)	ACTUAL WT.(mg)	CORRECTED WT.(mg)	FRACTION EVAPORATED
0	35.5	35.50	0.00
60	26.8	27.86	0.22
132	16.4	17.46	0.51
209	10.9	11.96	0.66
270	9.1	10.16	0.71
332	8.8	9.86	0.72
411	8.7	9.76	0.73
508	8.6	9.66	0.73

TABLE B8

EXPERIMENT NUMBER =105
CUSTARD(WT%) =40
AIR TEMPERATURE (C) =56
AIR VELOCITY(m/s) =0.97

TIME (sec)	ACTUAL WT.(mg)	CORRECTED WT.(mg)	FRACTION EVAPORATED
0	34.8	34.80	0.00
60	28.3	28.82	0.17
123	21.3	21.82	0.37
192	17.5	18.02	0.48
262	15.3	15.82	0.55
341	13.8	14.32	0.59
418	13.5	14.02	0.60
507	13.4	13.92	0.60
601	13.3	13.82	0.60

TABLE B9

EXPERIMENT NUMBER =37
CUSTERD(WT%) =20
AIR TEMPERATURE (C) =106
AIR VELOCITY(m/s) =0.95

TIME (sec)	ACTUAL WT.(mg)	CORRECTED WT.(mg)	FRACTION EVAPORATED
0	36	36.00	0.00
65	24.9	26.18	0.27
126	16.6	17.88	0.50
189	13.2	14.48	0.60
251	12.6	13.88	0.61
334	12.4	13.68	0.62
407	12.3	13.58	0.62

TABLE B10

EXPERIMENT NUMBER =161
CUSTERD(WT%) =20
AIR TEMPERATURE (C) =55
AIR VELOCITY(m/s) =0.49

TIME (sec)	ACTUAL WT.(mg)	CORRECTED WT.(mg)	FRACTION EVAPORATED
0	37	37.00	0.00
63	32.4	32.94	0.11
178	28	28.54	0.23
240	24.8	25.34	0.32
305	21.8	22.34	0.40
356	19	19.54	0.47
428	16.7	17.24	0.53
507	15.3	15.84	0.57
582	14.8	15.34	0.59
675	14.6	15.14	0.59
800	14.2	14.74	0.60
924	13.7	14.24	0.62
1099	13.6	14.14	0.62
1271	13.5	14.04	0.62

TABLE B11

EXPERIMENT NUMBER =97
GELATINIZED CUSTARD(WT%) =20
AIR TEMPERATURE (C) =22
AIR VELOCITY(m/s) =0.97

TIME (sec)	ACTUAL WT.(mg)	CORRECTED WT.(mg)	FRACTION EVAPORATED
0	36.4	36.40	0.00
60	35.4	35.62	0.02
126	34.1	34.32	0.06
197	32.8	33.02	0.09
280	31.7	31.92	0.12
368	30	30.22	0.17
461	28.8	29.02	0.20
551	27.7	27.92	0.23
643	26.8	27.02	0.26
769	24.7	24.92	0.32
883	23.6	23.82	0.35
1012	22.3	22.52	0.38
1130	20.9	21.12	0.42
1282	19.8	20.02	0.45
1414	18.9	19.12	0.47
1574	17.8	18.02	0.50
1743	17.1	17.32	0.52
1896	16.2	16.42	0.55
2090	15.2	15.42	0.58
2292	14.6	14.82	0.59
2444	14	14.22	0.61

TABLE B12

EXPERIMENT NUMBER =99
GELATINIZED CUSTARD(WT%) =20
AIR TEMPERATURE (C) =36.5
AIR VELOCITY(m/s) =0.99

TIME (sec)	ACTUAL WT.(mg)	CORRECTED WT.(mg)	FRACTION EVAPORATED
0	38.7	38.70	0.00
60	36.6	36.98	0.04
124	34.2	34.58	0.11
189	32.2	32.58	0.16
253	30.5	30.88	0.20
324	28.7	29.08	0.25
392	26.3	26.68	0.31
472	24.7	25.08	0.35
551	23.2	23.58	0.39
637	21.4	21.78	0.44
729	19.8	20.18	0.48
826	18.7	19.08	0.51
947	17.4	17.78	0.54
1062	16	16.38	0.58
1183	14.9	15.28	0.61
1308	14	14.38	0.63
1436	13	13.38	0.65
1567	12.4	12.78	0.67
1776	11.3	11.68	0.70
1977	10.7	11.08	0.71

TABLE B13

EXPERIMENT NUMBER =101
GELATINIZED CUSTARD(WT%) =20
AIR TEMPERATURE (C) =56.5
AIR VELOCITY(m/s) =0.97

TIME (sec)	ACTUAL WT.(mg)	CORRECTED WT.(mg)	FRACTION EVAPORATED
0	35.4	35.40	0.00
60	30.8	31.40	0.11
120	27	27.60	0.22
183	24	24.60	0.31
247	20.7	21.30	0.40
315	18.5	19.10	0.46
383	16.9	17.50	0.51
471	15.3	15.90	0.55
563	14.2	14.80	0.58
662	12.8	13.40	0.62
768	12	12.60	0.64
872	11.2	11.80	0.67
981	10.7	11.30	0.68
1103	10.3	10.90	0.69
1231	10	10.60	0.70
1380	9.6	10.20	0.71

B.2 RICE STARCH

TABLE B14

EXPERIMENT NUMBER =5
RICE STARCH(WT%) =20
AIR TEMPERATURE (C) =20.5
AIR VELOCITY(m/s) =0.98

TIME (sec)	ACTUAL WT.(mg)	CORRECTED WT.(mg)	FRACTION EVAPORATED
0	35.1	35.10	0.00
60	33	33.21	0.05
124	29.9	30.11	0.14
198	27.4	27.61	0.21
287	24.7	24.91	0.29
377	21.8	22.01	0.37
489	18.9	19.11	0.46
636	15.4	15.61	0.56
906	10.3	10.51	0.70
1053	8.6	8.81	0.75
1203	8	8.21	0.77
1433	7.7	7.91	0.77

TABLE B15

EXPERIMENT NUMBER =10
RICE STARCH(WT%) =30
AIR TEMPERATURE (C) =20.5
AIR VELOCITY(m/s) =0.97

TIME (sec)	ACTUAL WT.(mg)	CORRECTED WT.(mg)	FRACTION EVAPORATED
0	38.9	38.90	0.00
75	35.5	35.71	0.08
152	31.9	32.11	0.17
223	29	29.21	0.25
310	25.9	26.11	0.33
405	22.6	22.81	0.41
500	19.4	19.61	0.50
596	17.3	17.51	0.55
712	15.1	15.31	0.61
875	13.7	13.91	0.64
1016	12.6	12.81	0.67
1173	12	12.21	0.69
1353	11.5	11.71	0.70
1545	11.3	11.51	0.70
1798	10.9	11.11	0.71
2256	10.8	11.01	0.72

TABLE B16

EXPERIMENT NUMBER =15
RICE STARCH(WT%) =20
AIR TEMPERATURE (C) =20.5
AIR VELOCITY(m/s) =0.49

TIME (sec)	ACTUAL WT.(mg)	CORRECTED WT.(mg)	FRACTION EVAPORATED
0	36.5	36.50	0.00
80	33.9	34.09	0.07
154	32.2	32.39	0.11
234	30.2	30.39	0.17
322	27.5	27.69	0.24
393	25.3	25.49	0.30
490	23.3	23.49	0.36
595	21	21.19	0.42
710	18.5	18.69	0.49
830	16.3	16.49	0.55
965	13.2	13.39	0.63
1101	11.8	11.99	0.67
1248	9.5	9.69	0.73
1428	7.3	7.49	0.79
1633	6.7	6.89	0.81

TABLE B17

EXPERIMENT NUMBER =20
RICE STARCH(WT%) =20
AIR TEMPERATURE (C) =36
AIR VELOCITY(m/s) =0.98

TIME (sec)	ACTUAL WT.(mg)	CORRECTED WT.(mg)	FRACTION EVAPORATED
0	35.3	35.30	0.00
72	31.2	31.59	0.11
145	27.3	27.69	0.22
223	23.5	23.89	0.32
314	19.6	19.99	0.43
408	15.7	16.09	0.54
511	12.1	12.49	0.65
604	10.1	10.49	0.70
698	8.9	9.29	0.74
821	8.3	8.69	0.75
943	8.1	8.49	0.76
1099	7.9	8.29	0.77
1223	7.9	8.29	0.77

TABLE B18

EXPERIMENT NUMBER =24
RICE STARCH(WT%) =20
AIR TEMPERATURE (C) =54
AIR VELOCITY(m/s) =0.96

TIME (sec)	ACTUAL WT.(mg)	CORRECTED WT.(mg)	FRACTION EVAPORATED
0	38	38.00	0.00
65	31.8	32.38	0.15
132	25.9	26.48	0.30
203	20	20.58	0.46
276	14.5	15.08	0.60
356	9.3	9.88	0.74
447	6.8	7.38	0.81
523	6.7	7.28	0.81

TABLE B19

EXPERIMENT NUMBER =31
RICE STARCH(WT%) =20
AIR TEMPERATURE (C) =76
AIR VELOCITY(m/s) =0.97

TIME (sec)	ACTUAL WT.(mg)	CORRECTED WT.(mg)	FRACTION EVAPORATED
0	36.2	36.20	0.00
60	29.7	30.56	0.16
125	23.1	23.96	0.34
200	15.9	16.76	0.54
277	10.3	11.16	0.69
366	8.7	9.56	0.74
496	8.6	9.46	0.74
578	8.6	9.46	0.74

TABLE B20

EXPERIMENT NUMBER =36
RICE STARCH(WT%) =20
AIR TEMPERATURE (C) =90
AIR VELOCITY(m/s) =1

TIME (sec)	ACTUAL WT.(mg)	CORRECTED WT.(mg)	FRACTION EVAPORATED
0	33.1	33.10	0.00
60	24.9	25.95	0.22
121	17.1	18.15	0.45
183	10.1	11.15	0.66
244	7.5	8.55	0.74
322	7.4	8.45	0.74
408	7.3	8.35	0.75
498	7.3	8.35	0.75

B.3 GELATIN

TABLE B21

EXPERIMENT NUMBER =4
GELATIN(WT%) =20
AIR TEMPERATURE (C) =20.5
AIR VELOCITY(m/s) =0.98

TIME (sec)	ACTUAL WT.(mg)	CORRECTED WT.(mg)	FRACTION EVAPORATED
0	37	37.00	0.00
60	34.2	34.41	0.07
158	33.4	33.61	0.09
245	32.4	32.61	0.12
345	30.9	31.11	0.16
454	28.9	29.11	0.21
561	27.3	27.51	0.26
686	25.8	26.01	0.30
878	23.7	23.91	0.35
1060	22.3	22.51	0.39
1258	20.7	20.91	0.43
1467	19.1	19.31	0.48
1695	18.1	18.31	0.51
1940	17.2	17.41	0.53
2191	16.4	16.61	0.55
2538	15.6	15.81	0.57
2838	15.1	15.31	0.59

TABLE B22

EXPERIMENT NUMBER =164
GELATIN(WT%) =20
AIR TEMPERATURE (C) =55.5
AIR VELOCITY(m/s) =0.49

TIME (sec)	ACTUAL WT.(mg)	CORRECTED WT.(mg)	FRACTION EVAPORATED
0	35.6	35.60	0.00
67	31.5	32.04	0.10
132	28.5	29.04	0.18
200	25.5	26.04	0.27
303	21.9	22.44	0.37
383	18.2	18.74	0.47
467	16.7	17.24	0.52
572	15.1	15.64	0.56
693	13.7	14.24	0.60
823	12.3	12.84	0.64
999	11.1	11.64	0.67
1158	10.1	10.64	0.70
1317	9.8	10.34	0.71

TABLE B23

EXPERIMENT NUMBER =14
GELATIN(WT%) =20
AIR TEMPERATURE (C) =20
AIR VELOCITY(m/s) =0.49

TIME (sec)	ACTUAL WT.(mg)	CORRECTED WT.(mg)	FRACTION EVAPORATED
0	36.7	36.70	0.00
60	34.6	34.78	0.05
160	31.9	32.08	0.13
241	30.1	30.28	0.17
324	28.8	28.98	0.21
391	27.4	27.58	0.25
505	25.2	25.38	0.31
627	23.6	23.78	0.35
756	21.9	22.08	0.40
890	19.9	20.08	0.45
1022	18.5	18.68	0.49
1157	17.3	17.48	0.52
1309	16.3	16.48	0.55
1475	14.9	15.08	0.59
1652	13.7	13.88	0.62
1847	12.4	12.58	0.66
2059	11.6	11.78	0.68
2325	9.6	9.78	0.73
2511	9.5	9.68	0.74

TABLE B24

EXPERIMENT NUMBER =114
GELATIN(WT%) =40
AIR TEMPERATURE (C) =19.5
AIR VELOCITY(m/s) =1

TIME (sec)	ACTUAL WT.(mg)	CORRECTED WT.(mg)	FRACTION EVAPORATED
0	39	39.00	0.00
72	38	38.20	0.02
153	37.2	37.40	0.04
239	36.4	36.60	0.06
337	35.2	35.40	0.09
435	33.9	34.10	0.13
538	32.9	33.10	0.15
647	32.3	32.50	0.17
757	31.5	31.70	0.19
907	30.6	30.80	0.21
1027	29.6	29.80	0.24
1156	29.1	29.30	0.25
1300	28.4	28.60	0.27
1430	27.7	27.90	0.28
1591	27.1	27.30	0.30
1755	26.2	26.40	0.32
1930	25.9	26.10	0.33
2157	25.1	25.30	0.35
2374	24.6	24.80	0.36
2588	24	24.20	0.38
2861	23.6	23.80	0.39

TABLE B25

EXPERIMENT NUMBER =19
GELATIN(WT%) =20
AIR TEMPERATURE (C) =36
AIR VELOCITY(m/s) =0.98

TIME (sec)	ACTUAL WT.(mg)	CORRECTED WT.(mg)	FRACTION EVAPORATED
0	37.9	37.90	0.00
75	35.3	35.67	0.06
154	33.1	33.47	0.12
237	30.9	31.27	0.17
325	28.2	28.57	0.25
421	25.2	25.57	0.33
528	23.4	23.77	0.37
639	21.4	21.77	0.43
765	19.4	19.77	0.48
930	17.6	17.97	0.53
1078	15.6	15.97	0.58
1233	14.4	14.77	0.61
1404	13.2	13.57	0.64
1585	12.1	12.47	0.67
1821	11	11.37	0.70
2121	10	10.37	0.73

TABLE B26

EXPERIMENT NUMBER =25
GELATIN(WT%) =20
AIR TEMPERATURE (C) =54
AIR VELOCITY(m/s) =0.96

TIME (sec)	ACTUAL WT.(mg)	CORRECTED WT.(mg)	FRACTION EVAPORATED
0	38.1	38.10	0.00
70	32.4	32.95	0.14
146	28.9	29.45	0.23
237	25	25.55	0.33
336	21.8	22.35	0.41
427	19.8	20.35	0.47
525	18.3	18.85	0.51
613	17.1	17.65	0.54
704	15.8	16.35	0.57
830	14.7	15.25	0.60
986	13.4	13.95	0.63
1129	12.6	13.15	0.65
1282	11.5	12.05	0.68
1465	10.5	11.05	0.71
1738	9.7	10.25	0.73

TABLE B27

EXPERIMENT NUMBER =30
GELATIN(WT%) =20
AIR TEMPERATURE (C) =76
AIR VELOCITY(m/s) =0.97

TIME (sec)	ACTUAL WT.(mg)	CORRECTED WT.(mg)	FRACTION EVAPORATED
0	35.6	35.60	0.00
70	29.8	30.63	0.14
141	24.9	25.73	0.28
216	21.9	22.73	0.36
289	20	20.83	0.41
365	18.2	19.03	0.47
481	16.4	17.23	0.52
683	15.2	16.03	0.55
813	14.7	15.53	0.56
983	14.7	15.53	0.56

TABLE B28

EXPERIMENT NUMBER =35
GELATIN(WT%) =20
AIR TEMPERATURE (C) =91
AIR VELOCITY(m/s) =0.99

TIME (sec)	ACTUAL WT.(mg)	CORRECTED WT.(mg)	FRACTION EVAPORATED
0	32.3	32.30	0.00
65	26.2	27.24	0.16
131	21.4	22.44	0.31
194	18	19.04	0.41
268	16	17.04	0.47
358	13.6	14.64	0.55
448	12.4	13.44	0.58
606	10.5	11.54	0.64
789	10.2	11.24	0.65
949	10	11.04	0.66

B.4 SKIM MILK

TABLE B29

EXPERIMENT NUMBER =2
SKIM MILK(WT%) =20
AIR TEMPERATURE (C) =20
AIR VELOCITY(m/s) =0.98

TIME (sec)	ACTUAL WT.(mg)	CORRECTED WT.(mg)	FRACTION EVAPORATED
0	35	35.00	0.00
60	32.3	32.51	0.07
125	30	30.21	0.14
193	29	29.21	0.17
261	27.8	28.01	0.20
336	26.3	26.51	0.24
428	24.5	24.71	0.29
543	22.4	22.61	0.35
677	20.6	20.81	0.41
836	18.4	18.61	0.47
1033	16.7	16.91	0.52
1256	15.6	15.81	0.55
1616	15	15.21	0.57
1907	14.9	15.11	0.57
2447	14.8	15.01	0.57

TABLE B30

EXPERIMENT NUMBER =12
SKIM MILK(WT%) =20
AIR TEMPERATURE (C) =21
AIR VELOCITY(m/s) =0.49

TIME (sec)	ACTUAL WT.(mg)	CORRECTED WT.(mg)	FRACTION EVAPORATED
0	34	34.00	0.00
70	31.6	31.80	0.06
147	29.3	29.50	0.13
234	27.3	27.50	0.19
335	25.4	25.60	0.25
448	23.4	23.60	0.31
568	21.3	21.50	0.37
684	19.8	20.00	0.41
819	18.5	18.70	0.45
1003	16.3	16.50	0.51
1181	14.8	15.00	0.56
1368	13.3	13.50	0.60
1566	12.3	12.50	0.63
1786	12.3	12.50	0.63
1955	12.3	12.50	0.63

TABLE B31

EXPERIMENT NUMBER =17
SKIM MILK(WT%) =20
AIR TEMPERATURE (C) =36
AIR VELOCITY(m/s) =0.98

TIME (sec)	ACTUAL WT.(mg)	CORRECTED WT.(mg)	FRACTION EVAPORATED
0	35.2	35.20	0.00
70	31.7	32.09	0.09
144	28.1	28.49	0.19
218	25	25.39	0.28
313	22	22.39	0.36
388	19.7	20.09	0.43
470	18	18.39	0.48
585	16.4	16.79	0.52
709	15.3	15.69	0.55
831	14.4	14.79	0.58
983	14.3	14.69	0.58
1135	14.3	14.69	0.58

TABLE B32

EXPERIMENT NUMBER =163
SKIM MILK(WT%) =20
AIR TEMPERATURE (C) =55
AIR VELOCITY(m/s) =0.49

TIME (sec)	ACTUAL WT.(mg)	CORRECTED WT.(mg)	FRACTION EVAPORATED
0	35.7	35.70	0.00
66	32.5	33.03	0.07
132	29.5	30.03	0.16
203	26.9	27.43	0.23
277	24.6	25.13	0.30
361	22.6	23.13	0.35
496	21.2	21.73	0.39
587	20.2	20.73	0.42
710	19.5	20.03	0.44
863	18.7	19.23	0.46
1019	18.2	18.73	0.48
1207	18	18.53	0.48
1358	17.6	18.13	0.49
1583	17	17.53	0.51
1857	16.5	17.03	0.52
2045	16.2	16.73	0.53

TABLE B33

EXPERIMENT NUMBER =22
SKIM MILK(WT%) =20
AIR TEMPERATURE (C) =54
AIR VELOCITY(m/s) =0.96

TIME (sec)	ACTUAL WT.(mg)	CORRECTED WT.(mg)	FRACTION EVAPORATED
0	32.4	32.40	0.00
66	27	27.58	0.15
136	21.4	21.98	0.32
206	16.8	17.38	0.46
281	12.5	13.08	0.60
356	9.9	10.48	0.68
442	8.1	8.68	0.73
536	7.3	7.88	0.76
640	7.2	7.78	0.76
765	7.2	7.78	0.76

TABLE B34

EXPERIMENT NUMBER =28
SKIM MILK(WT%) =20
AIR TEMPERATURE (C) =76
AIR VELOCITY(m/s) =0.99

TIME (sec)	ACTUAL WT.(mg)	CORRECTED WT.(mg)	FRACTION EVAPORATED
0	34.3	34.30	0.00
60	27.7	28.55	0.17
120	22.5	23.35	0.32
181	18	18.85	0.45
249	14.4	15.25	0.56
314	11.5	12.35	0.64
390	9.3	10.15	0.70
508	9.2	10.05	0.71

TABLE B35

EXPERIMENT NUMBER =33
SKIM MILK(WT%) =20
AIR TEMPERATURE (C) =91
AIR VELOCITY(m/s) =0.99

TIME (sec)	ACTUAL WT.(mg)	CORRECTED WT.(mg)	FRACTION EVAPORATED
0	34.8	34.80	0.00
60	27.3	28.36	0.19
123	20.3	21.36	0.39
187	14.6	15.66	0.55
263	9.9	10.96	0.69
351	8.7	9.76	0.72
439	8.7	9.76	0.72
532	8.6	9.66	0.72

TABLE B36

EXPERIMENT NUMBER =113
SKIM MILK(WT%) =40
AIR TEMPERATURE (C) =19.5
AIR VELOCITY(m/s) =1

TIME (sec)	ACTUAL WT.(mg)	CORRECTED WT.(mg)	FRACTION EVAPORATED
0	34.8	34.80	0.00
60	34.4	34.60	0.01
126	33.4	33.60	0.03
198	32.6	32.80	0.06
275	31.4	31.60	0.09
362	30.6	30.80	0.11
448	29.4	29.60	0.15
550	28.4	28.60	0.18
663	27.5	27.70	0.20
784	26.8	27.00	0.22
896	26.4	26.60	0.24
1077	25.8	26.00	0.25
1255	25	25.20	0.28
1441	24.2	24.40	0.30
1651	24	24.20	0.30
1891	23.4	23.60	0.32

B.5 FRUCTOSE

TABLE B37

EXPERIMENT NUMBER =3
FRUCTOSE(WT%) =20
AIR TEMPERATURE (C) =20
AIR VELOCITY(m/s) =0.98

TIME (sec)	ACTUAL WT.(mg)	CORRECTED WT.(mg)	FRACTION EVAPORATED
0	37.2	37.20	0.00
60	35	35.21	0.05
132	32.4	32.61	0.12
210	30.2	30.41	0.18
283	28.2	28.41	0.24
362	26.1	26.31	0.29
440	24.6	24.81	0.33
519	23.1	23.31	0.37
603	21.3	21.51	0.42
710	19.2	19.41	0.48
834	17.3	17.51	0.53
981	15.6	15.81	0.58
1129	14.6	14.81	0.60
1302	13.7	13.91	0.63
1496	13.3	13.51	0.64
1772	12.8	13.01	0.65
1975	12.6	12.81	0.66
2155	12.4	12.61	0.66
2524	12.3	12.51	0.66

TABLE B38

EXPERIMENT NUMBER =13
FRUCTOSE(WT%) =20
AIR TEMPERATURE (C) =21
AIR VELOCITY(m/s) =0.49

TIME (sec)	ACTUAL WT.(mg)	CORRECTED WT.(mg)	FRACTION EVAPORATED
0	36.5	36.50	0.00
60	33.9	34.10	0.07
127	31.3	31.50	0.14
230	29.1	29.30	0.20
314	27.8	28.00	0.23
408	25.7	25.90	0.29
520	23.6	23.80	0.35
642	21.2	21.40	0.41
777	18.8	19.00	0.48
904	16.9	17.10	0.53
1050	14.9	15.10	0.59
1214	13.6	13.80	0.62
1373	12.8	13.00	0.64
1535	12.4	12.60	0.65
1749	11.7	11.90	0.67
1849	11.6	11.80	0.68
2077	11.4	11.60	0.68
2216	11.4	11.60	0.68

TABLE B39

EXPERIMENT NUMBER =18
FRUCTOSE(WT%) =20
AIR TEMPERATURE (C) =36
AIR VELOCITY(m/s) =0.98

TIME (sec)	ACTUAL WT.(mg)	CORRECTED WT.(mg)	FRACTION EVAPORATED
0	35.7	35.70	0.00
65	32.5	32.88	0.08
138	28.4	28.78	0.19
210	25.1	25.48	0.29
290	22.1	22.48	0.37
384	19.2	19.58	0.45
481	16.4	16.78	0.53
572	14.8	15.18	0.57
666	14	14.38	0.60
791	13.6	13.98	0.61
915	13.5	13.88	0.61
1041	13.4	13.78	0.61
1162	13.4	13.78	0.61
1307	13.4	13.78	0.61

TABLE B40

EXPERIMENT NUMBER =23
FRUCTOSE(WT%) =20
AIR TEMPERATURE (C) =54
AIR VELOCITY(m/s) =0.96

TIME (sec)	ACTUAL WT.(mg)	CORRECTED WT.(mg)	FRACTION EVAPORATED
0	38.4	38.40	0.00
70	31.9	32.48	0.15
141	26.1	26.68	0.31
211	21.4	21.98	0.43
305	15.9	16.48	0.57
395	12.5	13.08	0.66
492	10.8	11.38	0.70
594	10.1	10.68	0.72
737	9.3	9.88	0.74
859	9.3	9.88	0.74

TABLE B41

EXPERIMENT NUMBER =29
FRUCTOSE(WT%) =20
AIR TEMPERATURE (C) =76
AIR VELOCITY(m/s) =0.99

TIME (sec)	ACTUAL WT.(mg)	CORRECTED WT.(mg)	FRACTION EVAPORATED
0	33.8	33.80	0.00
70	25.9	26.76	0.21
137	18.6	19.46	0.42
208	12.7	13.56	0.60
295	9.3	10.16	0.70
388	8.1	8.96	0.73
526	8	8.86	0.74
705	8	8.86	0.74
803	8	8.86	0.74

TABLE B42

EXPERIMENT NUMBER =34
FRUCTOSE(WT%) =20
AIR TEMPERATURE (C) =91
AIR VELOCITY(m/s) =0.99

TIME (sec)	ACTUAL WT.(mg)	CORRECTED WT.(mg)	FRACTION EVAPORATED
0	32.3	32.30	0.00
60	24.9	25.94	0.20
123	17	18.04	0.44
188	10.5	11.54	0.64
274	8.6	9.64	0.70
368	8.2	9.24	0.71
489	8	9.04	0.72
578	8	9.04	0.72

TABLE B43

EXPERIMENT NUMBER =115
FRUCTOSE(WT%) =40
AIR TEMPERATURE (C) =19.5
AIR VELOCITY(m/s) =1

TIME (sec)	ACTUAL WT.(mg)	CORRECTED WT.(mg)	FRACTION EVAPORATED
0	38	38.00	0.00
72	37.6	37.80	0.01
153	36.6	36.80	0.03
251	35.3	35.50	0.07
336	34.3	34.50	0.09
426	33.3	33.50	0.12
522	32.5	32.70	0.14
628	31.8	32.00	0.16
743	31.3	31.50	0.17
865	30.9	31.10	0.18
1004	30.7	30.90	0.19
1138	30.5	30.70	0.19
1288	30.2	30.40	0.20
1468	30	30.20	0.21
1649	29.8	30.00	0.21
1829	29.6	29.80	0.22
2030	29.5	29.70	0.22
2270	29.4	29.60	0.22
2483	29.3	29.50	0.22
2723	29.3	29.50	0.22
3084	29.2	29.40	0.23

TABLE B44

EXPERIMENT NUMBER =165
FRUCTOSE(WT%) =20
AIR TEMPERATURE (C) =55.5
AIR VELOCITY(m/s) =0.49

TIME (sec)	ACTUAL WT.(mg)	CORRECTED WT.(mg)	FRACTION EVAPORATED
0	35.9	35.90	0.00
68	32.5	32.96	0.08
137	28.3	28.76	0.20
213	24.5	24.96	0.30
293	20.8	21.26	0.41
384	17.7	18.16	0.49
484	13.8	14.26	0.60
574	10.8	11.26	0.69
691	8.7	9.16	0.74
788	8.3	8.76	0.76
874	8.3	8.76	0.76

APPENDIX C

TABULATION OF EXPERIMENTAL CORE TEMPERATURE MEASUREMENTS FOR THE DRYING OF DROPLETS OF SKIN FORMING MATERIALS

Tables	Material
C1 - C3	Custard
C4 - C5	Rice Starch
C6 - C7	Gelatin
C8 - C9	Skim Milk
C10 - C12	Fructose

TABLE C1

EXPERIMENTAL CORE TEMPERATURE MEASUREMENTS

EXPERIMENTAL NUMBER =53
CUSTARD (WT%) =20
AIR TEMPERATURE (C) =36
AIR VELOCITY (m/s) =0.98

TIME (sec)	TEMP. (C)
0	23.3
20	21.3
50	20.3
80	20.7
110	21.3
150	22
190	22.5
210	22.8
260	23.2
320	23.5
380	23.9
440	24.1
500	24.7
590	27
650	27.9
710	28.4
800	28.7
920	28.9
1040	29.2
1130	29.7
1250	30.4
1340	30.9
1430	31.8
1490	32.5
1580	33.4
1670	34
1760	34.6
1940	35.3
2090	35.6

TABLE C2

EXPERIMENTAL CORE TEMPERATURE MEASUREMENTS

EXPERIMENTAL NUMBER =58
CUSTARD (WT%) =20
AIR TEMPERATURE (C) =54
AIR VELOCITY (m/s) =0.96

TIME (sec)	TEMP. (C)
0	21.8
30	21.6
60	23.3
80	24.2
100	24.9
130	25.8
170	26.7
210	27.3
240	28
280	29
320	30.3
370	31.7
420	33.2
480	34.5
540	35.8
580	36.8
620	37.9
680	38.5
760	39.5
820	40.1
920	41
1020	41.7
1140	42.4
1240	43.2
1320	44.1
1460	45
1600	46
1740	48.6
1940	50.7
2090	51.4
2270	51.9
2450	52.3
2690	52.7
2890	52.9
3170	53

TABLE C3

EXPERIMENTAL CORE TEMPERATURE MEASUREMENTS

EXPERIMENTAL NUMBER =87
CUSTARD (WT%) =20
AIR TEMPERATURE (C) =76
AIR VELOCITY (m/s) =0.99

TIME (sec)	TEMP. (C)
0	23.3
30	29.9
60	35.4
90	39.1
120	42.1
150	44.5
180	46.6
210	48.5
250	51.1
290	53.5
340	56
390	57.6
450	60
510	63.1
580	65.2
640	66.2
720	67.1
800	67.6
900	68
1040	68.3
1160	68.5
1310	68.6
1490	68.8
1730	69
1910	69.1
2150	69.2

TABLE C4

EXPERIMENTAL CORE TEMPERATURE MEASUREMENTS

EXPERIMENTAL NUMBER =49
RICE STARCH (WT%) =20
AIR TEMPERATURE (C) =20.5
AIR VELOCITY (m/s) =0.98

TIME (sec)	TEMP. (C)
0	22.4
30	15.9
60	13.4
90	12.6
120	12.5
150	12.6
190	12.7
235	12.8
275	12.9
325	13
380	13.1
470	13.2
560	13.4
650	13.6
740	14
830	14.3
920	14.7
1010	15.1
1100	15.8
1190	16.9
1280	17.5
1370	18.3
1460	19.3
1510	19.8
1560	20.1
1630	20.4

TABLE C5

EXPERIMENTAL CORE TEMPERATURE MEASUREMENTS

EXPERIMENTAL NUMBER =59
RICE STARCH (WT%) =20
AIR TEMPERATURE (C) =54
AIR VELOCITY (m/s) =0.96

TIME (sec)	TEMP. (C)
0	23.4
30	21.8
60	22.5
90	23.5
120	24.4
150	25.1
180	25.5
220	25.9
260	26.1
300	26.3
350	26.7
400	27.3
450	28
500	28.7
560	29.2
620	30.2
680	31.5
740	32.8
800	34.1
860	35.6
930	37.7
1000	40.6
1070	41.8
1140	43.3
1210	44.8
1280	46.4

TABLE C6

EXPERIMENTAL CORE TEMPERATURE MEASUREMENTS

EXPERIMENTAL NUMBER =57
GELATIN (WT%) =20
AIR TEMPERATURE (C) =36
AIR VELOCITY (m/s) =0.98

TIME (sec)	TEMP. (C)
0	24
30	19.8
60	20.6
90	21.3
120	22
150	22.4
180	22.7
210	23
250	23.3
290	23.5
340	23.7
400	24
460	24.3
520	24.9
580	25
660	25.5
740	25.9
820	26.2
920	26.9
1020	27.6
1120	28.3
1200	28.6
1300	29.1
1400	29.5
1520	29.9
1610	27.8
1700	28.2
1820	28.7
1940	29.5
2060	30.1
2180	30.9
2300	31,6
2420	32,4
2540	33,1
2660	33,7
2780	34,4
2900	35
2990	35,3
3080	35.5
3180	35,6

TABLE C7

EXPERIMENTAL CORE TEMPERATURE MEASUREMENTS

EXPERIMENTAL NUMBER =62
GELATIN (WT%) =20
AIR TEMPERATURE (C) =54
AIR VELOCITY (m/s) =0.96

TIME (sec)	TEMP. (C)
0	22
20	21.1
60	23.8
90	25.1
120	25.8
150	26.5
180	27.4
210	28
250	28.7
290	29.4
340	30.7
390	32.1
450	33.8
510	35.2
570	36.5
630	37.9
700	39.4
770	40.6
840	41.5
920	42.4
1000	43.2
1080	43.9
1160	44.5
1260	45.2
1360	45.6
1460	46.1
1580	46.6
1700	47.1
1820	47.4
1940	47.7
2060	48.2

TABLE C8

EXPERIMENTAL CORE TEMPERATURE MEASUREMENTS

EXPERIMENTAL NUMBER =60
SKIM MILK (WT%) =20
AIR TEMPERATURE (C) =54
AIR VELOCITY (m/s) =0.96

TIME (sec)	TEMP. (C)
0	23.5
20	22.2
60	27
90	29.3
120	30.8
150	31.5
180	32.3
220	33.4
260	34.8
300	36.5
350	38.6
400	40.6
450	42.4
510	44.1
570	45.1
630	46.7
690	47.6
760	48.2
830	48.7
900	48.8
980	49.4
1070	50
1140	50.4

TABLE C9

EXPERIMENTAL CORE TEMPERATURE MEASUREMENTS

EXPERIMENTAL NUMBER =69
SKIM MILK (WT%) =20
AIR TEMPERATURE (C) =76
AIR VELOCITY (m/s) =0.99

TIME (sec)	TEMP. (C)
0	23.1
30	27.5
60	31.3
90	35.7
120	39.6
150	42.6
180	45.2
220	47.7
260	52.4
300	55.9
340	58.9
380	61.7
420	64
460	65.8
500	67.3
540	68.5
580	69.5
620	70.3
660	71
700	71.6
740	72
800	72.6

TABLE C10

EXPERIMENTAL CORE TEMPERATURE MEASUREMENTS

EXPERIMENTAL NUMBER =50
FRUCTOSE (WT%) =20
AIR TEMPERATURE (C) =20
AIR VELOCITY (m/s) =0.98

TIME (sec)	TEMP. (C)
0	22.7
30	16.1
60	14.4
90	14
120	14.2
150	14.5
180	14.9
210	15.1
250	15.4
280	15.6
320	15.8
380	16
440	16.1
500	16.2
560	16.3
650	16.5
740	16.6
800	16.7
860	16.8
950	17
1040	17.2
1130	17.5
1220	17.8
1310	18.1
1430	18.6
1550	19.2
1670	19.7
1780	20

TABLE C11

EXPERIMENTAL CORE TEMPERATURE MEASUREMENTS

EXPERIMENTAL NUMBER =55
FRUCTOSE (WT%) =20
AIR TEMPERATURE (C) =36
AIR VELOCITY (m/s) =0.98

TIME (sec)	TEMP. (C)
0	20.4
30	19.1
60	19.1
80	19.4
100	19.7
120	20.3
150	21.2
180	22.1
210	22.7
240	23.3
280	24
320	24.5
370	25
420	25.4
480	25.8
530	26.1
590	26.7
650	27.2
710	27.8
770	28.5
860	29.8
950	31
1040	32
1130	32.9
1220	33.6
1310	34.1
1430	34.6
1550	34.9
1670	35
1790	35.5

TABLE C12

EXPERIMENTAL CORE TEMPERATURE MEASUREMENTS

EXPERIMENTAL NUMBER =61
FRUCTOSE (WT%) =20
AIR TEMPERATURE (C) =54
AIR VELOCITY (m/s) =0.96

TIME (sec)	TEMP. (C)
0	23.5
30	25.7
60	29.1
90	31.5
120	32.9
150	33.9
180	34.6
220	35.2
260	35.7
300	36.4
340	37.2
390	38.8
440	41.3
490	44
540	46.4
590	48.1
640	49.2
700	50.2
760	50.7
820	51.4
900	51.8
980	52.2
1060	52.4
1160	52.6
1260	52.7
1380	52.9

APPENDIX D

SKIN FORMATION MATHEMATICAL MODEL

D.1 VARIABLES USED IN MODEL

D.2 COMPUTER PROGRAMME LISTINGS

Programme Filename: FTSFM MODEL

APPENDIX D

D.1 VARIABLES USED IN MODEL

Initial Droplet Diameter (Custard and Starch) = 5×10^{-3} m

Initial Concentration of Custard and Starch = 20% wt.

Specific Heat Capacity of Solid (Custard) = 1445 J/kg K

Specific Heat Capacity of Solid (Starch) = 1389.5 J/kg K

Air Velocity = 0.1 m/s

Initial Concentration of custard in = 220.2 kg/m^3 Suspension
the Suspension of Custard

Initial Concentration of Starch in = 214.9 kg/m^3 Suspension
the Suspension

Initial Concentration of Water = 880.7 kg/ m^3 Suspension
in Custard Suspension

Initial Concentration of Water = 859.7 kg/m^3 Suspension
in Starch Suspension

Gelatinisation Temperature of Custard = 63 ^oC

Gelatinisation Temperature of Starch = 71 ^oC

Heat Capacity of Air

$$C_{pa} = 1017.441 - 0.13356588\ T'_a + 3.39147 \times 10^{-4}\ T'^2_a$$

D.2 COMPUTER PROGRAMME LISTING

Programme Filename: FTSFM MODEL

```
  10 REM MATHEMATICAL MODEL FOR SKIN FORMATION
  20 REM                    NOMENCLATURE
  22 REM                    ------------
  30 REM CPA(J)=SPECIFIC HEAT CAPACITY OF AIR.
  40 REM CPD(J)=SPECIFIC HEAT CAPACITY OF DROPLET.
  50 REM CPS   =SPECIFIC HEAT CAPACITY OF SOLID.
  60 REM CSO   =INITIAL CONCENTRATION OF SOLID.
  70 REM CPW   =SPECIFIC HEAT CAPACITY OF WATER.
  80 REM CWO   =INITIAL CONCENTRATION OF WATER.
  90 REM
 100 REM DA(J) =AIR DENSITY.
 120 REM DW(J) =DENSITY OF WATER.
 130 REM DV(J) =DIFFUSIVITY OF VAPOUR IN AIR.
 140 REM DP(J) =DROPLET DIAMETER.
 150 REM HG(J) =HEAT TRANSFER COEFFICIENT.
 160 REM K(J)  =THERMAL COND. OF AIR.
 170 REM KG(J) =MASS TRANSFER COEFFICIENT;UNITS:M/S.
 175 REM KGT(J)=MASS TRANSFER COEFFICIENT;UNITS:Kg/m^2 S Pa.
 180 REM LA(J) =LATENT HEAT OF EVAP.
 190 REM MWA   =MOLECULAR WEIGHT OF AIR.
 200 REM NU(J) =NUSSELT NUMBER.
 210 REM PI    =PIE (3.14159).
 220 REM PR(J) =PRANDTL NO. OF AIR.
 230 REM PWD(J)=VAPOUR PRESSURE OF WATER.
 240 REM PWI(J)=PARTIAL PRESSURE OF WATER VAP. IN AIR.
 250 REM R(J)  =RADIUS OF THE DROPLET AT THE
                GELATINIZATION TEMP.
 260 REM RE(J) =REYNOLDS NO.
 265 REM RO(J) =INITIAL RADIUS OF THE DROPLET.
 270 REM RC    =UNIVERSAL GAS CONSTANT.
 280 REM SC(J) =SCHMIDT NO. OF AIR.
 290 REM SH(J) =SHERWOOD NO.
 300 REM TA    =AMBIENT TEMP.
 310 REM TD(J) =DROPLET TEMP.
 311 REM TE(J) =EXPERIMENTAL TIME AT WHICH SKIN FORMS.
 312 REM TG    =GELATINIZATION TEMP.
 320 REM TI(J) =AIR TEMP.
 322 REM T0(J) =INITIAL DROPLET TEMP.
 330 REM V     =AIR VELOCITY.
 340 REM VA(J) =VISCOSITY OF AIR.
 350 REM X(J)  =THICKNESS OF THE BOUNDARY LAYER OF THE DROPLET.
 400 REM
 410 DIM CPD(40),TE(40),T0(40),R(40),HG(40),NU(40),RE(40)
 420 DIM PR(40),K(40),T1(40),TD(40),SH(40),SC(40),DV(40),
       KG(40),T(40)
 430 DIM PWD(40),VA(40),DA(40),LA(40),CPA(40),X(40),KGT(40),
       WW(40)
 433 DIM NU1(40),NU2(40)
 440 REM
 450 REM CALCULATIONS
 460 REM INPUT NUMBER OF SETS OF THEORETICAL DATA
 470 READ N1
 480 REM INPUT THE RUN NOS.
 490 FOR J=1 TO N1
 500 READ WW(J)
 510 NEXT J
 520 REM
>
```

```
530 REM INPUT AIR TEMP.
540 FOR J=1 TO N1
550 READ TI(J)
560 NEXT J
570 REM INPUT DROPLET TEMP.
580 FOR J=1 TO N1
590 READ TD(J)
600 NEXT J
610 REM INPUT INITIAL DROPLET TEMP.
620 FOR J=1 TO N1
630 READ T0(J)
640 NEXT J
650 REM INPUT GELATINIZTION TEMP.
654 READ TG
660 REM INPUT INITIAL DROPLET RADIUS
670 READ RO
680 REM INPUT DROPLET RADIUS AT GELATINAZATION TEMP.
690 FOR J=1 TO N1
700 READ R(J)
710 NEXT J
720 REM
730 REM INPUT VAPOUR PRESSURE OF WATER
740 FOR J=1 TO N1
750 READ PWD(J)
760 NEXT J
770 REM INPUT PARTIAL PRESSURE OF WATER VAP. IN AIR
780 READ PWI
790 REM INPUT AIR VELOCITY
800 READ V
803 REM INPUT UNIVERSAL GAS CONSTANT AND MOLECULAR WEIGHT
805 READ RC
807 READ MWA
860 REM SET VALUE FOR CONSTANT
870 LET PIE=22/7
880 REM
890 REM INPUT SPECIFIC HEAT CAPACITY OF SOLID
900 READ CPS
910 REM INPUT SPECIFIC HEAT CAPACITY OF WATER
920 READ CPW
930 REM INPUT INITIAL CONCENTRATION OF SOLID
940 READ CSO
950 REM INPUT INITIAL CONCENTRATION OF WATER
960 READ CWO
970 REM INPUT WATER DENSITY
975 FOR J=1 TO N1
980 READ DW
985 NEXT J
990 REM INPUT AMBIENT TEMP.
1000 READ TA
1010 REM
1020 REM EVALUATE PHYSICAL PROPS.
1030 FOR J=1 TO N1
1040 LET VA(J)=4.568E-8*(TI(J)+TD(J))/2+1.720E-5
1050 NEXT J
1060 FOR J=1 TO N1
1070 LET DA(J)=1.2929*273.15/(273.15+TI(J))
1080 NEXT J
>
```

```
1082 FOR J=1 TO N1
1083 LET K(J)=(4.2956E-5*(TI(J)+TD(J))/2+.014)*1.7307
1085 NEXT J
1090 REM
1100 REM CONVERT TEMP. TO K
1110 FOR J=1 TO N1
1120 LET TI(J)=TI(J)+273.15
1130 LET TD(J)=TD(J)+273.15
1140 NEXT J
1150 REM
1160 FOR J=1 TO N1
1170 LET LA(J)=(1075.95-1.0246*(TD(J)-273.15))*2.326E3
1180 NEXT J
1190 REM
1200 FOR J=1 TO N1
1210 LET DV(J)=0.22E-4*((TI(J)+TD(J))/2/273.15)^1.75
1220 NEXT J
1260 FOR J=1 TO N1
1270 LET CPA(J)=1017.441-.1356588*TI(J)+(3.39147E-4)*TI(J)^2
1280 NEXT J
1320 REM
1330 REM MODEL PREDICTION
1332 FOR J=1 TO N1
1334 LET CPD(J)=4/3*PIE*(RO^3)*((CPS*CSO)+(CPW*(CWO-(DW*(1-(R(J)^3/
               RO^3))))))
1336 NEXT J
1340 FOR J=1 TO N1
1350 LET RE(J)=(V*DA(J)*(2*R(J)))/VA(J)
1360 NEXT J
1364 FOR J=1 TO N1
1366 PR(J)=CPA(J)*VA(J)/K(J)
1368 NEXT J
1370 FOR J=1 TO N1
1372 SC(J)=VA(J)/(DV(J)*DA(J))
1375 NEXT J
1380 FOR J=1 TO N1
1385 NU(J)=2+(.27*(LA(J)/(CPA(J)*(TI(J)-TD(J))))^.18)*RE(J)^.5
          *PR(J)^.33
1400 NEXT J
1405 REM HEAT TRANSFER COEFFICIENT CALCULATION
1410 FOR J=1 TO N1
1420 LET HG(J)=NU(J)*K(J)/(2*R(J))
1430 NEXT J
1440 REM
1450 FOR J=1 TO N1
1460 SH(J)=2.0+0.57*((TI(J)-TD(J))/TA)^-0.04*RE(J)^0.5*SC(J)^0.33
1470 NEXT J
1480 REM KG CALCULATION;UNITS M/S
1490 FOR J=1 TO N1
1500 LET KG(J)=DV(J)*SH(J)/(2*R(J))
1510 NEXT J
1520 REM KG$ CALCULATION;UNITS Kg/m^2 S Pa.
1530 FOR J=1 TO N1
1540 LET X(J)=DV(J)/KG(J)
1550 NEXT J
1560 FOR J=1 TO N1
1570 LET KGT(J)=DV(J)/(RC*X(J)*TI(J))
>
```

```
1580 NEXT J
1590 REM CALCULATION OF THE TIME AT WHICH THE SKIN FORMS.
1600 FOR J=1 TO N1
1610 T(J)=(CPD(J)/(4*PIE*R(J)^2)*(TG-T0(J)))/((HG(J)*(TI(J)
       -TD(J)))-(KGT(J)*LA(J)*(PWD(J)-PWI)))
1620 NEXT J
1630 REM
1635 REM INPUT THE EXPERIMENTAL RESULT TO COMPARE WITH
1636 REM MODEL PREDICTIONS
1640 FOR J=1 TO N1
1643 READ TE(J)
1646 NEXT J
1650 REM PRINTING THE RESULTS
1653 PRINT TAB(9);"TABLE 9.1"
1657 PRINT TAB(9);"---------"
1659 PRINT
1660 PRINT
1662 PRINT TAB(9);"MATHEMATICAL MODEL PREDICTIONS FOR DROPLETS OF
                  CUSTARD SUSPENSION"
1665 PRINT TAB(9);"-----------------------------------------------
                  ------------------"
1668 PRINT
1669 PRINT
1670 PRINT
1671 PRINT TAB(9);"EXP";
1672 PRINT TAB(16);"AIR";
1674 PRINT TAB(25);"REY";
1676 PRINT TAB(33);"SH";
1678 PRINT TAB(41);"NU";
1680 PRINT TAB(49);"EXPERIMENTAL";
1681 PRINT TAB(65);"THEORETICAL"
1682 PRINT TAB(9);"NO";
1684 PRINT TAB(16);"TEMP(C)";
1685 PRINT TAB(25);"NO";
1686 PRINT TAB(33);"NO";
1687 PRINT TAB(41);"NO";
1689 PRINT TAB(49);"TIME(sec)";
1691 PRINT TAB(65);"TIME(sec)"
1693 PRINT TAB(9);"---";
1694 PRINT TAB(16);"------";
1697 PRINT TAB(25);"---";
1700 PRINT TAB(33);"---";
1703 PRINT TAB(41);"---";
1706 PRINT TAB(49);"-------------";
1709 PRINT TAB(65);"------------"
1720 PRINT
1730 FOR J=1 TO N1
1735 %%=&90A
1738 PRINT TAB(9);WW(J);
1740 PRINT TAB(17);TI(J)-273.15;
1745 %%=&20209
1750 PRINT TAB(25);RE(J);
1760 PRINT TAB(33);SH(J);
1770 PRINT TAB(41);NU(J);
1780 PRINT TAB(53);TE(J);
1790 PRINT TAB(69);T(J)
1800 PRINT
1820 NEXT J
1882 PRINT TAB(10);"---";
2500 END
>
```